ANALYTICAL TECHNIQUES FOR DETERMINING TEMPERATURES, THERMAL STRAINS, AND RESIDUAL STRESSES DURING WELDING

by

VASSILIOS JOHN PAPAZOGLOU

Dipl., National Technical University, Athens, Greece
(1975)

S.M., Massachusetts Institute of Technology
(1978)

SUBMITTED IN PARTIAL FULFILLMENT
OF THE REQUIREMENTS FOR THE
DEGREE OF

DOCTOR OF PHILOSOPHY

at the

MASSACHUSETTS INSTITUTE OF TECHNOLOGY

May 1981

© Massachusetts Institute of Technology

Signature of Author _____
Department of Ocean Engineering
May 11, 1981

Certified by _____
Koichi Masubuchi
Thesis Supervisor

Accepted by _____
A. Douglas Carmichael
Chairman, Departmental Graduate Committee

ARCHIVES
MASSACHUSETTS INSTITUTE
OF TECHNOLOGY

JUL 14 1981

LIBRARIES

ANALYTICAL TECHNIQUES FOR DETERMINING TEMPERATURES, THERMAL STRAINS, AND RESIDUAL STRESSES DURING WELDING

by

VASSILIOS JOHN PAPAZOGLOU

Submitted to the Department of Ocean Engineering on May 11, 1981 in partial fulfillment of the requirements for the Degree of Doctor of Philosophy in Ocean Engineering

ABSTRACT

New and modifications of existing analytical and numerical techniques have been developed for predicting temperatures, thermal strains and residual stresses due to welding of high strength steels, especially HY-130.

A closed form solution was found for predicting temperatures during welding of thin plates using a new three-dimensional heat source model, improving upon the already existing ones based on the conventional point and line heat sources. Comparisons with experimental results show good correlation.

Using ADINAT, a nonlinear finite element model for solving the heat transfer problem during welding was devised. The obtained results were compared with experiments performed on medium thickness GMA welded HY-130 plates.

A model for taking into account the phase transformation strains during welding quenched and tempered steels was developed and incorporated into the finite element program ADINA. The analytical predictions were then compared with the above mentioned experiments yielding a good correlation.

Thesis Supervisor: Dr. Koichi Masubuchi.
Title: Professor of Ocean Engineering and Materials Science.

ACKNOWLEDGEMENTS

Sincere appreciation is expressed to my advisor Professor Koichi Masubuchi for his friendship, guidance, and support throughout my graduate studies at M.I.T. Special thanks are also extended to Professor Klaus-Jürgen Bathe for providing me the finite element program ADINA and for his guidance during the course of this investigation. I would also like to thank Professors Warren Rohsenow and Joao de Oliveira for their invaluable help.

The author wishes to acknowledge the Office of Naval Research for the financial support they provided without which this study would not have been possible.

To Tony Zona and the late Fred Merlis many thanks are due for their support during the experimental part of this work. Further, I wish to thank Tricia Hollum and Marjorie Katz for the efficient typing of parts of this thesis.

Last, but not least, I would like to express my sincere thanks to my wife Nada for her expert typing of the mathematical formulae and part of the text, but mainly for her continuous encouragement and the sacrifices she had to make during the course of this study.

To Nada

TABLE OF CONTENTS

	Page
ABSTRACT	2
ACKNOWLEDGMENT	3
TABLE OF CONTENTS	5
LIST OF FIGURES	9
LIST OF TABLES	14
I. INTRODUCTION	16
1.1 Sources of Residual Stresses	18
1.2 Methodology	20
1.3 Problem Characteristics	20
1.4 Objectives	22
II. ANALYTICAL TREATMENT OF HEAT FLOW DURING WELDING	25
2.1 Literature Review	26
2.1.1 Fundamental Solutions	26
2.1.2 Experimental Verifications	30
2.1.3 Variable Material Properties	33
2.2 Heat Input Modeling	34
2.3 Three-Dimensional Finite Heat Source Model	43
2.3.1 Governing Equation	45
2.3.2 Boundary Conditions	50
2.3.3 Solution	54
2.4 Parametric Investigation	69
2.5 Comparison with Other Solutions and Experiments	77

Page

III. MATERIAL CHARACTERISTICS OF HY-130 STEEL 89

3.1 General Characteristics 90

3.2 Experimentally Derived Transformation Kinetics 96

3.2.1 Isothermal Kinetics 96

3.2.2 Continuous Cooling Kinetics 99

3.3 Temperature Dependence of Material Properties. 107

3.3.1 Mechanical Properties 110

3.3.2 Physical Properties 120

3.4 Computed Continuous Transformation Diagram from Isothermal Data 130

3.4.1 Application in the Case of HY-130 Steel. 136

IV. NUMERICAL SOLUTION OF HEAT FLOW DURING WELDING. 141

4.1 Literature Survey 142

4.2 Finite Element Procedure 143

4.3 Weld Model 145

4.3.1 Two-Dimensionality of Problem 145

4.3.2 Boundary Conditions 150

4.3.3 Material Properties 153

4.3.4 Weld Metal Modeling 154

4.3.5 Heat Input 157

4.4 Description of Experiments 157

4.4.1 Specimen Geometry 158

4.4.2 Instrumentation 161

4.4.3 Welding Procedure 163

Page

4.5 Comparison of Numerical and Experimental Results 165

V. TRANSIENT STRAINS, TRANSIENT STRESSES AND RESIDUAL STRESSES DUE TO WELDING 179

5.1 Literature Survey 180

5.2 One-Dimensional Analysis 182

5.3 Finite Element Formulation 186

5.4 Phase Transformation Effects 191

5.4.1 Microstructure Prediction 192

5.4.2 Calculation of Transformation and Thermal Strains 198

5.5 Weld Model Using the FEM 203

5.5.1 Geometry - Boundary Conditions 203

5.5.2 Material Properties 204

5.5.3 Solution Strategy 206

5.6 Results 207

VI. CONCLUSIONS AND RECOMMENDATIONS 221

6.1 Conclusions 221

6.2 Recommendations for Future Research 223

REFERENCES 226

APPENDIX A - COMPUTER IMPLEMENTATION OF THE THREE-DIMENSIONAL FINITE HEAT SOURCE SOLUTION 238

A.1 Solution of the Transcedental Equation (2.43). 238

A.2 Numerical Calculation of Integral (2.63) . . . 240

Page

A.3 Calculation of Maximum Heat Flux 242

A.4 Calculation of Bessel Functions 244

A.5 Program Listing 245

APPENDIX B - MODIFICATION OF THE CONVENTIONAL POINT HEAT SOURCE SOLUTION 266

B.1 Program Listing 269

APPENDIX C - DERIVATION OF SCHEMATIC CONTINUOUS COOLING TRANSFORMATION DIAGRAMS 276

C.1 The Grange-Kiefer Approach 276

C.2 The Manning-Lorig Approach 278

C.3 Log-linear Cooling Rates 281

C.4 Computer Implementation 282

APPENDIX D - EVALUATION OF COMBINED THERMAL AND TRANSFORMATION STRAIN 284

D.1 Heating Stage 284

D.2 Cooling Stage 286

LIST OF FIGURES

Figure		Page
1.1	Weldment Configuration	21
1.2	The Four Parts of a Weld Subjected to Different Thermal Histories	23
2.1	Schematic Diagram of Heat Flow Patterns	28
2.2	Distribution of Heat Flux Across the Hot Spot for a Normal Circular Source	38
2.3	Arc Heat Distribution for a Moving Finite Heat Source	44
2.4	Schematic Representation of Geometry for Boundary Value Problem	51
2.5	Superposition Used for Inner Solution	61
2.6	Effect of Heat Losses on Finite Heat Source Solution	71
2.7	Effect of Variation of Thermal Conductivity on Finite Heat Source Solution	72
2.8	Parametric Investigation of Finite Heat Source Solution (1.0 in)	73
2.9	Same (0.75in)	74
2.10	Same (0.5 in)	75
2.11	Same (0.284 in)	76
2.12	Effect of Heat Input on Finite Heat Source Solution (1.0 in)	78
2.13	Same (0.75 in)	79
2.14	Same (0.5 in)	80
2.15	Same (0.284 in)	81
2.16	Investigation of Point Heat Source Solutions (1.0 in from weld line)	83
2.17	Same (0.75 in from weld line)	84

Figure		Page
2.18	Same (0.5 in from weld line)	85
2.19	Same (0.284 in from weld line)	86
2.20	Comparison of Finite Heat Source Solution with Experimental Data for a 0.125 in thick Welded Plate	88
3.1	Isothermal Transformation Diagram for HY-130 Steel	97
3.2	Continuous Cooling Transformation Diagrams for HY-130 Steel	102
3.3	Continuous Cooling Transformation Diagrams for GMA Welded HY-130 Weld Metal (from 2000°F)	103
3.4	Typical Stress-Strain Diagram for HY-130 Steel at Room Temperature	111
3.5	Variation of Virgin Yield Stress with Temperature for HY-130 Steel	114
3.6	Variation of Young's Modulus with Temperature for HY-130	116
3.7	Variation of Tangent Modulus with Temperature for HY-130	118
3.8	Bilinear Stress-Strain Diagrams for HY-130 at Various Temperatures	119
3.9	Variation of Poisson's Ratio with Temperature for HY-130	121
3.10	Variation of Thermal Conductivity with Temperature for HY-130	125
3.11	Variation of Specific Heat with Temperature for HY-130	127
3.12	Variation of Average Thermal Expansion Coefficient with Temperature for HY-130	129
3.13	Variation of Density with Temperature for HY-130	131
3.14	Schematic CCT Diagrams for HY-130 Steel (Bainite Start Transformation Curves)	138

Figure		Page
4.1	Weldment Configuration	146
4.2	Test Plate Arrangement	159
4.3	Weld Joint Configuration	159
4.4	Test Plate Support Arrangement	160
4.5	Effect of Temperature on Apparent Strain (SR-4 Strain Gage)	162
4.6	Thermocouple and Strain Gage Location on HY-130 Specimen I	164
4.7	Thermocouple and Strain Gage Location on HY-130 Specimen II	164
4.8a	Finite Element Mesh Used in Heat Transfer Analysis (rightmost 11.5 in of cross-section)	167
4.8b	Finite Element Mesh Continued (center 1.0 in)	168
4.9	Heat Input Distribution (example)	170
4.10	Comparison of Finite Element Results with Experimental Data (weld pass no. 1)	172
4.11	Same	173
4.12	Comparison of Finite Element Results with Experimental Data (weld pass no. 2)	175
4.13	Same	176
4.14	Same	177
5.1	Longitudinal Transient Strain Histories for EB Welded Specimens (Experiment and Analysis)	185
5.2	Longitudinal Transient Strain Histories for GMA Welded Specimens (Experiment and Analysis)	185

Figure		Page
5.3	Idealized CCT Diagram	193
5.4	Typical Temperature History Inside the HAZ of a Weld	196
5.5	Typical Dialatational Curve Includinf Phase Transformation Effects	201
5.6	Constraints Applied to the Finite Element Model	208
5.7a	Finer Finite Element Mesh Used in Stress Analysis of Welding Problem	210
5.7b	Finer Finite Element Mesh, cont.	211
5.8	Accumulated Effective Plastic Strain at Various Distances from Weld Centerline (initial 5 sec)	212
5.9	Transient Stress History at Various Distances from Weld Centerline (initial 5 sec)	214
5.10	Comparison of Transverse Transient Strain Histories - Experimental Data vs. Analytical Predictions (initial 5 sec)	215
5.11	Accumulated Effective Plastic Strain History at Various Distances from the Weld Centerline	216
5.12	Longitudinal Stress Distribution at Several Time Instances	218
5.13	Comparison of Experimentally Measured Transverse Transient Strains on the Plate's Top Surface with Numerical Predictions	219
A.1	Representative Interval Used in Numerical Integration	243
B.1	Superposition of Heat Sources	267
C.1	Schematic Representation of the Grange-Kiefer Method	277

Figure		Page
C.2	Schematic Representation of the Manning-Lorig Method	280

LIST OF TABLES

Table		Page
2.1	Values of Arc Efficiency for Various Welding Processes	36
2.2	Experimental Values for the Concentration Coefficient	41
3.1	Compositional Ranges of HY-80 and HY-130 Steels	92
3.2	General Properties of HY-130 Type Steel	93
3.3	Analysis of Consumables for Welding HY-130 Type Steels	95
3.4	Results of Isothermal Transformation Studies on HY-130 Weld Metal Using AX-140 Wire	100
3.5	Measured Martensitic Start Transformation Temperature, M_s	105
3.6a	Summary of Mechanical Properties for HY-130 (Anglo-Saxonic units)	122
3.6b	Summary of Mechanical Properties for HY-130 (SI units)	123
3.7a	Summary of Physical Properties for HY-130 (Anglo-Saxonic units)	132
3.7b	Summary of Physical Properties for HY-130 (SI units)	133
4.1	Temperature Dependence of Heat Convection Coefficient	153
4.2	Strain Gage Specifications	161
4.3	Welding Conditions for HY-130 Specimens	165
4.4	Summary of Analyses	171
5.1	Values Used for the Calculation of Transformation Strains	202

Table		Page
5.2	Solution Parameters Used with ADINA	207
C.1	Values of Parameters A and B	281

CHAPTER I

INTRODUCTION

The welding processes have been and are extensively used for the fabrication of various structures ranging from bridges and machinery to all kinds of seagoing vessels to nuclear reactors and space vehicles. This is the case because of the many advantages it offers compared to other fabrication techniques — excellent mechanical properties, air and water tightness, good joining efficiency, to name but a few.

At the same time, however, welding creates various problems of its own that have to be solved. In the past these problems have been tackled through experimental investigations. Since low-carbon steel was the primary material used in the first two decades after World War II, extensive experimental parametric analyses were performed in an effort to solve these problems and hence produce satisfactory welded structures. As a consequence, a substantial amount of data has been collected over the years on welding low-carbon steel using conventional arc techniques.

A shortcoming of these types of experimental investigation, though, is the large amount of manpower required and the high cost. The question thus arises of what to do when conventional welding techniques are to be applied to other materials, such as high strength quenched and tempered steels, aluminum, and titanium or when modern welding techniques, such as electron beam and laser, are to be used. Fortunately enough, since the

advent of the computer, a new tool became available which, combined with limited experimental efforts, could give solutions to many of the problems due to welding.

One of the problems suitable for computer analysis is the one involving residual stresses and distortion due to welding. The uneven temperature distribution produced during welding gives rise to incompatible strains which in turn result in self equilibrating residual stresses and distortion that remain in the structure after it has cooled down to ambient temperature. The phenomena involved are very complex necessitating the use of numerical techniques and hence computers for their solution.

The next logical question coming to one's mind is why should one be concerned with residual stresses and distortion. The answer is that the effect they have on the service behavior of the welded structure can be detrimental. Brittle fracture can occur earlier because the presence of the residual stresses, combined with any external loading, can substantially decrease the critical flow size of the weldment. Compressive residual stresses in the regions located some distance away from the weld line can also substantially decrease the critical buckling stress of a structure, especially if it is composed of thin plates, causing structural instabilities. Similar effects occur in the areas of fatigue fracture, stress corrosion cracking, hydrogen embrittlement, etc.

It becomes, thus, evident from the above discussion that the existence of a methodology capable of predicting the residual stresses after the structure has cooled down is highly

desirable. The designer could then change the design or use different materials or welding processes in an effort to minimize the residual stresses and distortion and hence their adverse effects. This thesis is concerned with modifying the already available techniques in an effort to improve their predictive capabilities.

1.1 Sources of Residual Stresses

Residual stresses are those stresses that would exist in a body if all external loads were removed. If a material is heated uniformly, it expands uniformly and no thermal stress is produced. On the other hand, if the material is heated unevenly, thermal stresses are produced. Residual stresses will also be produced when unevenly distributed non-elastic strains, such as plastic strains exist. In the case of welding such plastic strains do occur in an area around the weld centerline caused primarily by the dramatic decrease of the material's yield stress at very high temperatures. As a consequence residual stresses are always produced in welded structures [1].

Three different sources of residual stresses due to welding can be identified according to Macherauch and Wohlfahrt [2], all contributing to the inelastic strain. One is the difference in shrinkage of differently heated and cooled areas of a welded joint. The weld metal, originally subjected to the highest temperatures, tends upon cooling to contract more than all other areas. This contraction is hindered by the other parts of the joint, thus resulting in the formation of high longitudinal stresses, σ_x, in the weld metal. Similar tensile

stresses, σ_y, arise in the transverse direction, too, but of smaller magnitude.

A second source is the uneven cooling in the thichness direction of the weld. Surface layers of the weld and the highly heated areas close to it usually cool more rapidly than the interior, especially in the case of thick plates. Thermal stresses thus arise over a cross-section which can lead to heterogenous plastic deformations and hence to residual stresses. These "quenching" residual stresses are expected to be compressive at the surface of the highly heated areas and to self-equilibrate with the tensile ones in the inner regions.

The final source of residual stresses will come from the phase transformations of austenite to ferrite, bainite, or martensite occuring during cooling. These transformations are accompanied by an increase in specific volume, causing the material being transformed (in the weld metal and the HAZ) to want to expand. But this expansion is hindered by the cooler material not being transformed, resulting in compressive stresses of the transformed material and tensile in the other regions.

The total residual stresses will thus be a combination of the above. In most previous analyses, though, only the first two sources were considered. This study will try to incorporate all three, in an effort to find the actual impact of phase transformations on the magnitude and distribution of transient and residual stresses.

1.2 Methodology

To accurately solve the welding problem, or for this matter any problem involving both thermal and stress analysis, one should start from first principles, which in this case is the first law of thermodynamics. This would mean, however, that one would have to solve a problem containing mechanical and thermal coupling, a fact that makes the analysis extremely complicated, if not impossible with the present state of knowledge. Mróz [3-5] has made initial attempts at formulating and investigating the problem of coupled thermoplasticity, but the whole process is still in its initial stages.

It becomes, therefore, necessary to uncouple the thermal and mechanical parts of the welding problem and solve each of them separately. Hibbitt [6] has examined the assumptions that have to be made in order to uncouple the problem and found them to be acceptable for the case of high strength quenched and tempered steels, such as HY-130.

The same approach was followed in this study. First, the problem of heat flow during welding was solved and then a strain and stress analysis was performed using as input, among others, the previously calculated temperature distribution.

1.3 Problem Characteristics

Figure 1.1 shows the physical phenomenon to be examined. A welding arc is travelling with a speed v between two plates causing them to coalesce by providing filler metal.

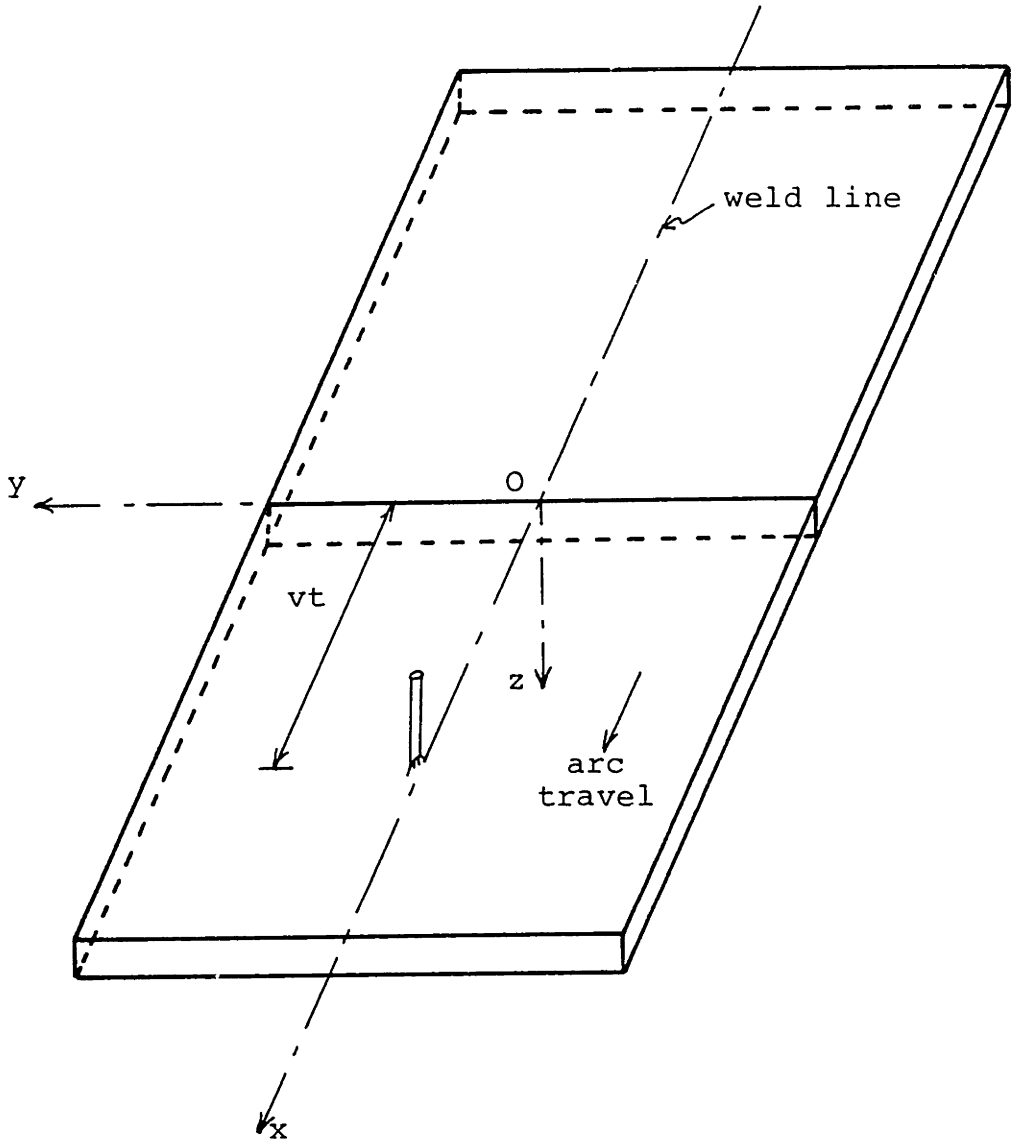

FIGURE 1.1 Weldment Configuration

The four parts of a weld that are subjected to different thermal histories are shown in Figure 1.2. Part 1 constitutes the filler metal which is deposited molten and later solidifies as cooling begins. Part 2 is the part of the joint that melts and later resolidifies during cooling. Both these parts define the weld metal. Part 3 is the heat affected zone (HAZ) defined as that part of the joint in which the maximum temperature reached is above the A_1 but below the solidus temperature. Finally, part 4 is the base metal.

Interest will be focused in this study in the first three parts. These are the ones in which the largest plastic deformations, causing the occurance of residual stresses, are exhibited. All phase transformations also occur in this region.

1.4 Objectives

This study is primarily concerned with the development of analytical and numerical techniques capable of predicting temperatures, thermal strains, transient strains, and residual stresses due to welding high strength quenched and tempered steels, especially the HY-130 steel. More specifically, the objectives are as follows:

1. Development of a closed form solution for predicting temperature distributions due to a moving three-dimensional heat source taking into account temperature dependent material properties and surface heat losses.

2. Comparison of the above solution with other closed-form ones and with experiments.

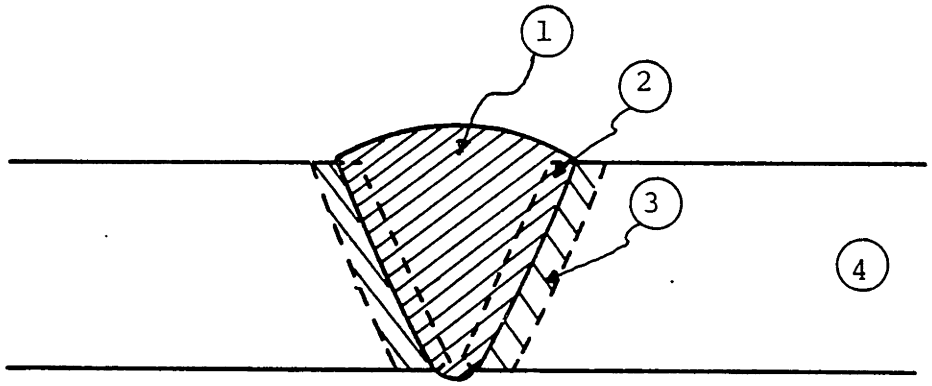

1, 2 Weld Metal

3 Heat Affected Zone

4 Base Metal

FIGURE 1.2 The Four Parts of a Weld Subjected to Different Thermal Histories.

3. Establishment of the transformation characteristics and the temperature dependence of material properties for the HY-130 steel.

4. Measurement of temperatures and transient strains during gas metal arc welding of 1 in (25.4 mm) thick HY-130 plates.

5. Modelling of the heat transfer problem during welding using the finite element method.

6. Comparison of the numerical results with the experimentally obtained ones.

7. Assessment of the accuracy of the one-dimensional stress analysis through comparisons with experiments.

8. Incorporation of phase transformation effects in the finite element nonlinear stress analysis program ADINA.

9. Modelling of the welding stress analysis using the finite element method.

10. Comparison of the results obtained in the previous step with experimental data.

CHAPTER II

ANALYTICAL TREATMENT OF HEAT FLOW DURING WELDING

The importance of accurately predicting the temperature distribution during welding has been recognized for many years by both scientists and engineers working with welding problems. This importance stems from the fact that most of the phenomena subsequently encountered, such as residual stresses, distortion, metallurgical changes, etc. have their origin in the uneven temperature distribution and the fast heating and cooling rates that occur during the welding operation.

All of the early attempts at solving the problem of heat flow during welding were analytical in nature since they were performed before the advent of the computer. As a consequence several simplifying assumptions had to be made to allow for the solution of the highly nonlinear governing partial differential equation and the accompanying boundary conditions. Starting in the mid-sixties, however, several investigators from around the world have used the computer to numerically predict the thermal history during welding with much greater accuracy, as it will be discussed in Chapter 4.

This chapter will exclusively deal with analytical solutions of the problem which, though not as accurate as the numerical ones, provide for the establishment of the general laws and thus facilitate a better understanding of the phenomena involved. A thorough literature review will first be presented dealing primarily with point and line heat source

solutions to the problem. A new model will then be developed based on a finite heat source and linear variation of the material thermal conductivity. Finally, comparisons will be made between the new model and the old ones, including some modifications of them, as well as with experimental results.

2.1 Literature Review

2.1.1 Fundamental Solutions

The first exact analytical solutions of the problem of heat flow during welding were obtained by Rosenthal [7 - 9] in the late 1930s and early 1940s, although a particular case was considered independently at around the same time by Boulton and Lance Martin [10]. Rosenthal solved the conventional heat conduction differential equation for constant point, line, and plane heat sources moving at a constant speed with respect to a fixed Cartesian coordinate system. To facilitate easier handling of the problem, he assumed that welding was performed over a sufficient length so that the temperature distribution around the heat source would not change if viewed from a coordinate system moving with the heat source. This phenomenon is called quasi-stationary or quasi-steady state. Additional assumptions were made as follows:

1. The physical properties of the conducting medium are constant.

2. The heat losses through the surface of the conducting medium to the surrounding atmosphere are neglected.

3. Heat created in electric welding by the Joule effect is negligible.

4. The phase changes and the accompanying absorption or release of latent heat in the conducting medium are neglected.

5. The conducting medium is infinitely large in the two-dimensional case (line heat source) and semi-infinitely large in the three dimensional case (point source).

Based on the above assumptions Rosenthal developed the following exact solutions for the two- and three-dimensional cases respectively (see Figures 1.1 and 2.1):

$$\theta - \theta_o = \frac{Q}{2\pi kH} \cdot e^{-\lambda v \xi} \cdot K_o(\lambda v r) \tag{2.1}$$

$$\theta - \theta_o = \frac{Q}{2\pi k} \cdot e^{-\lambda v \xi} \cdot \frac{e^{-\lambda v R}}{R} \tag{2.2}$$

where

θ_o = initial temperature

Q = total heat input

H = plate thickness

ξ = $x - vt$

v = welding (or arc travel) speed

t = time

(x,y,z) = fixed Cartesian coordinate system

r = $(\xi^2 + y^2)^{1/2}$

R = $(\xi^2 + y^2 + z^2)^{1/2}$

k = thermal conductivity

$1/2\lambda$ = $k/\rho c = \kappa$ = thermal diffusivity

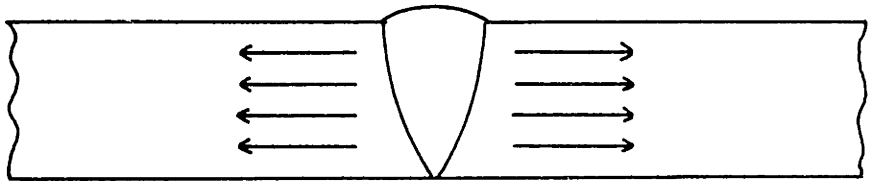

(a) Two-Dimensional Heat Flow:
Thin Plate

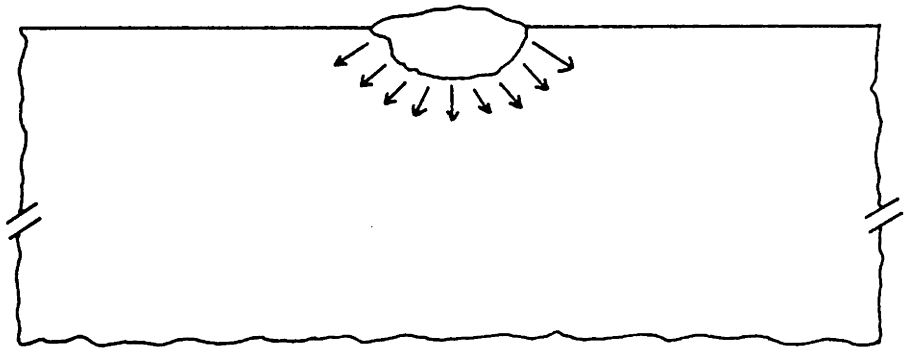

(b) Three-Dimensional Heat Flow:
Semi-infinite Plate

FIGURE 2.1 Schematic Diagram of Heat Flow Patterns

ρ = density

c = specific heat

$K_o(x)$ = modified Bessel function of second kind and zero order.

For the case of thin plates (two-dimensional solution) Rosenthal [8] and other investigators have suggested that heat losses through the surface to the surrounding atmosphere might have to be taken into account by replacing in the Bessel function of eqn. (2.1) the factor λv by

$$\left[(\lambda v)^2 + \frac{h_1+h_2}{kH}\right]^{1/2} \tag{2.3}$$

where h_1 and h_2 are the heat transfer coefficients, assumed constant, at the top and bottom of the plate respectively.

Futhermore, by using the so-called "method of images" or "image source method" [8], one can get solutions for the cases of large but finite thickness and/or finite breadth plates. For example, a three-dimensional solution for laying a weld bead on a finite thickness plate with adiabatic boundary conditions can be obtained by adding an infinite series to eqn. (2.2), yielding:

$$\theta - \theta_o = \frac{Q}{2\pi k} \cdot e^{-\lambda v \xi} \cdot \left\{ \frac{e^{-\lambda v R}}{R} + \sum_{n=1}^{\infty} \left(\frac{e^{-\lambda v R_n}}{R_n} + \frac{e^{-\lambda v R_{n'}}}{R_{n'}} \right) \right\} \tag{2.4}$$

where

$$R_n = \left(\xi^2 + y^2 + (2nH-z)^2\right)^{1/2}$$

$$R_{n'} = \left(\xi^2 + y^2 + (2nH+z)^2\right)^{1/2}$$

An extension of this concept to the case of multipass welding of thick plates will be described in Section 2.5.

2.1.2 Experimental Verifications

Following these initial developments many investigators tested the validity of the proposed equations experimentally. Although Myers et al [11] provide a thorough exposition of these works in their review paper, some of the most important research efforts will be cited here for completeness.

Rosenthal and Schmerber [12] tested the two-dimensional solution, eqn. (2.1), experimentally and reported satisfactory agreement of results only for distances far from the weld line. In the neighborhood of the arc the computed isotherms were further away from the arc than the measured ones, a fact that can be attributed to the simplified, but unrealistic, assumptions of a concentrated heat source and constant material properties.

In 1941, Mahla and co-workers [13] proposed a new solution for the case of a point source moving on the top surface of a semi-infinite conducting medium which is adiabatic along its boundaries. By integrating an appropriate Green's function they found the following equation:

$$\theta - \theta_o = \frac{Q}{2\pi kR} \cdot e^{-\lambda v(\xi+R)} \cdot (1-\hat{\gamma}) \qquad (2.5)$$

where

$$\hat{\gamma} = \frac{\beta}{\lambda vR} \left(1 + \frac{1}{\lambda vR}\right)$$

$$\beta = \frac{(\lambda v)^2}{24} (4p^2 + d^2)$$

p = weld penetration

d = weld width

Despite the fact, however, that the introduced correction factor, $\hat{\gamma}$, tends to reduce the temperatures compared to the ones predicted by Rosenthal's solution, the formula was still found to yield too high maximum temperatures and excessive cooling rates when correlated with experimental results.

A somewhat different approach was taken by Wells [14] who developed an equation relating the width of the melting isotherm to the amount of heat input based on the moving line heat source theory. He reports good agreement with data from Jackson and Shrubsall [15]. Apps and Milner, however, during their investigation of heat flow during argon-arc welding [16] found that Wells' equation does not correlate very well with experimental measurements of weld pool contours.

To test the infinite plate assumption made in most

analytical solutions, Roberts and Wells [17] examined the effect of bounding planes on the temperature distribution due to welding using Rosenthal's solution, Wells' correlation, and the "image source method". They concluded that a plate with half-width greater than ten times the width of the fusion zone approaches the thermal condition of an infinite plate.

Various other investigators looked at comparisons between predicted and measured values of peak temperatures and cooling rates, two parameters crucial for the determiniation of the metallurgical structure of the base metal after the welding operation. Adams [18 - 19], among others, derived engineering relationships, on the basis of extensive experimental results, giving peak temperatures and cooling rates directly as functions of welding, thermal, and geometric variables. He concluded that cooling rates at a constant temperature are comparatively independent of distance from the weld centerline within the heat affected zone region and that cooling rates can be predicted within 25% if the above mentioned variables are known with sufficient accuracy. The computed values, however, are always higher than the experimental ones, a fact that can be attributed to the omission of the latent heat effects near the heat source region.

Finally, in another investigation Christensen and co-workers [20 - 21] found good agreement only with trends for the width, depth, and cross-sectional area of the molten zone in the three-dimensional case. They concluded that the transfer of heat from the welding arc to the base metal is a

complicated process making it difficult to perform accurate calculations.

2.1.3 Variable Material Properties

Looking at data on thermal conductivity, specific heat, and density one finds that all these parameters are highly dependent upon temperature, thus making the constant properties assumption of the analytical solutions unrealistic, especially for the regions close to the heat source where the material exhibits very high temperatures. It is desirable to predict the high temperature region as accurately as possible, however, since it is this region that is directly related to the size of the plastic zone and the accompanying residual stresses and distortion.

Grosh, et al., [22 - 23] have formulated an analytical expression for the temperature distribution during welding assuming that thermal conductivity, k, and the product of density and specific heat, ρc, vary in the same manner with temperature so that their ratio, the thermal diffusivity, remains constant. For the simple, special case of two-dimensional temperature distribution with both k and ρc varying linearly with temperature, the solution is

$$\theta = \frac{1}{\gamma}\left[\left(\frac{\gamma Q}{\pi k_o H} \cdot e^{-\lambda v \xi} \cdot K_o(\lambda v r) + (1+\gamma\theta_o)^2\right)^{1/2} - 1\right] \quad (2.6)$$

where

$$k = k_o \cdot (1+\gamma\theta)$$

$$\rho c = (\rho c)_o \cdot (1+\gamma\theta)$$

This linearity assumption can be valid in some aluminum alloys. For other materials k and ρc cannot be assumed to vary according to the same law, making the analytical treatment very complex.

Researchers at the Massachusetts Institute of Technology [24 - 26] adopted the iteration method to take into account the temperature dependence of material properties. The fundamental heat source solution with material properties at some temperature, say 300°C, provides the first approximate solution at a particular point. This temperature is compared with the initial guess and if the two temperatures disagree by more than 0.5°C, new properties are found for a temperature halfway inbetween. These new values are used to obtain a new temperature estimate. The process is repeated until covergence is reached. It should be pointed out that although this iteration method generally gives good predictions outside the fusion zone, there is no guarantee that it will converge to the correct solution since the approximation used may not satisfy the energy conservation law.

2.2 Heat Input Modeling

Most investigators agree that perhaps the most critical input required for the welding thermal analysis is the power, Q, that enters the plate or section being welded. It is customary to express this total heat input by the formula

$$Q = \eta_a \cdot V \cdot I \qquad (2.7)$$

where V and I are the arc voltage and current respectively, their product giving the electric arc power. The other

parameter in the above equation, η_a, is called arc efficiency; it represents the ratio of the power introduced by the arc into the metal to the total electric arc power. In other words it provides a semi-empirical way of taking into account the various heat losses that occur through electrode tip heating, radiation to the surrounding atmosphere, metal spatter, etc.

Arc efficiency, η_a, is heavily dependent on the welding process used, the penetration achieved, the shielding gas and many other factors that make it very difficult to predict. It is therefore measured experimentally using the so-called calorimetry method which consists of measuring the temperature rise of a water bath after immersion of a just welded metal specimen. Christensen and co-workers [20 - 21] made extensive measurements using this approach and found approximate ranges of the arc efficiency for various welding processes. Table 2.1 is a summary of the values proposed by Christensen. Included in the same table are also values proposed by Rykalin and co-workers [27 - 28].

Several other investigators have tried a different approach to the problem of estimating the arc efficiency. Among the latest efforts is that of Tsai [29] who tried to correlate the arc efficiency with the weld width in the case of thin plates. Dividing the conducting medium into a solid and liquid region, he derived an equation of the form:

$$Q = 2\pi k_{\ell} H \cdot f(d) \qquad (2.8)$$

TABLE 2.1 Values of Arc Efficiency for Various Processes

	Christensen	Rykalin	Tsai
GMAW	-	0.65-0.85	-
Mild Steel	0.66-0.70	-	0.80-0.90
Aluminum	0.70-0.85	-	-
SAW	0.90-0.99	0.90-0.99	0.85-0.98
SMAW	-	-	-
Mild Steel, ac	0.66-0.85	0.65-0.85	0.55-0.90
GTAW	-	-	-
Mild steel, ac	0.22-0.48	0.20-0.50	-
Mild steel, dc	0.36-0.46	0.45-0.75	-
Aluminum, ac	0.21-0.43	0.20-0.50	-

Nomenclature

GMAW = Gas Metal Arc Welding
SAW = Submerged Arc Welding
SMAW = Shielded Metal Arc Welding
GTAW = Gas Tungsten Arc Welding

Then, by experimentally measuring the weld width, d, he was able to calculate the total heat input, Q, and then estimate the arc efficiency using eqn. (2.7). His estimates are also shown in Table 2.1, the values being similar to those of the other investigators with the exception of GMAW where he predicts higher arc efficiencies.

Of equal importance to the magnitude of the total heat input is its distribution. At the solutions presented in Section 2.1 a point or line heat source was assumed. As Rykalin [28 - 30] and other investigators report, however, a more realistic approach is to assume a Gaussian radial heat flux distribution of the form (see Fig. 2.2)

$$q\ (r) = q_o \cdot e^{-Cr^2} \qquad (2.9)$$

where

q_o = maximum heat flux at the center of the heat spot, [W/cm^2]

C = heat flux concentration coefficient, [cm^{-2}]

r = radial distance from the center of the heat spot, [cm]

A stationary source with such a heat flux distribution may be called normal circular. The concentration coefficient C evaluates the source concentration: the higher C is, the more concentrated a heat source is and the smaller the diameter d_h of the heat spot is.

The distance $r_h = d_h/2$ can be defined for all practical

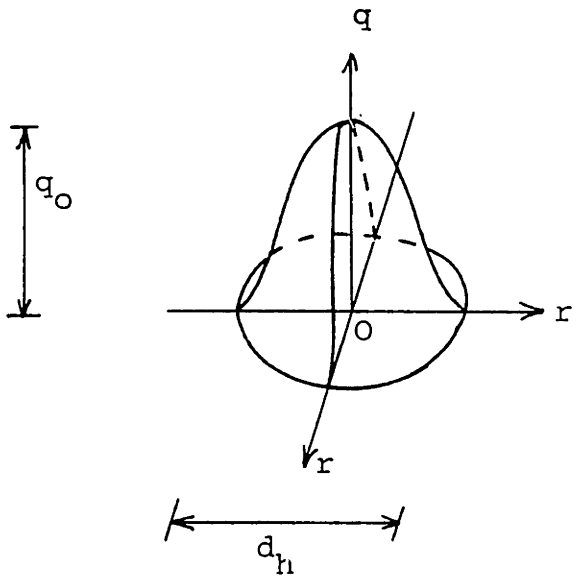

FIGURE 2.2 Distribution of Heat Flux Across the Hot Spot for a Normal Circular Source.

purposes as this at which the heat flux $q(r_h)$ falls to 0.05 of the maximum heat flux q_o. Then

$$q\ (r_h) = q_o \cdot e^{-Cr_h^2} = 0.05\ q_o$$

from which

$$e^{-Cr_h^2} = 0.05$$

or

$$Cr_h^2 = 3.0$$

The conventional diameter of the heat spot

$$d_h = 2\sqrt{3.0/C} = \frac{3.46}{\sqrt{C}} \qquad (2.10)$$

is thus inversly proportional to the square root of the concentration coefficient C, as previously mentioned.

Furthermore, if the total power absorbed by the workpiece, Q, is known, the distribution function, eqn. (2.9), may be integrated to give

$$Q = \int_0^\infty q(r) \cdot 2\pi r \cdot dr$$

$$= 2\pi q_o \int_0^\infty r \cdot e^{-Cr^2} dr$$

or

$$Q = \pi q_o/C \qquad (2.11a)$$

from which the maximum heat flux at the center of the heat spot can be calculated to be

$$q_o = \frac{CQ}{\pi} \tag{2.11b}$$

where Q is given by eqn. (2.7).

Experimental data on ranges of C for the various welding processes are shown in Table 2.2 after Rykalin and Nikolaev [28].

The above equations are valid for a stationary arc. High speed cinematography reveals, however, that during welding, when the arc is moving, the arc column is not radially symmetric but rather distorted backwards. This observation led Tsai [29] to propose the following equation for the arc heat distribution instead of eqn. (2.9):

$$q(r,\xi) = q_o \cdot e^{-Cr^2-\lambda v\xi} \tag{2.12}$$

where all the symbols have been previously defined.

Equation (2.12) can also be written in terms of a moving cylindrical coordinate system as

$$q(r,\psi) = q_o \cdot e^{-Cr^2-\lambda vr\cos\psi} \tag{2.13}$$

where $\xi = r.\cos\psi$.

This last expression, if calculated at a constant radial distance, r, from the center of the arc column, clearly represents the backward distortion of the arc heat distribu-

TABLE 2.2 Experimental Values for the Concentration Coefficient [28]

Welding Process	C, [cm^{-2}]	Polarity, Current
GMAW	1.26-1.32	ac, 550-1100A
SAW	1.00-2.50	ac, 550-1200A
SMAW	1.26-1.32	ac, 550-1100A
GTAW, steel	6.00-14.00	dcsp, 40-200A
Carbon electrode	1.00-3.50	dcsp, 95-2500A

tion: more heat enters the plate behind the arc ($\pi/2 < \psi < 3\pi/2$) than ahead of it ($0 < \psi < \pi/2$ and $3\pi/2 < \psi < 2\pi$). Futhermore, for the special case of the weld centerline ($y = 0$, $r = |\xi|$), the maximum arc heat flux can be found from eqn. (2.12) to be located at

$$\xi = -\frac{\lambda v}{2C}$$

i.e. behind the center of the arc, and to have a value equal to

$$q_{max} = q_o \cdot e^{\frac{(\lambda v)^2}{4C}}$$

i.e. greater than q_o.

The two unknowns, q_o and C, appearing in eqns. (2.12) and (2.13) can be found by employing two conditions. The first one uses the total heat input to the plate in a similar manner that produced eqn. (2.11a):

$$Q = 2q_o \int_o^{r_h} \int_o^{\pi} e^{-Cr^2-\lambda vr\cos\psi} \, rdrd\psi \qquad (2.14)$$

The second condition stems from the heat input model proposed by Apps and Milner [16]. According to them, the heat input from an argon arc, Q, can be expressed as the sum of the concentrated intense heat, Q_c, uniformly distributed in the cylindrical arc column of radius r_a, and the diffused heat, Q_d, dispersed around the arc column and over the heat spot due to radiation, convection, and conduction from the

arc column to the plate. The following formulae were proposed:

$$Q_c = a \cdot I \tag{2.15a}$$

$$Q_d = b \cdot l_{ac} \cdot I \tag{2.15b}$$

where l_{ac} is the arc length and a and b are constants. For an argon arc in air a/b was reported to be equal to 1.59.

Accepting this model, one can then write the following

$$\frac{Q_c}{Q_d} = \frac{\int_0^{r_a}\int_0^{\pi} e^{-Cr^2 - \lambda v r\cos\psi} \cdot r \cdot d\psi \cdot dr}{\int_0^{r_h}\int_0^{\pi} e^{-Cr^2 - \lambda v r\cos\psi} \cdot r \cdot d\psi \cdot dr - \int_0^{r_a}\int_0^{\pi} e^{-Cr^2 - \lambda v r\cos\psi} \cdot r \cdot d\psi \cdot dr}$$

$$= \frac{a}{b} \cdot \frac{1}{\ell_{ac}} \tag{2.16}$$

Equations (2.14) and (2.16), if solved numerically, give values of q_o and C if all other parameters are known. Figure 2.3 shows an example of the ensuing arc heat distribution assuming that a/b is 1.59cm and v is 9ipm (0.06 cm/sec). Given the fact, however, that several of the required parameters, e.g. a/b, ℓ_{ac}, r_a, are not generally known with accuracy, only eqn. (2.14) will be used in later calculations for the determination of q_o (see Appendix A); the concentration coefficient C will be estimated from eqn. (2.10).

2.3 Three-Dimensional Finite Heat Source Model

The discussion of the previous two sections leads to

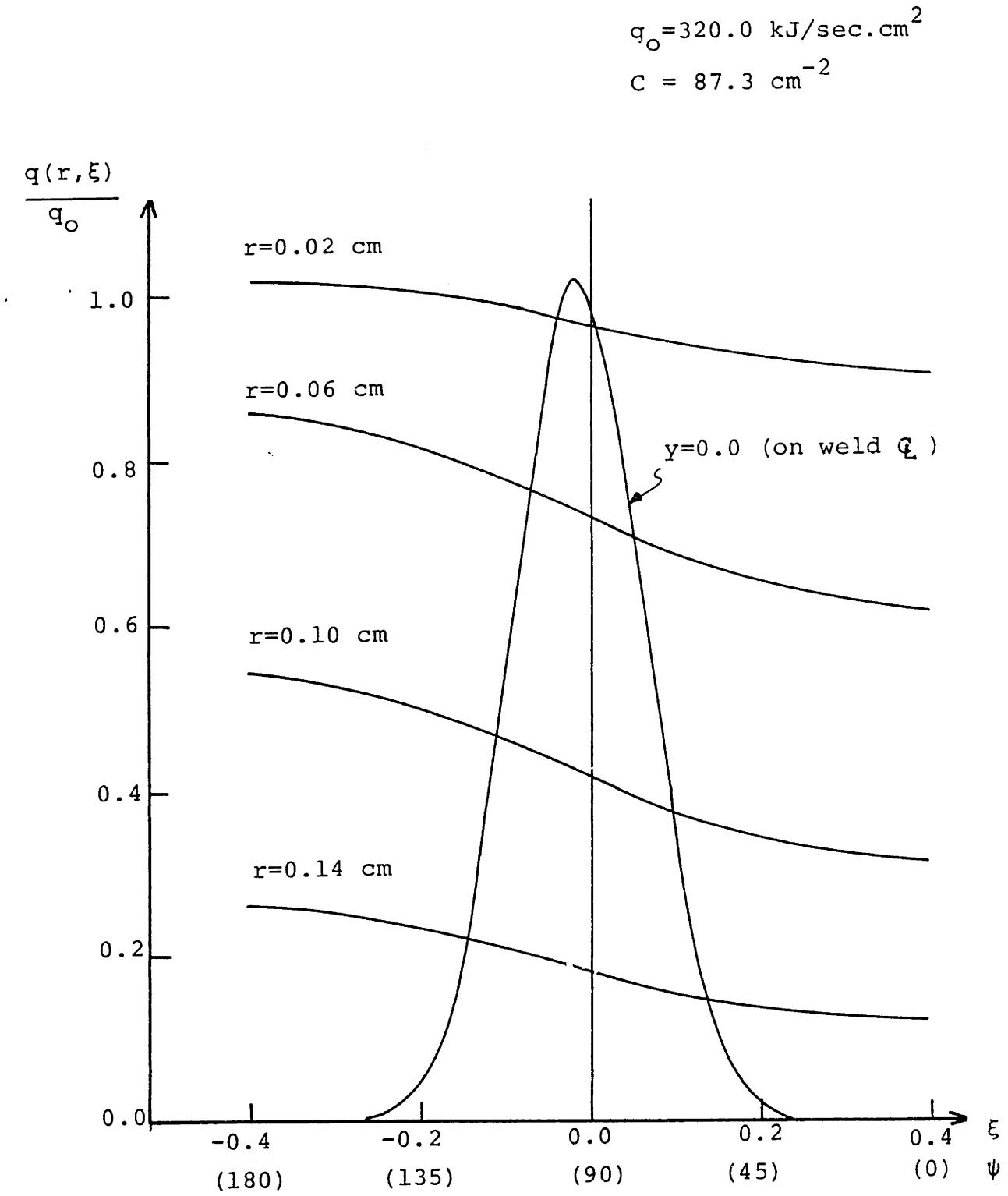

FIGURE 2.3 Arc Heat Distribution for a Moving Finite Heat Source.

the conclusion that in order to more accurately describe the temperature distribution and cooling rates in the region close to the weld more realistic assumptions should be employed. In this section a model will be developed under the following general assumptions:

1. Quasi-stationary state

2. The heat input will be provided by a moving three-dimensional skewed normally distributed heat source (eqn. 2.12), instead of a line or point source.

3. The thermal conductivity of the material will be assumed to be a linear function of temperature.

4. The thermal diffusivity of the material will be assumed to be constant.

5. Convective and radiation boundary heat losses will be taken into account through a constant average "effective" heat transfer coefficient.

6. Phase transformation and Joule heating effects will be neglected.

7. The initial temperature of the plate, θ_o, can be different from the environmental (ambient) temperature, θ_e, to allow for preheating.

2.3.1 Governing Equation

The governing equation of heat flow during welding is the partial differential equation (P.D.E.) of heat flow in a conducting medium [11, 31], namely

$$\frac{\partial}{\partial x}\left(k\frac{\partial\theta}{\partial x}\right)+\frac{\partial}{\partial y}\left(k\frac{\partial\theta}{\partial y}\right)+\frac{\partial}{\partial z}\left(k\frac{\partial\theta}{\partial z}\right)=\rho c\frac{\partial\theta}{\theta t}-W_i \qquad (2.17)$$

where W_i is the internal heat generation rate per unit volume and the other variables as previously defined.

Letting

$$T = \theta - \theta_o \tag{2.18}$$

where θ_o is the initial temperature, eqn. (2.18) can be written as

$$\frac{\partial}{\partial x}\left(k\,\frac{\partial T}{\partial x}\right) + \frac{\partial}{\partial y}\left(k\,\frac{\partial T}{\partial y}\right) + \frac{\partial}{\partial z}\left(k\,\frac{\partial T}{\partial z}\right) = \rho c\,\frac{\partial T}{\partial t} - W_i \tag{2.19}$$

Using the so-called Kirchhoff's transformation [31] the new variable u can be defined

$$u = \frac{1}{k_o}\int_o^T k(\eta)\,d\eta \tag{2.20}$$

where k_o is the value of thermal conductivity at $T = 0$ $(\theta = \theta_o)$, and $k(\eta)$ is the function describing the temperature dependence of the material thermal conductivity. Assuming that this function is linear

$$k(T) = k_o\,(1 + \gamma\,T) \tag{2.21a}$$

or

$$k(\theta) = k_o\,[1 + \gamma(\theta - \theta_o)] \tag{2.21b}$$

equation (2.20) can be solved to give

$$\theta = \theta_o + \frac{1}{\gamma} (\sqrt{1 + 2\gamma u} - 1) \tag{2.22}$$

Furthermore, noting that

$$\frac{\partial u}{\partial t} = \frac{k}{k_o} \cdot \frac{\partial T}{\partial t}$$

$$\vec{\nabla} u = \frac{k}{k_o} \vec{\nabla} T$$

eqn. (2.19) can be written as

$$\nabla^2 u = \frac{1}{\kappa} \cdot \frac{\partial u}{\partial t} - \frac{1}{k_o} \cdot W_i \tag{2.23}$$

where $\kappa = k/\rho c$ is the thermal diffusivity, assumed constant (recall that, as mentioned in section 2.1.3, this assumption is particularly valid for aluminum alloys) and ∇^2 is the Laplacian operator.

Equation (2.23) was derived with respect to a stationary Cartesian coordinate system (x,y,z). A coordinate system moving with the welding arc can now be defined through the transformation

$$\xi = x - vt, \quad y = y, \quad z = z$$

and noting that

$$\frac{\partial u}{\partial x} = \frac{\partial u}{\partial \xi} \cdot \frac{\partial \xi}{\partial x} = \frac{\partial u}{\partial \xi}$$

$$\left.\frac{\partial u}{\partial t}\right|_{SS} = \frac{\partial u}{\partial \xi} \cdot \frac{\partial \xi}{\partial t} + \left.\frac{\partial u}{\partial t}\right|_{MS} = - v \cdot \frac{\partial u}{\partial \xi} + \left.\frac{\partial u}{\partial t}\right|_{MS}$$

where SS denotes the stationary and MS the moving system, eqn. (2.23) can be written in the new system as

$$\frac{\partial^2 u}{\partial \xi^2} + \frac{\partial^2 u}{\partial y^2} + \frac{\partial^2 u}{\partial z^2} = -2\lambda v \frac{\partial u}{\partial \xi} + 2\lambda \left.\frac{\partial u}{\partial t}\right|_{MS} - \frac{1}{k_o} W_i \tag{2.24}$$

where $2\lambda = 1/\kappa$.

Given the fact that a solution in the quasi-stationary state is sought, the time dependence can be dropped; moreover, since it is assumed that no heat is generated internally, i.e. that both the Joule and transformation effects can be neglected, the last term of the above equation can also be dropped. Equation (2.24) therefore becomes

$$\frac{\partial^2 u}{\partial \xi^2} + \frac{\partial^2 u}{\partial y^2} + \frac{\partial^2 u}{\partial z^2} + 2\lambda v \frac{\partial u}{\partial \xi} = 0 \tag{2.25}$$

To further simplify this equation it is appropriate at this point to briefly mention a type of boundary conditions that will be fully investigated in the next section. The reference is to the heat losses from the plate's surfaces through natural convection and radiation which are expressed in equations having terms that include the quantity $(\theta-\theta_e)$, where θ_e is the environmental temperature. This temperature can be smaller or equal to the plate's initial temperature θ_o depending on whether a plate preheating operation has taken place or not respectively. It should be mentioned that it is important for the solution to be able to handle the preheating case since the operation is used extensively when welding high

strength quenched and tempered steels to prevent cracking and also as a measure to reduce distortion. Based on the considerations just described, a new variable is introduced by

$$\hat{u} = u + (\theta_o - \theta_e) \tag{2.26}$$

where the operation is legitimate since the variable u has, according to eqn. (2.20), the same dimensions as temperature. Note that eqn. (2.25) is then transformed into

$$\frac{\partial^2 \hat{u}}{\partial \xi^2} + \frac{\partial^2 \hat{u}}{\partial y^2} + \frac{\partial^2 \hat{u}}{\partial z^2} + 2\lambda v \cdot \frac{\partial \hat{u}}{\partial \xi} = 0 \tag{2.25a}$$

Furthermore, the simple solutions presented in section 2.1.1 and experimental data show that the temperature distribution, as viewed by an observer travelling with the welding arc, is steeper ahead of than behind the arc. This behavior can be simulated by invoking the function $\exp(-\lambda v \xi)$ through the following transformation

$$\hat{u} = e^{-\lambda v \xi} \cdot \phi(\xi, y, z) + (\theta_o - \theta_e) \tag{2.27a}$$

under which eqn. (2.25a) becomes

$$\frac{\partial^2 \phi}{\partial \xi^2} + \frac{\partial^2 \phi}{\partial y^2} + \frac{\partial^2 \phi}{\partial z^2} - (\lambda v)^2 \cdot \phi = 0 \tag{2.28a}$$

Using cylindrical coordinates (r, ψ, z) the last two equations can be written as

$$\hat{u} = e^{-\lambda v \xi} \cdot \phi(r, z) + (\theta_o - \theta_e) \tag{2.27b}$$

$$\frac{\partial^2 \phi}{\partial r^2} + \frac{1}{r} \cdot \frac{\partial \phi}{\partial r} + \frac{\partial^2 \phi}{\partial z^2} - (\lambda v)^2 \cdot \phi = 0 \tag{2.28b}$$

where $r^2 = \xi^2 + y^2$

$\xi = r.\cos\psi$

The angle dependence has been dropped from the function ϕ because of the symmetrical form of eqn. (2.28a) with respect to ξ and y and the circularity of the boundary conditions as it will become evident in the next section.

Equation (2.28b) is the final equation whose solution is sought.

2.3.2 Boundary Conditions

Let r_h be the radius of the heat input circle on the top surface of the plate, z = H (see Figure 2.4). The solution to equation (2.28b) will be divided into an inner solution $\phi^i(r,z)$ for $r \leq r_h$ and an outer solution $\phi^o(r,z)$ for $r \geq r_h$ which will be matched on the common boundary $r = r_h$. Boundary conditions will accordingly be divided.

First the boundary conditions will be expressed in the original variable θ as follows:

for $r \leq r_h$

$$k(\theta^i) \cdot \frac{\partial\theta^i}{\partial z} - \hat{h}_2 \cdot (\theta^i - \theta_e) = 0 \text{ at } z = 0, \text{ all } r \leq r_h \quad (2.29a)$$

$$-k(\theta^i) \cdot \frac{\partial\theta^i}{\partial z} + q_o \cdot e^{-Cr^2 - \lambda v\xi} - \hat{h}_1 \cdot (\theta^i - \theta_e) = 0 \text{ at } z = H, \text{ all } r \leq r_h \quad (2.29b)$$

$$\frac{\partial\theta^i}{\partial r} = 0 \qquad \text{at } r = 0, \text{ all } z \quad (2.29c)$$

for $r \geq r_h$

$$k(\theta^o) \cdot \frac{\partial\theta^o}{\partial z} - \hat{h}_2 \cdot (\theta^o - \theta_e) = 0 \quad \text{at } z = 0, \text{ all } r \geq r_h \quad (2.29d)$$

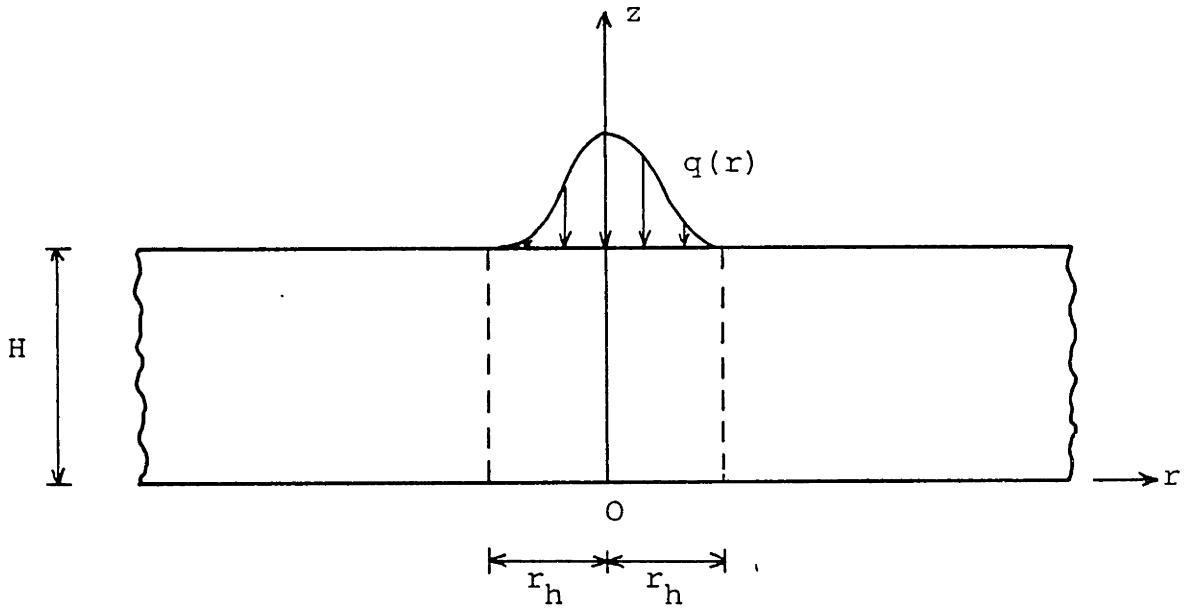

FIGURE 2.4 Schematic Representation of Geometry for Boundary Value Problem.

$$-k(\theta^o) \cdot \frac{\partial\theta^o}{\partial z} - \hat{h}_1 \cdot (\theta^o - \theta_e) = 0 \qquad \text{at } z = H, \text{ all } r \geq r_h \tag{2.29e}$$

$$\theta^o \to \theta_o \qquad \text{as } r \to \infty, \text{ all } z \tag{2.29f}$$

for $r = r_h$

$$\theta^i = \theta^o \qquad \text{at } r = r_h, \text{ all } z \tag{2.29g}$$

$$\frac{\partial\theta^i}{\partial r} = \frac{\partial\theta^o}{\partial r} \qquad \text{at } r = r_h, \text{ all } z \tag{2.29h}$$

where $\hat{h}_1$ and $\hat{h}_2$ are the heat transfer coefficients at the top and bottom surfaces of the plate that take into account the heat losses to the surrounding atmosphere through convection and radiation. They are defined as:

$$\hat{h} = h_c + \sigma \cdot \varepsilon \cdot A \cdot (\theta^2 + \theta_e^2) \cdot (\theta + \theta_e) \tag{2.30}$$

where h_c = temperature dependent convection coefficient

σ = Stefan-Boltzman constant

ε = emmisivity of the surface

A = shape function

θ_e = environmental (ambient) temperature

The boundary conditions as expressed above are non-linear, owing to the temperature dependence of the coefficients k, $\hat{h}_1$, and $\hat{h}_2$. As a first step towards linearizing them the assumption will be made that the heat transfer coefficients $\hat{h}_1$ and $\hat{h}_2$ are constant and equal to an average value over the temperature history of the plate; these average values will be denoted h_1 and h_2. As a second step use will have to be made of equations (2.18), (2.20), (2.26), and (2.27) to transform the boundary conditions to ones having the variable ϕ and to

linearize them wherever necessary. As an example of this process eqn. (2.29a) will be worked on.

Using transformation (2.18), eqn. (2.29a) can be written

$$k(T^i) \cdot \frac{\partial T^i}{\partial z} - h_2 \cdot [T^i + (\theta_o - \theta_e)] = 0 \qquad (2.31)$$

From the Kirchhoff transformation (2.20) and noting that $\partial T/\partial z = (k_o/k) \cdot \partial u/\partial z$, eqn. (2.31) can be further written

$$k(T^i) \cdot \frac{k_o}{k(T^i)} \cdot \frac{\partial u^i}{\partial z} - h_2 \cdot [T^i(u) + (\theta_o - \theta_e)] = 0$$

or

$$k_o \cdot \frac{\partial u^i}{\partial z} - h_2 \cdot [T^i(u) + (\theta_o - \theta_e)] = 0 \qquad (2.32)$$

To find an approximation for $T^i(u)$, $k(\eta)$ is expanded in a Taylor series around 0

$$k(\eta) = k(0) + k'(0) \cdot \eta + k''(0) \cdot \frac{\eta^2}{2} + O(\eta^3)$$

or

$$k(\eta) = k_o + \eta \cdot k'(0) + \frac{1}{2} \cdot \eta^2 \cdot k''(0) + O(\eta^3)$$

and substituted into eqn. (2.20) to give

$$u = T + \frac{k'(0)}{2k_o} \cdot T^2 + \frac{k''(0)}{6k_o} \cdot T^3 + O(T^4)$$

Thus, to a first approximation

$$u = T + O(T^2)$$

or

$$u \simeq T$$

Eqn. (2.32) can then be written to a first approximation:

$$k_o \cdot \frac{\partial u^i}{\partial z} - h_2 \cdot [u^i + (\theta_o - \theta_e)] = 0 \qquad (2.33)$$

Finally, invoking eqns. (2.26) and (2.27b), the above expression becomes

$$\frac{\partial \phi^i}{\partial z} = \frac{h_2}{k_o} \cdot \phi^i \quad , \quad z = 0,\ r < r_h \qquad (2.34a)$$

Working similarly on the other boundary conditions the following equations were derived:

$$\frac{\partial \phi^i}{\partial z} = \frac{q_o}{k_o} \cdot e^{-Cr^2} - \frac{h_1}{k_o} \cdot \phi^i,\ z = H,\ r < r_h \qquad (2.34b)$$

$$\frac{\partial \phi^i}{\partial r} = 0 \ , \qquad r = 0,\ \text{all } z \qquad (2.34c)$$

$$\frac{\partial \phi^o}{\partial z} = \frac{h_2}{k_o} \cdot \phi^o \ , \qquad z = 0,\ r > r_h \qquad (2.34d)$$

$$\frac{\partial \phi^o}{\partial z} = -\frac{h_1}{k_o} \cdot \phi^o \qquad z = H,\ r > r_h \qquad (2.34e)$$

$$\phi^o \to 0 \ , \qquad r \to \infty,\ \text{all } z \qquad (2.34f)$$

$$\phi^o = \phi^i \ , \qquad r = r_h\ ,\ \text{all } z \qquad (2.34g)$$

$$\frac{\partial \phi^o}{\partial r} = \frac{\partial \phi^i}{\partial r} \ , \qquad r = r_h\ ,\ \text{all } z \qquad (2.34h)$$

2.3.3 Solution

The governing equation (2.28b) will be solved using the method of separation of variables [32]. Let

$$\phi(r,z) = R(r) \ . \ Z(z) \qquad (2.35)$$

Substituting the above equation into eqn. (2.28b) and regrouping the similar terms, the following two ordinary differential equations can be derived:

$$\frac{1}{R(r)} \cdot [R''(r) + \frac{1}{r} \cdot R'(r)] - (\lambda v)^2 = \pm \omega^2 \tag{2.36}$$

$$- \frac{1}{Z(z)} \cdot Z''(z) = \pm \omega^2 \tag{2.37}$$

where the sign of ω^2 will be chosen such that the boundary-value problem of the homogeneous direction leads to a characteristic-value problem [33]. Constant ω will be determined by the boundary conditions.

A. <u>Outer solution</u>. For the outer solution, $r \geq r_h$, the above equations become

$$R^{o''}(r) + \frac{1}{r} \cdot R^{o'}(r) - [\omega^2 + (\lambda v)^2] \cdot R^o(r) = 0 \tag{2.38a}$$

$$Z^{o''}(z) + \omega^2 \cdot Z^o(z) = 0 \tag{2.38b}$$

and the boundary conditions (2.34d) - (2.34f)

$$Z^{o'}(0) - \frac{h_2}{k_o} \cdot Z^o(0) = 0 \tag{2.39a}$$

$$Z^{o'}(H) + \frac{h_1}{k_o} \cdot Z^o(H) = 0 \tag{2.39b}$$

$$R^o(r) \to 0 \quad \text{as } r \to \infty \tag{2.39c}$$

Note that $+\omega^2$ was selected so that the orthogonal trigonometric functions will be the characteristic functions of the homogeneous z-direction; $-\omega^2$ would have resulted in hyperbolic functions which are not orthogonal.

Letting

$$\xi^2 = \omega^2 + (\lambda v)^2 \tag{2.40}$$

the general solutions to eqns. (2.38) can be written as

$$R^o(r) = A_1 \cdot I_o(\zeta \cdot r) + A_2 \cdot K_o(\zeta \cdot r) \tag{2.41a}$$

$$Z^o(z) = B_1 \cdot \sin(\omega \cdot z) + B_2 \cdot \cos(\omega \cdot z) \tag{2.41b}$$

where A_1, A_2, B_1, B_2 are arbitrary constants and $I_o(x)$ and $K_o(x)$ are the modified Bessel functions of the first and second kind respectively and of zero order.

Invoking eqn. (2.39c) it can be found that $A_1 = 0$. Furthermore, using boundary conditions (2.39a) and (2.39b), eqn. (2.41b) gives

$$(k_o \cdot \omega) \cdot B_1 - h_2 \cdot B_2 = 0 \tag{2.42a}$$

and

$$\left[\frac{h_1}{k_o} \cdot \sin(\omega H) + \omega \cdot \cos(\omega H)\right] \cdot B_1 + \left[\frac{h_1}{k_o} \cdot \cos(\omega H) - \omega \cdot \sin(\omega H)\right] \cdot B_2 = 0 \tag{2.42b}$$

respecitvely. To get nontrivial solutions for B_1 and B_2, the determinant of the above homogeneous system of equations should vanish, providing an equation for the characteristic values ω_n, $n = 0,1,2...$ of the z-direction solution

$$(k_o^2 \cdot \omega_n^2 - h_1 \cdot h_2) \cdot \tan(\omega_n H) = k_o \cdot \omega_n \cdot (h_1 + h_2) \tag{2.43}$$

For the case of adiabatic boundary conditions ($h_1 = h_2 = 0$), the characteristic values will be given by

$$\omega_n = \frac{n\pi}{H}, \qquad n = 0,1,2,... \tag{2.43a}$$

Note that both eqns. (2.43) and (2.43a) give $\omega_o = 0$. The question thus arises whether this characteristic value is acceptable in one and/or both cases. To resolve it, use will be made of energy considerations and in particular of the heat that flows out of a cylindrical surface with radius r, $r \geq r_h$,

$$Q(r) = 2\int_0^H\int_0^\pi - k.\frac{\partial\theta}{\partial r}.r.d\psi.dz$$

which, by making the appropriate substitutions, can be written as

$$Q(r) = -2.k_o.\int_0^H\int_0^\pi e^{-\lambda vr.\cos\psi}.R^{o'}(r).Z^o(z).r.d\psi.dz \tag{2.44}$$

or

$$Q(r) = -2.k_o.r.R^{o'}(r).I.P \tag{2.45}$$

where

$$I = \int_0^H Z^o(z).dz \tag{2.46}$$

$$P = \int_0^\pi e^{-\lambda vr.\cos\psi}.d\psi \tag{2.47}$$

Interest here will be focused on I which, using eqn. (2.38b), integrating by parts and then using eqns. (2.39a), (2.39b), and (2.41b), may be written as

$$I=\frac{1}{k_o\omega^2}\cdot[h_2\cdot B_2+h_1\cdot B_1\cdot\sin(\omega H)+h_1\cdot B_2\cdot\cos(\omega H)]$$

or, making the appropriate substitution from eqns. (2.42),

$$I=B_1\cdot H\cdot\frac{1-\cos(\omega H)}{\omega H}+B_2\cdot H\cdot\frac{\sin(\omega H)}{\omega H} \tag{2.48}$$

For the general case of non-adiabatic boundary conditions, $h_1\cdot h_2 \neq 0$, the constant B_2 can be expressed from eqn. (2.42a) as

$$B_2=\frac{k_o\omega}{h_2}\cdot B_1$$

Equation (2.48) then gives

$$I=B_1\cdot H\cdot\left[\frac{1-\cos(\omega H)}{\omega H}+\frac{k_o\cdot\omega}{h_2}\cdot\frac{\sin(\omega H)}{\omega H}\right] \tag{2.49a}$$

so that $I = 0$ when $\omega = 0$ for finite B_1. In other words, the characteristic value $\omega_o = 0$ and its associated characteristic function do not contribute to the transfer of energy and can thus be neglected. As a consequence, the characteristic functions can be written from eqns. (2.41b) and (2.42a) as

$$\frac{h_2}{k_o\cdot\omega_n}\cdot\sin(\omega_n z)+\cos(\omega_n z),\quad n=1,2,3,\ldots$$

The outer solution is thus expressed as

$$\phi^o(r,z)=\sum_{n=1}^{\infty}C_n\cdot K_o(\zeta_n r)\cdot\left[\frac{h_2}{k_o\cdot\omega_n}\cdot\sin(\omega_n z)+\cos(\omega_n z)\right] \tag{2.50}$$

where $C_n = A_{2n}\cdot B_{2n}$, $n = 1,2,3,\ldots$

For the case of adiabatic boundary conditions, $h_1 = h_2 = 0$, eqn. (2.42a) gives $B_1 = 0$ so that eqn. (2.48)

can be written as

$$I = B_2 H \cdot \frac{\sin(\omega H)}{\omega H} \tag{2.49b}$$

When $\omega = 0$ the integral I is B_2H, that is finite and nonzero, making it necessary to include the zero characteristic value in the solution. The characteristic functions now are $\cos(n\pi z/H)$, $n = 0,1,2,\ldots$ and the outer solution can be expressed as

$$\phi^o(r,z) = C_o \cdot K_o(\lambda v r) + \sum_{n=1}^{\infty} C_n \cdot K_o(\zeta_n \cdot r) \cdot \cos\left(\frac{n\pi z}{H}\right) \tag{2.50a}$$

where again $C_n = A_{2n} \cdot B_{2n}$, $n = 1,2,3,\ldots$ To find the constant C_o, eqn. (2.45) will be applied at $r = r_h$. Since there are no heat losses from the surface $Q(r_h) = Q$, so after some algebra

$$C_o = \frac{Q}{2 \cdot k_o \cdot \lambda v \cdot r_h \cdot H \cdot K_1(\lambda v r_h) \cdot P} \tag{2.51}$$

where Q is the total heat input, $K_1(x)$ is the modified Bessel function of second kind and order one, and P is given by eqn. (2.47). The other constants C_n, $n = 1,2,3,\ldots$ will be found from the ones of the non-adiabatic solution by setting $h_1 = h_2 = 0$.

The situation previously described can be intuitively explained as follows. In the adiabatic case, and concentrating on the "frequency domain", one sees that the zeros of the energy integral I, eqn. (2.49b), are also the characteristic values ω_n, $n= 1,2,3,\ldots$ So each time the terms of the series

expansion of the solution attempt to make a contribution to the energy integral they become zero, the only exception being the first term where $\omega_o = 0$ is not a zero of I. In other words the dominant term of the outer solution is the first one with the others playing a modulation role. This could be expected due to the simplicity of the adiabatic boundary conditions.

On the other hand in the general case, $h_1 \cdot h_2 \neq 0$, the zeros of the energy integral I, eqn. (2.49a), are different from the characteristic values ω_n, n= 1,2,3,... given by eqn. (2.43). All terms of the series expansion of the outer solution contribute therefore to the energy flown through the cylindrical surface, making the solution more complicated, as expected.

B. <u>Inner solution</u>. For the inner domain one observs that there are two homogeneous and two non-homogeneous boundary conditions, the latter ones at $r = r_h$ and $z = H$, so that the method of separation of variables cannot be applied. Fortunately, however, the fact that the problem is linear allows the application of the superposition principal, leading to the separation of the inner solution into two parts (see Fig. 2.5),

$$\phi^i(r,z) = \phi_I^i(r,z) + \phi_{II}^i(r,z) \tag{2.52}$$

each one having only one non-homogeneous boundary condition.

B1. In part I the homogeneous direction is the r-direction. The $-\omega^2$ constant is thus chosen in eqns. (2.36) and (2.37) in order to get the orthogonal Bessel functions as

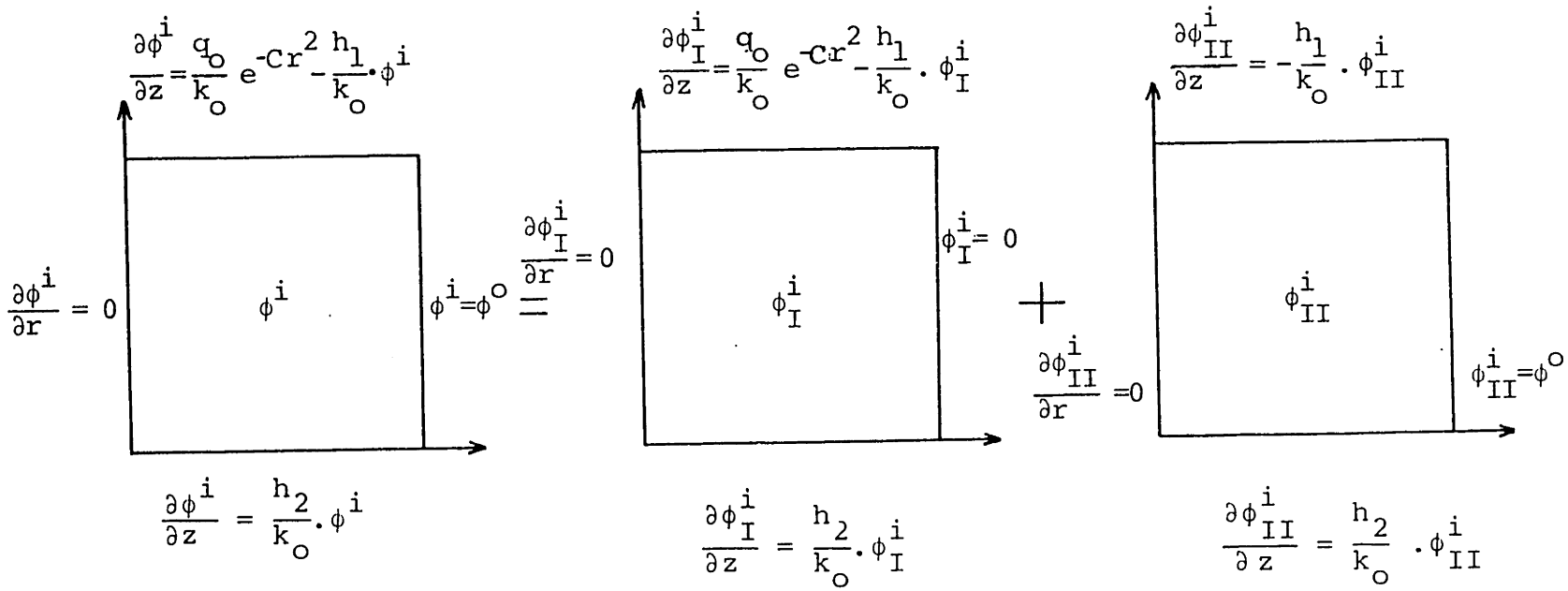

FIGURE 2.5 Superposition Used for Inner Solution.

the characteristic functions for the r-equation. The governing equations thus are

$$R_I^{i''}(r) + \frac{1}{r} \cdot R_I^{i'}(r) + \delta^2 \cdot R_I^{i}(r) = 0 \tag{2.53a}$$

$$Z_I^{i''}(z) - \chi^2 \cdot Z_I^{i}(z) = 0 \tag{2.53b}$$

where χ stands for the constant ω in eqns. (2.36) and (2.37) and

$$\delta^2 = \chi^2 - (\lambda v)^2 \tag{2.54}$$

The boundary conditions, according to eqns. (2.34a) - (2.34c) and Fig. 2.5, can be expressed as

$$R_I^{i'}(0) = 0 \tag{2.55a}$$

$$R_I^{i}(r_h) = 0 \tag{2.55b}$$

$$Z_I^{i'}(0) - \frac{h_2}{k_o} \cdot Z_I^{i}(0) = 0 \tag{2.55c}$$

The general solutions of eqns. (2.53) can then be written as

$$R_I^{i}(r) = A_1' \cdot J_o(\delta_n r) + A_2' \cdot Y_o(\delta_n r) \tag{2.56a}$$

$$Z_I^{i}(r) = B_1' \cdot \sinh(\chi_n z) + B_2' \cdot \cosh(\chi_n z) \tag{2.56b}$$

where A_1', A_2', B_1', B_2' are arbitrary constants (the primes do not denote differentiation) and $J_o(x)$ and $Y_o(x)$ are the Bessel functions of first and second kind respectively and of zero order.

By differentiating eqn. (2.56a) and using condition (2.55a) it can be found that $A_2' = 0$. Moreover, using condition

(2.55b), eqn. (2.56a) gives

$$J_o(\delta_n . r_h) = 0, \quad n=1,2,3,.. \tag{2.57}$$

i.e. the characteristic values (eigenvalues) δ_n can be found from the zeros of $J_o(x)$. Finally, the use of boundary condition (2.55c) in conjunction with eqn. (2.56b) results in the following relation between constants B_1' and B_2'

$$B_1' = \frac{h_2}{\chi . k_o} . B_2' \tag{2.58}$$

The first part of the inner solution can now be written as

$$\phi_I^i(r,z) = \sum_{n=1}^{\infty} D_n . J_o(\delta_n r) . \left[\frac{h_2}{\chi_n . k_o} . \sinh(\chi_n z) + \cosh(\chi_n z)\right] \tag{2.59}$$

To find constants D_n the fourth boundary condition of the first part of the inner solution

$$\frac{\partial \phi_I^i(r,H)}{\partial z} = \frac{q_o}{k_o} . e^{-Cr^2} - \frac{h_1}{k_o} . \phi_I^i(r,H) \tag{2.60}$$

will be invoked (see Fig. 2.5), to give

$$\sum_{n=1}^{\infty} D_n . J_o(\delta_n r) . \chi_n . \left[\frac{h_2}{\chi_n . k_o} . \cosh(\chi_n H) + \sinh(\chi_n H)\right]$$

$$= \frac{q_o}{k_o} . e^{-Cr^2} - \frac{h_1}{k_o} . \sum_{n=1}^{\infty} D_n . J_o(\delta_n r) . \left[\frac{h_2}{\chi_n . k_o} . \sinh(\chi_n H) + \cosh(\chi_n H)\right] \tag{2.61}$$

Multiplying both sides of the above equation by $r.J_o(\delta_m r)$, integrating from 0 to r_h, and utilizing the following orthogonality property of Bessel functions

$$\int_0^{r_h} r.J_o(\delta_n r) \;.\; J_o(\delta_m r)\,dr = 0 \qquad \text{if } \delta_m \neq \delta_n$$

$$= \frac{r_h^2}{2}.J_1^2(\delta_n r_h) \quad \text{if } \delta_m = \delta_n$$

where $J_1(x)$ is the Bessel function of first kind and order one, the constant D_n can be found as

$$D_n = \frac{2.q_o.K_n}{k_o.J_1^2(\delta_n r_h).\left[\left(\frac{h_1+h_2}{k_o}\right).\cosh(\chi_n H)+\left(\chi_n+\frac{h_1 h_2}{\chi_n.k_o^2}\right).\sinh(\chi_n H)\right]} \tag{2.62}$$

where

$$K_n = \int_0^1 x.e^{-C.r_h^2.x^2} \;.\; J_o(\delta_n.r_h.x) \;.\; dx \tag{2.63}$$

The first part of the inner solution is therefore

$$\phi_I^i(r,z) = \sum_{n=1}^{\infty} \frac{2.q_o.K_n.J_o(\delta_n r).[h_2.\sinh(\chi_n z)+k_o.\chi_n.\cosh(\chi_n z)]}{J_1^2(\delta_n r_h).[k_o\chi_n.(h_1+h_2).\cosh(\chi_n H)+(k_o^2\chi_n^2+h_1 h_2).\sinh(\chi_n H)]} \tag{2.64}$$

Note, that in the case of adiabatic boundary conditions ($h_1 = h_2 = 0$) the above solution becomes

$$\phi_I^i(r,z) = \sum_{n=1}^{\infty} \frac{2.q_o.K_n.J_o(\delta_n r).\cosh(\chi_n z)}{k_o.\chi_n.J_1^2(\delta_n r_h).\sinh(\chi_n H)} \tag{2.64a}$$

B2. For part II of the inner solution note that the boundary conditions in the z-direction are similar to those of the outer solution. The general solutions should thus be similar to eqns. (2.41), namely

$$R_{II}^i(r) = A_1'' \;.\; I_o(\bar{\zeta}.r) + A_2'' \;.\; K_o(\bar{\zeta}.r) \tag{2.65a}$$

$$Z^{i}_{II}(z) = B''_1 \cdot \sin(\bar{\omega}.z) + B''_2 \cdot \cos(\bar{\omega}.z) \tag{2.65b}$$

where A''_1, A''_2, B''_1, B''_2, and $\bar{\omega}$ are constants to be determined and

$$\bar{\zeta}^2 = \bar{\omega}^2 + (\lambda v)^2 \tag{2.66}$$

The boundary conditions can be expressed, according to Fig. 2.5, as

$$R^{i'}_{II}(0) = 0 \tag{2.67a}$$

$$Z^{i'}_{II}(0) - \frac{h_2}{k_o} \cdot Z^{i}_{II}(0) = 0 \tag{2.67b}$$

$$Z^{i'}_{II}(H) + \frac{h_1}{k_o} \cdot Z^{i}_{II}(H) = 0 \tag{2.67c}$$

Condition (2.67a) demands that $A''_2 = 0$. Furthermore, using the other two boundary conditions and following an approach similar to the one for the outer solution it can be found that

$$B''_1 = \frac{h_2}{\bar{\omega}.k_o} \cdot B''_2 \tag{2.68}$$

and

$$\tan(\bar{\omega}_n.H) = \frac{k_o.\bar{\omega}_n.(h_1+h_2)}{k_o^2.\bar{\omega}_n^2 - h_1.h_2}, \quad n = 1,2,3,... \tag{2.69}$$

Comparing the above equation with eqn. (2.43) it can be concluded that

$$\bar{\omega}_n = \omega_n, \quad n = 1,2,3,... \tag{2.70}$$

and thus $\bar{\zeta}_n = \zeta_n$, $n = 1,2,3,...$

One can therefore obtain the second part of the inner solution in the following series form

$$\phi^{i}_{II}(r,z) = \sum_{n=1}^{\infty} E_n . I_o(\zeta_n r) . \left[\frac{h_2}{\omega_n . k_o} . \sin(\omega_n z) + \cos(\omega_n z)\right] \tag{2.71}$$

or, for the case of adiabatic boundary conditions ($h_1 = h_2 = 0$)

$$\phi^{i}_{II}(r,z) = E_o . I_o(\lambda v r) + \sum_{n=1}^{\infty} E_n . I_o(\zeta_n r) . \cos\left(\frac{n\pi z}{H}\right) \tag{2.71a}$$

C. Matching region. To complete the solution, that is to find the constants C_n and E_n, the boundary conditions at the interface $r = r_h$ will have to be invoked.

The first condition, stating that the inner and outer solutions should match on the interface, can be expressed according to Fig. 2.5 as

$$\phi^{o}(r_h, z) = \phi^{i}_{II}(r_h, z) \tag{2.72a}$$

or, using eqns. (2.50) and (2.71),

$$\sum_{n=1}^{\infty} C_n . K_o(\zeta_n r_h) \cdot \left[\frac{h_2}{\omega_n . k_o} \cdot \sin(\omega_n z) + \cos(\omega_n z)\right]$$

$$= \sum_{n=1}^{\infty} E_n . I_o(\zeta_n r_h) \cdot \left[\frac{h_2}{\omega_n . k_o} \cdot \sin(\omega_n z) + \cos(\omega_n z)\right] \tag{2.72b}$$

Since the above equation must hold for all z, it is concluded that

$$E_n = \frac{K_o(\zeta_n r_h)}{I_o(\zeta_n r_h)} \cdot C_n \ , \quad n = 1,2,3,... \tag{2.73}$$

Based on the above and eqns. (2.52), (2.64), and (2.71) the complete inner solution can now be written as

$$\phi^{i}(r,z)=\sum_{n=1}^{\infty}\left[\frac{2.q_o.K_n.J_o(\delta_n r).[h_2.\sinh(\chi_n z)+k_o.\chi_n.\cosh(\chi_n z)]}{J_1^2(\delta_n r_h).[k_o\chi_n(h_1+h_2).\cosh(\chi_n H)+(k_o^2\chi_n^2+h_1h_2).\sinh(\chi_n H)}\right.$$

$$\left.+\,C_n.K_o(\zeta_n r_h).\frac{I_o(\zeta_n r)}{I_o(\zeta_n r_h)}.\left[\frac{h_2}{\omega_n.k_o}.\sin(\omega_n z)+\cos(\omega_n z)\right]\right] \qquad (2.74)$$

For the case of adiabatic boundary conditions ($h_1 = h_2 = 0$) the inner solution can be similarly written

$$\phi_i(r,z) = \frac{Q}{2.k_o.\lambda v.r_h.H.P}\cdot\frac{K_o(\lambda v r_h)}{K_1(\lambda v r_h)}\cdot\frac{I_o(\lambda v r)}{I_o(\lambda v r_h)}$$

$$+\sum_{n=1}^{\infty}\left[\frac{2.q_o.K_n.J_o(\delta_n r).\cosh(\chi_n z)}{k_o.\chi_n.J_1^2(\delta_n r_h).\sinh(\chi_n H)}+C_n.K_o(\zeta_n r_h).\frac{I_o(\zeta_n r)}{I_o(\zeta_n r_n)}.\cos(\omega_n z)\right] \qquad (2.74a)$$

The second condition at the interface states that

$$\frac{\partial\phi^{o}(r_h,z)}{\partial r}=\frac{\partial\phi^{i}(r_h,z)}{\partial r} \qquad (2.75)$$

Substituting the outer and inner solutions from eqns. (2.50) and (2.74) respectively and using the orthogonality conditions

$$\int_0^H\left[\frac{h_2}{\omega_n.k_o}.\sin(\omega_n z)+\cos(\omega_n z)\right]\cdot\left[\frac{h_2}{\omega_m.k_o}.\sin(\omega_m z)+\cos(\omega_m z)\right]dz=0$$

for $\omega_n \neq \omega_m$, and

$$\int_0^H\left[\frac{h_2}{\omega_n.k_o}.\sin(\omega_n z)+\cos(\omega_n z)\right]^2 dz=\frac{H}{2}\left(1+\frac{h_2^2}{\omega_n^2.k_o}\right)$$

$$+\frac{1}{4\omega_n}\left(1-\frac{h_2^2}{\omega_n^2.k_o^2}\right).\sin(2\omega_n H)+\frac{h_2}{\omega_n^2.k_o}.\sin^2(\omega_n H)$$

one can find the following expression for the constants C_n

$$C_n=\frac{1}{a_n}.\sum_{m=1}^{\infty}\frac{2.q_o.K_m.\delta_m.[r_{mn}.\tanh(\chi_m H)+s_{mn}]}{(\chi_m^2+\omega_n^2).(J_1(\delta_m r_h).[d_m+e_m.\tanh(\chi_m H)]}\ ,\ n=1,2,3,\ldots \qquad (2.76)$$

where

$$a_n = b_n \cdot c_n \qquad (2.77a)$$

$$b_n = \zeta_n \cdot \left[K_1(\zeta_n r_h) + K_o(\zeta_n r_h) \cdot \frac{I_1(\zeta_n r_h)}{I_o(\zeta_n r_h)}\right] \qquad (2.77b)$$

$$c_n = \frac{H}{2}.\left(1+\frac{h_2^2}{\omega_n^2.k_o^2}\right)+\frac{1}{4\omega_n}.\left(1-\frac{h_2^2}{\omega_n^2.k_o^2}\right).\sin(2\omega_n H)+\frac{h_2}{\omega_n^2.k_o}.\sin^2(\omega_n H) \qquad (2.77c)$$

$$d_m = k_o \cdot \chi_m \cdot (h_1 + h_2) \qquad (2.77d)$$

$$e_m = k_o^2 \cdot \chi_m^2 + h_1 \cdot h_2 \qquad (2.77e)$$

$$r_{mn} = h_2.\left(\omega_n+\frac{\chi_m^2}{\omega_n}\right).\sin(\omega_n H)+\left(k_o\chi_m^2-\frac{h_2^2}{k_o}\right).\cos(\omega_n H) \qquad (2.77f)$$

$$s_{mn} = \chi_m \cdot \left(k_o.\omega_n+\frac{h_2^2}{k_o.\omega_n}\right).\sin(\omega_n H) \qquad (2.77g)$$

In the case of adiabatic boundary conditions ($h_1 = h_2 = 0$), the constants C_n, $n = 1,2,3,\ldots$ are given by

$$C_n = (-1)^n \cdot \frac{4q_o}{k_o.H.b_n} \cdot \sum_{m=1}^{\infty}\frac{K_m.\delta_m}{(\chi_m^2+\omega_n^2).J_1(\delta_m r_h)} \qquad (2.76b)$$

The final solution can be written as

$$\theta = \theta_o + \frac{1}{\gamma} \cdot \left(\sqrt{1+2\gamma.e^{-\lambda v\xi}.\phi(r,z)} - 1\right) \tag{2.78}$$

where

$$\phi(r,z) = \phi^i(r,z) \cdot [u_{-1}(r)-u_{-1}(r-r_h] + \phi^o(r,z) \cdot u_{-1}(r-r_h) \tag{2.79}$$

with $u_{-1}(r-a)$ being the unit step function and $\phi^i(r,z)$, $\phi^o(r,z)$ being given by eqns. (2.50) and (2.74). All other variables have been previously defined.

A computer program has been written in the FORTRAN IV language to perform the necessary calculations. Appendix A provides some details of the program.

2.4 Parametric Investigation

The computer program developed for the three-dimensional finite heat source solution discussed in the previous section was used to perform a parametric investigation in an effort to study the effects the arc efficiency, η_a, the concentration coefficient, C, and the average heat loss coefficient, h, have on the predicted temperature distribution.

As a case study, the laying of a bead on the top surface of a 1 in (25.4 mm) thick HY-130 plate using the GMA welding process was chosen. The plate measured 24in x 24in (610mm x 610mm) so that the quasi-stationary state could be assumed to hold in the mid-length region of the weld. Two arc efficiencies, 0.50 and 0.60, were assumed. For the concentration coefficient C the values of 39.50 and 8.2 in^{-2} (6.12 and 1.28

cm^{-2}) were investigated corresponding to a heat spot radius r_h of 0.275 and 0.600 in (7. and 15.2 mm) respectively. The average heat loss coefficient for both surfaces ranged from 0. to 0.0006 Btu/sec.in^2.^{o}F corresponding to adiabatic boundary conditions and to heat losses at high temperatures respectively. Finally the cases of constant thermal conductivity (γ=0.) and of linearly varying thermal conductivity (γ=0.0001) were examined, the latter value being computed from data for the HY-130 steel (see Section 3.3.1) using least squares approximation.

The effect of heat losses from the surface at a point 0.5 in (12.7 mm) from the weld centerline is shown in Figure 2.6. As expected, the adiabatic case exhibits unreasonably high temperatures and slower cooling rate than the ones for finite heat losses. In Figure 2.7 the case of variable versus constant thermal conductivity is depicted. At lower temperatures the difference between the two assumptions is not great, whereas at higher temperatures the variable k case tends to predict somewhat lower temperatures.

Figures 2.8 through 2.11 show the temperature distribution at 1, 0.75, 0.50, and 0.284 in (25.4, 19.1, 12.7, and 7.2 mm) from the weld centerline for η_a = 0.60 and various values of C, γ, and h. It is observed that the smaller concentration coefficient (larger heat spot radius) predicts higher temperatures at all points, if all other parameters are kept constant, as expected. The effect of γ and h is also similar

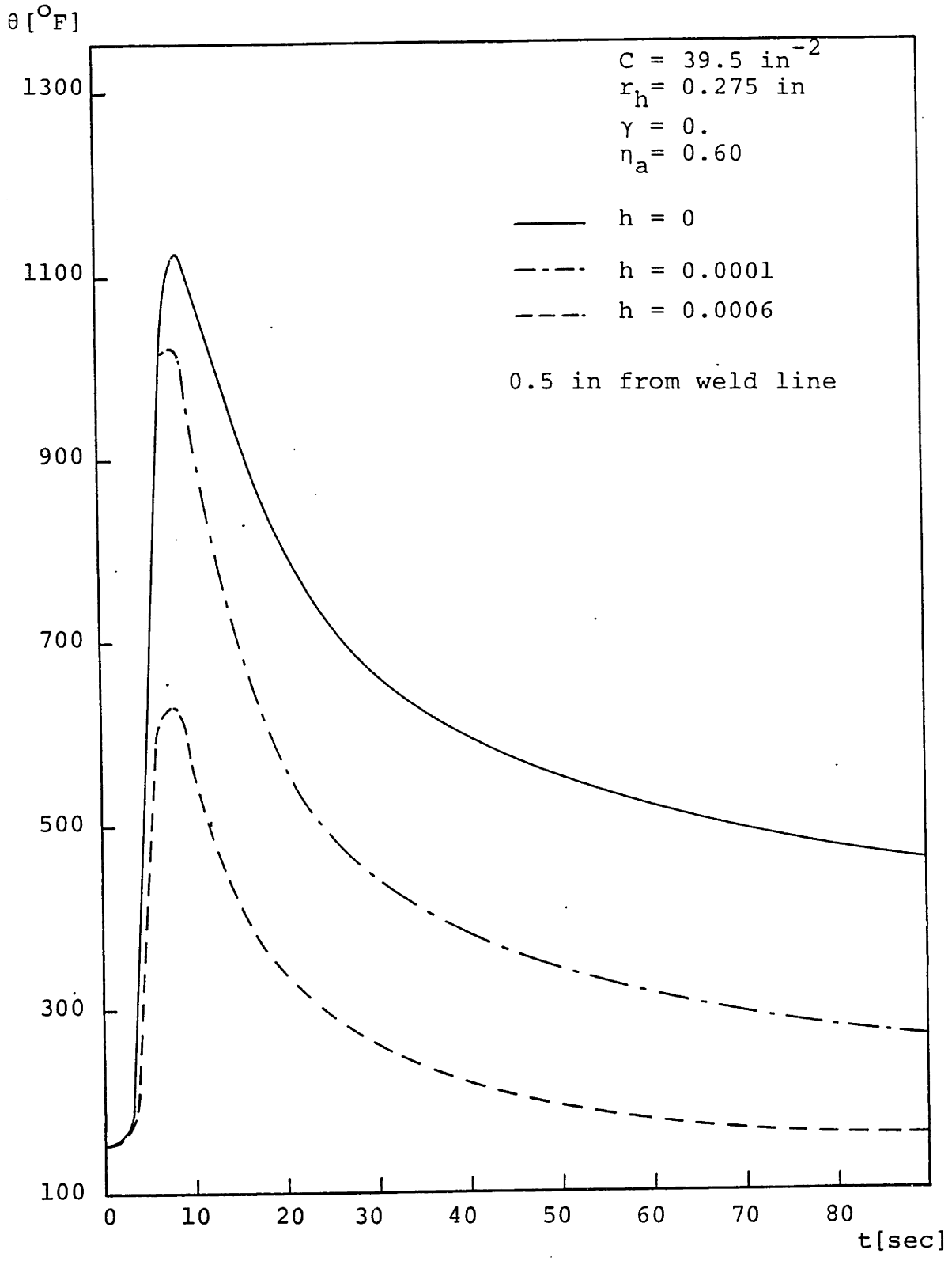

FIGURE 2.6 Effect of Heat Losses on Finite Heat Source Solution.

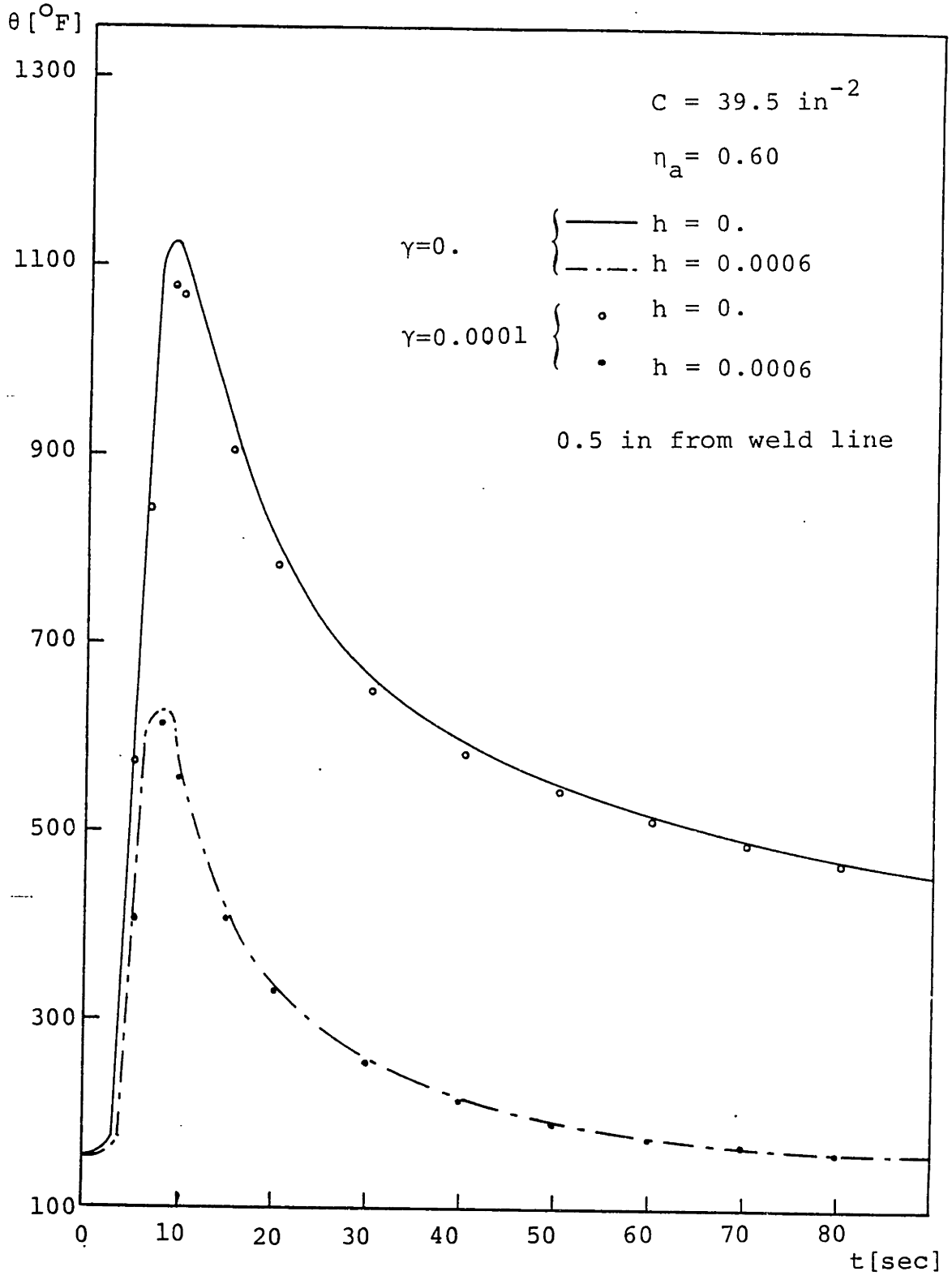

FIGURE 2.7 Effect of Variation of Thermal Conductivity on Finite Heat Source Solution.

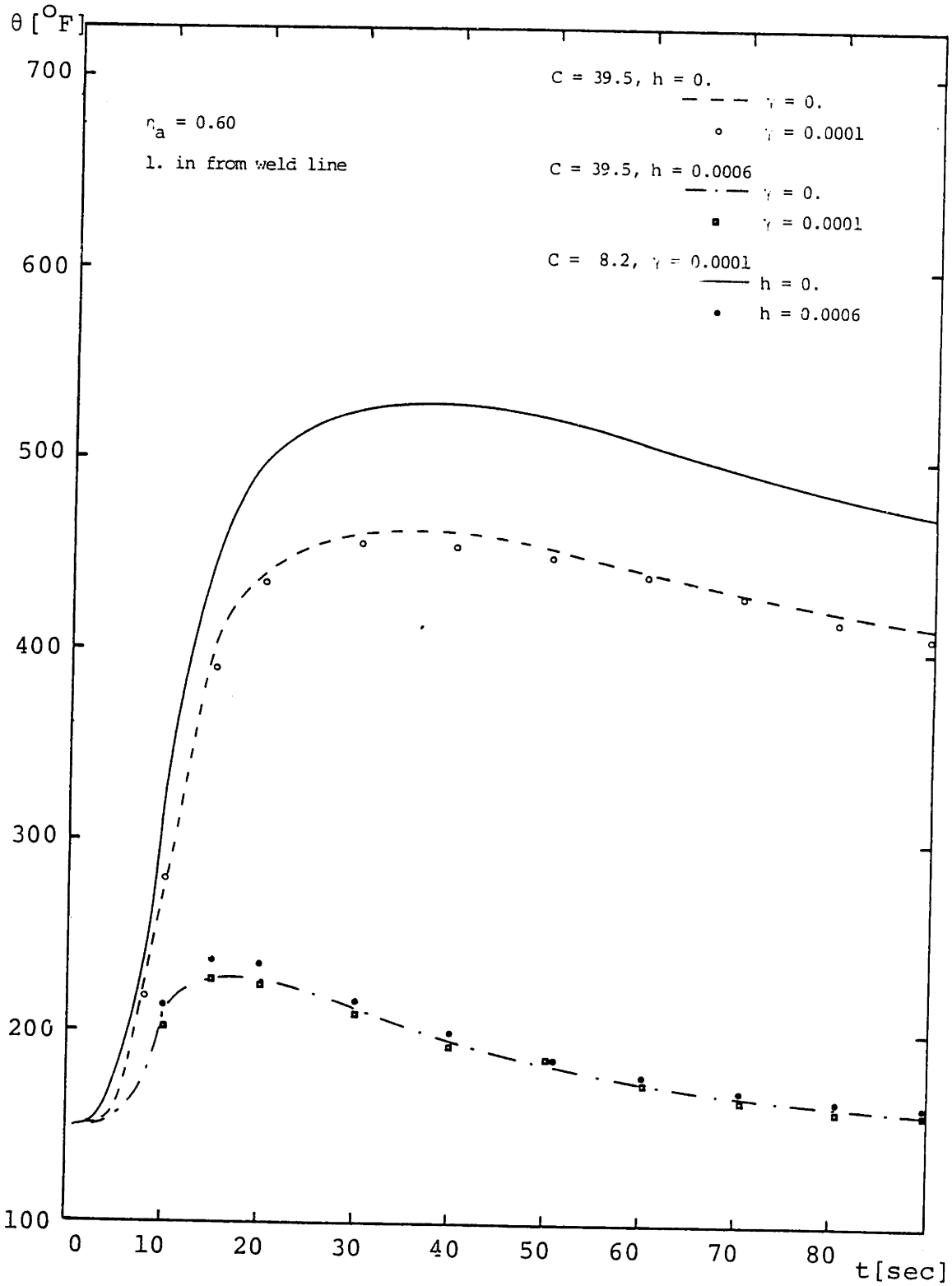

FIGURE 2.8 Parametric Investigation of Finite Heat Source Solution (1.0 in).

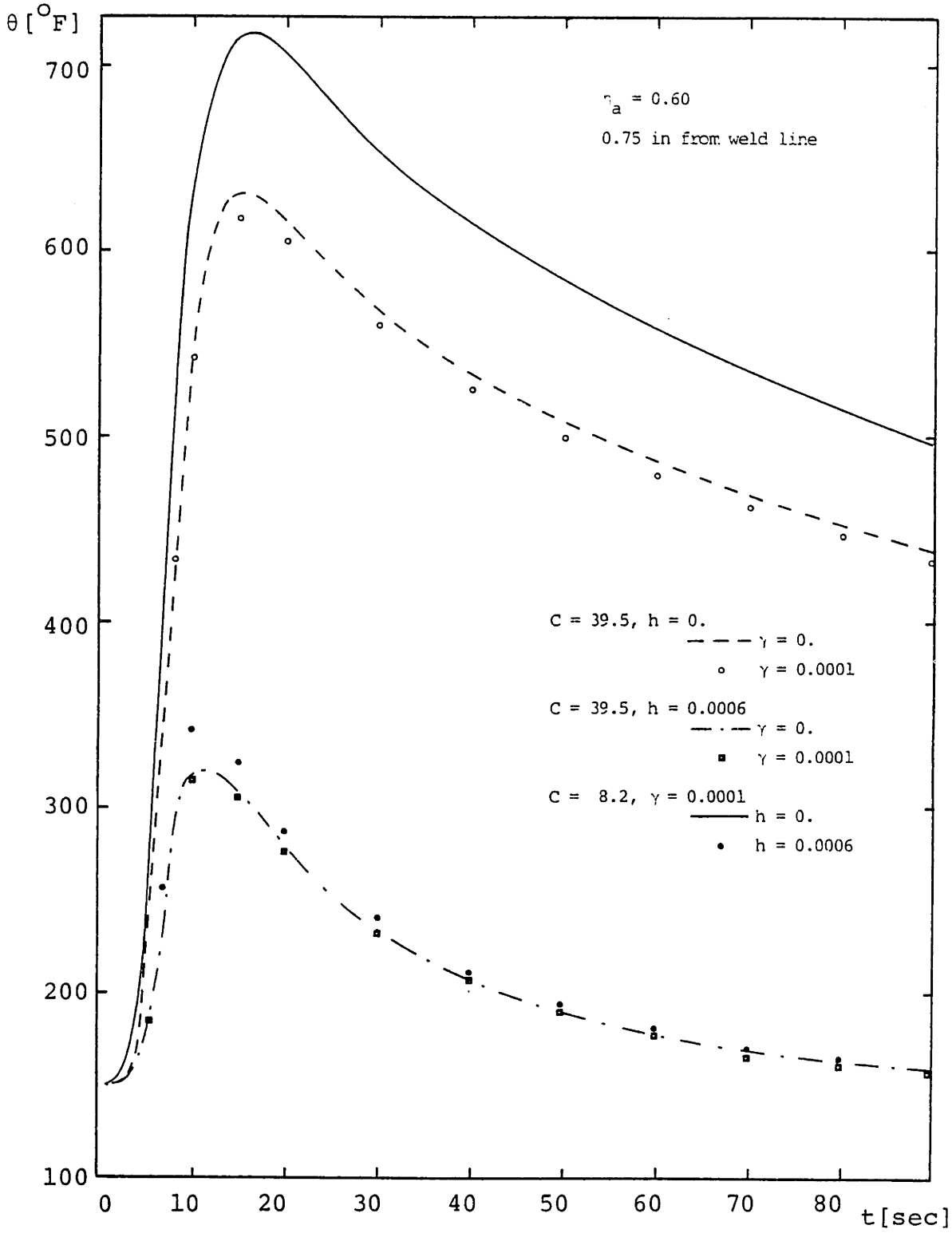

FIGURE 2.9 Parametric Investigation of Finite Heat Source Solution (0.75 in).

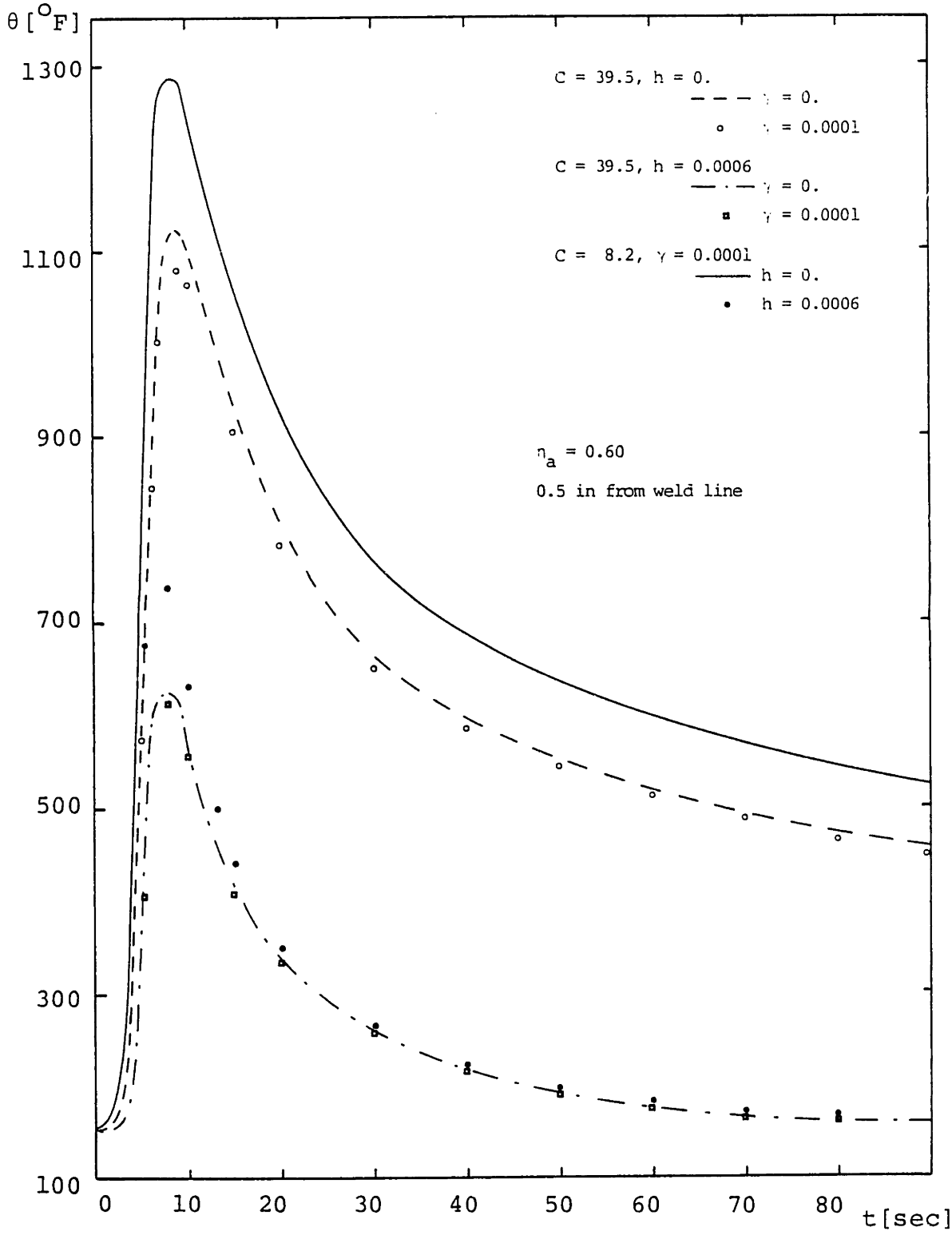

FIGURE 2.10 Parametric Investigation of Finite Heat Source Solution (0.5 in).

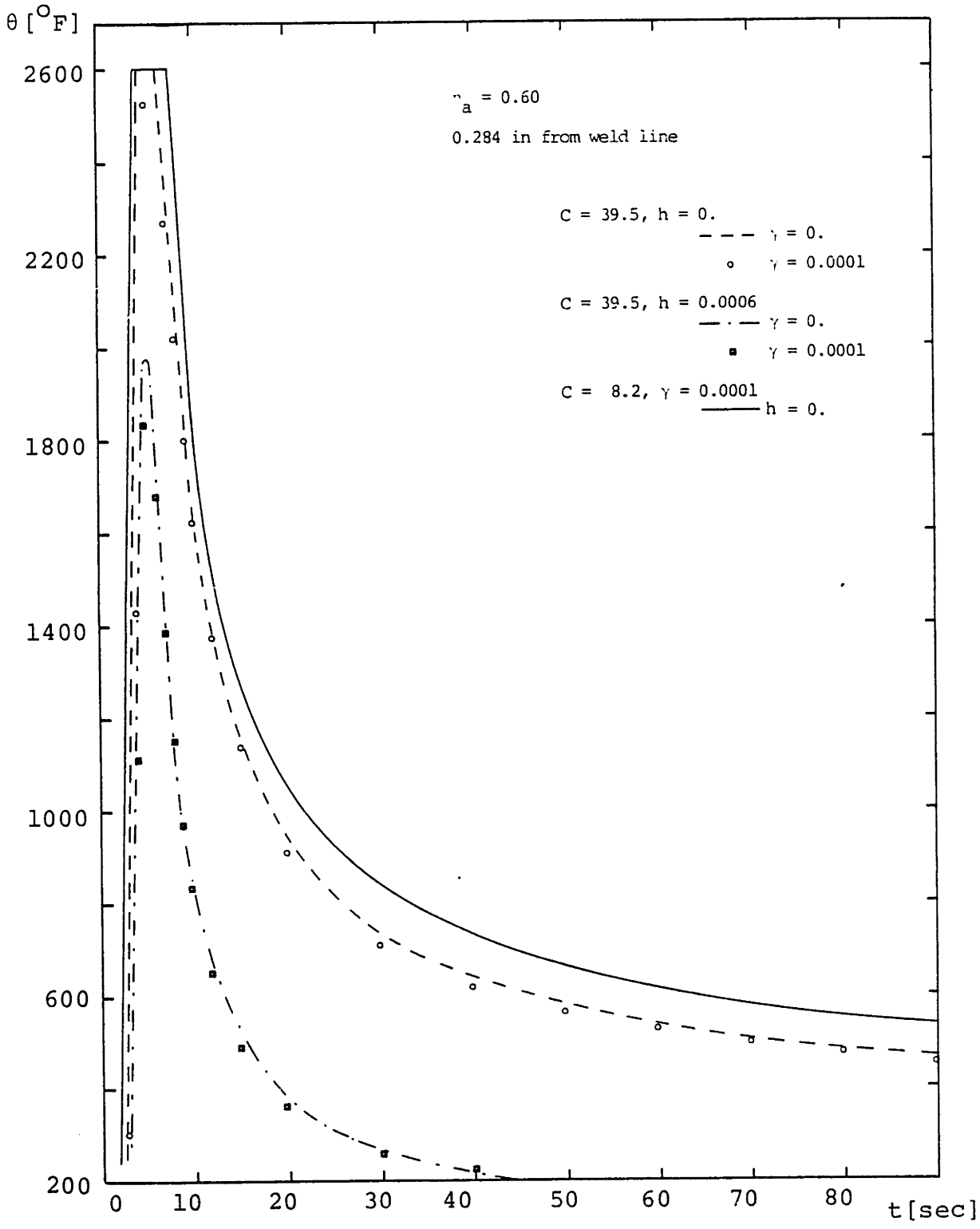

FIGURE 2.11 Parametric Investigation of Finite Heat Source Solution (0.284 in).

to the one explained in the previous paragraphs.

The effect of the arc efficiency on the temperature history of the same four points is illustrated in Figures 2.12 through 2.15. The curves shown were all calculated using the same C and γ. Two values of the heat loss coefficient were used. Again the same observation can be made with the additional one that larger arc efficiencies result in higher temperatures, all other things being equal.

In conclusion thus it can be said that the impact the various parameters have on the temperature distribution during welding is as follows:

1. Larger arc efficiencies result in higher temperatures.

2. The smaller the concentration coefficient (i.e the larger the heat spot radius) the higher the temperatures. This effect is more pronounced at the high temperature range.

3. The inclusion of linearly varying thermal conductivity does not alter by much the temperature distribution predicted by constant thermal conductivity calculation. Only in high temperature regions (inside the HAZ) is the effect pronounced, resulting in lower temperatures.

4. The average heat loss coefficient (from convection and radiation) has the largest impact on the temperature distribution with the adiabatic boundary conditions resulting in unreasonably high temperatures.

2.5 Comparison with Other Solutions and Experiments

The conventional point heat source closed form solution

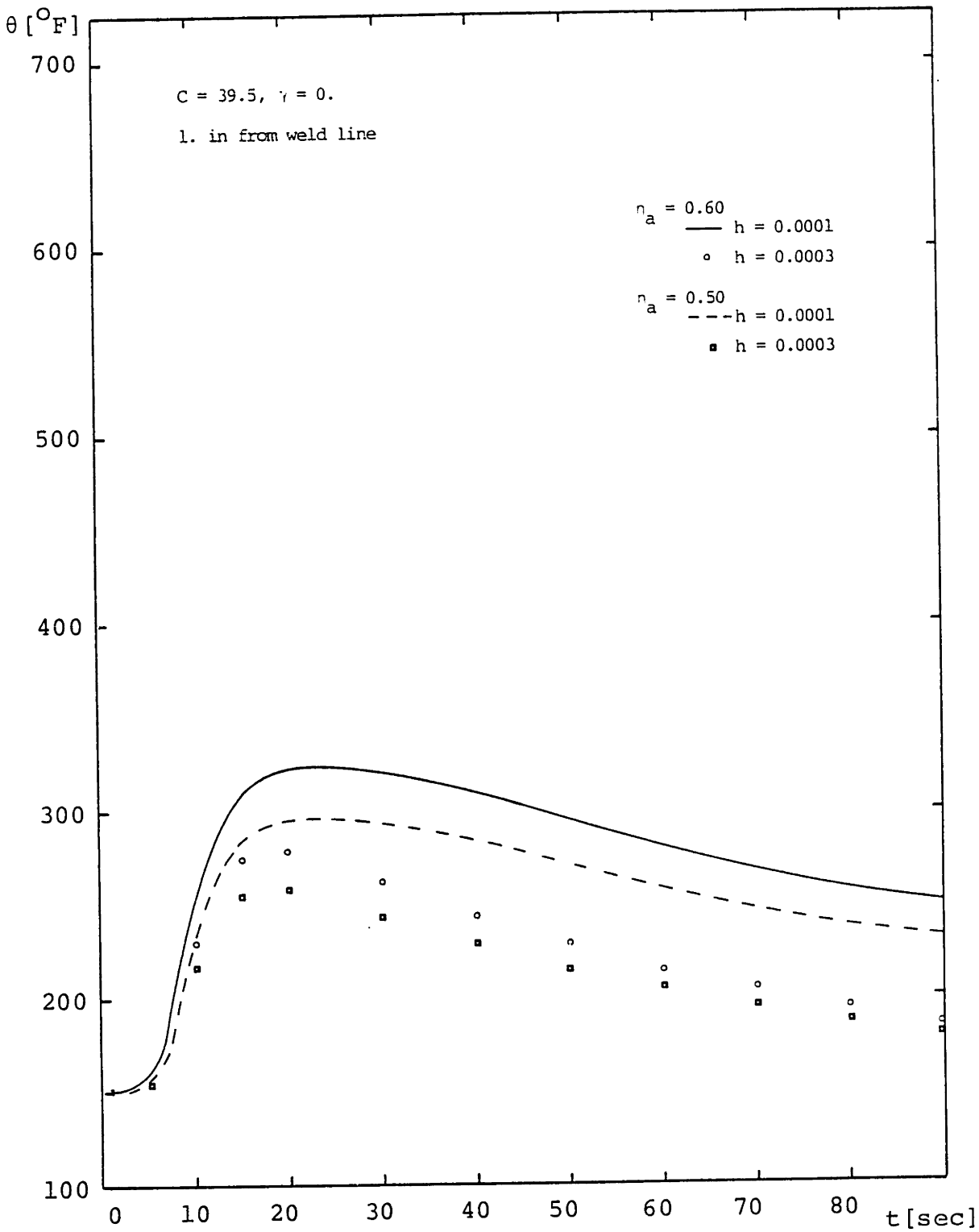

FIGURE 2.12 Effect of Heat Input on Finite Heat Source Solution (1.0 in).

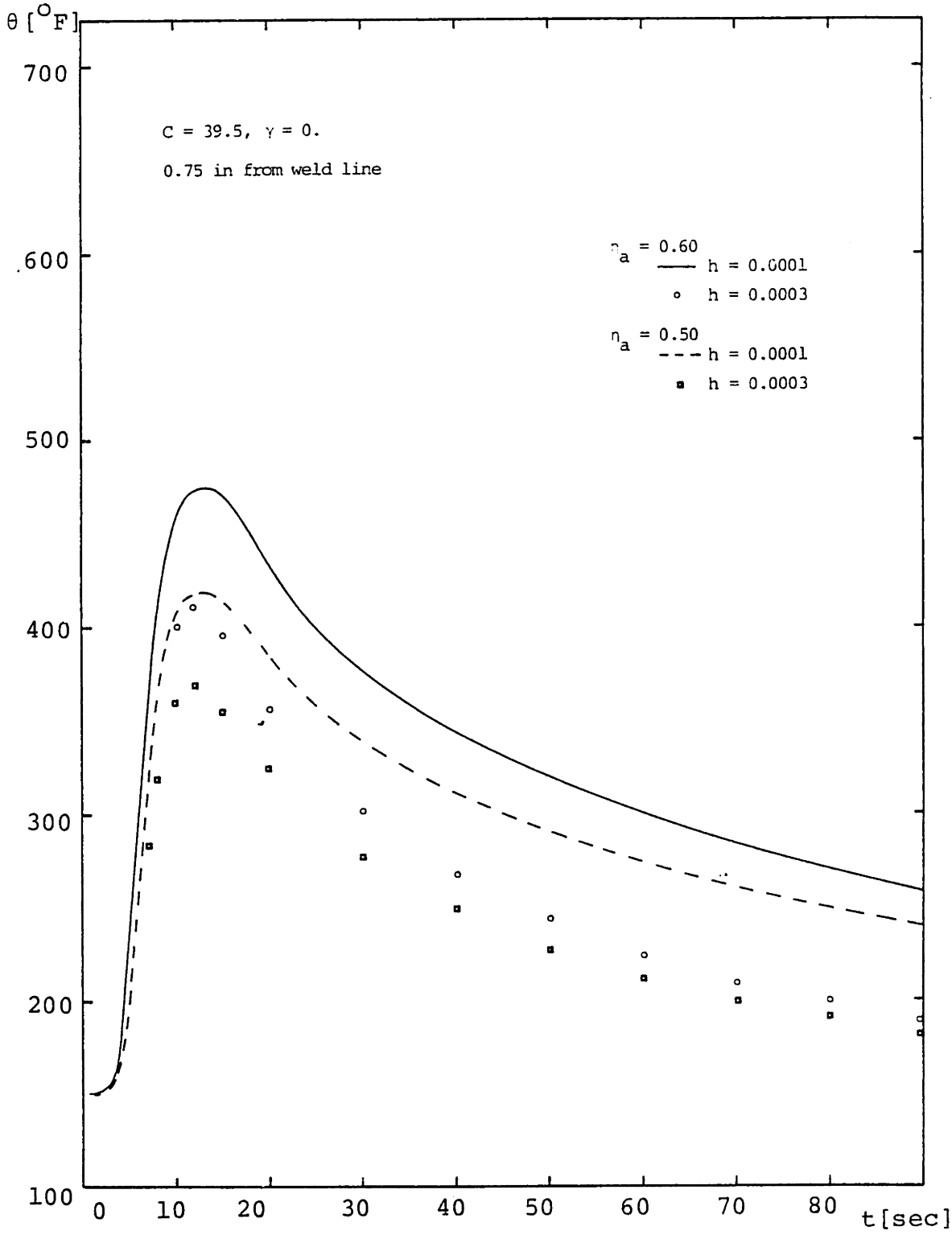

FIGURE 2.13 Effect of Heat Input on Finite Heat Source Solution (0.75 in).

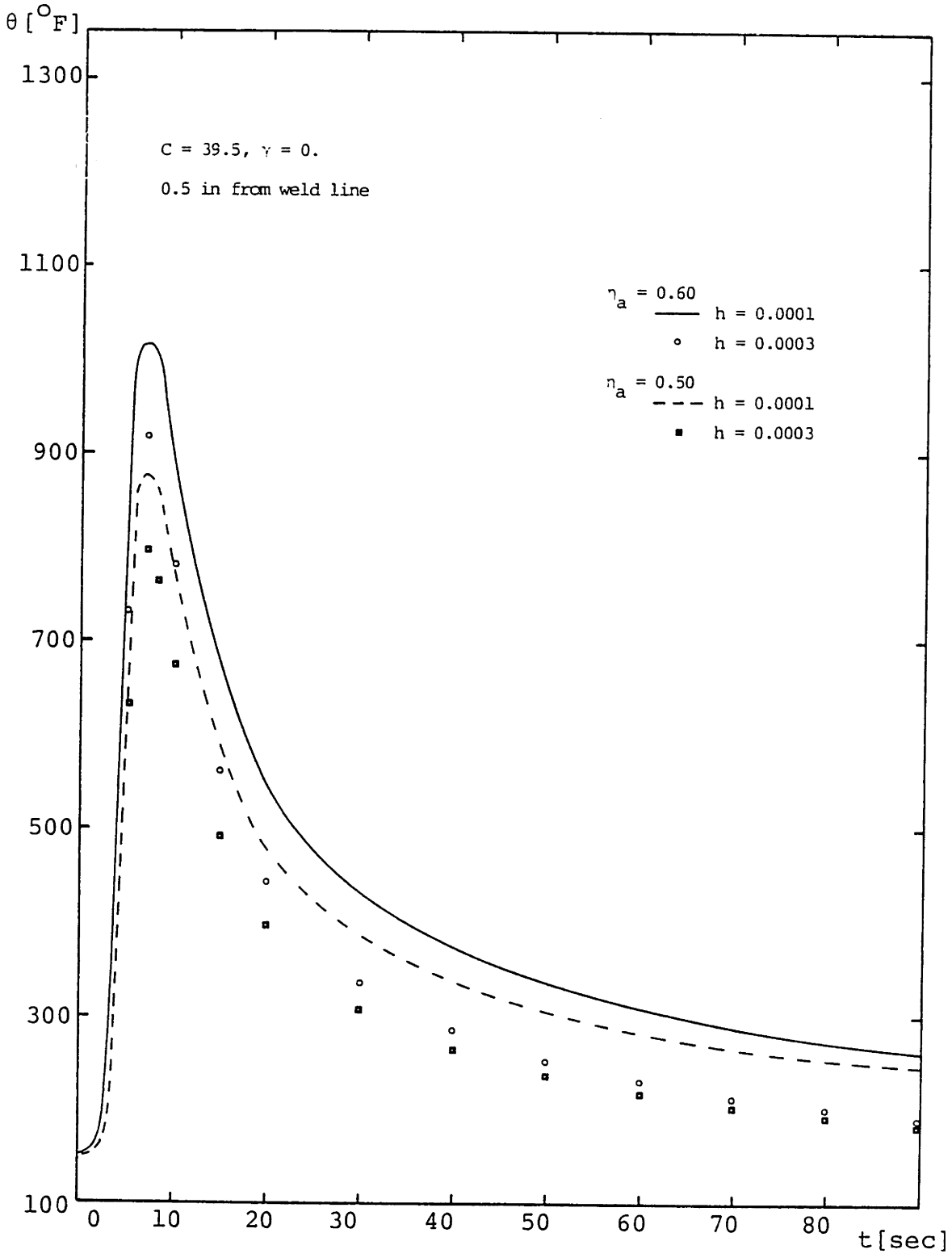

FIGURE 2.14 Effect of Heat Input on Finite Heat Source Solution (0.5 in).

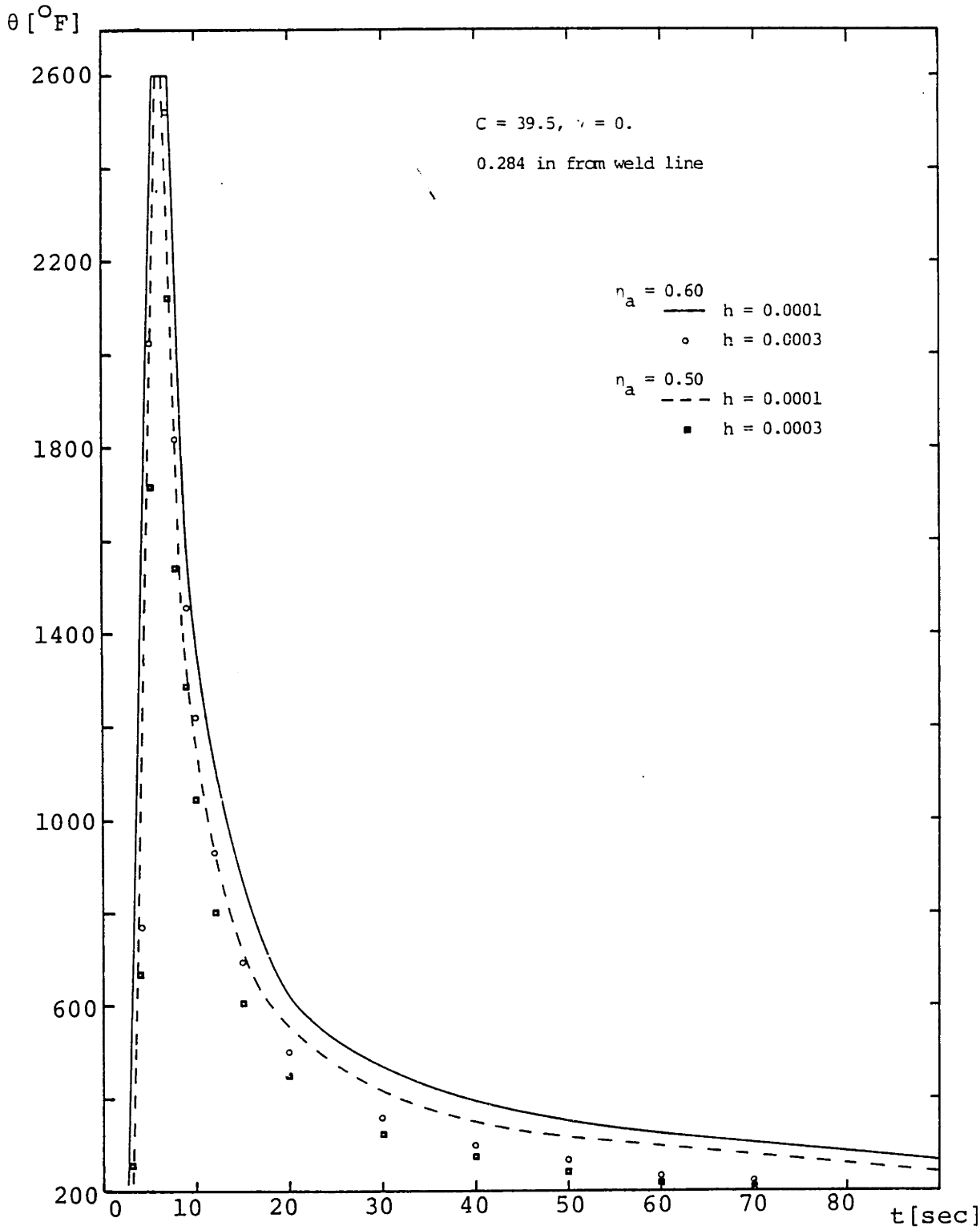

FIGURE 2.15 Effect of Heat Input on Finite Heat Source Solution (0.284 in).

was modified in this study to be able to simulate multipass welds. This modification, explained in Appendix B, involves the possibility of the point source being located at any point within the plate thickness as well as the inclusion of the effect the joint shape has on the temperature distribution. The point source can thus be located on the geometric center of each weld pass and not just on the top surface of the plate as was the case with the conventional solutions.

Both the conventional and modified point source solutions were applied to the same case as the one for the three-dimensional heat source model. Figures 2.16 through 2.19 depict the results obtained for four points located at various distances from the weld centerline. Shown are the cases of constant properties with the point source on the top surface of the plate and at a distance 0.4375 in (11.1 mm) from the top (simulating the first pass of the welding experiments described in detail in Section 4.4) and the case of variable properties using the iterative approach outlined in Section 2.1.3.

The results show clearly the overestimation of temperatures for points located on the top surface of the plates if the conventional point source solution is applied even if the temperature variation of material properties is considered. This overestimation is even more pronounced in the high temperature regions close to the weld centerline. At the same time the experimental results (see Section 4.4) seem to have a good correlation with the ones obtained using the modified approach.

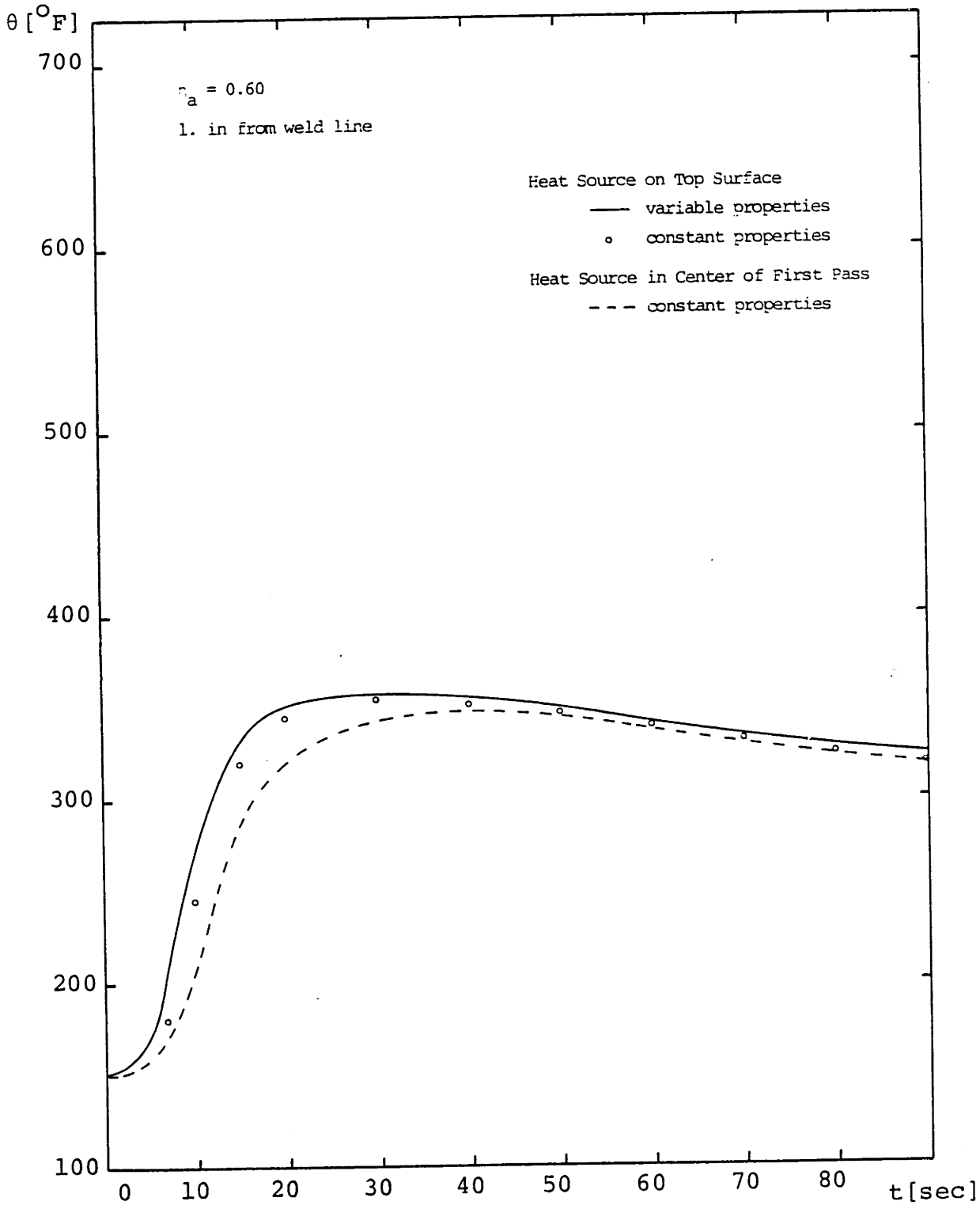

FIGURE 2.16 Investigation of Point Heat Source Solutions (1.0 in from weld line).

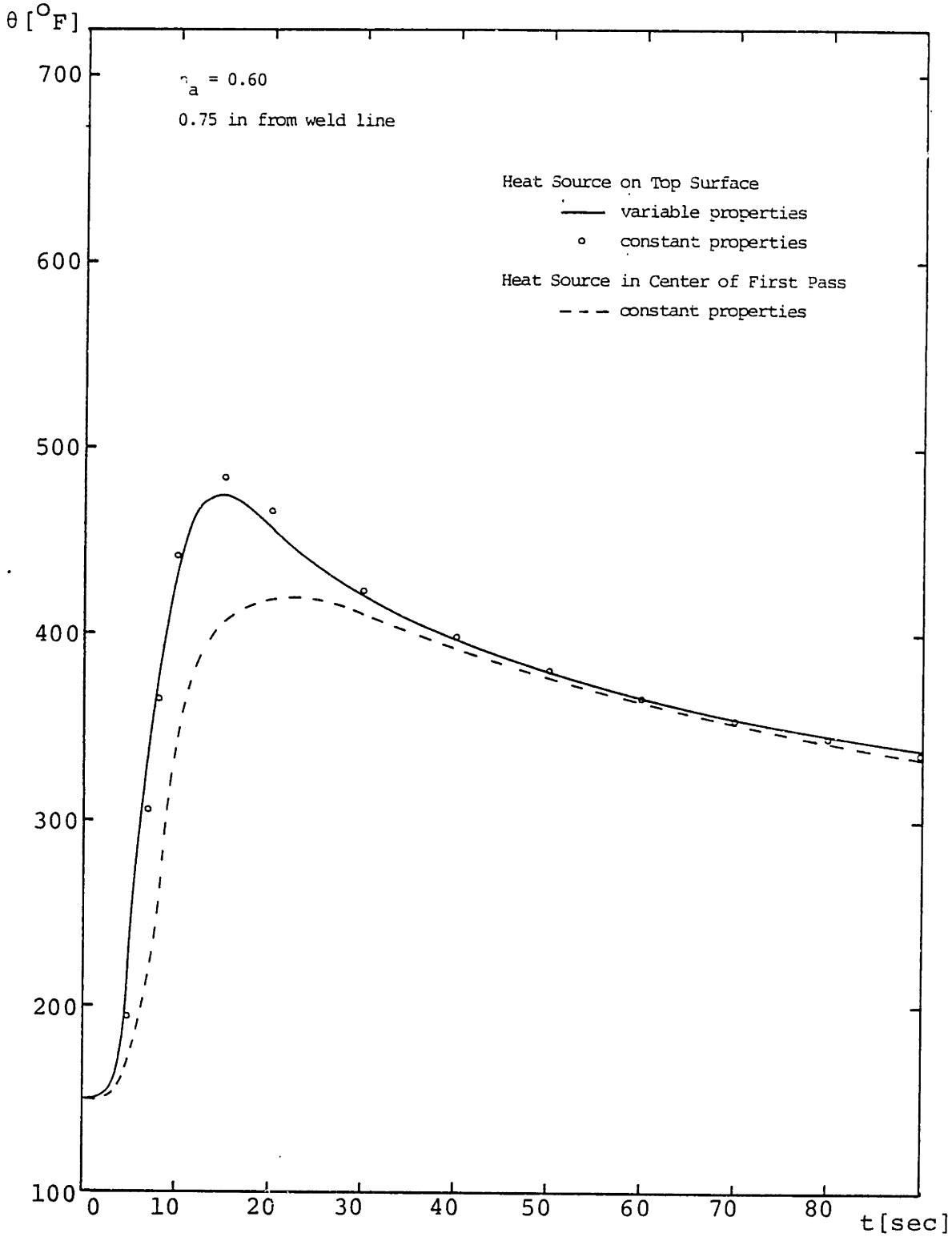

FIGURE 2.17 Investigation of Point Heat Source Solutions (0.75 in from weld line).

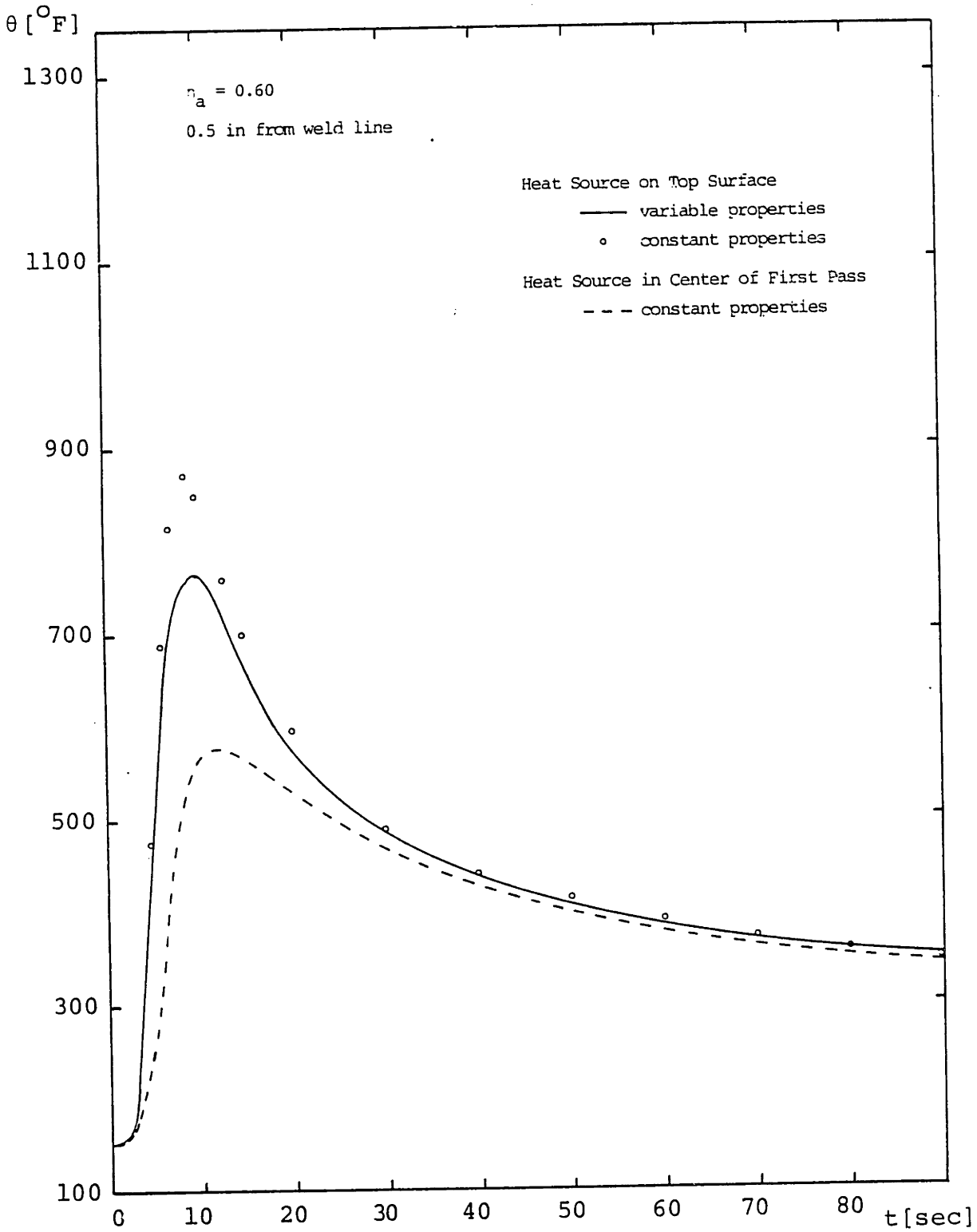

FIGURE 2.18 Investigation of Point Heat Source Solutions (0.5 in from weld line).

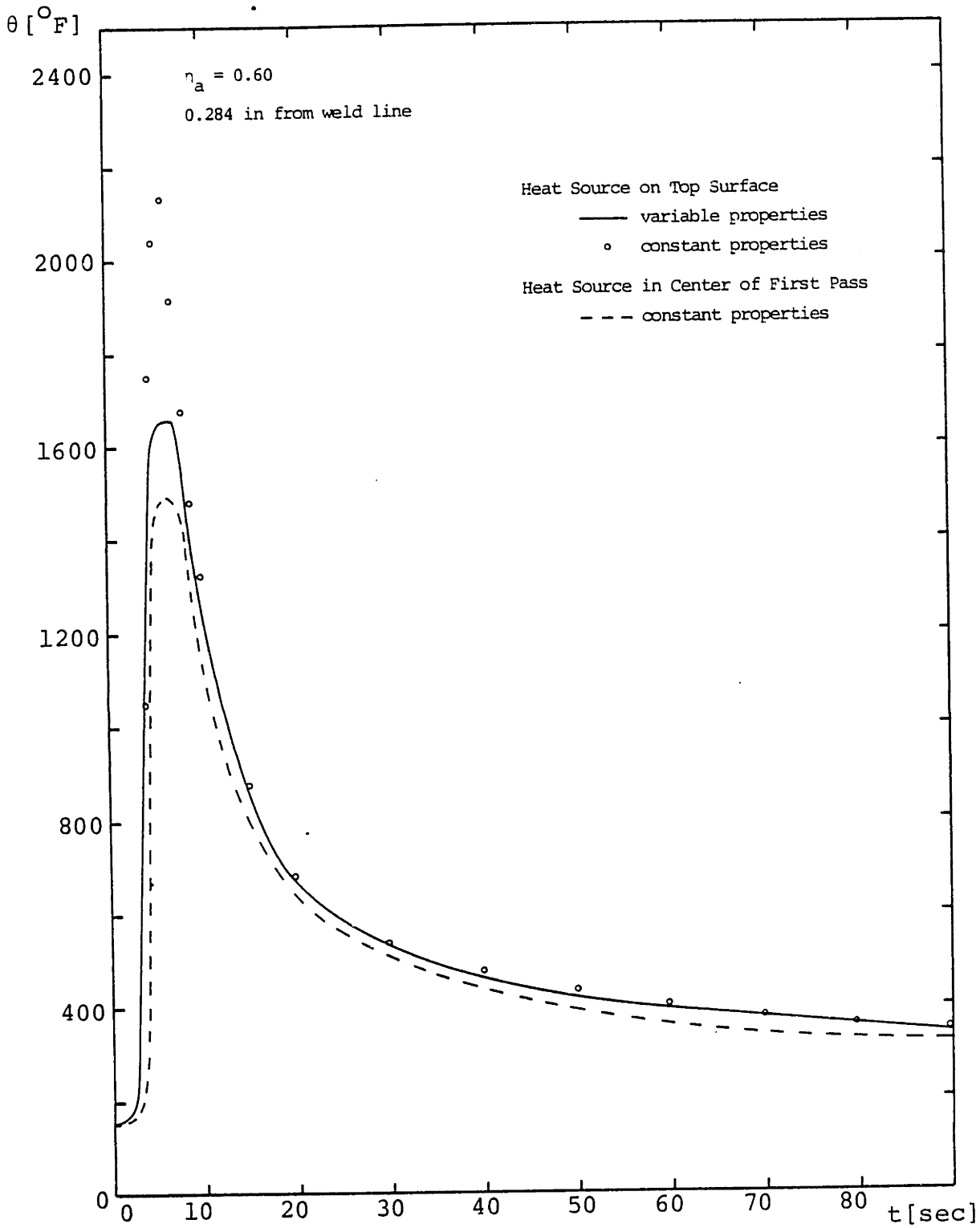

FIGURE 2.19 Investigation of Point Heat Source Solutions (0.284 in from weld line).

Furtheromore, a comparison of the modified point heat source results with the ones obtained using the three dimensional finite heat source approach (see Figures 2.12 through 2.15) reveals that the latter predicts too high cooling rates if the maximum temperatures reached are matched for the two solutions. The situation is even worse if the results for the first pass of the multipass welding experiments are compared.

These results should not be of a surprise, however. The assumptions involved in the development of the three- dimensional heat source model make its use more appropriate in the cases of thin plates. A better correlation with experimental results should therefore be expected in these situations.

To test this proposition an analysis of experimental results obtained by Tsai [29] during laying a bead on a 0.125 in (3.2 mm) low carbon steel plate was attempted. The welding speed was 9 ipm and the arc power 5000 J/sec. Figure 2.20 shows the comparison between experiments and analysis at two points located 0.4 and 0.7 in (10.2 and 17.8 mm) away from the weld centerline. As postulated, the three dimensional heat source model gives good results in this thin plate test case.

In summary, the new finite heat source model developed for predicting temperature distributions during welding can be applied when welding thin plates, preferably made of materials exhibiting a linear temperature dependence of the thermal conductivity (such as aluminum).

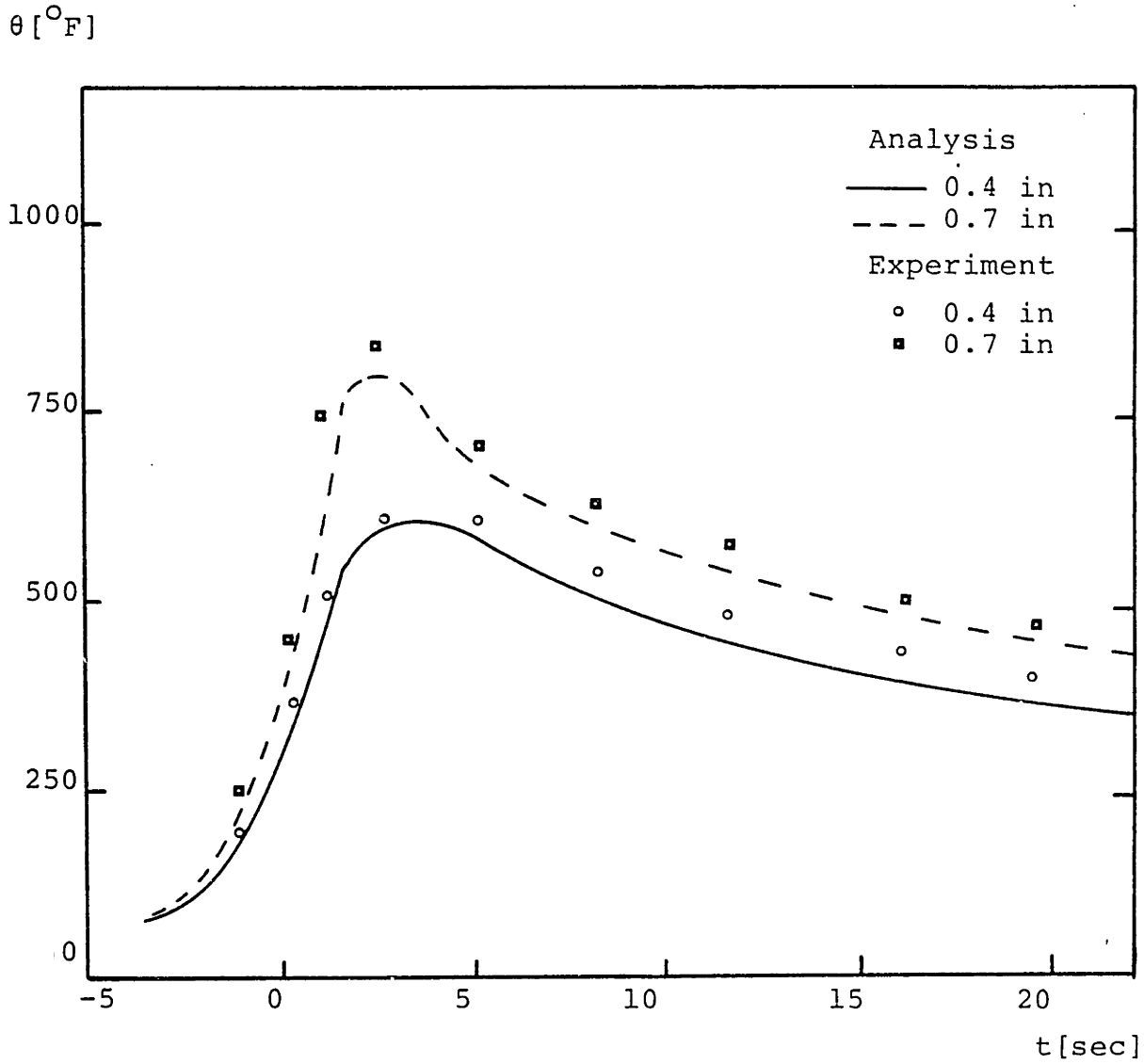

FIGURE 2.20 Comparison of Finite Heat Source Solution with Experimental Data for a 0.125 in thick Welded Plate.

CHAPTER III

MATERIAL CHARACTERISTICS OF HY-130 STEEL

This study is primarily concerned with temperature, transient strain, and residual stress distributions due to welding of high strength quenched and tempered steels, and in particular of HY-130 steel. It is thus appropriate to devote a chapter to the characterization of this material.

The first section deals with general characteristics of the HY-130 steel, including its composition, desired mechanical properties, welding consumables and the problems encountered during welding.

This is followed by a section reviewing the available experimental data on the transformation kinetics of HY-130. Isothermal (TTT) and cooling (CCT) transformation diagrams are presented for the base and weld metal.

The third section details an effort towards a rational determination of the temperature dependence of the HY-130 mechanical and physical properties, in the absence of any available experimental data. Such an effort was deemed necessary because the properties are required input to both the thermal and stress analyses.

The final section, returning to the subject of transfromation kinetics, deals with proposed methods for the analytical derivation of the CCT diagram on the basis of the experimentally available isothermal one. These methods will be applied and commented upon for the case of HY-130 steel.

3.1 General Characteristics

HY-130 was develoepd as an upgrading of the HY-80 class of Naval hull-construction alloys. The developmental effort started in the early sixties at Westinghouse Electric Corporation [34, 35]. In 1962 a contract was placed with the U.S. Steel Co. by the U.S. Navy for the systematic development of a steel with a minimum yield strength in the 130 to 150ksi (895 to 1030 MPa) range and of associated welding procedures and consumables [36]. The steel development program was actually carried out in the U.S. Steel Co. laboratories, whereas the consumable development was subcontracted to the McKay Company and the Arcos Corporation for shielded metal arc electrode development, and to the Air Reduction Company (Airco) primarily for the development of GMA welding consumables [37].

The steel developed at the U.S. Steel Co. is based on 5% nickel and contains chromium, molybdenum and vanadium. In going through the literature of the 1960s and before the final standarization of the alloy's name to HY-130, one encounters several other designations such as 5Ni-Cr-Mo-V, HY-150, HY-140, HY-130/150, and HY-130(T), all being used to describe the same alloy in different stages of development [38]. These designations reflect the progressive lowering of the desired minimum yield strength from 150 to 130ksi (from 1030 to 895 MPa) through the realization of the inherrent fracture toughness limitations of this class of alloy steel at high yield strengths.

Table 3.1 provides the compositional ranges of the HY-130 steel and compares them with those of the HY-80 alloy [37]. Both of them are intended for use in the quenched-and-tempered condition, in which the microstructure is primarily tempered martensite. More about the transformation kinetics will be discussed in a later section.

The mechanical properties of HY-130 in the as-received quenched and tempered condition are typically as follows [38, 39]:

(a) Yield strength of at least 130ksi (895MPa) at the center of a 4 in. (101.6mm) plate - it should be noted that yield stress of as high as 160ksi (1100MPa) has been reported in heats of 1.5 in (38mm) plates [40].

(b) Elongation in 2 in. (50mm) of 15 to 20% for 1 in (25.4mm) thick plates.

(c) Reduction of area equal to 50-64% transversely and 70% through thickness.

(d) A Charpy-V-notch impact energy absorption of 60ft-lb (81.3J) at 0°F (-17.8°C) in the ductile fracture region ("shelf").

Other general properties of the HY-130 steel are presented in Table 3.2 as reported in a 1964 paper by Manganello et al [41]; some of these constants could not be found in the more recent literature. Nevertheless the values connected with transformation kinetics will be discussed in another section.

Consumables for welding HY-130 have been developed for

TABLE 3.1 Compositional Ranges of HY-80 and HY-130 steels (weight, %) [37]

Element	HY-80	HY-130
C	0.18 max	0.08-0.12
Mn	0.10-0.40	0.60-0.90
Si	0.15-0.35	0.20-0.35
Ni	2.00-3.25	4.75-5.25
Cr	1.00-1.80	0.40-0.70
Mo	0.20-0.60	0.30-0.65
V	0.03 max	0.05-0.10
S	0.025 max	0.010 max
P	0.025 max	0.010 max
S+P	0.045 max	-
Ti	0.02 max	0.02 max
Cu	0.25 max	0.25 max

TABLE 3.2 General Properties of HY-130 Type Steel [41]

A_{c_1} Temperature	1210°F (654°C)
A_{c_3} Temperature	1415°F (768°C)
M_s Temperature	715°F (379°C)
Recommended final austenitizing temperature	1500°F (815°C)
Microstructure (as quenched, mid-thickness)	
0.5in (12.2mm) plate	100% martensite
4.0in (101mm) plate	60-75% martensite, remainder bainite
Recomended tempering temperature range	1000-1150°F(538-621°C)
Magnetic properties	
B_{sat}	20,520 G (2.052 T)
H_{sat}	2,190 O (1.7×10^5 A/m)
μ_{max}	630

both the shielded metal arc (SMA) and gas metal arc (GMA) welding [42, 43]. Table 3.3 provides the compositional ranges for the three available consumables: the Navy specifications for a low-hydorgen type E14018 electrode to be used with SMAW; the AX-140 GMAW wire as developed by Airco; and the Navy specifications for the 140S GMAW wire. Comparing Tables 3.1 and 3.3 it can be seen that the carbon content of the consumables is below that of the base metal because of the carbon's tendency to cause cracking. Similarly, manganese content is relatively high because it imparts toughness; nickel content is lowered to avoid cracking known to be caused by high nickel contents; and chromium content is raised for increased hardenability.

Generally speaking hydrogen induced HAZ cold cracking, hot tearing, and lamellar tearing are not considered to be a probelm with HY-130 welds. Weld metal solidification cracking could be a high risk for HY-130 welds; it is believed, however, that the reduced phosphorus and sulfur contents necessary for good weld metal toughness are adequate for avoiding the problem [37]. Many investigators [36, 38, 43] have reported that weld metal hydrogen cracking is perhaps the most serious problem facing the production of HY-130 welds. A compilation of the various recommendations proposed for avoiding this type of cracking, such as preheating, moisture control in electrodes, and maximum heat input, can be found in the Welding Institute review paper by Shackleton [37].

TABLE 3.3 Analysis of Consumables for Welding HY-130 Type Steels

Element	MIL-14018[1]	AX-140[2]	MIL-140S[3]
C	0.10 max	0.07-0.11	0.12 max
Mn	0.75-1.35	1.70-2.00	1.50-2.00
Si	0.65 max	0.25-0.45	0.30-0.50
S	0.010 max	∿ 0.007	0.010 max
P	0.013 max	∿ 0.006	0.010 max
Cr	0.35-1.20	0.85-1.20	0.65-1.05
Mo	0.30-0.90	0.50-0.60	0.40-1.00
Ni	3.10-3.90	2.00-2.50	1.95-3.10
Al	-	∿ 0.018	0.04 max
Ti	-	∿ 0.01	0.04 max
Zr	-	-	0.04 max
Cu	-	-	0.15 max

Notes:
1. MI-30-CE/3 specification requirements; electrode E14018 manufactured by McKay Co.
2. Technical data provided by Air Reduction Co.
3. MI-30-BE/1 specification requirements; wire Linde 140S manufactured by the Union Carbide Co.

3.2 Experimentally Derived Transformation Kinetics

3.2.1 Isothermal Kinetics

The isothermal transformation characteristics for the base HY-130 steel could only be found in a 1967 U.S. Steel Co. report compiled by Manganello, et al [44]. For lack of other data and although these characteristics pertain to the alloy still in its developmental stages, the time-temperature-transformation (TTT) diagram is reproduced here in Figure 3.1 in the hope that the basic attributes have been carried over to the finalized alloy. The TTT diagram shown has been experimentally determined from a heat having the following composition: 0.09% C, 0.75% Mn, 4.98% Ni, 0.61% Cr, 0.54% Mo, and 0.07% V; the steel was austenitized at 1500°F (815°C) and had an ASTM grain size number between 7 and 8.

The three major transformation temperatures were determined to be as follows (see also Table 3.2):

A_{c3} = 1415°F (768°C)

A_{c1} = 1210°F (654°C)

M_s = 715°F (379°C)

One can compare these temperatures with the ones predicted by the empirical formulae proposed by Andrews [45], since the HY-130 composition is within the ranges for which the formulae can be used. The predicted values for the M_s and A_{c1} temperatures are 713°F (378.5°C) and 1204°F (651°C) respectively, i.e. very close to the experimentally obtained ones; the A_{c3} temperature was predicted to be 1430°F (777°C), 15°F (8°C) higher than the experimental one.

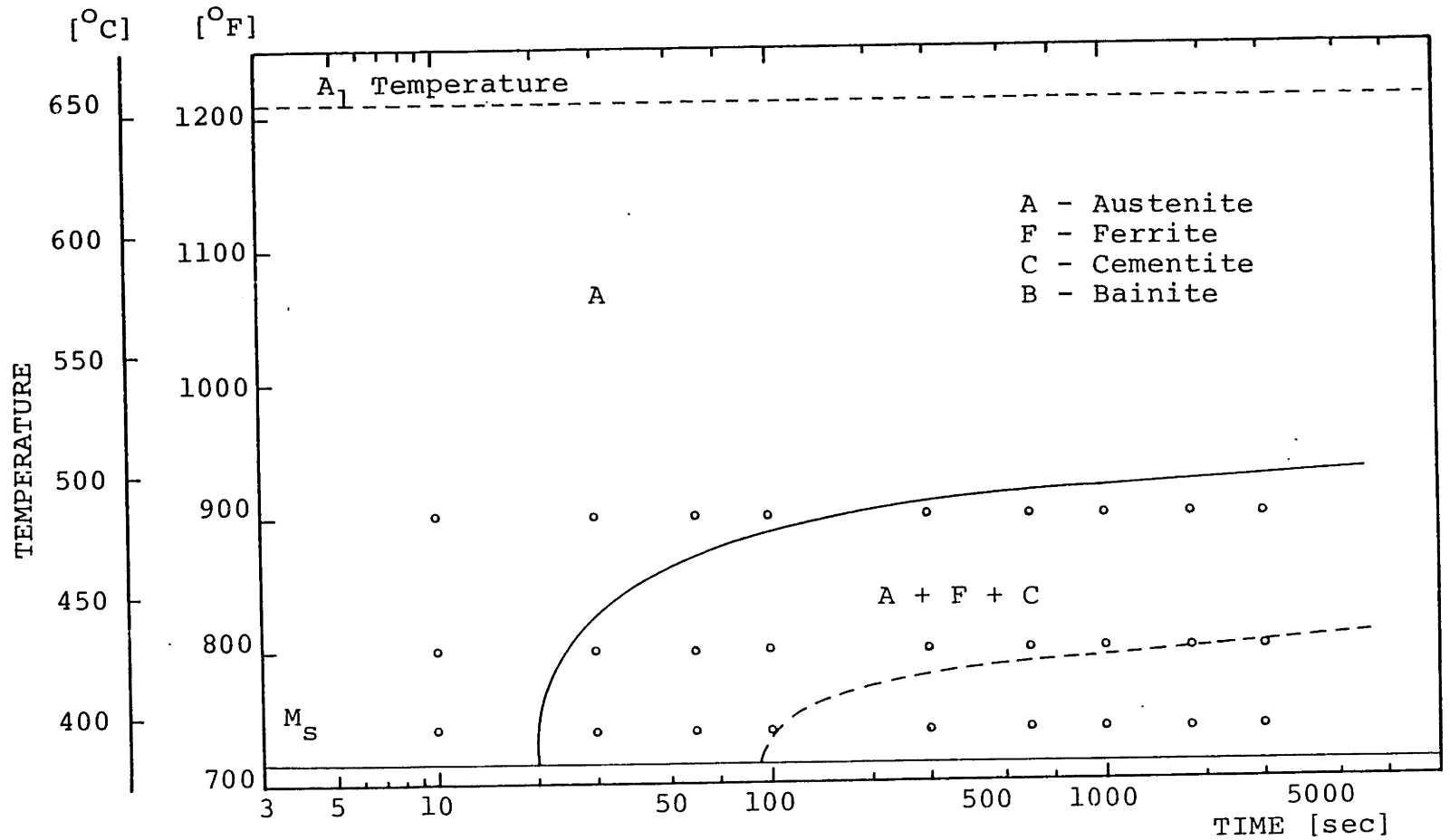

FIGURE 3.1 Isothermal Transformation Diagram for HY-130 Steel.

During the isothermal study it was noted that transformation to ferrite, at temperatures just below the A_1 temperature, were suppressed to times in excess of 10^4 seconds. Given the fact that such time scales at so high temperatures do not occur during the welding cycle, it follows that this allotropic transformation is of no interest to the welding problem and it is therefore not shown in Fig. 3.1. Furthermore, the TTT diagram shows that transformation to lower bainite can occur in as short a time as 20 seconds at temperatures just above the M_s temperature. As a consequence, heavy plates may end up having a bainitic microstructure around their midthickness as compared to the tempered martensitic structure prevailing in the remaining volume.

A limited isothermal transformation study of the HY-130 weld metal welded using 1/16 inch (1.5mm) Airco AX-140 GMA filler wire was conducted as a part of a larger investigation by Holsberg [46]. In the study heating was controlled to reach peak temperature in 8 seconds at a linear rate; the peak was maintained 5 seconds before cooling. Free cooling was then used up to the preselected isothermal temperature and after the desired hold time the specimens were freely cooled to ambient temperature. These thermal cycles were produced in a Duffer's Gleeble apparatus [47,48]. Note that the described thermal cycles are not the same as the conventional ones used in isothermal studies, but rather ones reminiscent of the actual welding cycle. In particular the 5 seconds during which the specimen is held at the peak temperature might not

be enough for full austenitization to take place.

In all cases a martensitic transformation was observed during free cooling from the isothermal temperature, even after long hold times. This is in agreement with the base metal isothermal study referred to above. Holsberg reports an M_s temperature of 760°F (405°C) and notes that this temperature was depressed (see Table 3.4) whenever a bainitic transformation preceeded the martensitic one, owing to segregation of alloying elements into the remaining austenite. Table 3.4 reproduces the results of the study.

3.2.2 Continuous Cooling Kinetics

Although isothermal transformation diagrams, as the one for HY-130 shown in Fig. 3.1, are easily obtained experimentally, they are not very useful in predicting microstructures during practical applications. The reason is that TTT diagrams show in an approximate way the transformation kinetics over time for constant temperatures, whereas in practical applications, such as casting and welding, the temperature does not remain constant but changes with time. The need thus arises for diagrams showing the transformation kinetics in non-isothermal cases. Such diagrams, called continuous cooling transformation (CCT) diagrams, although difficult and time consuming to experimentally obtain, have been derived for a limited number of alloys under conditions of constant cooling rates and/or of previously specified cooling patterns [49].

A few cooling transformation studies have been conducted, mostly at the DTNSRDC, for the HY-130 steel and its weld metal,

TABLE 3.4 Results of Isothermal Transformation Studies on HY-130 Weld Metal Using AX-140 Wire (Holsberg [46])

Peak Temperature		Isothermal Temperature		Hold Time	M_s Temperature	
°F	°C	°F	°C	min	°F	°C
		900	480	60	710	380
2000	1090	825	440	360	575	300
		750	400	60	ND	ND
		900	480	5	715	380
1600	820	750	400	60	585	305

ND - not determined

all using the Duffer's Gleeble apparatus mentioned earlier. Schreitz and Thompson [50] studied the HY-130 base metal and the weld metal deposited using the Airco AX-140 GMA wire; Wyckoff, et al [51] concentrated on the McKay 14018 and Linde 140S weld metal microstructures; finally Holsberg [46] reexamined the Airco AX-140 weld metal.

In all these studies the peak temperature was reached in 8 seconds, held there for 5 seconds, and then the specimen was allowed to cool down according to predetermined cooling rates. The cooling rates from 1000° to 800°F (538° to 427°C) ranged between 67 and 4°F/sec (37 and 2°C/sec) for the 1600°F (870°C) and between 55 and 2°F/sec (31 and 1°C/sec) for the 2000°F (1090°C) peak temperature. Hardness measurements were taken in all cases; in addition, Schreitz and Thompson [50] measured the yield strength and the Charpy V-notch impact toughness of the specimens after the imposition of the thermal cycles.

Figure 3.2 shows the continuous cooling transformation diagram for the HY-130 steel as obtained experimentally for both peak temperature cases [50]. Figure 3.3 presents similar diagrams for the Airco AX-140 and Linde 140S GMAW weld metals for a peak temperature of 2000°F (1090°C) [46,50,51]. It should also be noted that the CCT diagram for the McKay 14018 SMAW metals, not shown here, is similar to the Airco AX-140 GMAW metal at slow cooling rates and the Linde 140S metal at rapid cooling rates [50].

A careful observation of the two figures indicates that

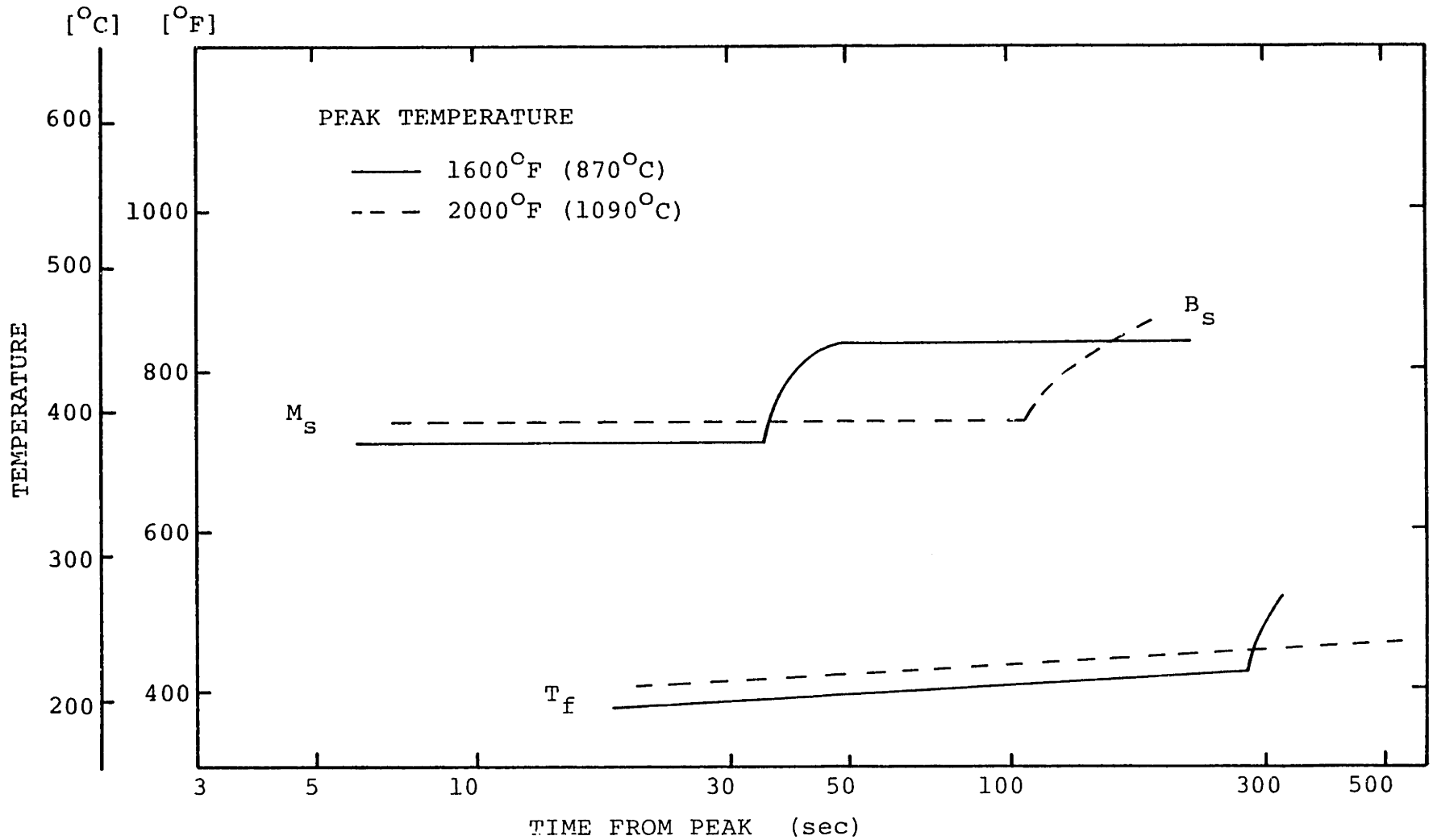

FIGURE 3.2 Continuous Cooling Transformation Diagrams for HY-130 Steel.

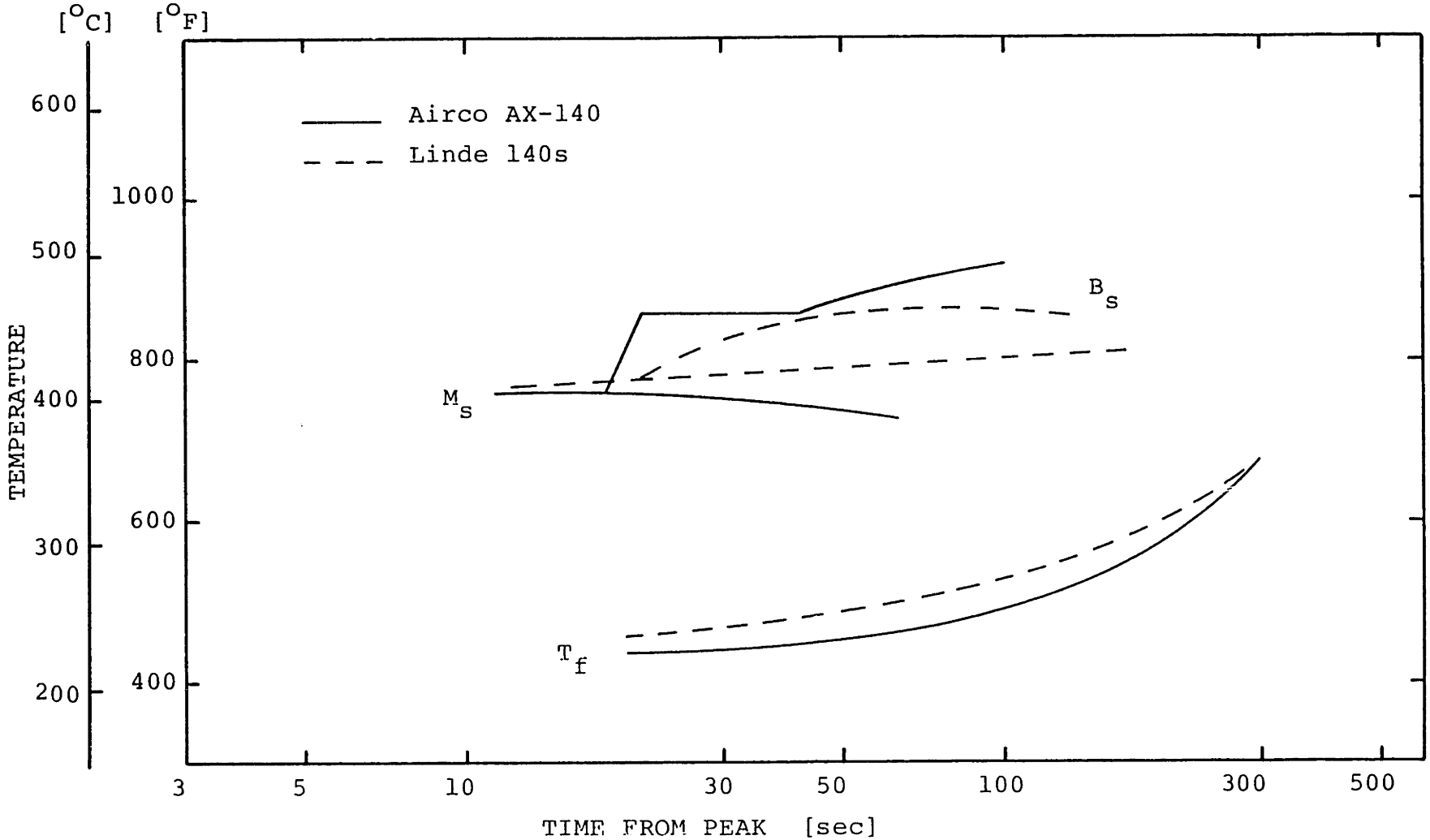

FIGURE 3.3 Continuous Cooling Transformation Diagrams for GMA Welded HY-130 Weld Metal (from 2000°F).

at high cooling rates a wholly martensitic structure is always the end result. Bainite starts forming at slower cooling rates, typically below 15°F/sec (8°C/sec), and at temperatures ranging from about 900°F (480°C) to the M_s temperature; greater amounts of bainite are formed, as expected, with a decrease in the cooling rate. Furthermore, a comparison of the HY-130 and weld metal CCT diagrams reveals that bainite is formed sooner in the weld metal, i.e. at higher cooling rates. More specifically, in the case of HY-130 bainite starts forming at 14°F/sec (8°C/sec) for the 1600°F (870°C) peak and at 4.5°F/sec (2.5°C/sec) for the 2000°F (1090°C) peak; in the case of the AX-140 weld metal this happens at 24°F/sec (13°C/sec) for the 1600°F peak and at 15°F/sec (8°C/sec) for the 2000°F peak; and in the case of the 140S weld metal bainite starts forming at 15°F/sec (8°C/sec) for the 2000°F peak. Given the fact that typical production welding conditions for 1 in. (25mm) thick HY-130 plates involve cooling rates in excess of 25°F/sec (14°C/sec) around the weld area, it can be safely assumed that the final microstructure will be wholly martensitic in this region.

Regarding the martensite start transformation temperature, M_s, Table 3.5 was compiled using data from the previously mentioned studies. For the HY-130 base metal it can be seen that the isothermal studies report a somewhat lower M_s temperature as compared to the continuous cooling one. Since such a discrepancy is not theoretically justifiable because

TABLE 3.5 Measured Martensitic Start Transformation Temperature, M_s

	M_s °F	M_s °C
Isothermal		
HY-130	715	379
AX-140	760	405
Continuous Cooling		
HY-130	720±10	382±5
AX-140	760±25	405±15
140S	770±10	410±5

of the athermal nature* of the martensitic transformation - assuming the same material and the same stress conditions - it is believed that the difference can be due either to experimental error or to small differences in the material chemical composition, the latter being known as heavily influencing M_s. For the purpose of this study, which is rather macroscopic in nature, it is felt that a reasonable approximation for the M_s temperature of the HY-130 base metal can be set at the 720°F (380°C) level.

With respect to the M_s temperatures of the Airco AX-140 and Linde 140S GMA weld metals, Table 3.5 reveals much higher values compared to the HY-130 one. It is believed that these differences can be attributed to the differences in the base and weld metal chemical compositions (compare Tables 3.1 and 3.3) which tend to suppress the base metal's M_s temperature (see also the various empirical formulae for predicting M_s based on chemical composition, as the one proposed by Andrews [45]).

One further note is in order at this point. The various M_s temperatures discussed above pertain to the cases where the cooling rates are so high so as to exclusively form martensite in the specimen. At lower cooling rates, when bainite is also formed, the M_s temperature cannot be accurately determined. This is due to the fact that the bainitic reaction also produces material expansion tending to mask the expansion of the

---

*More about it will be discussed in the appropriate chapter.

martensitic reaction. For the purposes of this study, however, it will be assumed that the same, constant M_s temperature exists for all cooling rates regardless of the prior formation or no formation of bainite.

A recent study by Stoop and Metzbower [52] looked into the metallurgical characterization of HY-130 steel welds made using the shielded metal arc (SMA) with E14018 electrodes, gas metal arc (GMA) with 140S wire, electron beam (EB), and laser beam (LB) welding processes. Specimens having 1/4 in. (6.35mm) and 1/2 in. (12.7mm) thicknesses were used. The microstructures of the SMA and GMA weldments were found to be similar, consisting primarily of a large percentage of acicular ferrite with somewhat small percentages of bainite and martensite. The EB and LB weldments were also similar in microstructure, composed mostly of martensite with smaller amounts of bainite.

3.3 Temperature Dependence of Material Properties

The analytical and numerical study of temperature, thermal strain and residual stress distributions due to welding requires the knowledge of the temperature dependence of both the physical and mechanical properties of the material under consideration. More specifically, in the heat transfer analysis the temperature variations of thermal conductivity, k, specific heat, c, and density, ρ, are used, whereas for the stress analysis the variations of the thermal expansion coefficient, α, virgin yield stress, σ_{yv}, Young's modulus, E, tangent modulus, E_T, and Poisson's rat .o, ν, with temperature are

required. This is due to the fact that during the welding cycle the material experiences temperatures ranging from room to melting and it is well established that all material properties exhibit severe changes within that range.

In so much, however, as the temperature dependence of material properties is such a critical input for the accurate calculation of temperatures, strains, and stresses due to welding, a quick look through the available literature shows a rather disappointing situation. Tall [53] in his pioneering 1964 study on residual stresses in welded plates, as well as many other investigators after him, including this author, have observed a great variation in the temperature dependence of properties among materials differing only slightly in chemical composition. On top of that, most available data on the properties do not include the high side of the temperature range of interest, the reason being the great difficulties encountered in the measurement of properties at elevated temperatures.

The combination of the above facts has thus left analysts with no other alternative but to approximate the elevated temperature properties through careful extrapolations, or even worse, to approximate the non-available properties of some materials from the available ones of materials with similar chemical compositions through an averaging process. It is obvious, though, that such or similar techniques do not only lack adequate accuracy but can, in some cases, lead to significant errors. This situation tends to improve in recent years

especially with respect to materials widely used in critical structures, such as stainless steels in nuclear reactors, and where accurate analyses are of paramount importance from the safety standpoint.

As far as the welding problem is concerned, however, particularly in the case of high strength quenched and tempered steels, such as HY-80 and HY-130, the situation has not improved. The availability of elevated temperature properties of these materials is at best scant, if not nonexistent. The problem is further complicated by the presence of the molten pool, becoming the weld metal when solidified, which exhibits different properties than the base metal, something due to both chemical composition differences and differences in the heat treating it is subjected to during the welding cycle. Most investigators, though, have chosen to neglect this latter effect not because it complicates the problem but because of the high uncertainty involved; in other words the assumption of same material properties for the weld and base metals is as good as any in the absence of concrete information.

Having made the above observations, an effort will be undertaken in the next two subsections to approximate the temperature dependence of the HY-130 properties in the best possible way. A similar effort made by Schrodt [39] in 1974 will be utilized as the starting point coupled with information that has become available since then, especially on the material's transformation kinetics.

3.3.1 Mechanical Properties

An estimated stress-strain curve at room temperature for HY-130 is shown in Fig. 3.4 as developed by the author using data from Willner and Salive [54] and Schrodt [39], and pertaining to tension. In the case of compression Flax et al [38] report that the σ-ε curve is displaced by about 10-15 ksi (70-105 MPa) higher; for the purposes of this study, however, it will be assumed that the same curve can represent both tension and compression.

The figure reveals that at room temperature HY-130 has a Young's modulus, E, equal to 30×10^3ksi (2×10^5 MPa) and that the 0.2% offset yield stress (point A) is equal to 143 ksi (986 MPa).

At this point some notes on the modeling to be used for the stress-strain relationships are in order. During the welding thermal history part of the material undergoes plastic deformation at high temperatures accompanied by conditions of loading and unloading reminiscent of cases involving cyclic stress-strain responses. For these kinds of responses, it is a well established fact [55,57] that they are highly dependent on past history of the material - for example, in uniaxial cyclic tests it was found that the σ-ε curves depend strongly on the strain range. It would be thus impossible to realistically model such cases in an analysis, especially since no such experimentally confirmed σ-ε curves exist nor do proven multiaxial theories that can adequately predict the nonlinear, history-dependent material behavior under arbitrary no radial

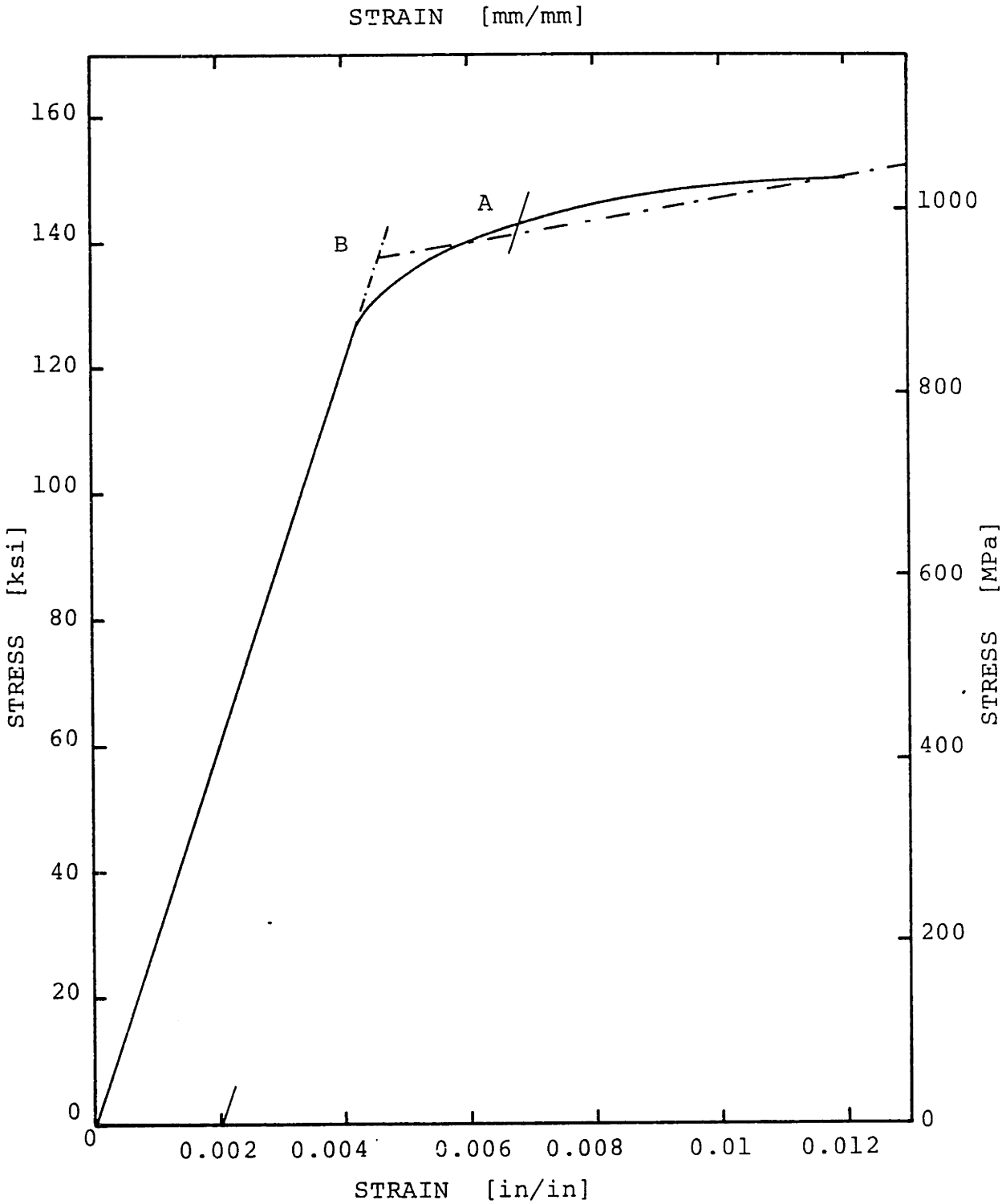

FIGURE 3.4 Typical Stress-Strain Diagram for HY-130 Steel at Room Temperature.

loading.

As a way out researchers at the Oak Ridge National Laboratory [57] have proposed the use of an approximating theory based on the bilinear representation of the uniaxial stress-strain curve for the virgin material in the case of initial loading; their similar proposal for subsequent loading cycles are of no relevance to the welding problem. According to this approach, which is claimed to be conceptually and mathematically consistent for general non-proportional loadings, the elastic segment of the bilinear curve is represented by a straight line determined by the initial response of the material, i.e. a line having a slope equal to the material's Young's modulus; and the elastic-plastic segment of the curve is represented by a straight line connecting the stress point at the maximum expected elastic plus plastic strain, ε_{max}, to the stress point, at strain $\varepsilon_{max}/2$*. The intersection of these two lines will then determine a point defined as the virgin yield point, σ_{yv}; furthermore, the slope of the elastic-plastic segment defines the material tangent modulus, E_T.

Following the procedure described above and assuming, based on experimental data, a maximum strain equal to 1.2%, the bilinear representation of the HY-130 uniaxial stress-

---

*Note that in the case of multiaxial strain state the maximum strain should be assessed on the basis of the effective strain, $\bar{\varepsilon}$, defined by

$$\bar{\varepsilon} = \left(\frac{2}{3}\,\varepsilon_{ij}\varepsilon_{ij}\right)^{1/2}$$

strain curve at room temperature was constructed as shown in Fig. 3.4. The room temperature values of the virgin yield stress, σ_{yv}, (point B) and tangent modulus, E_T, can then be read as 138 ksi (950 MPa) and 1.6×10^3 ksi (11×10^3 MPa) respectively.

Yield stress. The approximate effect of temperature on the virgin yield stress is shown in Fig. 3.5 as developed from available data on T-1 steel (a commercially available quenched and tempered high strength steel with mechanical properties close to those of HY-80) [58] and a low alloy high strength Ni-Cr-Mo-V steel [59]. Note that although the available data pertained to the 0.2% offset yield stress, it was assumed that a similar behavior would be expected for the virgin yield stress, σ_{yv}. Furthermore, most of the elevated temperature data run up to about 1200°F (650°C) making it necessary to extrapolate for higher temperatures and up to the solidus; this was done bearing in mind that at very high temperatures the material loses most of its strength, becoming unable to sustain any strength in its molten state.

A comparison of Fig. 3.5 with similar ones proposed by Hibbitt [6,60] and Cacciatore and Morante [61] for the HY-130 steel reveals many qualitative similarities, although the latter ones pertain to the 0.2% offset yield strength and have been idealized by straight line approximations. Quantitative differences include a faster reduction in yield stress with temperature as compared to Fig. 3.5 and higher values in

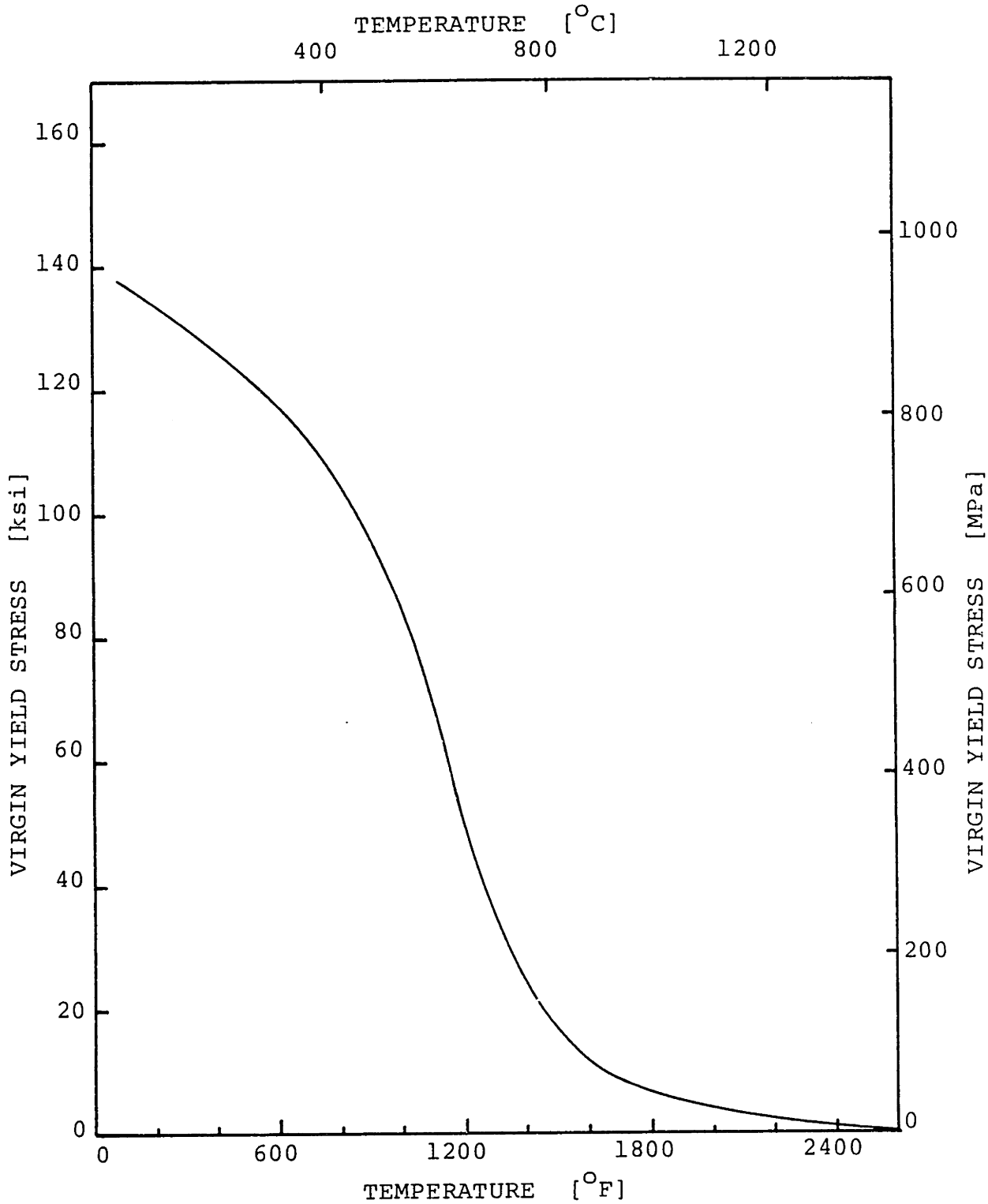

FIGURE 3.5 Variation of Virgin Yield Stress with Temperature for HY-130.

the transformation temperatures, depicted in the diagrams by changes in the curves' slopes.

Young's modulus. Figure 3.6 presents the approximate effect of temperature on the Young's modulus for HY-130. It was developed using again data from the T-1 steel [58]. The observations made above with respect to the virgin yield stress hold here as well for the most part.

Tangent modulus. Looking at most uniaxial stress-strain curves one observes that the tangent (or plastic or work-hardening) modulus, represented by the slope at any point of the elastic-plastic segment of the stress-strain curve, changes with the stress level; and that for the case of work-hardenable materials it decreases with increasing stress level. This is not the case, however, for the bilinear representation of the stress-strain curve where a unique tangent modulus is defined at each temperature.

Having said that, the question arises on how to evaluate the temperature dependence of the tangent modulus, given the fact that nowhere in the literature does such data exist and that the investigators who have studied the HY-130 welding response have assumed an elastic-perfectly plastic material [6,60,61]. The answer can be given by assuming a proportionality between the tangent and Young's moduli at all temperatures which leads to the following equation:

$$E_T(\theta) = \frac{E_T(\theta_e)}{E(\theta_e)} \cdot E(\theta)$$

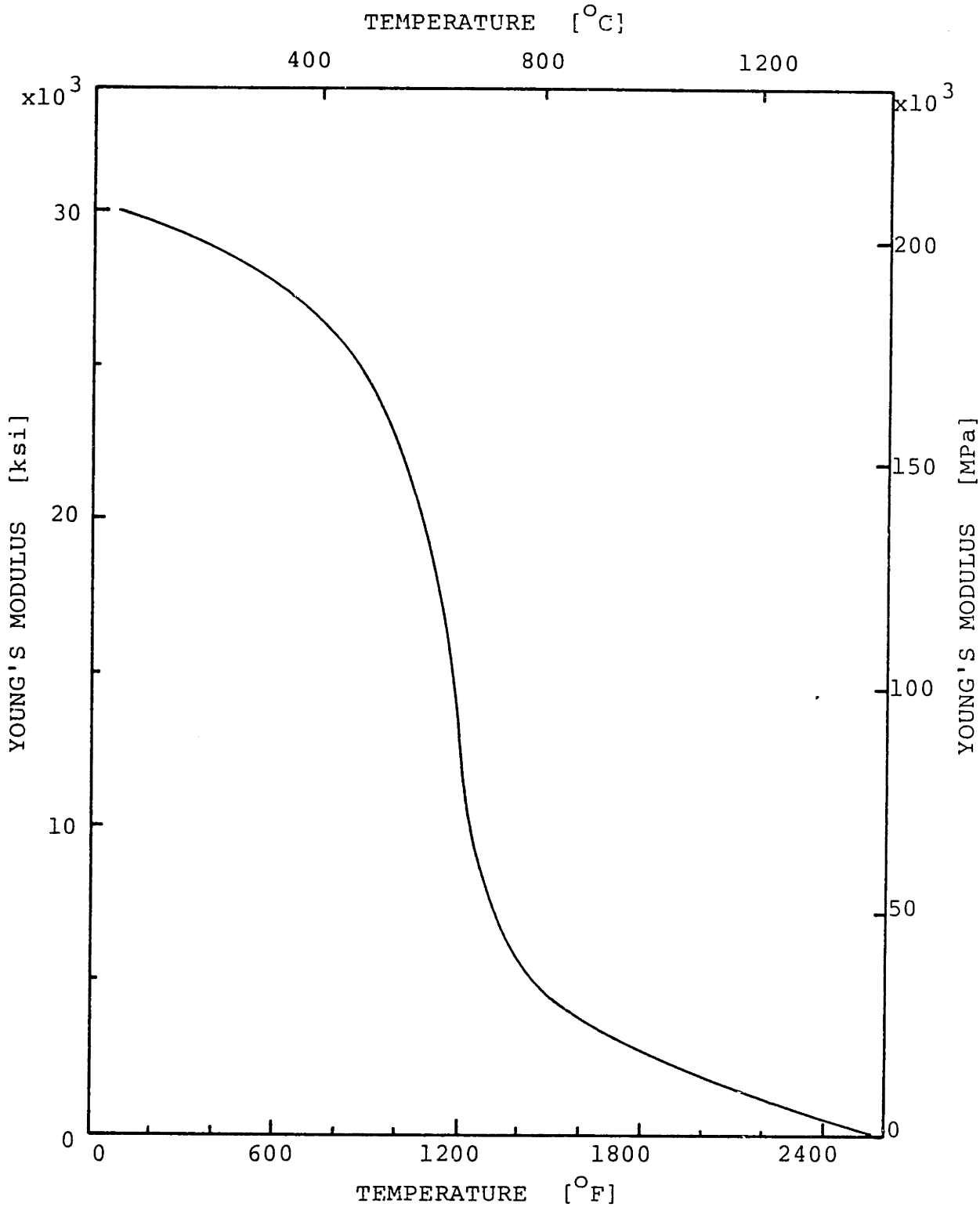

FIGURE 3.6 Variation of Young's Modulus with Temperature for HY-130.

where $E_T(\theta_e)$ and $E(\theta_e)$ are the values of the tangent and Young's moduli at room temperature, and $E_T(\theta)$ and $E(\theta)$ the corresponding values at any other temperature.

Based on the above assumption and Fig. 3.6, Fig. 3.7, showing the approximate variation of tangent modulus with temperature, was constructed.

Stress-strain diagram. On the basis of the temperature variation of σ_{yv}, E, and E_T as earlier depicted, Fig. 3.8 was made showing the bilinear approximations of the HY-130 stress-strain diagrams at various temperatures ranging from room to 2000°F (1090°C). The figure clearly depicts the effects of a temperature change on the material. A decrease in the yield strength and the elastic region is a consequence of a temperature increase, making it possible for plastic flow to occur under constant stress even if the material was fully elastic at lower temperatures. This phenomenon is even more pronounced at very high temperatures where plastic flow can be initiated at very low stress levels. Such a behavior is obviously of paramount importance in welding and is the cause of residual stress formation. Moreover, a temperature increase results in a reduction of the tangent modulus, which means that for a specimen under constant applied stress and already exhibiting plastic flow, the further increment of plastic flow corresponding to a given temperature increment will decrease as the temperature level is increased. On the other hand, a decrease in temperature under constant stress will not result in any plastic strain decrease (since plastic strain is

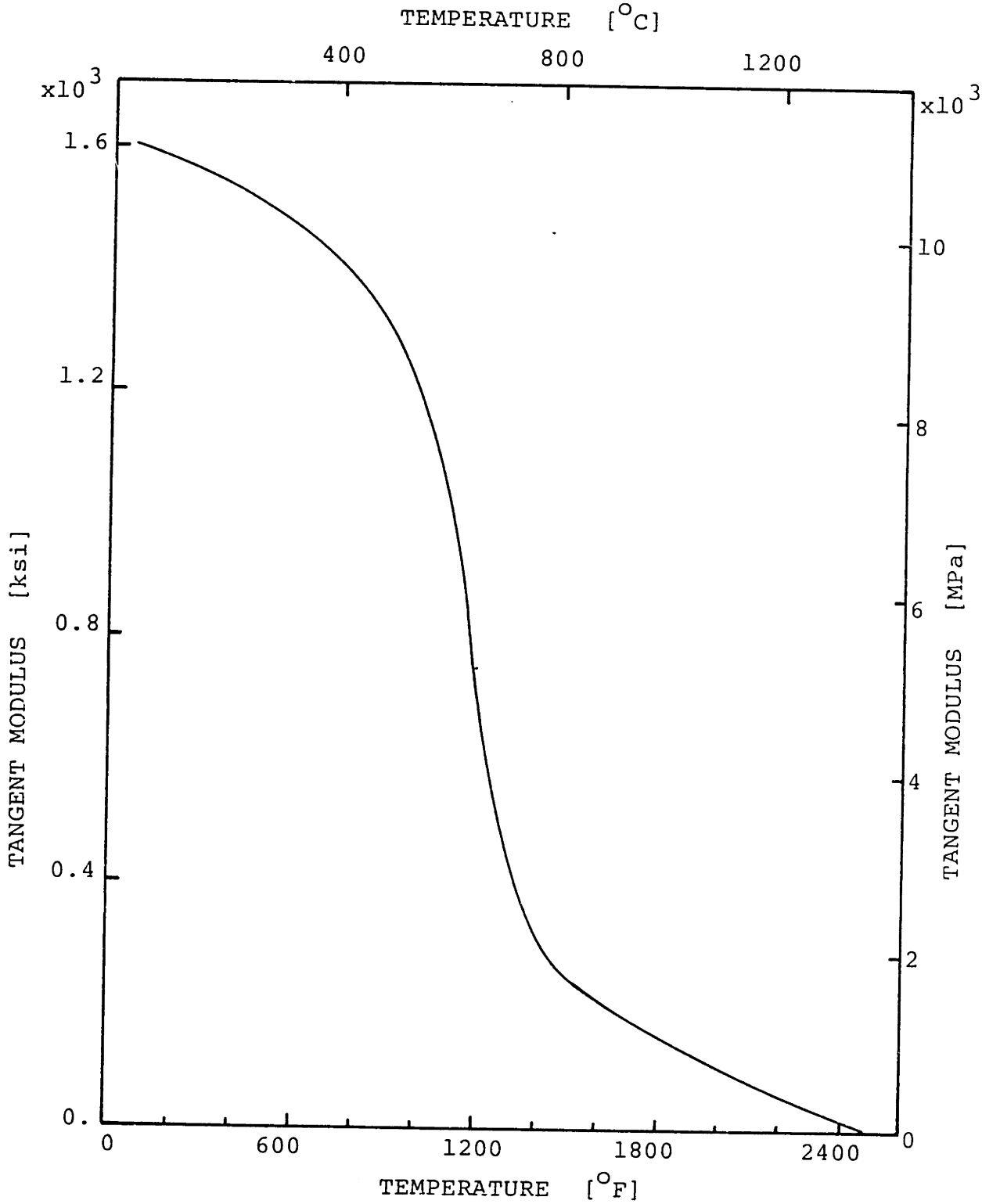

FIGURE 3.7 Variation of Tangent Modulus with Temperature for HY-130.

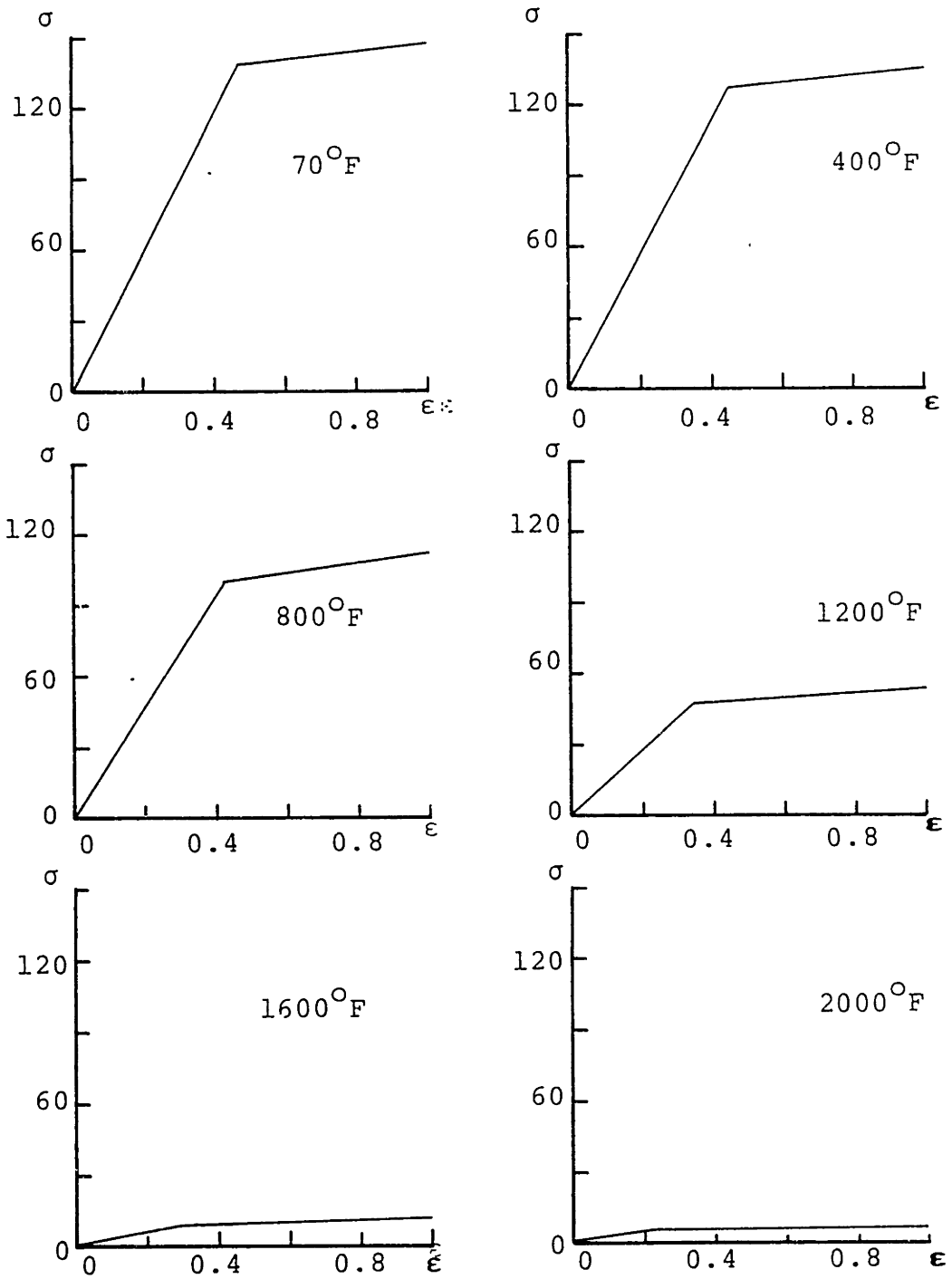

FIGURE 3.8 Bilinear Stress-Strain Diagrams for HY-130 at Various Temperatures.

irrecoverable) but rather in a small elastic strain decrease, owing to an increase in the Young's modulus.

Poisson's ratio. The variation of Poisson's ratio with temperature is shown in Fig. 3.9 as proposed by Hibbitt [6]. A linear variation is shown from a value of 0.30 to 0.454 as temperature varies from room temperature to 2600°F (1430°C); in other words, Poisson's ratio tends to a value of one half as temperature increases, but it does not reach it in the melting region because of volume change considerations (at 0.50 there would be no volume change in the molten pool).

Friedman [62], in a welding thermomechanical analysis involving the Iconel Alloy 600, reports that a better choice for the Poisson's ratio's temperature variation would be one which, when coupled with the Young's modulus' variation, would always provide for a constant bulk modulus, $B = E/3(1-2\nu)$, equal to its room temperature value. He claims that by following this approach possible ill-behavior of the solution can be avoided and convergence facilitated. This proposition was not verified in the present study since the solution converged using the assumed variations outlined above.

To summarize the variation of the mechanical properties of HY-130 with temperature, Tables 3.6a and 3.6b were prepared and presented here.

3.3.2 Physical Properties

The effect of temperature on the thermal conductivity, k, specific heat, c, average thermal expansion coefficient, α, and density, ρ, will be discussed in this section.

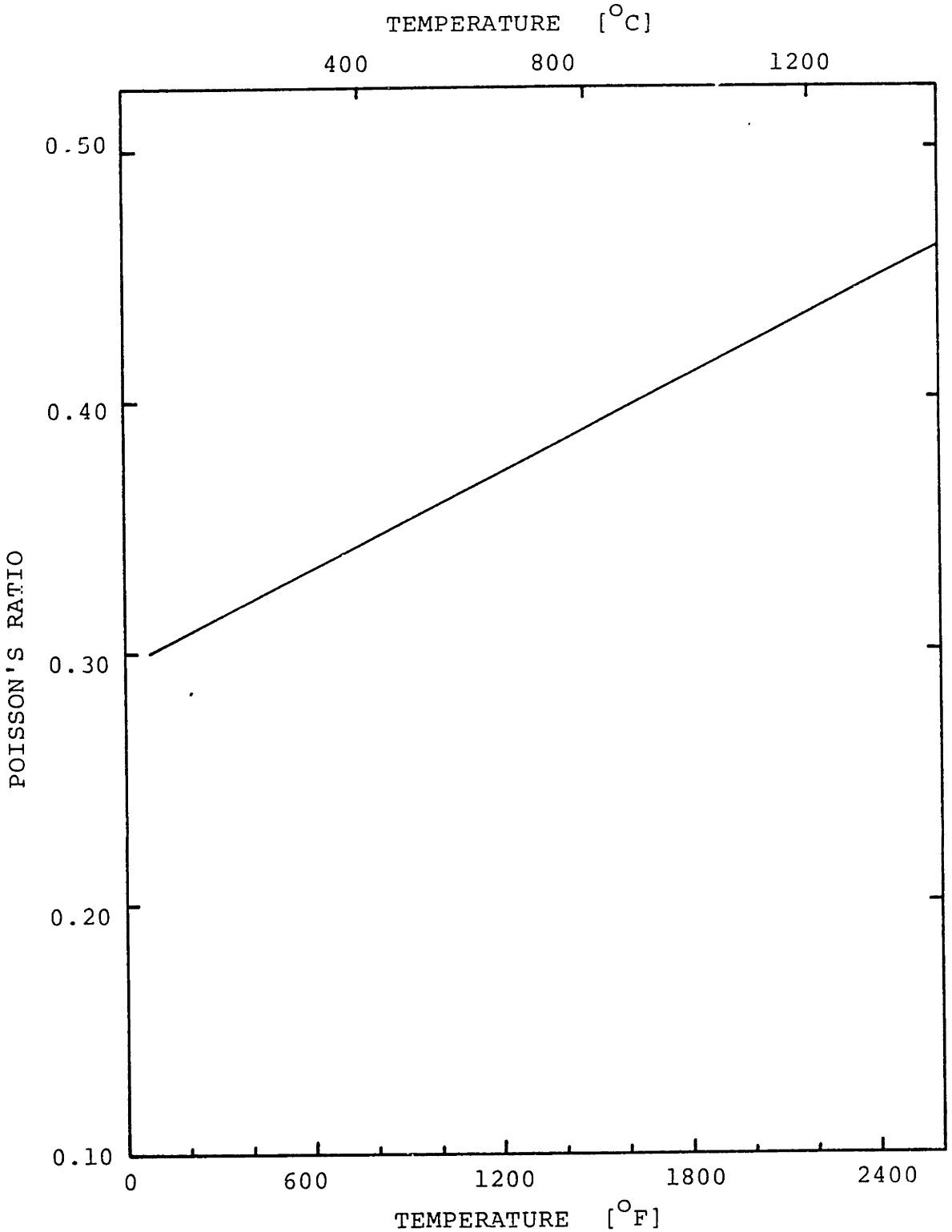

FIGURE 3.9 Variation of Poisson's Ratio with Temperature for HY-130.

TABLE 3.6a Summary of Mechanical Properties for HY-130 (Anglo-Saxonic units)

θ	70	200	400	600	800	1,000	1,200	1,400	1,600	1,800	2,000	2,200	2,400	2,600	2,700	2,800
σ_{yv}	138	133.5	126.7	117	106	85	49	24.5	11	5.8	4	2	1	0	0	0
E	30	29.6	28.8	27.7	26	22.7	14	5	4	3	2	1.2	0.4	0	0	0
E_T	1.60	1.58	1.54	1.48	1.39	1.21	0.75	0.27	0.21	0.16	0.11	0.06	0.02	0	0	0
ν	0.300	0.308	0.321	0.334	0.346	0.359	0.372	0.384	0.397	0.410	0.422	0.435	0.447	0.454	0.454	0.454

Nomenclature

θ = Temperature (^{o}F)

σ_{yv} = Virgin Yield Stress (ksi)

E = Young's Modulus (ksi x 10^{-3})

E_T = Tangent Modulus (ksi x 10^{-3})

ν = Poisson's Ratio

TABLE 3.6b Summary of Mechanical Properties for HY-130 (SI units)

θ	20	200	300	400	500	600	700	800	900	1,000	1,100	1,200	1,300	1,400	1,500
σ_{yv}	950	872	820	751	648	472	248	124	69	41	27.6	17.2	8.3	3.2	0
E	206	200	192	183	167	132	56.5	33.1	25.5	20	14.5	9.6	2.8	0.4	0
E_T	11	10.7	10.3	9.8	8.9	7	3	1.8	1.4	1.1	0.8	0.5	0.15	0.02	0
ν	0.300	0.320	0.331	0.342	0.353	0.364	0.374	0.385	0.396	0.407	0.418	0.429	0.440	0.451	0.462

Nomenclature

θ = Temperature (^{o}C)

σ_{yv} = Virgin Yield Stress (MPa)

E = Young's Modulus (MPa x 10^{-3})

E_T = Tangent Modulus (MPa x 10^{-3})

ν = Poisson's Ratio

Thermal conductivity. In the absence of any information regarding the temperature variation of the HY-130 steel's thermal conductivity, Fig. 3.10 was constructed based on data for a low alloy 3.4 Ni-Fe steel [63]. These data were available up to a temperature of 1400°F (760°C); from this temperature and up to the solidus (2600°F or 1430°C) line a linearly increasing variation was assumed based on the fact that an increase is expected with temperature*. Note that this assumption is different from that made by other investigators who usually treat the thermal conductivity as constant from the highest temperature for which data exists and up to the solidus temperature. The adequacy of either assumption is of course open to question, and only the experimental determination of the required high temperature data can serve to test their validity.

A much more formidable problem is the one concerning the characteristics of heat transfer in the liquid metal. Although this problem will be addressed in some detail in the next chapter, a few words are in order here as far as the thermal conductivity is concerned. Tsai [29], Hibbitt [6], and other investigators have assumed that the thermal conductivity in the weld molten pool is much lower than the one of the solid metal, sometimes an order of magnitude lower. This assumption,

*Heat is conducted through metals by two distinct mechanisms: one involves the transfer of thermal energy by the free electrons in the metal, and the other results from the coupling together of the vibrations of the atoms in the crystal [49]. Both contributions are expected to result in an increase in thermal conductivity at high temperatures.

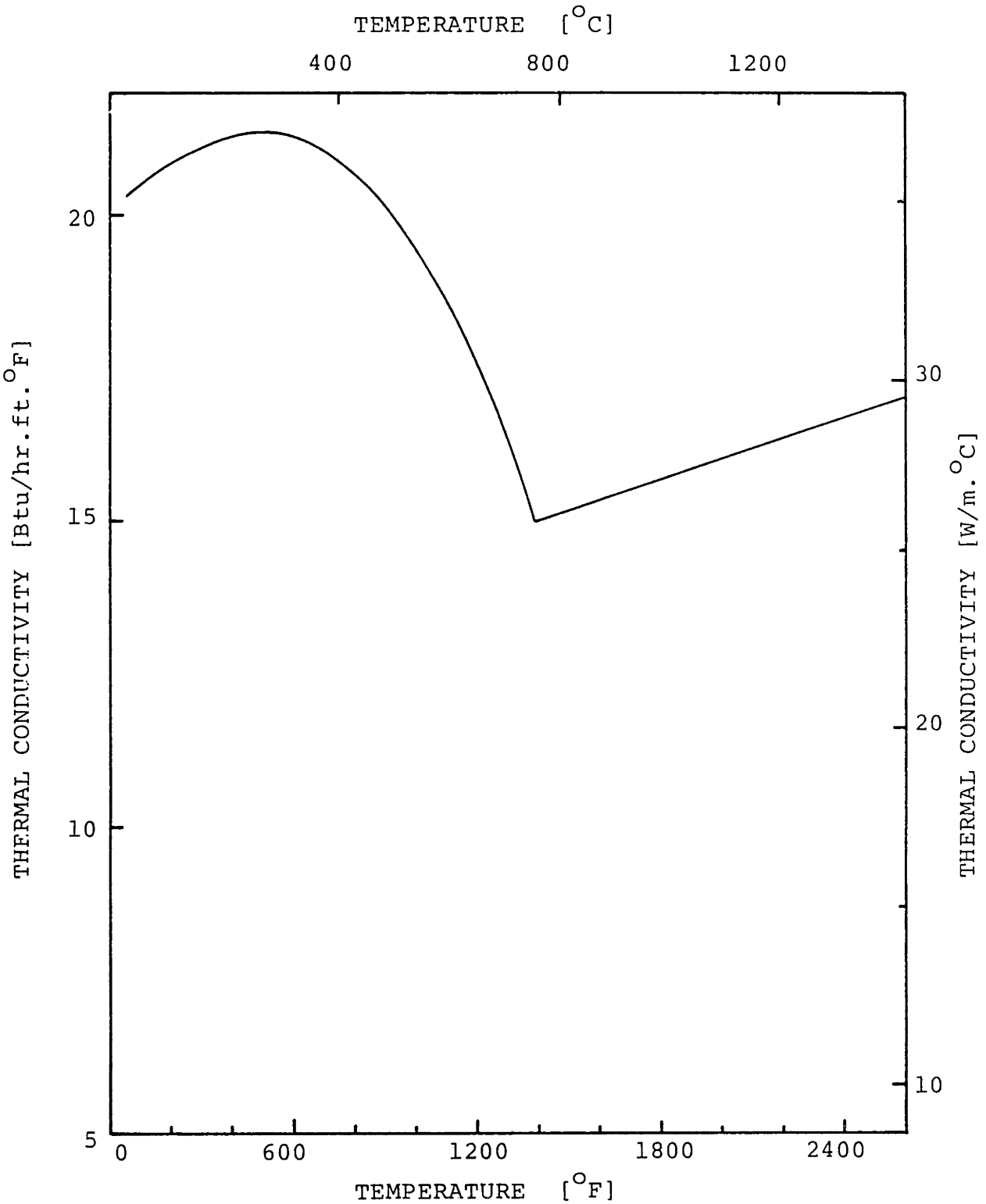

FIGURE 3.10 Variation of Thermal Conductivity with Temperature for HY-130.

although consistent with the fact that metal liquids have smaller thermal conductivity than the corresponding solid metals, does not take into account the question regarding the actual heat transfer mechanism in the weld pool, a mixture of conduction and convection. Although this mechanism has not been adequately modeled yet, several researchers, Friedman [64] among them, have maintained that the molten metal thermal conductivity, an equivalent and not a true one, can be assumed to realize a value much higher than the solid metal one. In other words, the convective part of the heat transfer mechanism is expected to increase the heat flow to a level above the one explained by pure conduction.

This latter approach was followed in the present study. Details of the actual values of k tested will be presented at the appropriate places in the next chapter.

Specific heat. The same difficulties, as the ones described for the thermal conductivity, were encountered in the case of the temperature variation of HY-130 steel's specific heat, c. Figure 3.11 was constructed on the basis of a low-alloy carbon steel, having a carbon content of 0.10 percent [63]. The graph shown includes a high peak of 0.354 Btu/lbm.°F (1.48kJ/kg.°C) at 1400°F (760°C) signifying the inclusion of the latent heat (16.4 Btu/lbm) in the allotropic phase transformation that takes place at the temperature range around this temperature (ferrite to austenite upon heating and vice versa upon cooling) under equilibrium conditions. It is understood that this inclusion of the latent heat is very approximate

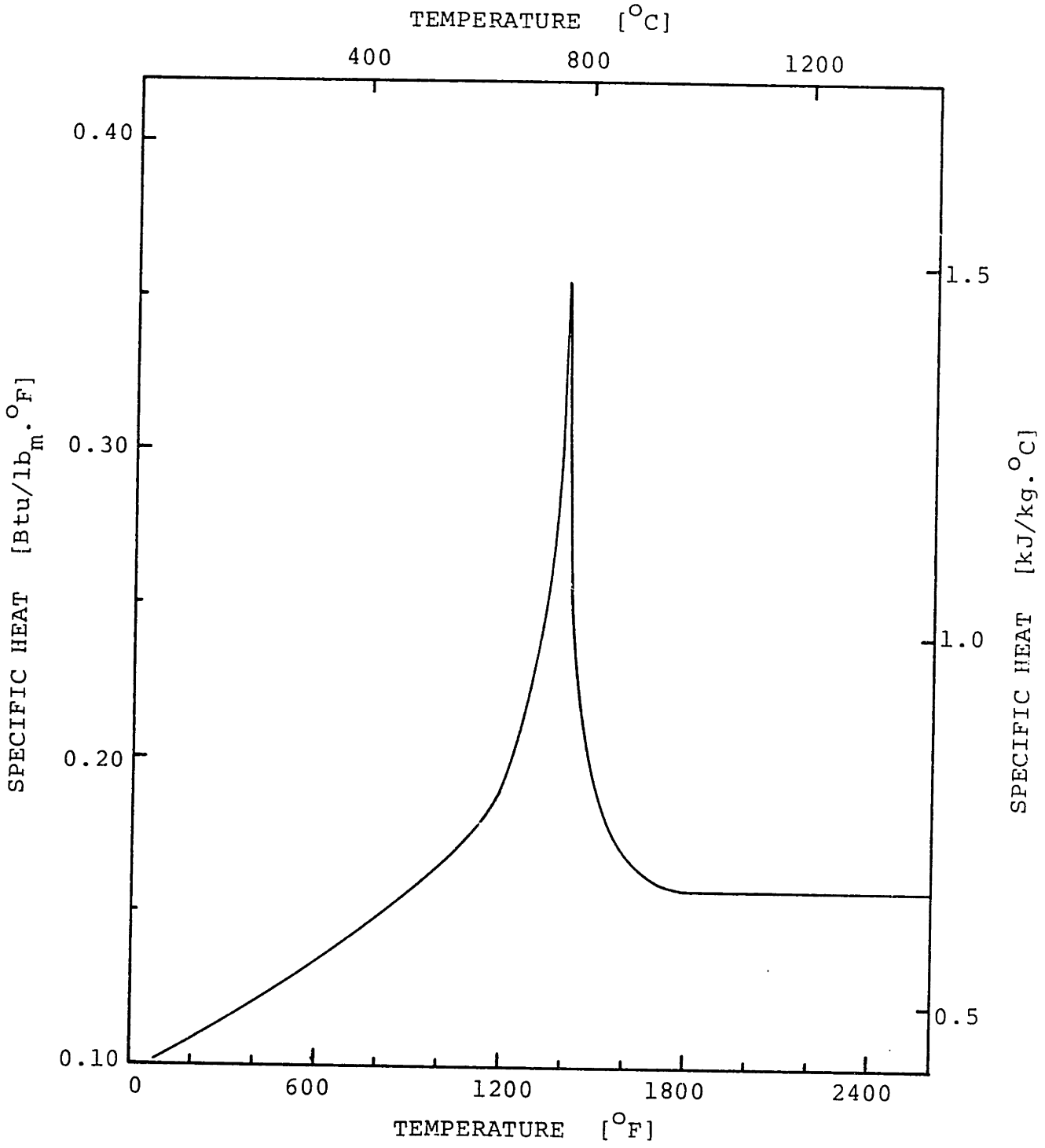

FIGURE 3.11 Variation of Specific Heat with Temperature for HY-130.

since it does not take into account the nonequilibrium transformations that take place during the cooling stage of the welding cycle (austenite to bainite and/or martensite); in the absence of any other data, however, this is the best one can do.

As far as the high temperature region (close to the solidus line) is concerned, a constant specific heat was assumed owing again to the absence of data. Beyond the solidus temperature, where a solid-liquid transformation takes place, the latent heat effect is not shown as an equivalent increase in the specific heat, but is treated explicitely in the numerical calculations, as discussed in the next chapter. The latent heat value chosen is the one proposed by Hibbitt [6] for both the HY-130 and HY-80 steels and is equal to 118 Btu/lbm (275 kJ/kg).

Average thermal expansion coefficient. The temperature variation of the average thermal expansion coefficient, α, for HY-130 is shown in Fig. 3.12 and is based on values of the same low-alloy carbon steel used for the specific heat's temperature dependency [63]. Note the abrupt reversal in slope that takes place at around 1400°F (760°C) which is due to the allotropic phase transformation occuring under equilibrium conditions upon heating or cooling.

It should be emphasized at this point that Fig. 3.12 pertains to equilibrium conditions only, i.e. it assumes similar allotropic transformations occuring in both the heating and cooling stages of a temperature cycle. This is not the case,

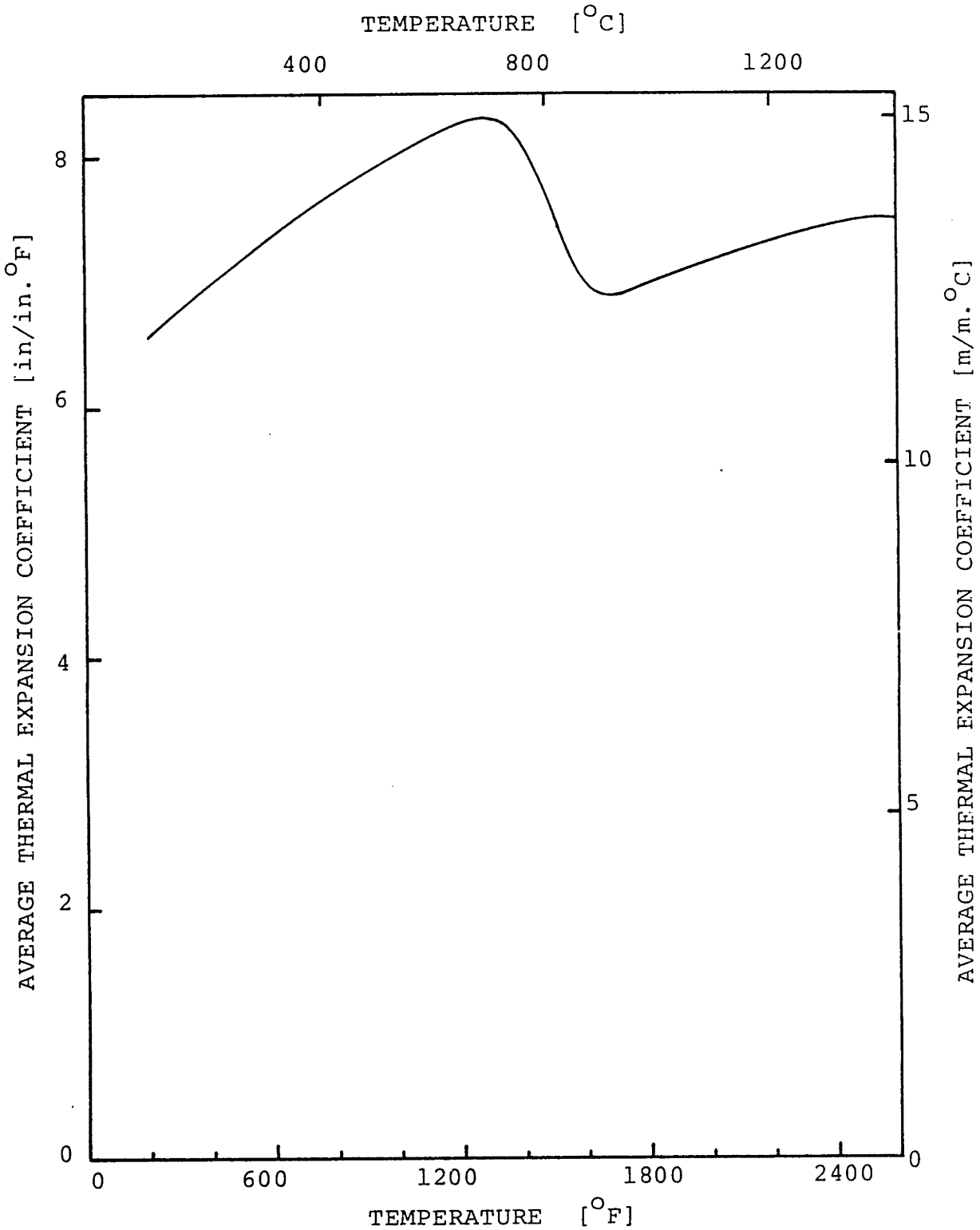

FIGURE 3.12 Variation of Average Thermal Expansion Coefficient with Temperature for HY-130.

however, for welding where nonequilibrium conditions prevail and where the allotropic phase transformations upon heating (ferrite or martensite to austenite) and cooling (austenite to bainite and/or martensite) are different and take place within different temperature intervals. As a consequence, Fig. 3.12 cannot be strictly applied. Instead, a more fundamental approach based on first principles should be devised. Such an approach is outlined in detail in Chapter 5.

Density. Figure 3.13 shows the variation with temperature of the density, ρ, of HY-130. It was calculated on the basis of a measured density of 0.284 lbm/in^3 (7.86×10^3 kg/m^3) at 70°F (21°C) and the thermal expansion data presented in Fig. 3.12.

To summarize the variation of the physical properties of HY-130 with temperature, Tables 3.7a and 3.7b were prepared and presented here.

3.4 Computed Continuous Transformation Diagram from Isothermal Data

As mentioned in Section 3.2.2, continuous cooling transformation (CCT) diagrams are more appropriate than isothermal transformation (TTT) diagrams for predicting the steel microstructures during the cooling stage of the welding cycle. Today, experimentally derived CCT diagrams exist for several steel alloys (see for example Cavanagh [65] for an extended bibliography), thus making such predictions possible. There are, however, alloys -- the HY-130 steel being

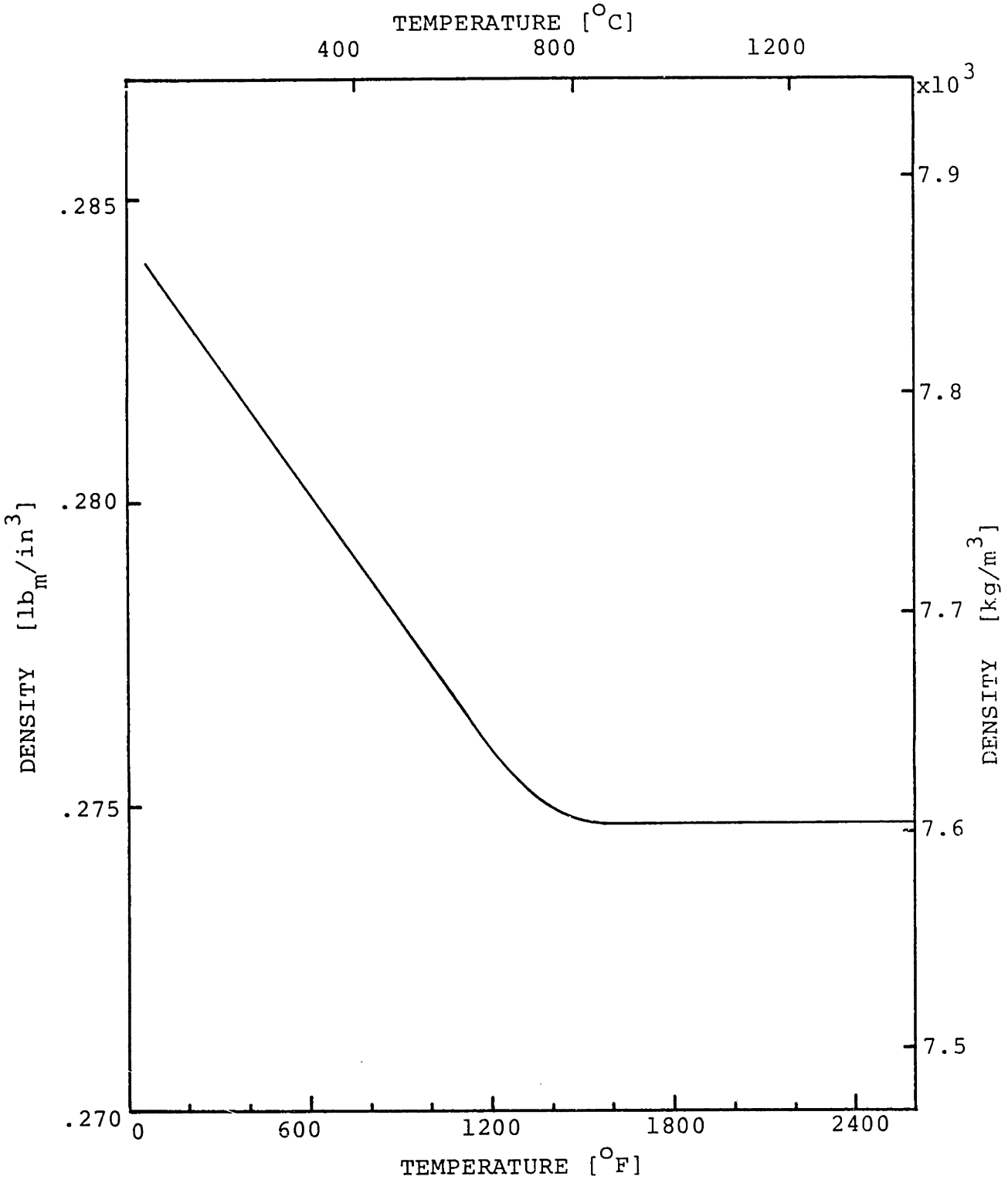

FIGURE 3.13 Variation of Density with Temperature for HY-130.

TABLE 3.7a Summary of Physical Properties for HY-130 (Anglo-Saxonic units)

θ	70	200	400	600	800	1,000	1,200	1,400	1,600	1,800	2,000	2,200	2,400	2,600
k	20.03	20.9	21.3	21.03	20.7	19.5	17.6	14.9	15.3	15.7	16	16.4	16.7	17
c	0.102	0.110	0.120	0.132	0.148	0.166	0.190	0.354	0.168	0.156	0.156	0.156	0.156	0.156
ρ	0.2839	0.2830	0.2816	0.2802	0.2788	0.2773	0.2759	0.2749	0.2747	0.2747	0.2747	0.2747	0.2747	0.2747
α	--	6.55	6.97	7.35	7.75	8.06	8.23	8.15	6.95	7	7.18	7.30	7.45	7.50

Nomenclature

θ = Temperature (^{o}F)

k = Thermal Conductivity (Btu/hr.ft.^{o}F)

c = Specific Heat (Btu/lb_m.^{o}F)

ρ = Density (lb_m/in^3)

α = Average Thermal Expansion Coefficient ($in/in^{o}F \times 10^{-6}$)

TABLE 3.7b Summary of Physical Properties for HY-130 (SI units)

θ	20	200	300	400	500	600	700	760	900	1,000	1,100	1,200	1,300	1,400	1,500
k	35.1	36.8	36.8	36.2	34.6	32.0	28.5	25.8	26.6	27.2	27.8	28.4	29.0	29.6	--
c	0.427	0.502	0.548	0.602	0.665	0.741	0.481	0.686	0.653	0.653	0.653	0.653	0.653	0.653	--
ρ	7.860	7.795	7.759	7.725	7.690	7.654	7.620	7.609	7.604	7.604	7.604	7.604	7.604	7.604	--
α	--	12.51	13.18	13.77	14.27	14.87	14.94	14.67	12.42	12.60	12.92	13.14	13.36	13.50	--

Nomenclature

θ = Temperature (^{o}C)

k = Thermal Conductivity ($W/m.^{o}C$)

c = Specific Heat ($kJ/kg.^{o}C$)

ρ = Density ($kg/m^3 \times 10^{-3}$)

α = Average Thermal Expansion Coefficient ($m/m.^{o}C$)

one of them -- for which CCT diagrams are not available. In such instances the analyst would like to be able to compute a schematic CCT diagram based on available isothermal data and resembling as closely as possible the experimentally obtained one.

Bain [66] is credited with the first such schematic cooling diagrams; it indicated the beginning of transformation and the structures produced by several typical cooling rates for a eutectoid steel.

Grange and Kiefer [67] were among the first to theoretically compute a CCT diagram from a TTT one. The essence of their method consists of representing any stage of the cooling by a point on the isothermal diagram which indicates, by its position, the equivalent amount of transformation that has occurred on cooling to that temperature at the specified rate. In other words, on cooling through a limited temperature range, the amount of transformation is assumed equal to that indicated with an isothermal curve at an average temperature and for an equal time interval and transformation extent. More details on the method will be included in Appendix C. Their method predicted curves possessing the same general shape but lying to the left and above the measured curves.

Although the above method resulted in reasonably close agreement between experimental and calculated CCT curves for a Ni-Cr-Mo eutectoid steel, Manning and Lorig [68] were re-

luctant to apply the same technique to any steel composition, claiming it to be entirely empirical. Working with five steels of varying Cr content, they instead upheld the validity of the additivity concept when restricted to one austenitic decomposition mechanism at a time. This concept, first proposed by Scheil [69], states that the time spent at a particular temperature divided by the time required for beginning transformation isothermally at that temperature represents a fraction of the incubation requirement. Transformation thus begins when the sum of these fractions reaches unity. In mathematical terms this rule of additivity can be stated as follows: Suppose that an isothermal reaction has reached a certain fraction of completion, f_o, at time τ which is a function of temperature. Then on continuous cooling, the fraction completed will be f_o at that time t and temperature θ at which

$$\int \frac{dt}{\tau} = \int \frac{d\theta}{\tau\left(\frac{d\theta}{dt}\right)} = \int \frac{df}{\tau\left(\frac{df}{dt}\right)} = 1$$

The results obtained by Manning and Lorig using this technique (described in more detail in Appendix C) were of the same general nature as the ones previously derived by Grange and Kiefer.

A question thus arose regarding the validity of the additivity rule. Cahn [70] in 1956 finally eliminated much of the confusion by supporting its application if one of

two cases existed:

(a) the transformation process is "isokinetic", i.e., the nucleation and growth rates are proportional over a range of temperature

(b) the nucleation is restricted to the beginning of the transformation product formation, i.e., the transformation is growth-dependent which usually means temperature-dependent.

The second case exists at relatively high cooling rates, which is the situation encountered in the heat affected zone (HAZ) of welds.

Since the advent of the computer several other investigations, including Markowitz and Richman [71] and Kennon [72], tried to improve upon the calculated CCT curves by using the methods previously described but with much smaller time increments. The discrepancy they found with the experimental curves was usually smaller and in the reverse direction.

3.4.1 Application in the Case of HY-130 Steel

Given the fact that no comprehensive CCT diagram existed for the HY-130 steel, it was decided to apply the two methods, Grange-Kiefer and Manning-Lorig, in an effort to calculate such a diagram based on the isothermal one described in Section 3.2.1 and depicted in Figure 3.1.

One important note has, however, first to be made. The CCT diagram is heavily dependent not only on the type of alloy considered, but also, for the same alloy, on the cool-

ing rate. All of the methods described previously utilize linear cooling rates, although the authors point out that the procedures can be modified to encompass any type of cooling rate. On the other hand, looking at the temperature curves during welding (see Chapters 2 and 4), it is obvious that the cooling rates encountered are far from linear. Plotting them, however, on a semilogarithmic graph (linear scale for temperatures, logarithmic scale for time), the emerging picture can be adequately represented by straight lines (the cooling stage of the welding temperature cycle only).

Based on the above observations a modification of the two approaches was made to enable them to handle log-linear cooling curves. The details of these modifications are described in Appendix C.

Figure 3.14 shows the schematic CCT diagrams calculated using both linear and log-linear cooling curves. In the linear case both the Grange-Kiefer and Manning-Lorig approaches predict almost identical bainite start, B_s, transformation curves. This was expected and confirms results obtained by previous investigators. Comparing the obtained curves with the experimental ones shown in Figure 3.2 and 3.3 (although the latter ones are not CCT curves but have been measured using log-linear cooling curves), it is observed that the schematic curves lie below and to the right of the experimental ones, again confirming the more recent investigations

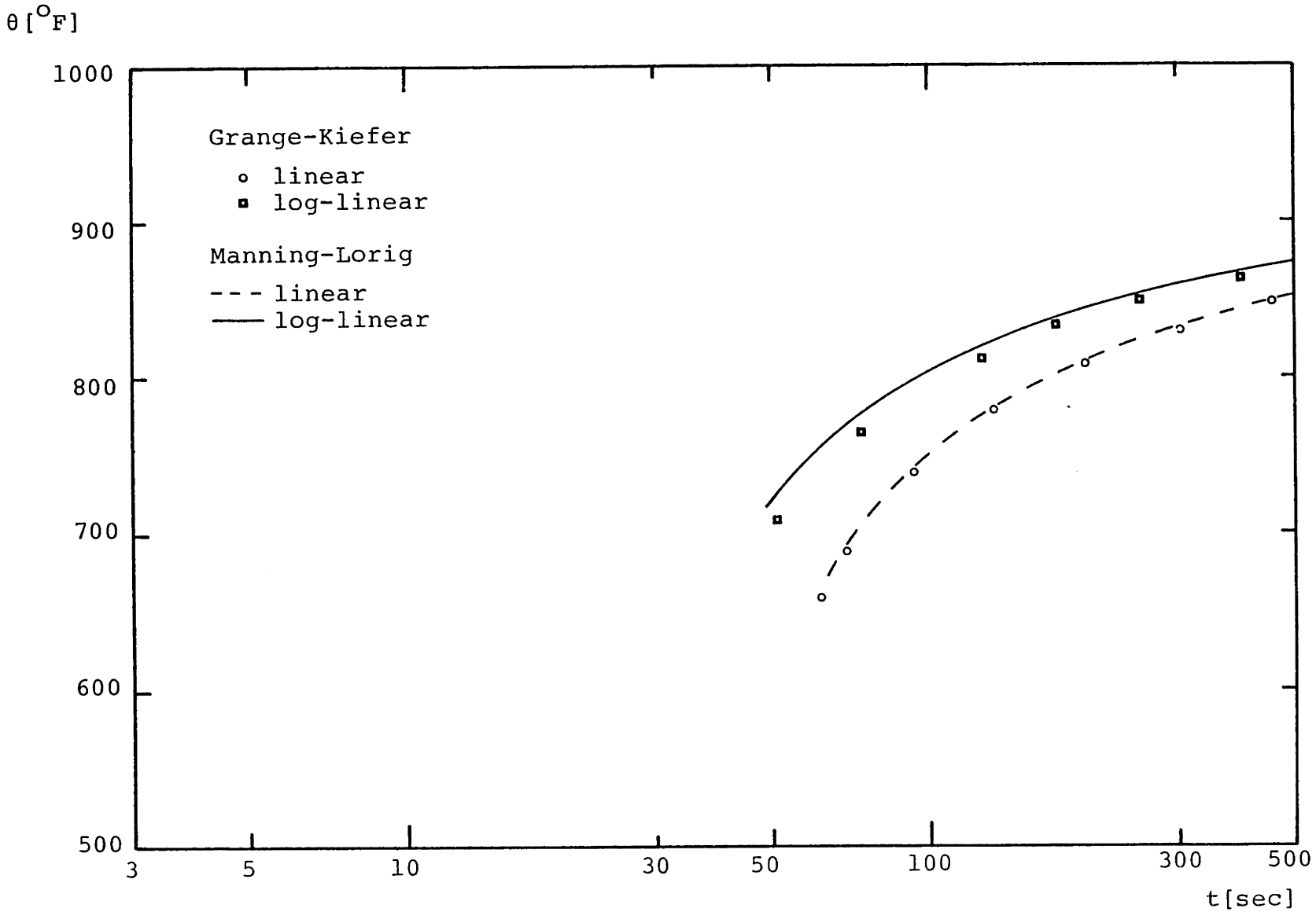

FIGURE 3.14 Schematic CCT Diagrams for HY-130 Steel (Bainite Start Transformation Curves).

[71].

Regarding the log-linear case, the curves derived from both approaches lie above and to the left of the linear ones, with the one predicted using the Manning-Lorig method being slightly further away. As a consequence, both log-linear curves are much closer to the experimentally obtained ones.

It can therefore be concluded that the application of the methods using log-linear cooling curves results in schematic CCT diagrams that are closer to the ones appropriate for predicting microstructures in the HAZ and the weld metal of a weldment. It should be pointed out, however, that an even better approximation can be obtained if the microstructure prediction is based on rate equations. Efforts in this direction have been made for a very few steel alloys, primarily of eutectoid composition (see for example McCullough [73]), and much more research in the materials science field is needed for the development of similar rate equations for more complicated alloys, like the quenched and tempered HY-130 steel. Until such developments are made the above described methods with the proposed modifications are thought to be adequate in describing the phase transformations from an applied mechanics (macroscopic) point of view.

The previous discussion pertained to the bainite start, B_s, transformation temperature and can be extended to include any similar nucleation and growth transformation, such as the ferritic one. As far as the martensite transformation

is concerned, the situation is different. Austenite transforms to martensite athermally (no thermal activation is involved). This means that once the martensite start transformation temperature, M_s, is known, the extent of the transformation is dependent only on the amount of undercooling below the M_s temperature (Burke [74]). It can therefore be assumed that the constant M_s temperature found in the TTT diagram can be carried over to the CCT diagram. As Cavanagh [65] and others have pointed out, however, with the precipitation of ferrite and/or bainite, the build-up of carbon and/or alloy elements in the remaining austenite will alter its M_s temperature, resulting in slightly depressed M_s temperature at slower cooling rates. Although such effects are recognized here, it is felt that due to the uncertainty of the amount of depression and for the purposes of this study, they can be neglected. Similar considerations have been taken into account for the martensite finish, M_f, transformation temperature.

CHAPTER IV

NUMERICAL SOLUTION OF HEAT FLOW DURING WELDING

In Chapter II some analytical solutions to the problem of heat flow during welding were discussed and analyzed. The general conclusion was that these closed form solutions, however complicated they may be, cannot very accurately predict the temperature distribution during welding, especially close to the weld line (i.e., in the weld metal and the HAZ). This is primarily due to the highly nonlinear nature of the problem. Nevertheless, such solutions are very useful in providing insight to the problem and allow for extensive parametric analyses due to their low cost.

On the other hand, there are occasions when an accurate description of the temperature is necessary, as for example when a metallurgical characterization of the weld metal and HAZ is needed, or when a subsequent stress analysis is required to determine the transient strains and residual stresses. In these cases a numerical analysis using the finite difference or finite element method is more appropriate.

In this chapter concern will be focused on the finite element method for solving the heat transfer problem during welding. After a brief literature survey, the model will be discussed in some detail and an assessment of its limitations

will be made.

The results obtained using this model will then be compared with experimentally obtained data. The experiments themselves will also be briefly discussed.

4.1 Literature Survey

Since the advent of the electronic digital computer several serious efforts have been made to numerically solve field, and in particular heat transfer, problems. And although the finite difference method had initially the edge, the advantages of the finite element method, especially if coupled with thermal stress analysis, are more and more recognized today.

Many finite element programs have thus been developed over the years capable of performing heat transfer analyses. Several of these codes can take various nonlinearities into account in a more or less sophisticated manner. One of the most sophisticated ones, and the one actually chosen in this study to solve the welding heat flow problem, is ADINAT (Automatic Dynamic Incremental Nonlinear Analysis for Temperatures) developed by Bathe and co-workers [75 - 77] over a period of years. Some details of this program will be discussed later. It suffices here to mention that ADINAT can take into account temperature dependent material properties as well as nonlinear convection and radiation boundary conditions.

The discussion so far dealt with multipurpose heat trans-

fer finite element method (FEM) programs. Concurrently, however, several investigators concerned with the welding problem have developed similar programs. Hibbitt and Marcal [6, 60] developed such a program in 1973 which was later used by other investigators including Hsu [78] and Nickell [79]. At the Massachusetts Institute of Technology a team headed by Masubuchi has also developed similar programs in the early 1970s [24, 80 - 83]. Friedman [62, 64, 84, 85] has also made substantial contributions in the case of GTA welding working at the Westinghouse Electric Corporation's Bettis Atomic Power Laboratory.

The way each of the above individuals approached the various aspects of the welding problem will be discussed at the appropriate places in the next sections where the way in which the current model was developed will be detailed.

4.2 Finite Element Procedure

As mentioned previously, the welding heat flow analysis was performed using ADINAT. The governing incremental isoparametric finite element equations for this problem have been derived by Bathe [77] and are

$$({}^{t}\underline{K}^{k} + {}^{t}\underline{K}^{c} + {}^{t}\underline{K}^{r})\ \Delta\underline{\theta}^{(i)} = {}^{t+\alpha\Delta t}\underline{Q}$$

$$+ {}^{t+\alpha\Delta t}\underline{Q}^{c(i-1)} + {}^{t+\alpha\Delta t}\underline{Q}^{r(i-1)} - {}^{t+\alpha\Delta t}\underline{Q}^{k(i-1)} \qquad (4.1a)$$

or

$$ {}^{t}\hat{\underline{K}}\ \Delta\theta^{(i)} = {}^{t+\alpha\Delta t}\hat{\underline{Q}}^{(i-1)} \tag{4.1b} $$

where ${}^{t}\hat{\underline{K}}$ is the effective conductivity matrix at time t consisting of the conductivity, nonlinear convection, and radiation matrices; ${}^{t+\alpha\Delta t}\underline{Q}$ is the heat flow vector including the effects of surface heat flow inputs, internal heat generation and temperature-dependent heat capacity; ${}^{t+\alpha\Delta t}\hat{\underline{Q}}^{(i-1)}$ is the effective heat flow vector; and $\Delta\theta^{(i)}$ is the increment in nodal-point temperatures in iteration i,

$$ {}^{t+\alpha\Delta t}\underline{\theta}^{(i)} = {}^{t+\alpha\Delta t}\underline{\theta}^{(i-1)} + \Delta\underline{\theta}^{(i)} \tag{4.2} $$

Equations (4.1) represent the heat flow equilibrium of the body at time $t+\alpha.\Delta t$, where $0 \leq \alpha \leq 1$ and α is chosen to obtain optimum stability and accuracy in the solution. Furthermore, the solution using eqn. 4.1 corresponds to a modified Newton-Raphson iteration.

Boundary conditions. Convection and radiation boundary conditions are taken into account by including the matrices ${}^{t}\underline{K}^{c}$ and ${}^{t}\underline{K}^{r}$ and the vectors ${}^{t+\alpha\Delta t}\underline{Q}^{c}$ and ${}^{t+\alpha\Delta t}\underline{Q}^{r}$ in eqn. (4.1a). Additional external heat flow input on the boundary is specified in ${}^{t+\alpha\Delta t}\underline{Q}$ as surface heat flow input. Prescribed temperature conditions can also be specified.

Time integration schemes. A family of one-step methods [86] is considered for the time integration using the para-

meter α. The scheme was found [77] to be unconditionally stable for $\alpha \geq 1/2$ and to generally give better solution accuracy when $\alpha = 1$ (Euler backward method). Finally the modified Newton iteration is guaranteed to converge provided the time step Δt is small enough.

4.3 Weld Model

In this section all the necessary considerations for the modelling of a multipass weldment between two relatively thick plates -- thickness on the order of 1 inch (25 mm) -- will be discussed. They include the two-dimensionality of the problem, the boundary conditions except the heat input, the material properties, the weld metal and the heat input.

4.3.1 Two-Dimensionality of Problem

The heat flow pattern resulting from a moving welding arc is generally three-dimensional; temperature gradients exist through the weldment's thickness direction, as well as in directions parallel and transverse to the arc travel (welding) one. A closer examination of the physics of the process, however, reveals that the necessary assumptions for the transformation of the problem from a three- to a two-dimensional one are reasonable.

As a starting point and referring to the fixed coordinate system (x,y,z) depicted in Figure 4.1, let's consider the general heat flow equation for a differential element inside the conducting medium:

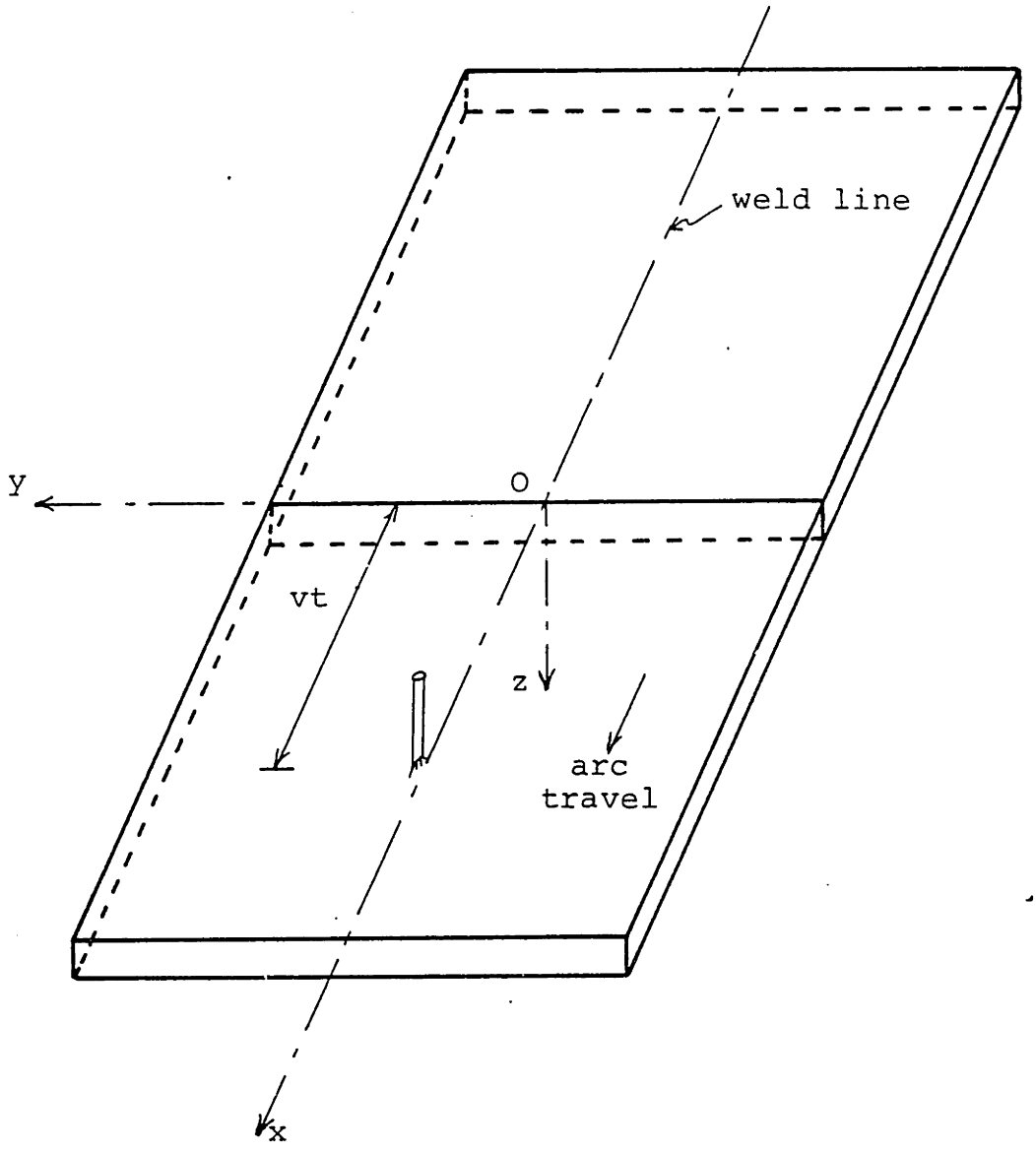

FIGURE 4.1 Weldment Configuration

$$\frac{\partial}{\partial x}\left(k\frac{\partial\theta}{\partial x}\right) + \frac{\partial}{\partial y}\left(k\frac{\partial\theta}{\partial y}\right) + \frac{\partial}{\partial z}\left(k\frac{\partial\theta}{\partial z}\right) + W_i = \rho c\frac{\partial\theta}{\partial t} \qquad (4.3)$$

where all parameters have been previously defined.

For the case of a stationary arc situated above the origin 0 of the coordinate system, the above three-dimensional equation can be solved numerically with no simplifications. Closer examination of the process, however, reveals that the stationary arc (being modeled either as a point source or as a bell shaped function in space) results in heat flow being supplied axisymmetrically to the weldment. Therefore, if the weldment is geometrically regular (a flat plate for example), heat transfer in the weld can be idealized as radially symmetric in the high temperature region of interest -- or everywhere if the dimensions in the xy-plane are large compared to the thickness so as to be for all practical purposes infinite. As a consequence, the welding thermal cycle can be analyzed using a two-dimensional, axisymmetric heat conduction model. This method of analysis was actually used by Friedman [64] in the case of a stationary gas tungsten arc, providing much useful data and insight on the effects of the heat input magnitude and distribution on weld penetration and fusion zone shape.

The problem becomes complicated, however, when the more realistic moving welding arc is considered. A first simpli-

fication of the problem can be attained by assuming that the welding heat source (arc) is moving at a constant speed on a regular path (i.e., a straight line in a planar weld, or a circle in an axisymmetric weld) and that end effects resulting from either initiation or termination of the heat source can be neglected. Under these assumptions quasi-steady state conditions are attained for the fixed coordinate system (x,y,z). Alternatively, the problem can be treated as a steady state one with respect to the moving coordinate system (ξ=x-vt, y,z), where v is the speed of the heat source. To be more precise, introducing the new variable $\tau = t - x/v$, equation (4.3) can be transformed into

$$\frac{\partial}{\partial y}\left(k\frac{\partial\theta}{\partial y}\right) + \frac{\partial}{\partial z}\left(k\frac{\partial\theta}{\partial z}\right) + \frac{1}{v^2}\cdot\frac{\partial}{\partial\tau}\left(k\frac{\partial\theta}{\partial\tau}\right) + W_i = \rho c\frac{\partial\theta}{\partial\tau} \qquad (4.4)$$

With this formulation, the time dependent solution at any section, say x=0, normal to the welding direction is expressed as a function of the variables y,z, and τ. Knowing this temperature distribution, the temperature can be evaluated directly for any other section using the transformation

$$\theta(x,y,z,t) = \theta(0,y,z,\tau + \frac{x}{v}) \qquad (4.5)$$

The problem is, therefore, reduced to finding the two-dimensional, unsteady temperature field at a section normal to the weld line (e.g., at the section x=0). A planar analysis may

be used for this purpose when the weld speed is sufficiently high, relative to a characteristic diffusion rate for the material. In this case, the net heat flow across any infinitesimally thin slice of the weldment normal to the weld line is assumed to be negligible relative to the heat being conducted within the slice itself. If this assumption is justified, and it is, then the third term in the left hand side of equation (4.4) can be dropped, resulting into the final equation:

$$\frac{\partial}{\partial y}\left(k\frac{\partial\theta}{\partial y}\right) + \frac{\partial}{\partial z}\left(k\frac{\partial\theta}{\partial z}\right) + W_i = \rho c\frac{\partial\theta}{\partial\tau} \qquad (4.6)$$

Friedman [85] notes that the restriction of high weld speed can be relaxed, accounting for net heat flow in the x-direction by approximating the third term of equation (4.4) and including it in the formulation as an equivalent internal heat generation term. The two-dimensional character of the formulation can thus be retained for any welding speed.

It should be mentioned at this point that attempts for the solution of the three-dimensional moving arc problem using the finite element method have been undertaken by several investigators (Muraki [83], Nishida [25], etc.) but with little success, due mainly to the prohibitively high computational cost. Tsai [29] was able, however, to develop a three-dimensional formulation with the finite-difference method using a semi-empirical iterative approach by eliminating the

molten pool area through an inner boundary condition.

Finally, two dimensional finite element programs have been developed [83] for use when welding thin plates. In these programs the problem is formulated in the x-y plane, by assuming that the temperature gradient in the thickness direction is zero.

In conclusion, the approximation of the three-dimensional character of the problem by a two-dimensional one is rational for relatively high welding speeds.

4.3.2 Boundary Conditions

The boundary conditions relevant to the welding problem will be discussed in this section. An exception will be made of the heat input which will be described separately.

Prescribed temperatures. It is rare that the need for specifying temperatures at points and/or surfaces of a weldment arises. An exception can be the presence of a large heat sink in contact with the weldment, but such a case will not be considered in this study.

Convection. Heat is lost from the surface of the weldment by two mechanisms, one of which is natural (or, more rarely, forced) convection -- the other is radiation discussed separately. Linear Newton convection cooling is assumed in the model according to

$$q^s = h \cdot (\theta_e - \theta^s) \tag{4.7}$$

where h is the temperature dependent convection coefficient, θ_e the environmental temperature, and θ^s the surface temperature at the point under consideration. Note that slag formation is not considered in the thermal model, possibly causing overestimation of the heat losses through natural convection at the lower temperatures at which slag is formed. It is believed, however, that the error involved is small.

The estimation of the convection coefficient, h, is not an easy task. This is particularly true if the temperature dependence of h is to be taken into account, something that most previous investigators did not. Hibbitt and Marcal [60], for example, in their analysis of gas metal arc axisymmetric welds assumed a constant h equal to 2×10^{-6} Btu/in^{2}sec°F (5.88 W/m^{2}K) for most part of the weld history, except for the weld-side surface during the weld deposit operation when they took h to be equal to 1.5×10^{-5} Btu/in^{2}sec°F (44.1 W/m^{2}K) to take some account of the additional heat removal due to the shielding gas flow. On the other hand, Andersson [87], analyzing submerged arc welds, assumed a constant h equal to 4.1×10^{-6} Btu/in^{2}sec°F (12 W/m^{2}K). Finally, Friedman [64] in his investigation of stationary GTA welds utilized an empirical correlation equation for natural convection over horizontal plates with the hot surface facing up, yielding h equal to $1.566\ (\theta - 480)^{1/4}$ W/m^{2}K.

In this study use was made of a temperature dependent convection coefficient based on semi-empirical studies made

by Tsai [29]. Table 4.1 provides three different sets of values used. Discussion of the obtained results will be deferred until Section 4.5.

Radiation. In the vicinity of the weld metal radiation heat losses are significant because of the large difference between the surface and environmental temperatures. These losses are modeled according to the quartic Stefan-Boltzman law

$$q^s = \sigma\varepsilon A(\theta_r^4 - \theta^{s4}) \tag{4.8}$$

where σ = Stefan-Boltzman constant

ε = emissivity of the surface

A = shape function

θ_r = sink temperature

θ^s = surface temperature

The above equation can also be written as

$$q^s = \kappa(\theta_r - \theta^s) \tag{4.9a}$$

where

$$\kappa = \sigma\varepsilon A(\theta_r^2 + \theta^{s2})(\theta_r + \theta^s) \tag{4.9b}$$

Radiation heat losses have been taken into account by many of the previously mentioned investigators. In this study the shape factor A was taken to be unity and the emis-

sivity coefficient ε 0.8. The Stefan-Boltzman constant is 0.33044×10^{-14} Btu/sec.in^2°R^4 (5.67×10^{-8} W/m^2°K^4).

TABLE 4.1 Temperature Dependence of Heat Convection Coefficient

$\theta^s - \theta_e$ [°R]	h [Btu/sec.in^2°R]		
	Case 1	Case 2	Case 3
0	0	0	0
100	$.2 \times 10^{-5}$	$.2 \times 10^{-5}$	$.1 \times 10^{-4}$
500	$.5 \times 10^{-5}$	$.1 \times 10^{-4}$	$.6 \times 10^{-4}$
1000	$.1 \times 10^{-4}$	$.2 \times 10^{-4}$	$.1 \times 10^{-3}$
5000	$.58 \times 10^{-3}$	$.58 \times 10^{-4}$	$.6 \times 10^{-3}$
50000	$.12 \times 10^{-2}$	$.12 \times 10^{-2}$	$.12 \times 10^{-2}$

Note: θ^s = surface temperature

θ_e = environmental temperature

4.3.3 Material Properties

The temperature dependence of the thermal conductivity, k, the specific heat, c, and the density, ρ, of the HY-130 steel was described in detail in Section 3.3.2. The values reported there were utilized as input in the finite element heat transfer analysis.

4.3.4 Weld Metal Modelling

The heat transfer mechanism in the weld metal, when molten, is extremely complex and its physics are not well understood as of today. These complexities arise not only from the difficulty involved in modelling the welding arc heat flux correctly, but also from the behaviour of the convective motion of the molten metal; the thermal properties of the molten metal (inlcuding the phase transformations that take place during melting and solidification), the electric heating due to the current flow in the base metal; the boundary conditions for heat losses, etc. Many investigators have recognized these difficulties and have tried to find ways to approximate the phenomena involved.

A look at the available literature reveals that there are generally three ways for handling the problem. The first one, still at its developing stages, tries to understand and subsequently mathematically model the physical phenomena involved through sophisticated experimental and analytical techniques. Since no conclusive results are yet available, this approach will not be discussed any further.

A second way of handling the problem stems from the following thoughts: since the physics involved in the weld pool are not well understood, the problem will be divided into two parts. In the first part, an effort will be undertaken to predict the shape of the molten pool, and then in the second part the energy equations will be solved numerically in the

solid metal using the melting isotherm as a boundary condition. This approach was first hinted by Apps and Milner [16], was first applied by Pavelic et al. [88] to calculate temperature distributions when Gas Tungsten Arc welding thin plates, and was further expanded by Tsai [29] in the underwater welding case. All investigators have reported good correlation between experiments and analysis. The method works especially when the temperature distribution in the heat affected zone is required in order to predict the resulting microstructures in this area.

Some aspects and limitations of this approach are:

1. The shape of the molten pool is determined semi-empirically by measuring the weld bead width and the ripple length.

2. There is no need to estimate an arc efficiency for the welding process since the two weld bead shape parameters previously mentioned can be correlated to the heat input into the welded plate.

3. All investigations have been confined to thin plates only (less than 1 inch thick).

4. The case of multipass welding has not been examined.

The third and final way by which the problem seems to be handled in the literature is by assuming thermal properties of the molten metal such that its behaviour can be best approximated [6, 78, 79, 84]. For example, most investigators [64] use a value for the thermal conductivity of the molten

metal an order of magnitude higher than that of the material at the solidus temperature, in an effort to simulate the convective heat transfer mechanism and electromagnetically induced circulation in the puddle. On the other hand, other investigators use a value for the thermal conductivity of the molten metal equal to one half of that for the solid material [6]. Such inconsistencies arise because of the lack of data for the thermal properties at such high temperatures. As mentioned in Section 3.3.2, however, it is believed that the higher thermal conductivity better approximates the actual phenomena.

In this study the ultimate goal is the successful prediction of transient strains and residual stresses in weldments. It is therefore necessary to know the temperature distribution not only outside the weld metal but also inside it, since most plastic deformations that cause the formation of residual stresses take place in that region. As a consequence, the second approach mentioned above cannot be utilized. Instead, the third approach was applied using as thermal conductivity for the molten metal a value an order of magnitude higher than the one for the solid metal just below the solidus temperature.

Finally, since the cases analyzed involved multipass welding, it was necessary to find a way to model the laying of the various beads during the welding cycle. This was made possible by the element birth-and-death capabilities of the

code used. In other words, the program ADINAT [76] is capable of giving birth to a predetermined number of elements at predetermined time instances, thus enabling one to model the laying of a bead by specifying the appearance of the elements representing it at the time it physically appears.

4.3.5 Heat Input

The general modelling of heat input during welding was extensively discussed in Section 2.2, where both its magnitude and distribution were described. It was then pointed out that the arc efficiency, η_a, is one of the most important parameters involved. In this study where a gas metal arc welded specimen is analyzed, three arc efficiencies were tested, namely 0.60, 0.65, and 0.70. Discussion of the obtained results is delayed until Section 4.5.

As far as the distribution of heat input is concerned, a consistent formulation was adopted [89] assuming uniform distribution in space over the top of each weld bead.

4.4 Description of Experiments

A description of the welding experiments performed on HY-130 steel to measure temperature histories and transient strains will be undertaken in this Section. The experimental results regarding temperatures will be compared with the ones obtained by the finite element analysis in the next section, whereas the transient strains will be discussed in Chapter 5. Note that all experimental data will be shown in the appro-

priate places as mentioned above.

4.4.1 Specimen Geometry

Two experiments using the GMA welding process on HY-130 steel plates were performed. Similar experiments using the EB and LB welding processes on identical specimens were performed by Coneybear [90], Rogalsky [91], Coumis [92], and Lipsey [93] as part of the same study.

In both experiments each plate measured 12" x 12" x 1" (305 mm x 610 mm x 25.4 mm) resulting after welding in a 24" x 24" x 1" (610 x 610 x 25.4 mm) configuration as shown in Figure 4.2. The weld length was chosen to be larger than 18 inches (457.2 mm) because previous experimental experience has shown that in such lengths the maximum stresses are developed and kept constant around the middle of the plate. Moreover, in such lengths the end effects can be neglected as far as the mid-length region of the weld is concerned, so that a quasi-stationary state can be assumed for the heat transfer analysis -- in other words it can be assumed that any cross-section in the vicinity of the middle of the plate experiences the same temperature history.

Figure 4.3 shows the weld joint configuration. It consists of a double-V groove with a 60° included angle in accordance with U.S. Navy specifications. This configuration was made by machining.

The test plate support arrangement is shown in Figure 4.4.

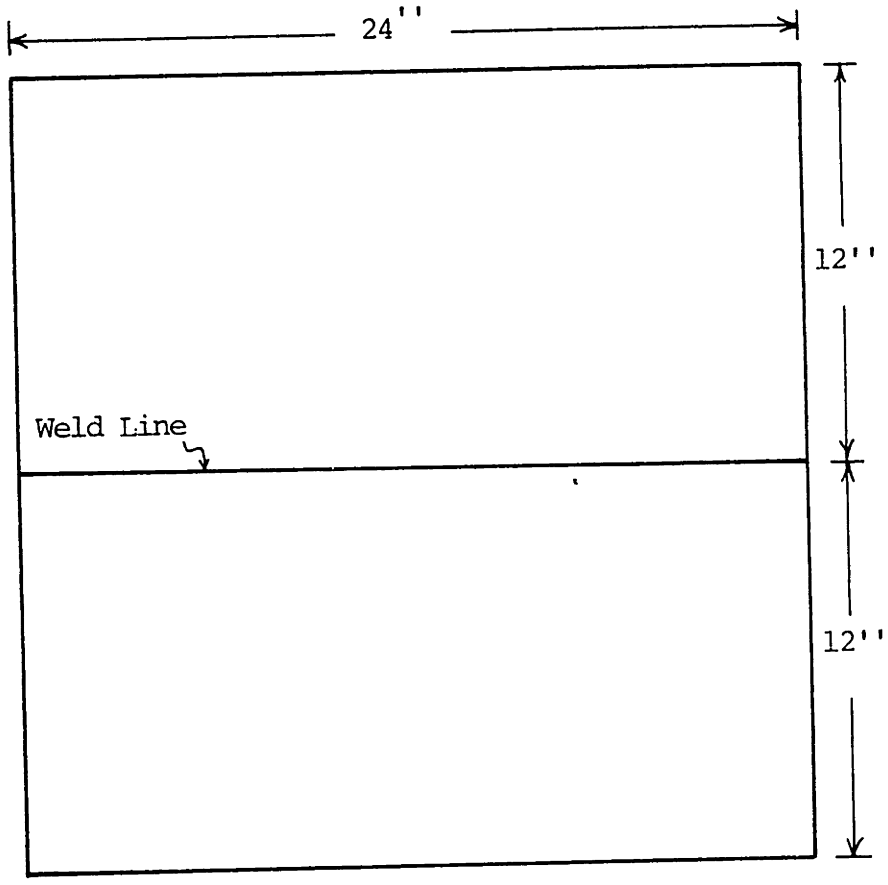

FIGURE 4.2 Test Plate Arrangement

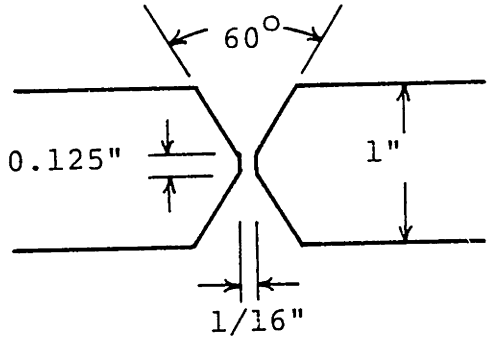

FIGURE 4.3 Weld Joint Configuration

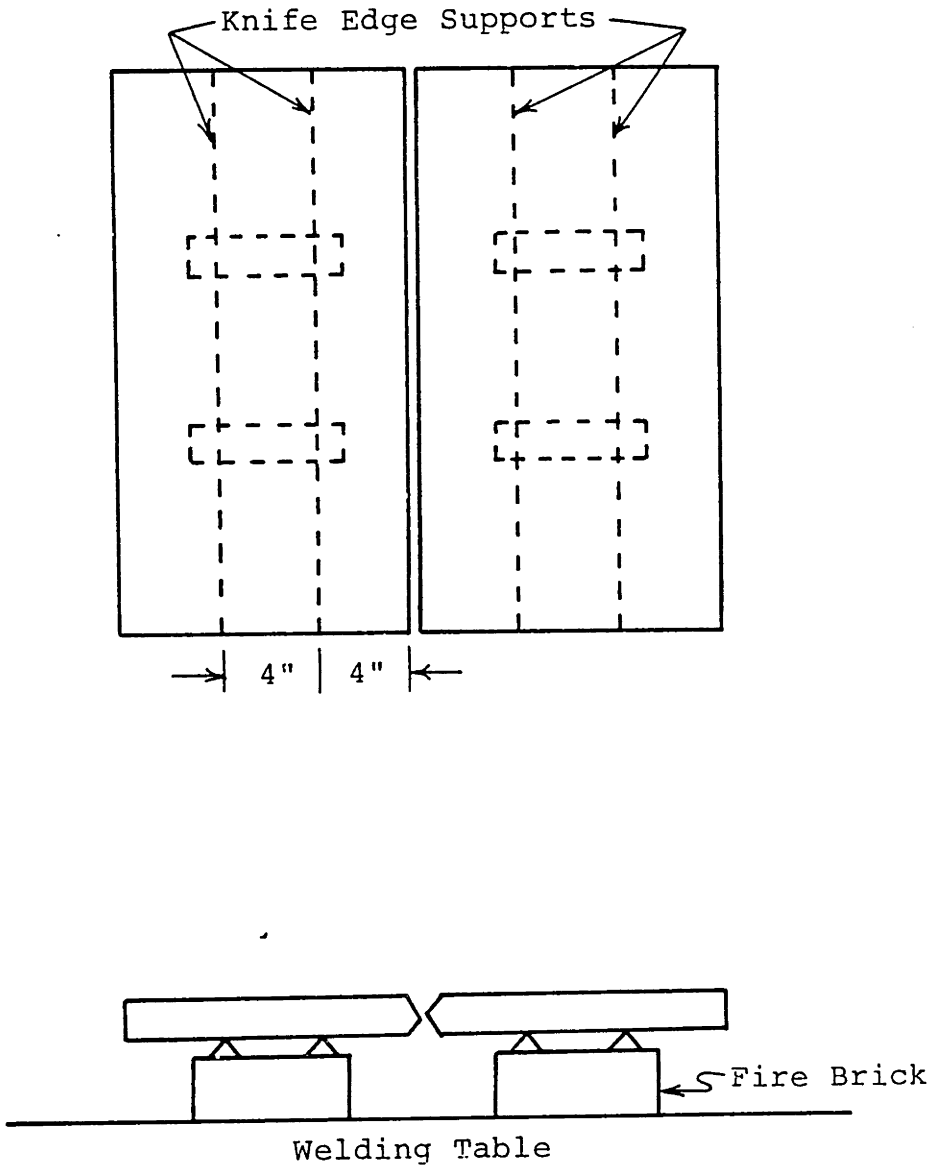

FIGURE 4.4 Test Plate Support Arrangement

It is the same one used by Lipsey [93] and consists of knife edge supports located through the whole specimen length at 5 and 8 inches (127 and 203.2 mm) from the weld centerline on either side. This way the experiments were performed with the specimens completely unrestrained.

4.4.2 Instrumentation

Temperatures on the top surface of the specimens were measured using Chromel/Alumel adhesive bonded thermocouples referenced at 32°F (0°C). Transient strains were also measured on the top surface of the specimens using 90° Rosette electric resistance strain gages which were cemented on the plates' surface. Table 4.2 provides the gages' specifications and Figure 4.5 shows the apparent strain curve supplied by the manufacturer, necessary to perform the temperature compensations on the raw data [94].

Temperatures and strains were simultaneously read out on a twelve channel, continuous recording Visicorder.

TABLE 4.2 Strain Gage Specifications

Gage	SR-4 90° Rosette
Designation	FAET-19D-12-S6
Manufacturer	BLH Electronics
Grid dimensions	0.19 in x 0.19 in
Temperature range	-100° to 500°F
Resistance	120 Ohms
Gage factor	1.98
Cement	EPY-500

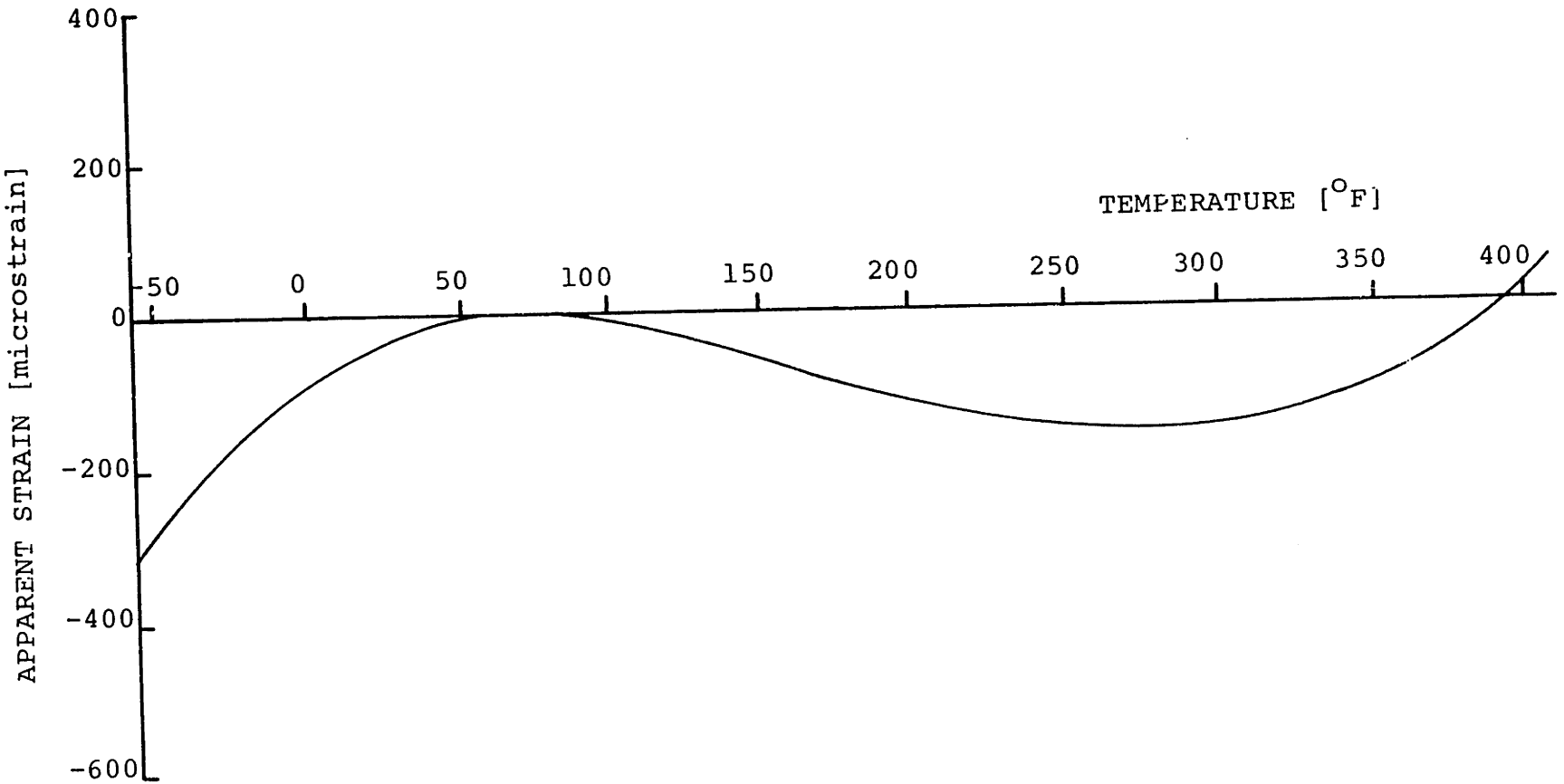

FIGURE 4.5 Effect of Temperature on Apparent Strain (SR-4 Strain Gage).

Figures 4.6 and 4.7 show the locations of the thermocouples and strain gages on the two specimens, I and II. In both cases the strain gages were located at the midlength of the weld (12 inches or 305 mm from the plates' edge) and at the transverse distances from the weld centerline shown in the figures. The thermocouples were located 1/2 inch (12.7 mm) ahead of the strain gages, assuming that the same temperature history was to be experienced at both locations with a time lag equal to the time spent by the arc to travel the two locations. This time lag was taken into account when reducing the data.

4.4.3 Welding Procedure

Welding on both tests was performed by the semiautomatic GMA method, using a SVI-300 power supply and associated controls manufactured by the Linde Division of the Union Carbide Corporation. Arc travel speed, voltage, and amperage were set prior to the start of each welding test so as to obtain the desired heat input (less than 45 kJ/in according to U.S. Navy specifications) and hence a sound weld. Preheating was also applied by resistance heaters, monitored by the installed thermocouples so as to be as uniform as possible and not exceed 175°F (80°C). Interpass temperature was also monitored.

The filler wire was 0.045 in (1.14 mm) in diameter and of the Linde-140s type described in Section 3.1. A mixture of argon plus 2% oxygen was used as the shielding gas.

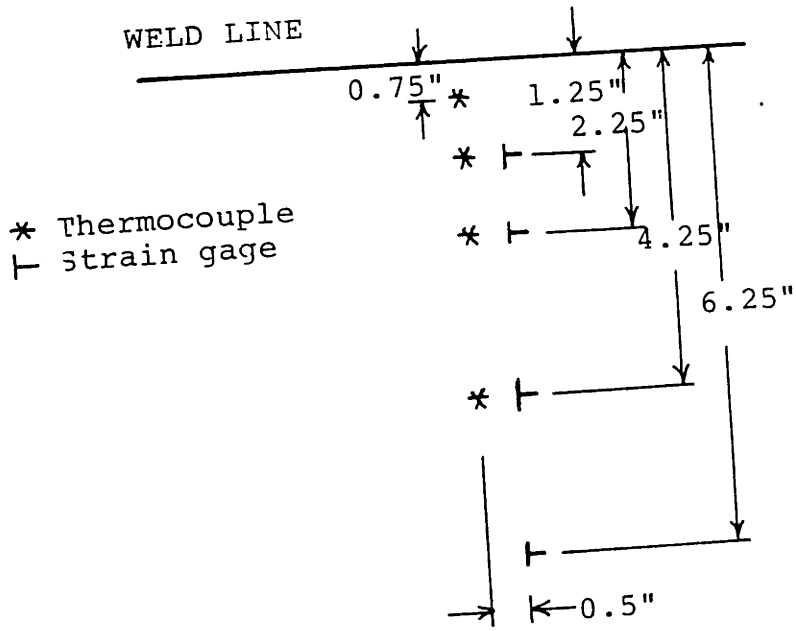

FIGURE 4.6 Thermocouple and Strain Gage Location on HY-130 Specimen I.

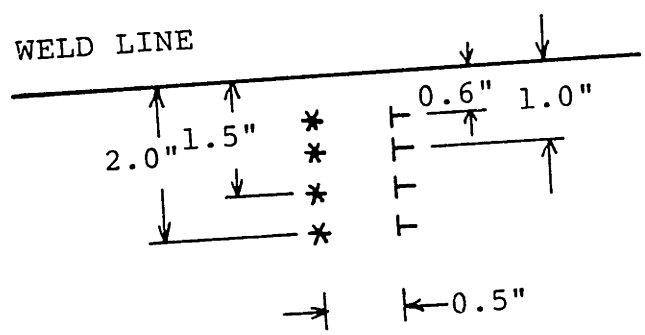

FIGURE 4.7 Thermocouple and Strain Gage Location on HY-130 Specimen II.

Six welding passes were required to fill the top half of the joint. The specimens were then turned over and six more passes were made to complete the joining.

Table 4.3 provides a summary of the welding conditions used.

TABLE 4.3 Welding Conditions for HY-130 Specimens

	I	II
Weld type	Butt	Butt
Process	GMA	GMA
Arc voltage	25	25
Polarity	d.c.r.p[1]	d.c.r.p.
Travel speed (ipm)	12	12
Heat input (kJ/in)	37	37
Filler wire	0.045" Linde 140s	
Shielding gas	Argon + 2% O_2	
Number of passes	12	12
Preheat temperature (°F)	150-175	
Interpass temperature (°F)	150-175	

[1]direct current reverse polarity

4.5 Comparison of Numerical and Experimental Results

The experiments described in the previous section were analyzed using the finite element program ADINAT [76] and the modelling procedures described in Section 4.3. Due to cost considerations and in order to perform a limited parametric analysis, a rather crude mesh was used. Four runs were totally made analyzing the first two weld passes.

Figures 4.8a and 4.8b show the finite element mesh used at a cross section of the plate in its mid-length. Note that Figure 4.8a shows the leftmost 11.5 inches (292.1 mm) of the plate with the rightmost 11.5 inches (292.1 mm) being exactly symmetric, whereas Figure 4.8b shows, in different scale, the middle 1 inch (25.4 mm) that includes the weld metal and the heat affected zone.

A total of 37 isoparametric elements were used divided into two groups of 30 and 7 elements, the second group representing the weld metal. Referring to Figure 4.8b, elements 3, 4, and 5 model the first welding pass, elements 1 and 2 the second, and elements 6 and 7 the third.* It is once more emphasized that during the analysis of each pass the elements representing the next passes remained inactive using the birth-and-death option of the program. Finally, a total of 72 nodes were used.

It should also be mentioned at this point that due to the fact that only the first welding pass is symmetric, the total cross-section, and not half of it, had to be modelled with finite elements.

The heat input was calculated using a consistent formulation as described in Section 4.3.5. It was then distribu-

---

*The general shape of each welding pass was found by cross-sectioning each specimen after all measurements have been made and etching the surface to reveal the weld pass boundaries.

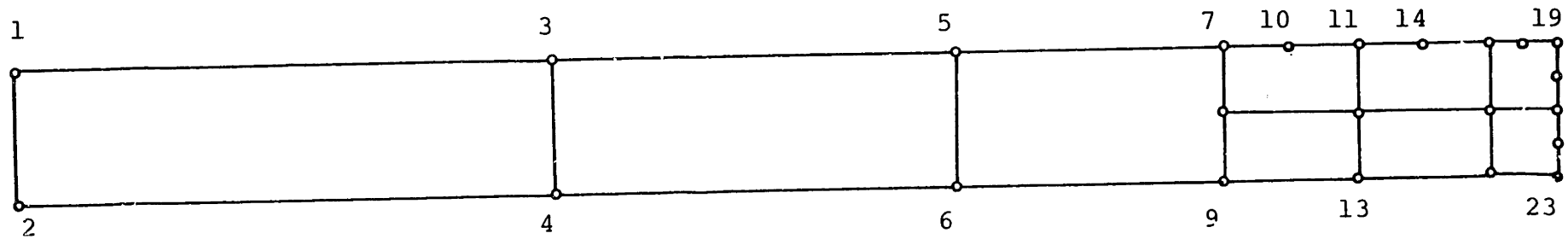

FIGURE 4.8a Finite Element Mesh Used in Heat Transfer Analysis (rightmost 11.5 in of cross-section)

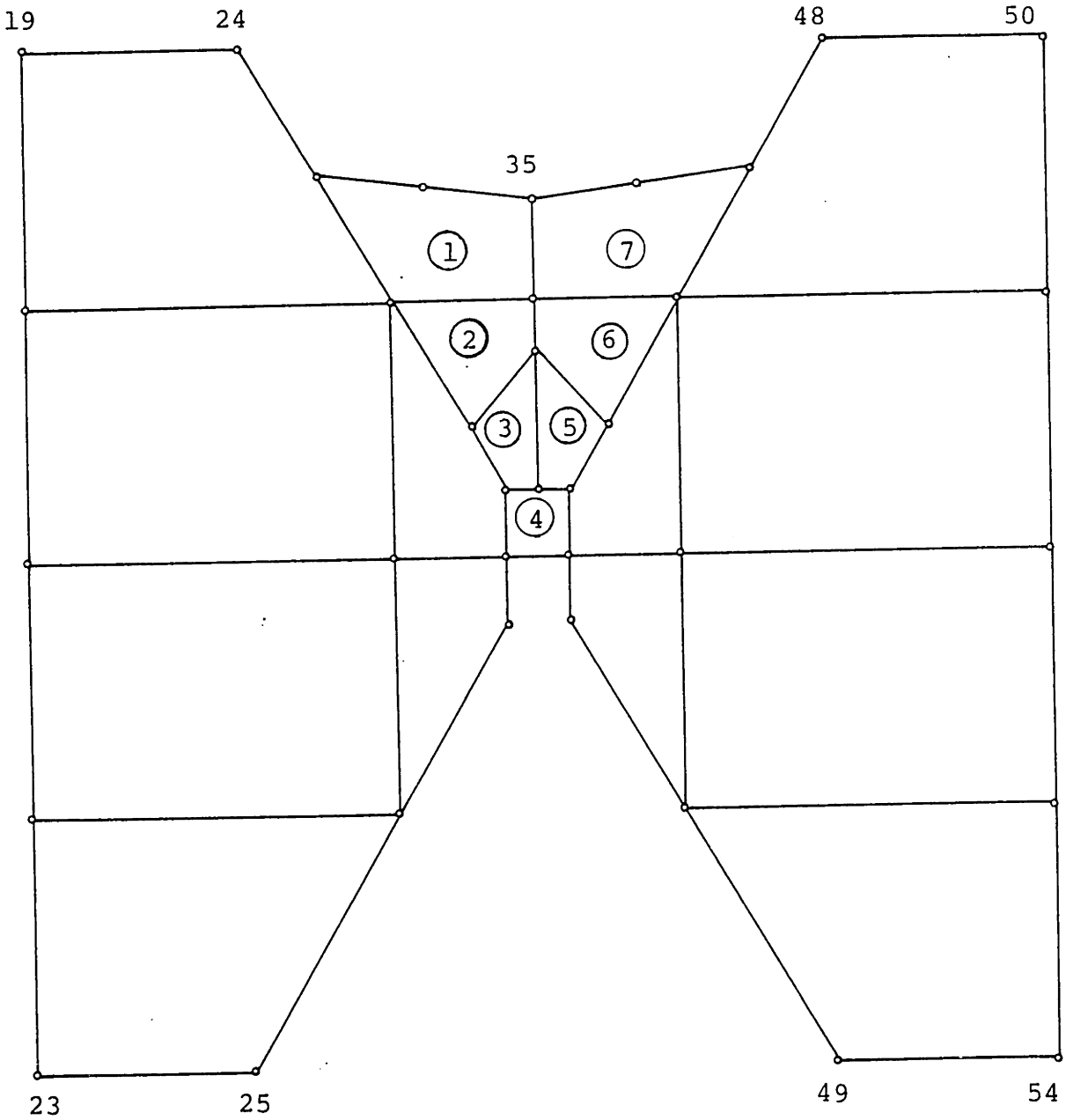

FIGURE 4.8b Finite Element Mesh Continued (center 1. in).

ted over 5.5 sec, as shown in Figure 4.9 for the case η_a=0.70, to simulate the passing of the arc traveling at 12 in/min (0.2 in/sec) over the 1 in thickness of the cross-section.

Table 4.4 summarizes the four analyses performed. Two parameters were varied, the arc efficiency, η_a, and the temperature variation of the convection coefficient, h, given the fact that some uncertainty exists regarding their true values. All other variables were kept constant in the four cases, assuming the values referred to in previous Sections.

Figures 4.10 and 4.11 show results for the first welding pass. In Fig. 4.10 the temperature history at a point on the plate's top surface 0.5 in (12.7 mm) away from the weld centerline as predicted by cases A1 and A2 (refer to Table 4.4) is depicted. With the only difference between the two cases being the arc efficiency (i.e. amount of heat input), the curve for case A1 (η_a=0.65) shows, as expected, higher temperatures than case A2 (η_a=0.60). The cooling rates are about the same, although both predict too slow cooling if compared with the experimental data. This latter observation means that the values chosen for the heat convection coefficient are probably low.

Cases A2, A3, and A5 are compared with the experimentally obtained results in Figure 4.11 for the same point as the one of the previous figure. Considering the same heat input (η_a=0.60) little difference is found between cases A2 and A3. This is due to the fact that although higher values for the

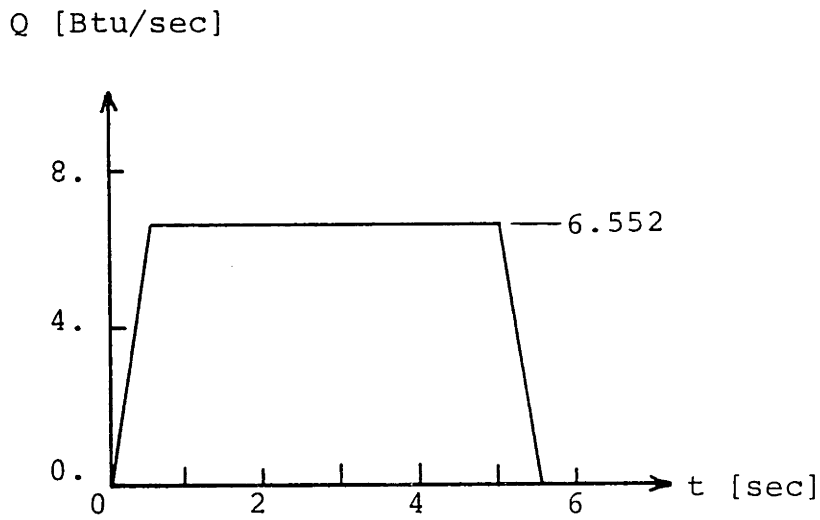

$$Q = \eta_a VI = (0.70)(25)(395) = 6.552 \text{ Btu/sec}$$

$$H = \frac{Q}{v} = \frac{(6.552)}{(0.2)} = 32.76 \text{ Btu/in}$$

$$\text{Area} = 2(0.5)(6.552) + (4.5)(6.552) = 32.76 \text{ Btu/in}$$

FIGURE 4.9 Heat Input Distribution (example).

TABLE 4.4 Summary of Analyses

Analysis	η_a[1]	h case[2]
A1	0.65	1
A2	0.60	1
A3	0.60	2
A4	0.70	3

Notes: [1] η_a is the arc efficiency utilized.

[2] Refers to the cases presented in Table 4.1

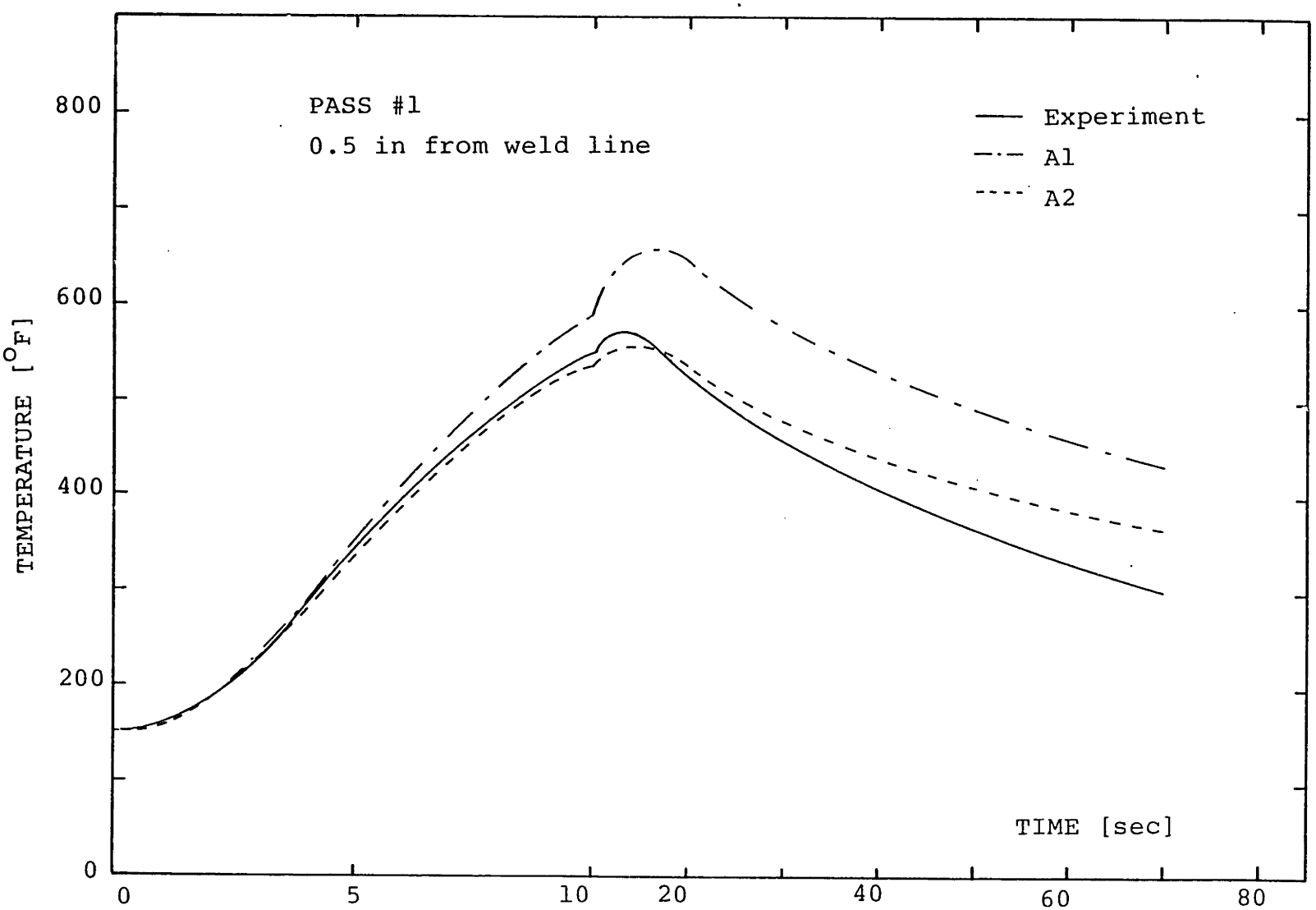

FIGURE 4.10 Comparison of Finite Element REsults with Experimental Data (weld pass no. 1)

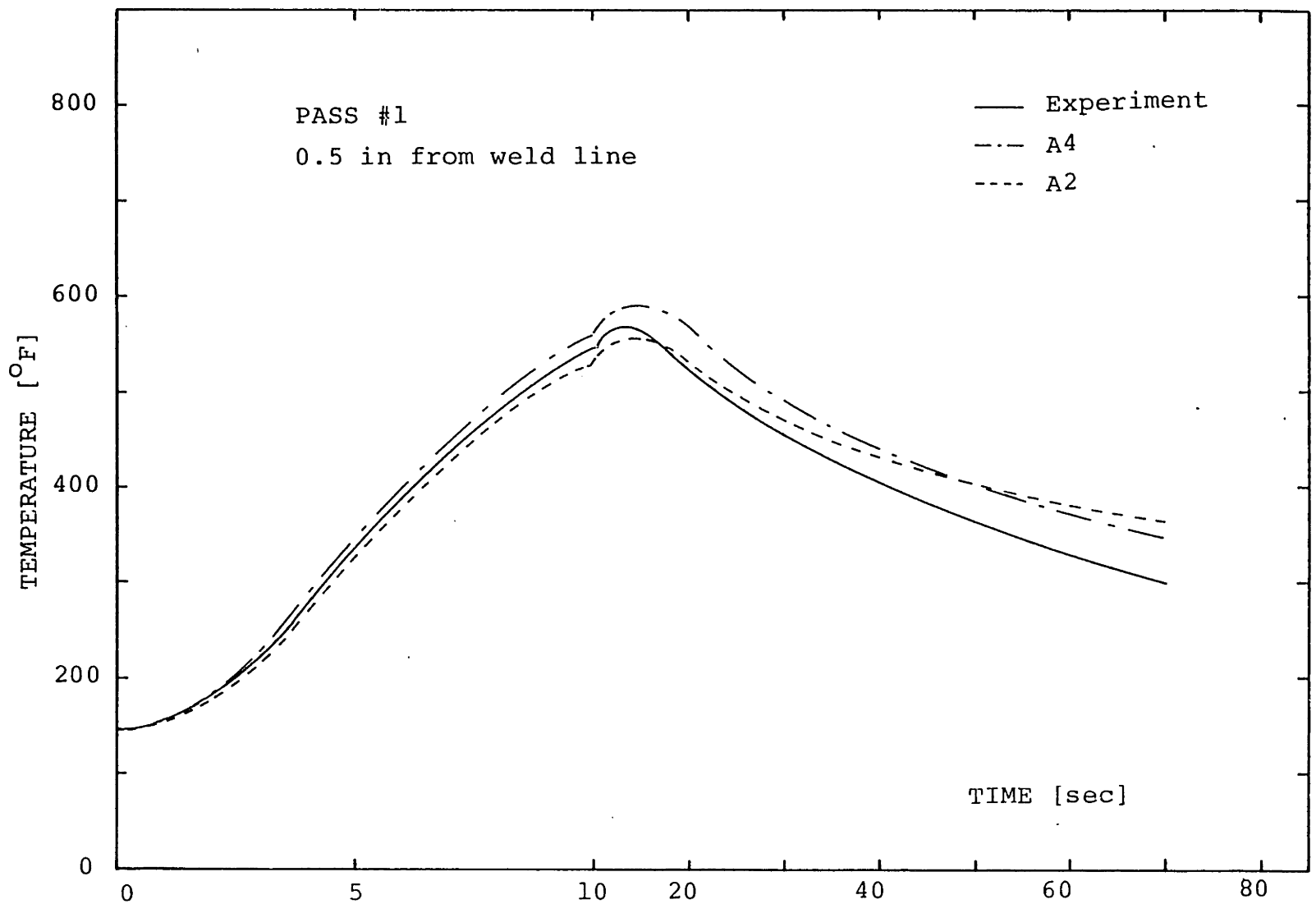

FIGURE 4.11 Comparison of Finite Element Results with Experimental Data (weld pass no. 1).

convection coefficient were chosen in analysis A3, these values were not high enough to significatly alter the heat losses from the top and bottom surfaces of the plate and consequently the temperature distribution. A substantial increase in the convection coefficient was therefore chosen for case A4; at the same time, however, an increase in the arc efficiency was made to partially compensate for the higher h and thus to obtain a good estimate of the maximum temperature reached. As seen in Fig. 4.11 the combination of values used in this latter analysis succeeded in bringing the cooling rate much closer to the experimental one. At the same time a 4% overprediction of the maximum temperature is observed. The difference, however, was very small so that any further analysis was not felt necessary.

Similar results were found at other points of the plate. Case A4 came always closest at matching the experimentally obtained results.

Temperature distributions for the second welding pass are shown in Figures 4.12 through 4.14. Results for three points on the plate's surface located 0.5, 1.0, and 1.5 in (12.7, 25.4, and 38.1 mm) away from the weld centerline as predicted by the four cases analyzed are compared with experimental data. As was the case with the first welding pass, analysis A4 comes again closest at matching the experimentally obtained temperature histories.

The temperature histories calculated from analysis A4 were subsequently used as input to the stress analysis

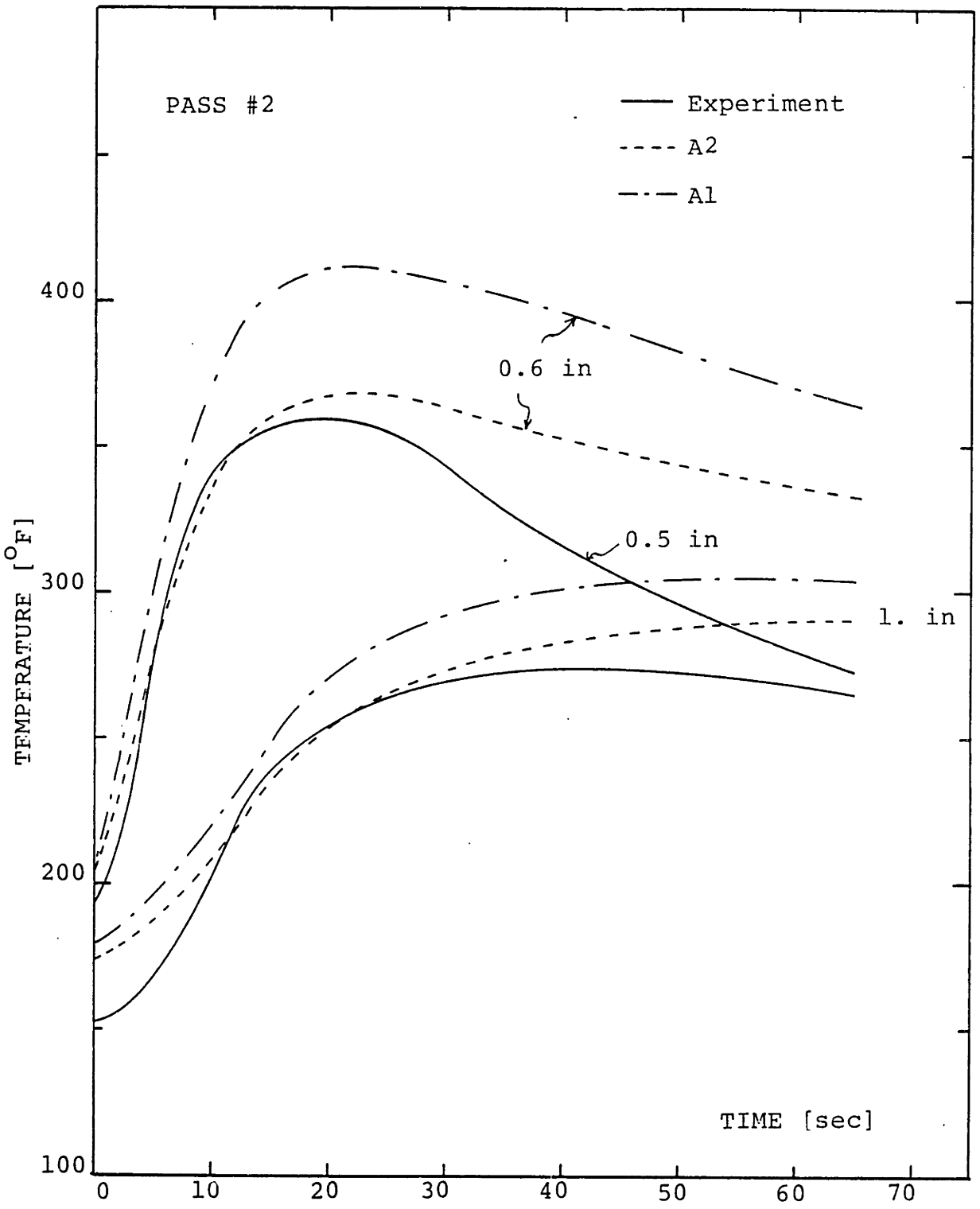

FIGURE 4.12 Comparison of Finite Element Results with Experimental Data (weld pass no. 2)

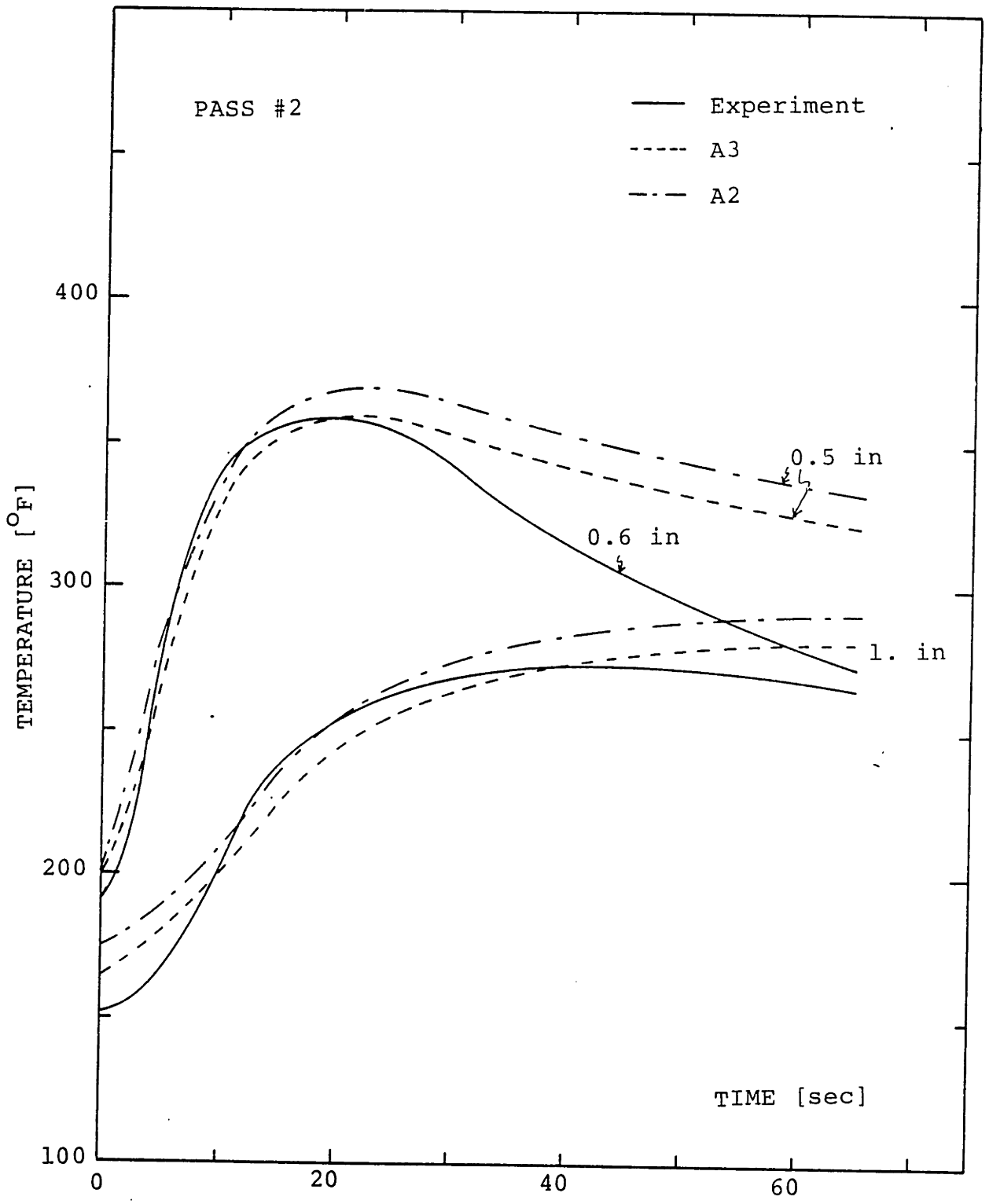

FIGURE 4.13 Comparison of Finite Element Results with Experimental Data (pass no. 2).

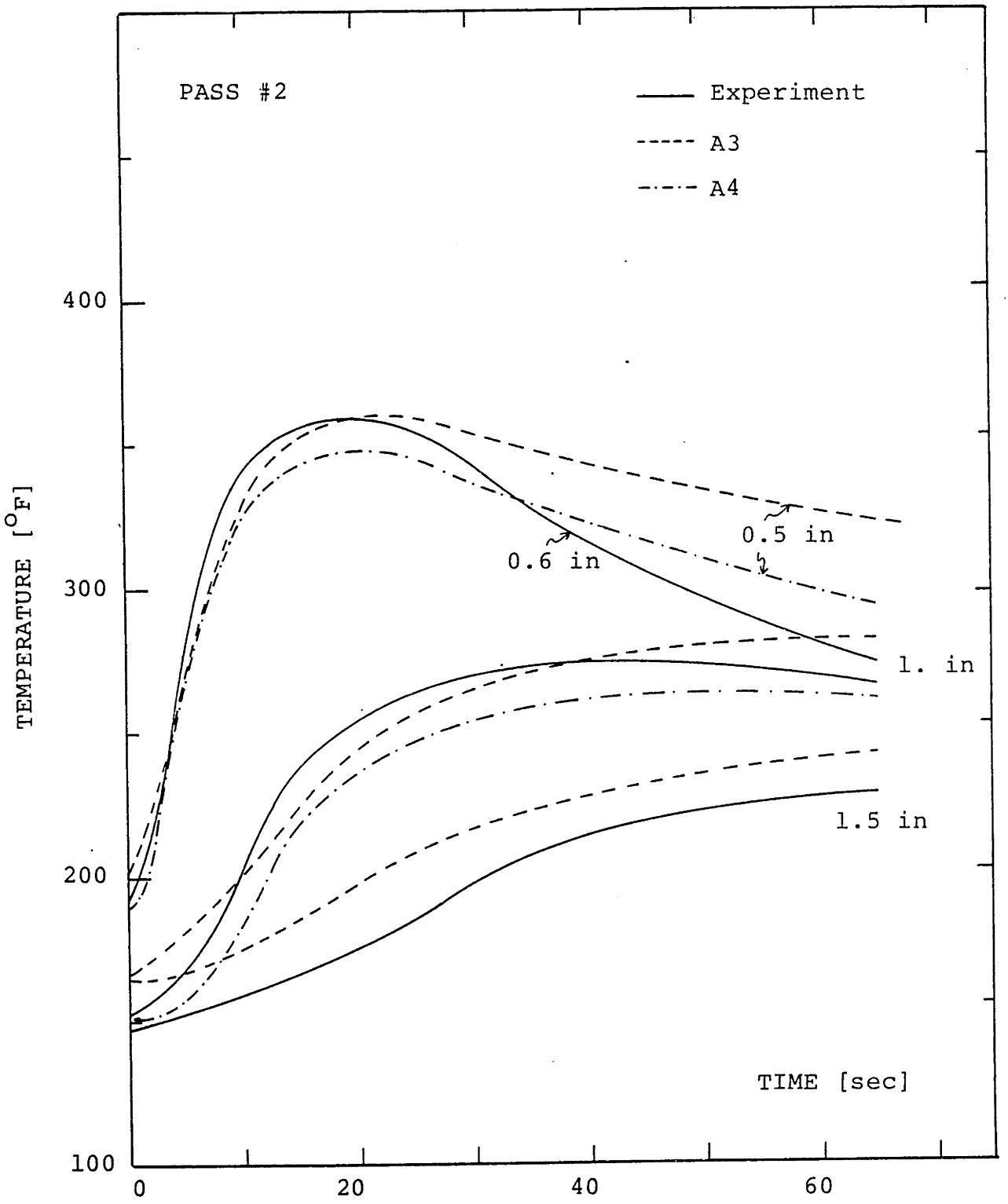

FIGURE 4.14 Comp cison of Finite Element Results with Experimental Data (pass no. 2).

discussed in Chapter 5. It should be noted that when this stress analysis failed to give accurate results using the finite element mesh shown in Figures 4.8a and 4.8b, the heat transfer analysis for the first welding pass was repeated with the finer mesh shown in Figures 5.7a and 5.7b. The same conditions as the ones for case A4 were used. No significant difference was observed between the temperatures calculated on this finer mesh and the ones with the more crude one.

Finally, some thoughts regarding the parametric analyses performed should be expressed. To many this would look like an exercise in curve-fitting, trying to match experiments and analysis. In reality, the problem is much more fundamental and has to do with the uncertainties involved in estimating several parameters required as input to the solution. The many complexities and the nonlinearity of the welding problem combined with the state-of-the-art in arc physics and heat transfer, do not allow at present the accurate calculation of, among others, the heat input to the plates beeing welded and the temperature dependence of the heat convection coefficient. Therefore, and until further developments in these areas are made, some parametric analyses will be necessary to better estimate the temperature distribution during welding. It is nevertheless hoped that analyses similar to the ones performed in this study would help future investigators in better selecting appropriate values for uncertain parameters.

CHAPTER V

TRANSIENT STRAINS, TRANSIENT STRESSES AND RESIDUAL STRESSES DUE TO WELDING

Using the temperature distributions predicted based on the techniques described in Chapters II and IV, one can calculate the transient strains, transient stresses and residual stresses due to welding since, under the conditions described in the Introduction, the problem was assumed to be uncoupled. The calculation of strains and stresses, however, poses a much more formidable problem than the one encountered in the heat transfer analysis, making the use of numerical techniques a necessity. These difficulties stem from the complicated thermal-elastic-plastic state developed in and around the weld metal during welding.

Two general techniques have been developed to solve the problem. One is a simple one-dimensional analysis and the other a more sophisticated one based on the finite element method. Both will be considered here, although emphasis will be placed on the latter.

After a brief literature survey, the one-dimensional analysis will be considered and applied to several cases. Based on the obtained results, the advantages and limitations of this method will be discussed.

The finite element method as applied to the welding problem will then be described. Particular emphasis here will be

given to the development of a model, incorporated in the finite element analysis, which can take into account the effects on strains and stresses produced by the allotropic phase transformations. These effects can be quite pronounced, as it will be seen, when considering quenched and tempered steels, like, for example, the HY-130 steel.

Finally, the results obtained by the finite element analysis will be compared with the experiments described in the previous Chapter.

5.1 Literature Survey

Two review articles, by Tall [95] and Masubuchi [82], provide the general picture as far as developments in the area of calculation of residual stresses is concerned. In this Section, part of their discussions will be borrowed, although much of what follows is relatively new.

The one-dimensional model for calculating stresses parallel to the weld line only was first developed in 1964 by Tall [53]. Using this model, Masubuchi, Simons, and Monroe [96] developed a computer program which was later modified and improved both at M.I.T. and elsewhere [26,97,98].

The complexities involved, however, in performing simple analytical studies of welding stresses and distortions for various weld configurations -- in particular, the complex effects of inelastic material response and material loading and unloading -- did not allow for the further development of similar studies. Instead, attention was focused on numerical

methods, predominantly the finite element method, which could be applied to the highly nonlinear, inelastic behavior of welded structures.

Fundamental aspects of the finite element method are discussed in many books and articles [89,99]. Nonlinear thermo-elastic-plastic procedures are described by Bathe and co-workers [100,103], Inoue and Tanaka [104] and others.

One of the first applications of the FEM to weld problems was presented by Hibbitt and Marcal [60], who considered a thermomechanical model for the welding and subsequent loading of a fabricated structure. Their model simulates GMA welding processes and accounts for temperature dependent material properties. This model has been subsequently used by other investigators, including Nickell and Hibbitt [79], Hsu [78], Lobitz and co-workers [105], and others. Friedman [62,85] also developed finite element analysis procedures for calculating stresses and distortions in longitudinal butt welds. These procedures are applicable to planar or axisymmetric welds. Rybicki and co-workers [106-108] have developed similar procedures. At the Massachusetts Institute of Technology a team headed by Masubuchi has also developed two-dimensional finite element programs capable of performing plane strain and plane stress analyses [80-83].

Japanese investigators have also been very active in the field. Ueda and co-workers [109-113], Satoh et al. [114], and more recently Fujita and Nomoto [115-117] have all

developed models to calculate transient strains and residual stresses due to welding based primarily on the initial strain method.

Efforts to include the effects of phase transformation on transient strains and residual stresses have been undertaken by some investigators, including Inoue and Tanaka [118], Toshioka [119-120], Jones and Alberry [121], and Andersson [87]. By and large their approach consists of dividing the area where phase transformations are expected (the weld metal and HAZ) into a number of regions, typically three, and assuming that the material exhibits a constant cooling rate in each of these regions. Based on that, they estimate one dilatational curve for each region and use it as the thermal strain curve for that region. A more fundamental approach has been developed in this study and will be extensively discussed in Section 5.4.

As a general assessment of the models developed so far, it can be said that they give reasonable results for the cases reported as compared to experiments, although the deviation from experimental data varies considerably.

5.2 One-Dimensional Analysis

The basic assumption inherent in the one-dimensional stress analysis is that the only stress present is the one parallel to the weld line, σ_x, and that this stress is a function of the transverse distance from the weld centerline only. As a consequence, the equilibrium conditions are not

satisfied. Despite this, however, it appears that the obtained solutions correlate reasonably well with experimental data in certain cases, as will be further explored.

The analysis lends basically the procedure originally proposed by Tall [53]; the computer code implementing the solution with the latest modifications can be found in [26].

The algorithm for solving the problem is based on the method of successive elastic solutions as proposed by Mendelson [122]. The program can take into account the temperature dependence of all material properties, any type of strain hardening and can solve bead-on-plate, edge, and butt welds of flat plates with finite width. One of the input requirements, the temperature distribution, can also be calculated if desired by the same program using the line heat source solution. The output at each time step consists of the temperature, total strain, mechanical strain, plastic strain, and stress at each of the predetermined points located at various transverse distances from the weld centerline.

Previous applications of the program have shown that it gives good results in the case of thin plates. This happens because in thin plates all stresses, except σ_x, are very small, sometimes an order of magnitude smaller than σ_x.

In the present study an analysis was undertaken of the experiments performed by Coneybear [90] on HY-130 specimens welded using the Electron Beam (EB) welding process, as well as of the GMA welded specimens described in Section 4.4. The

EB specimens had the same geometric configuration as the GMA welded ones, the only difference being the joint shape which was square butt in the case of EB welding.

Figure 5.1 shows the comparison between experiment and analysis of the longitudinal transient strain history, ε_x, in the EB specimen at two points 0.67 and 1 inch (17 and 25.4 mm) away from the weld centerline. Despite the thickness of the specimens (1 inch or 25.4 mm) the results show a remarkably good correlation of analysis and experiment. This can be attributed to the physics of the EB welding process which result in a relatively uniform through thickness temperature distribution and a narrow heat affected zone. As a consequence, stresses σ_y, τ_{xy}, and σ_z are small compared to σ_x, a fact substantiated by the experimental data (see Coneybear [90]). The assumption of the one-dimensional theory that σ_x is the only stress present is, therefore, approximately valid. It should be emphasized once more, however, that these results apply for the midlength of a relatively long plate (longer than 18 inches or 457.2 mm), where the maximum possible stresses have been developed and where the end effects can be neglected.

The comparison between experimental data and analytical results for the longitudinal transient strain history in the GMA welded specimens at two points 1.0 and 2.25 inches (25.4 and 57.2 mm) away from the weld centerline is shown in Figure 5.2. Here the story is completely different. The correlation

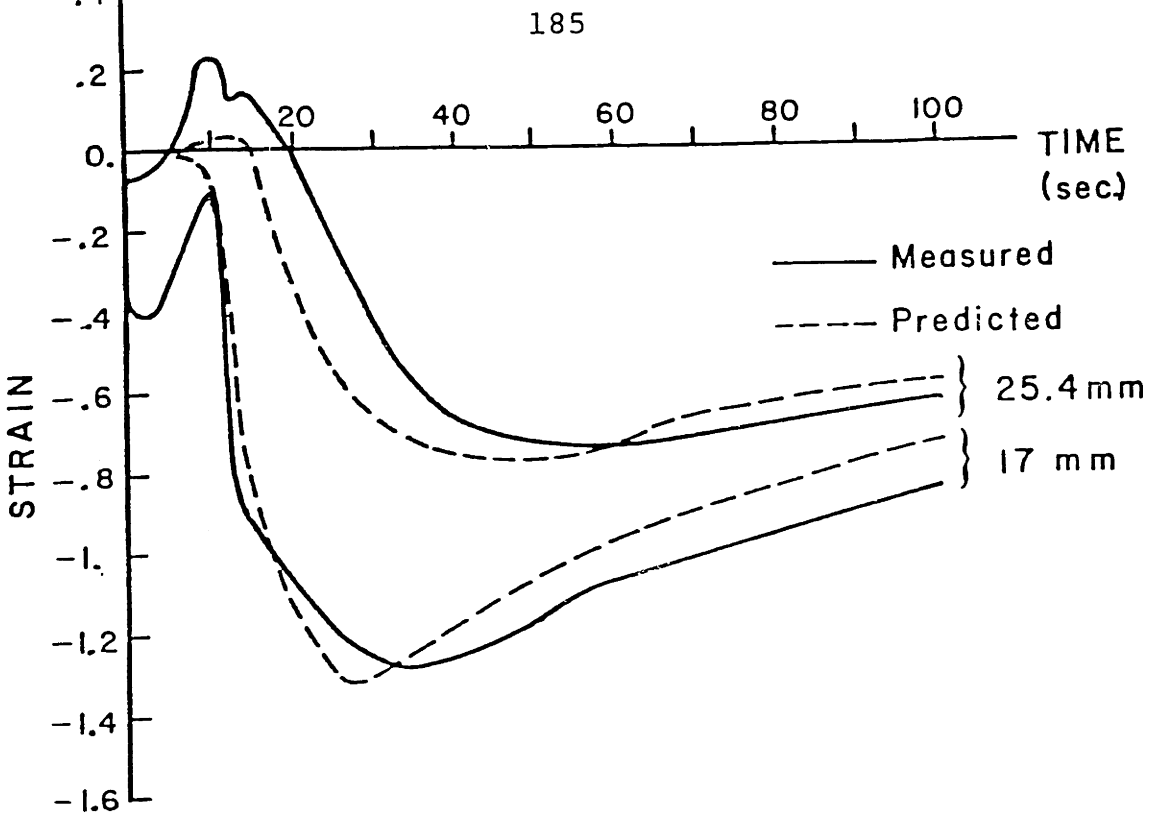

FIGURE 5.1 Longitudinal Transient Strain Histories for EB Welded Specimens (Experiment and Analysis)

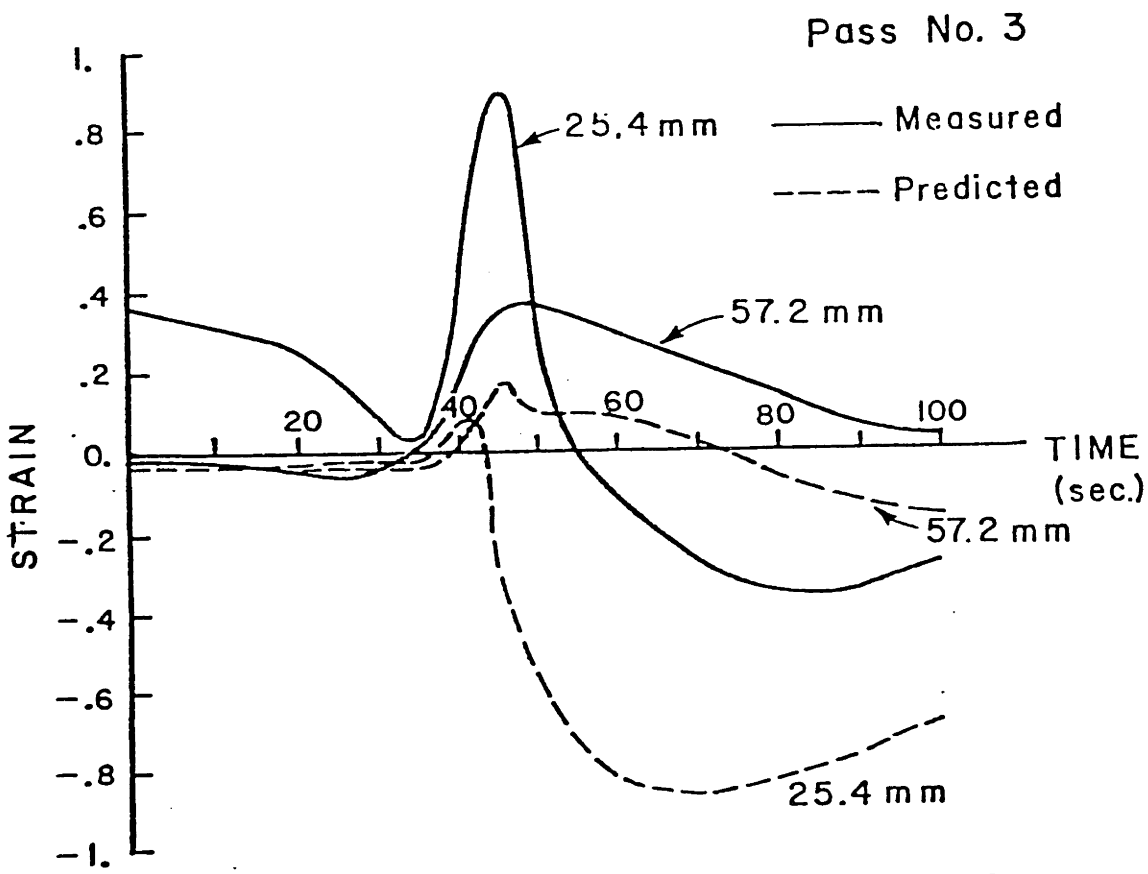

FIGURE 5.2 Longitudinal Transient Strain Histories for GMA Welded Specimens (Experiment and Analysis)

is not good, especially for the closest point; at around 45 sec from the commencement of welding, for example, the experimental data show a maximum positive longitudinal strain of about 0.9, whereas the analysis predicts a negative longitudinal strain 0.4 in magnitude. It is thus apparent that the assumptions involved in the one-dimensional analysis break down in the case of multipass GMA welds of thick plates. Experimental data actually confirm this by showing that the transverse strains are of the same order of magnitude as the longitudinal ones.

In conclusion, the one-dimensional program seems to be appropriate for analyzing thin plates or medium thickness plates welded by one of the high energy density processes (Electron Beam or Laser Beam). For the case of multipass welds the basic assumptions of the method do not hold and hence a more sophisticated technique, like the finite element method, seems to be necessary.

5.3 Finite Element Formulation

The thermal-elastic-plastic and creep constitutive model (with the phase transformation modification discussed in the next Section) of the multipurpose finite element program ADINA (Automatic Dynamic Incremental Nonlinear Analysis) will be used for predicting the transient strains, transient stresses, and residual stresses due to welding. The model was developed by Snyder and Bathe [103] in 1980. Some features of this model will be described in this Section

for completeness.

The governing incremental finite element equations for the problem can be written as [100],

$$ {}^{\tau}\underline{K}\ \Delta\underline{U}^{(i)} = {}^{t+\Delta t}\underline{R} - {}^{t+\Delta t}\underline{F}^{(i-1)} \qquad (5.1) $$

where ${}^{\tau}\underline{K}$ is the tangent stiffness matrix corresponding to time τ; ${}^{t+\Delta t}\underline{R}$ is the nodal-point external force vector at time $t+\Delta t$; ${}^{t+\Delta t}\underline{F}^{(i-1)}$ is a vector of nodal-point forces that are equivalent, in the virtual work sense, to the internal element stresses at time $t+\Delta t$ and iteration i-1

$$ {}^{t+\Delta t}\underline{F}^{(i-i)} = \int_V \underline{B}_L^T\ {}^{t+\Delta t}\underline{\sigma}^{(i-1)}\, dv \qquad (5.2) $$

and $\Delta\underline{U}^{(i)}$ is the increment in nodal-point displacement in iteration i

$$ {}^{t+\Delta t}\underline{U}^{(i)} = {}^{t+\Delta t}\underline{U}^{(i-1)} + \Delta\underline{U}^{(i)} \qquad (5.3) $$

The solution using eq.(5.1) corresponds to the modified Newton-Raphson iteration procedure which is helpful in improving the solution accuracy and in many cases in preventing the development of numerical instabilities. The convergence of the iteration can be accelerated using the Aitken method or, in complex material nonlinear cases (like the welding problem), improved using the BFGS (Broyden-Fletcher-Goldfarb-Shanno) matrix updating method [102].

In the thermo-elastic-plastic and creep model, and

assuming infinitesimal strains, the total strain at time τ, ${}^{\tau}e_{ij}$, is assumed to be given by

$$ {}^{\tau}e_{ij} = {}^{\tau}e^{E}_{ij} + {}^{\tau}e^{P}_{ij} + {}^{\tau}e^{C}_{ij} + {}^{\tau}e^{TH}_{ij} \tag{5.4} $$

where ${}^{\tau}e^{E}_{ij}$ = elastic strain

${}^{\tau}e^{P}_{ij}$ = plastic strain

${}^{\tau}e^{C}_{ij}$ = creep strain

${}^{\tau}e^{TH}_{ij}$ = thermal strain

so that at any time τ during the response the stress is given by the constitutive law for an isotropic thermo-elastic material

$$ {}^{\tau}\sigma_{ij} = {}^{\tau}C^{E}_{ijrs} \left({}^{\tau}e_{rs} - {}^{\tau}e^{P}_{rs} - {}^{\tau}e^{C}_{rs} - e^{TH}_{rs}\right) \tag{5.5} $$

with ${}^{\tau}C^{E}_{ijrs}$ denoting a component of the elastic constitutive tensor.

The thermal strains are

$$ {}^{\tau}e^{TH}_{rs} = {}^{\tau}\alpha_{m}({}^{\tau}\theta - \theta_{R})\,\delta_{rs} \tag{5.6} $$

where ${}^{\tau}\alpha_{m}$ is the average thermal expansion coefficient, θ_{R} is the reference temperature, and δ_{rs} the Kronecker delta. It is this term of eqn. (5.5) that will be modified in the next section to take into account the effects of phase transformation.

The creep strains, ${}^{\tau}e^{C}_{rs}$, are determined using the approach proposed by researchers at the Oak Ridge National Laboratory [56, 57]. Given that in the welding problem the time intervals at high temperatures are short, however, creep will not be considered in this study.

For the plastic strains, ${}^{\tau}e^{P}_{rs}$, the situation is more complicated. Although the classical theory of isothermal plasticity is a well tested one [122,123], extension of the theory to non-isothermal cases is difficult to experimentally substantiate. Several investigators have proposed modifications — Prager [124], Ziegler [125,126], Naghdi [127], Cyr and Teter [128], Sharifi and Yates [129], Chang [130] — but very few experiments have been performed. Corum et al. [57] and Phillips [55] have reported relatively good agreement between theory and experiments, but for temperatures up to about 1000°F only. During welding, though, the temperatures rise to above the A_1 temperature (1210°F for steel) inside the HAZ-base metal boundary and above the liquidus temperature in the weld metal. For lack of any alternative, however, the same non-isothermal theory of plasticity will be used throughout the temperature range encountered in welding problems.

The general form of the yield or loading function for multiaxial stress conditions is

$$ {}^{\tau}F = {}^{\tau}F({}^{\tau}\sigma_{ij}, {}^{\tau}\alpha_{ij}, {}^{\tau}\sigma_{y}) \qquad (5.7) $$

where ${}^{\tau}\alpha_{ij}$ and ${}^{\tau}\sigma_{y}$ are functions of the history of plastic

deformation and temperature. For elastic behavior, ${}^{\tau}F < 0$, and for plastic behavior ${}^{\tau}F = 0$. As a consequence of Drucker's postulate for stable plastic materials, ${}^{\tau}F$ defines a convex surface in the stress-temperature space. It is also assumed that the isothermal normality condition remains valid, so that

$$ {}^{\tau}\dot{e}^{P}_{rs} = {}^{\tau}\lambda \frac{\partial\, {}^{\tau}F}{\partial\, {}^{\tau}\sigma_{ij}} \tag{5.8} $$

where ${}^{\tau}\lambda$ is a positive scalar. The selection of a hardening rule is also required for the calculation of ${}^{\tau}\lambda$. In ADINA either isotropic or kinematic hardening can be assumed. Because cyclic plasticity is expected in the welding problem, the kinematic hardening mechanism, thought by many to better model the phenomena involved, was chosen. The assumptions involved in this mechanism are that the size of the yield surface depends on the temperature only, whereas the translation rate of the yield surface in the stress space depends on the plastic strain rate.

A very important aspect of the analysis is the accurate integration of stresses [103] at time t+Δt and iteration i

$$ {}^{t+\Delta t}\underline{\sigma}(i) = {}^{t+\Delta t}\underline{C}^{E}\left({}^{t+\Delta t}\underline{e}(i) - {}^{t+\Delta t}\underline{e}^{P}(i) - {}^{t+\Delta t}\underline{e}^{TH}(i)\right) \tag{5.9} $$

where

$$ {}^{t+\Delta t}\underline{e}^{P}(i) = {}^{t}\underline{e}^{P} + \int_{t}^{t+\Delta t(i)} d\, {}^{\tau}\underline{e}^{P} \tag{5.10} $$

and where it was assumed that creep strains are zero. The integration of eqn. (5.10) is performed using the α-method where $\alpha = 0$ and 1 correspond to the Euler forward (explicit) and Euler backward (implicit) methods, respectively. The implicit scheme can display considerably better stability characteristics but is more costly, requiring equilibrium iterations. Furthermore, the accuracy of the integration is enhanced with the use of subincrements in each time step, an important feature considering the rapidity with which some of the solution variables and material parameters vary with time during welding.

5.4 Phase Transformation Effects

In most previous stress analyses of the welding problem no consideration was given to the phenomenon of allotropic phase transformations. At the same time in cases where poor agreement was observed between experimental data and analytical results, the discrepancy was attributed exactly to the fact that phase transformations were not taken into account [6].

The limited number of efforts made by investigators to include the phase transformation effects have been outlined in Section 5.1. All of these efforts, however, were based on using dilatational curves and did not concentrate on the fundamentals of the phenomena involved. In this Section such an effort towards a more fundamental approach will be outlined.

The model developed starts with the prediction of the

history of microstructure formation during the cooling stages of the welding cycle using the CCT diagram. It should be understood that this is also an approximation of reality although more rational than the previously used ones. An even better approach would have made use of the rate equations for transformation kinetics. Such equations have not yet been adequately developed, however, for complex alloys, like the high strength quenched and tempered HY-130 steel.

Using the predicted microstructure history and the transformation strains for each allotropic phase change as well as the average thermal expansion coefficients appropriate for each phase, the combined transformation and thermal strains are then estimated. Finally, these calculated strains are incorporated into the finite element program ADINA replacing the conventional thermal strains, ${}^{\tau}e_{ij}^{TH}$.

Details of the model are described in the following subsections.

5.4.1 Microstructure Prediction

The usefuleness of the CCT diagrams for predicting the microstructures during cooling from temperatures higher than the A_1 temperature has been discussed in Section 3.2.2. At the same time, methods for calculating schematic CCT diagrams from isothermal data have been outlined and applied in the case of HY-130 steel in Section 3.4.

An idealization of the CCT diagram is shown in Figure 5.3. The basic assumption involved is that the bainite start,

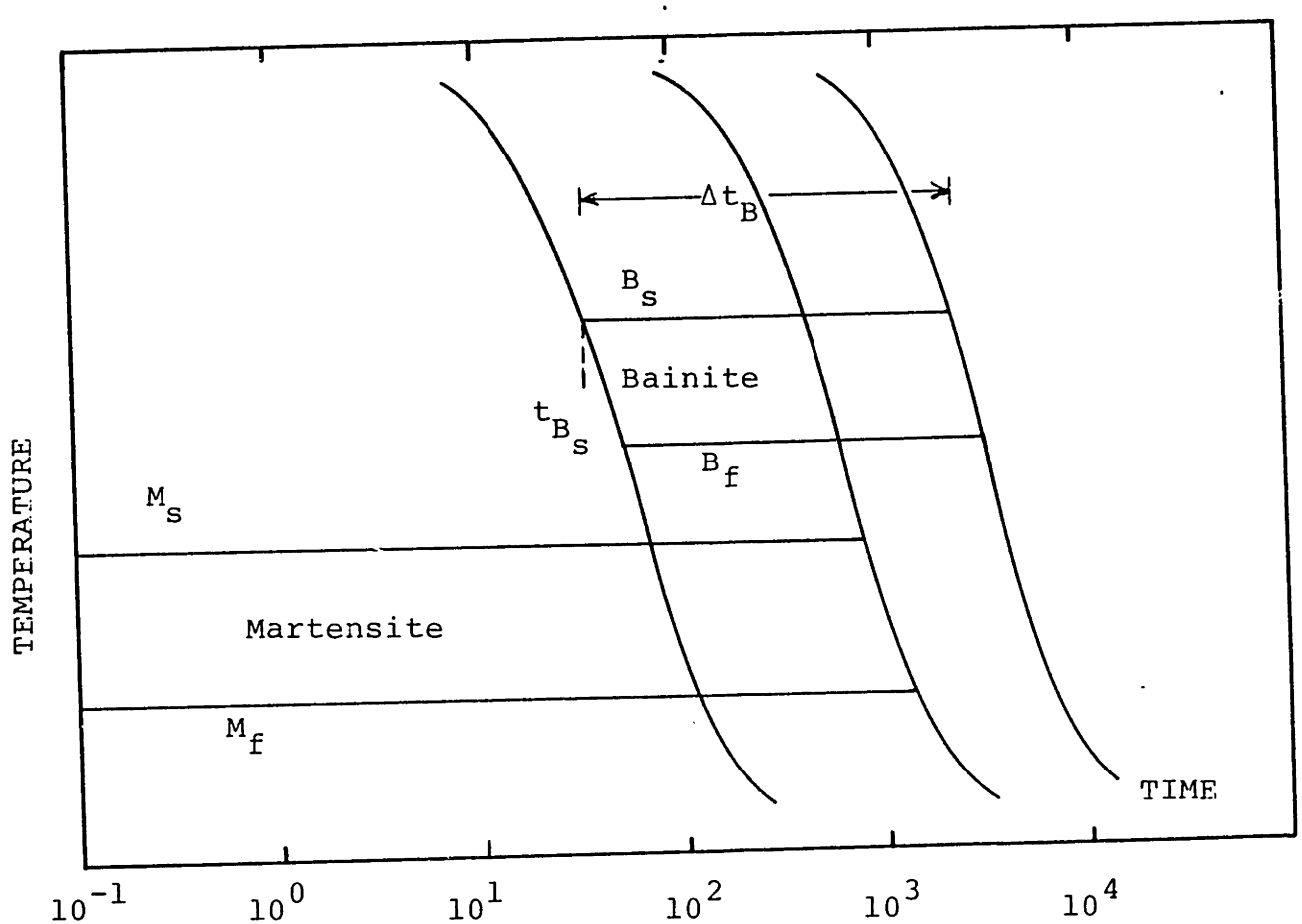

FIGURE 5.3 Idealized CCT Diagram

B_s, and bainite finish, B_f, transformation temperatures are constant, that is independent of the cooling rate, the maximum temperature (above the A_1 temperature) reached before cooling commences, and the time held at this maximum temperature. The last two assumptions require that full austenitization has taken place before, upon cooling, the A_1 temperature is reached and is thought to be reasonable for the welding case.

As far as the constant B_s temperature is concerned, a closer look of Figure 3.14 reveals that the approximation for the case of HY-130 steel is not unrealistic. Although some difference in the B_s temperatures is observed for different cooling rates, the range is not large. Moreover, the cooling rates observed in the weld metal and HAZ of a weld are relatively high, thus diminishing the range of possible B_s temperatures towards the lower size, In the present study the B_s temperature was taken equal to 840°F (449°C).

Furthermore, Figure 5.3 shows the B_f temperature to be in general different than the martensite start, M_s, one. For the case of HY-130, however, the two temperatures can be assumed to be equal. Finally, the assumption of constant M_s and M_f temperature is, as discussed in Section 3.4, a completely acceptable one, owing to the athermal nature of the transformation. Values of M_s and M_f were taken to be 715° and 415°F (379° and 213°C) respectively.

To predict the microstructures during the cooling stage of the welding process an incremental strategy is involved so

that the model can be compatible with the step-by-step solution of the nonlinear stress analysis using the finite element program ADINA. A procedure has therefore to be established that will enable one to calculate the proceeding of each transformation. The following equation, proposed by Toshioka [119], has been used for this purpose:

$$f = f_F \cdot \left[1-\left(\frac{\theta-\theta_f}{\theta_s-\theta_f}\right)^2\right] \qquad (5.11)$$

where f is the fraction of the product transformed at temperature θ, f_F the fraction of the product to be transformed at the transformation finish temperature, θ_f, and θ_s the start transformation temperature. Equation (5.11) is applied separately for each allotropic transformation, namely for the martensite to austenite one upon heating and for the austenite to bainite and austenite to martensite ones upon cooling.

For the calculation of f_F the following guidelines have been applied. Referring to Figure 5.4, the martensite to austenite transformation during the heating stage of the welding cycle takes place progressively within the temperature range bounded by the A_1 and A_3 temperatures. Since full austenitization is assumed to occur as soon as the A_3 temperature is exceeded, f_F for this transformation has been taken to be equal to unity regardless of the heating rate.

The situation is somewhat different in the case of the austenite to bainite phase transformation, which takes place

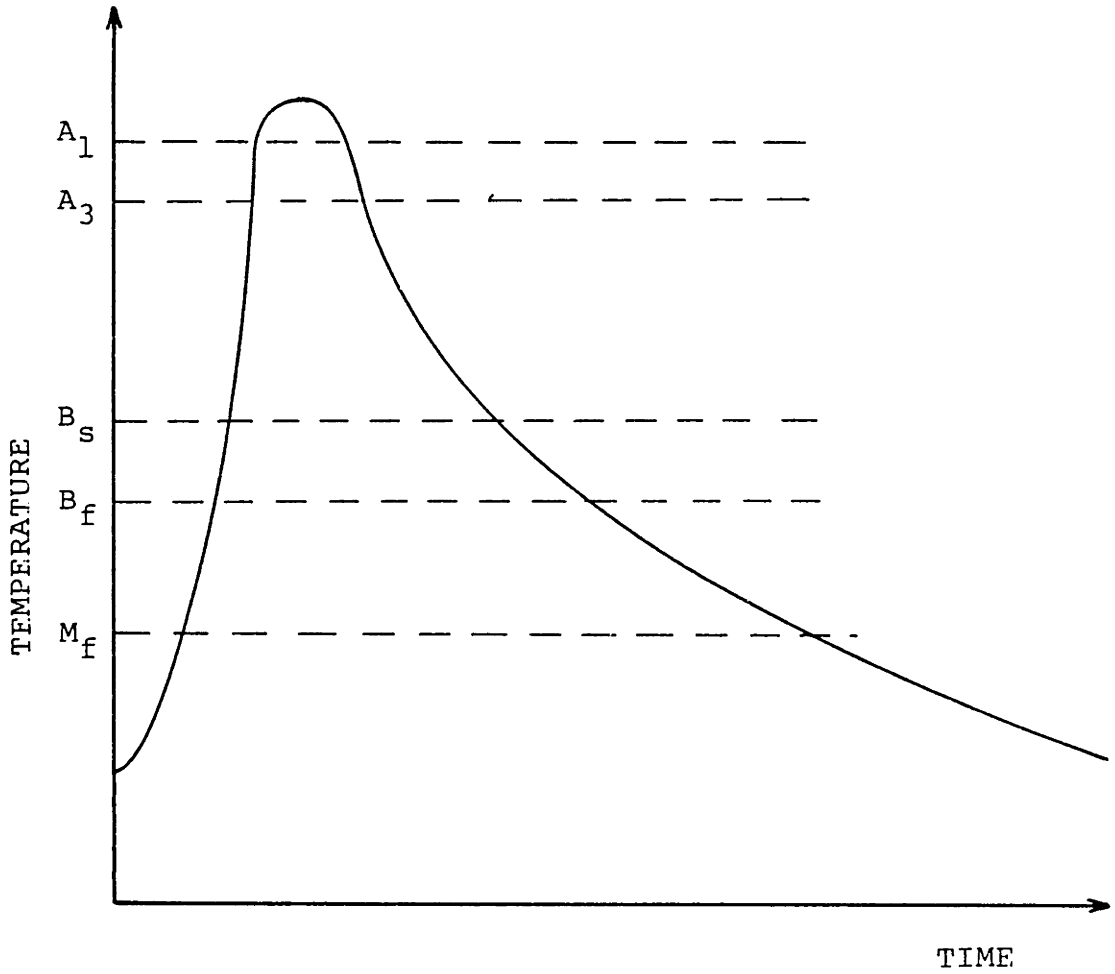

FIGURE 5.4 Typical Temperature History Inside the HAZ of a Weld.

between the B_s and M_s temperatures. A major parameter is the cooling rate. If it exceeds a critical value then, as shown in Figure 5.3, no bainite is formed. Alternatively, if for a particular cooling curve the time elapsed between the instance the curve passes the A_1 temperature and the instance it passes the B_s temperature is less than the precipitation start time for bainite, t_{B_s}, the bainite reaction will not take place. This latter criterion was the one used in this study. Furthermore, if the bainite reaction does occur, its extent will depend again on the cooling rate, with slower cooling rates resulting in the final formation of larger fractions of bainite, f_F. The occurance of this phenomenon has been modeled by calculating f_F using

$$f_F = (\Delta t)_B \cdot (\log_{10} t^*_{B_s} - t_{B_s}) \qquad (5.12)$$

where $(\Delta t)_B$ is the time interval over which the bainite reaction can take place (see Fig. 5.3), $t^*_{B_s}$ is the time elapsed between the instances the cooling curve passes the A_1 and B_s temperatures, and t_{B_s} has been previously defined. Note that f_F has to be smaller or equal to 1.

For the case of the martensite reaction things are simpler. Since this is an athermal transformation, it is not dependent on the cooling rate. As a consequence, f_F is equal to the remaining austenite fraction (the one that has not been already transformed to bainite). For the case in which no bainite reaction has taken place (cooling rate higher than the

critical one), it is obvious that f_F is equal to unity.

Finally, it should be mentioned that in the previous discussion it was assumed that full austenitization has taken place, i.e. that the maximum temperature reached was higher than the A_3 temperature. If, on the other hand, the maximum temperature lied between A_1 and A_3, in which case only partial austenitization took place, all equations giving f_F will have to be multiplied by the fraction of austenite formed as given by eqn. (5.11).

5.4.2 Calculation of Transformation and Thermal Strains

Based on the microstructure predictions calculated by the methodology outlined in the previous subsection, the transformation and thermal strains developed during the welding cycle can be calculated. The importance of including these transformation strains has been recognized by several authors, including Linnert [131], especially for thick weldments. This importance stems from the expansion associated with allotropic phase changes, as opposed to the contraction due to cooling.

To qualitatively show the phenomena involved, the cooling of a thick section in air will be considered. The surface of the section cools quicker than the interior, thus reaching the transformation start temperature (for the bainite or martensite reaction) quicker. As a consequence the surface expands. To accommodate this surface expansion the metal in the center region, which is still austenitic and much hotter,

is pulled towards the surface causing the ends of the section to be forced inwards and thus resulting in a concave shape. As the cooling proceeds, the center also reaches the transformation start temperature and starts expanding. The surface layers must, therefore, also expand. At this stage, however, the surface is contracting due to thermal strains, so that the surface expansion can take place by plastic flow only. After the center has gone through the transformation, it again starts contracting but at a higher rate than the surface (owing to the higher temperature of the former). This contraction difference tends to pull the surface inwards. For self-equilibrating purposes this tensile pull of the center must be balanced by the compressive strength of the surface. At room temperature the section thus ends up with compressive residual stresses at the surface and tensile ones in the center.

To calculate these expansions and contractions, the combined thermal and transformation strain, e_{rs}^{TH}, can be written as

$$e_{rs}^{TH} = (e_1+e_2+e_3) \cdot \delta_{rs} \qquad (5.13)$$

where e_1 is the thermal strain in a mixture of phases, e_2 the transformation strain, e_3 the thermal strain in a single phase, and δ_{rs} the Kronecker delta.

The estimation of the thermal strains e_1 and e_3 requires knowledge of the microstructures present and of the average thermal expansion coefficients of austenite, α_A, bainite, α_B,

and martensite, α_M. Similarly, to calculate the transformation strain, e_2, one has to also know the transformation strains for each separate phase change, namely from martensite to austenite, $e^{TR}_{M\to A}$, from austenite to bainite, $e^{TR}_{A\to B}$, and from austenite to martensite, $e^{TR}_{A\to M}$. Table 5.1 shows the values used in this study, taken from a variety of sources [119,131].

The equations used for calculating each term in eqn. (5.13) depend on the temperature history the considered location has undergone. Appendix D gives in detail these equations for all possible cases encountered during the welding cycle.

To show the impact the inclusion of phase transformation effects has on the thermal strain of a section which is free to expand or contract, Figure 5.5 is constructed. The solid line depicts for a specific temperature history the thermal strain during the heating stage of this history, including the phase transformation effects (phase change from martensite to austenite). This is the usual curve assumed as input in previous stress analyses using the finite element method. Upon cooling, the same curve was usually assumed, thus neglecting the phase changes from austenite to bainite and/or martensite. By contrast, the intermittent line shows clearly the effect the expansion accompanying these transformations has on the thermal strain.

It becomes evident from the previous discussion that the model developed captures the main characteristics of the phase transformation effects. The accuracy of the analysis will, of

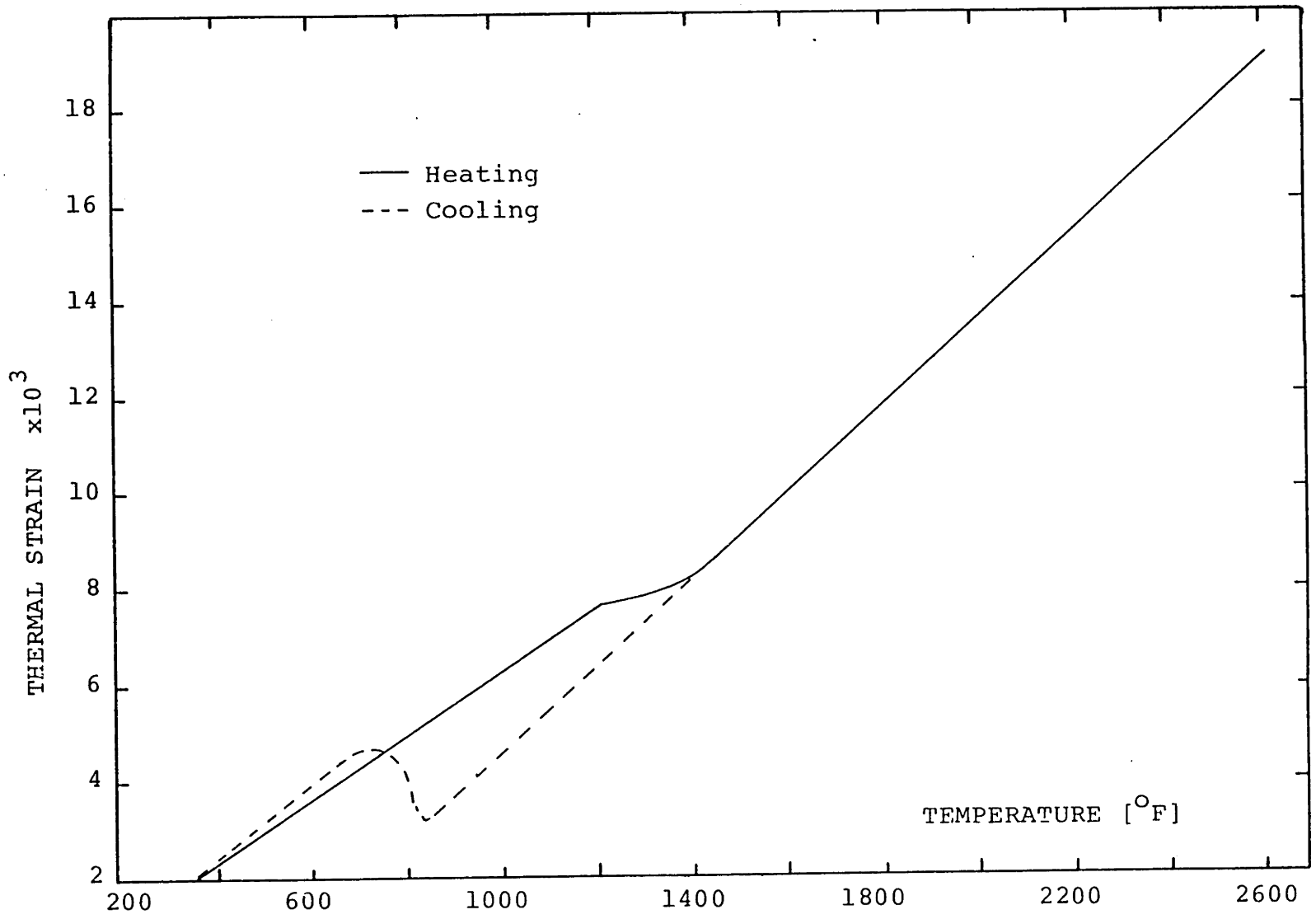

FIGURE 5.5 Typical Dialatational Curve Including Phase Transformation Effects.

TABLE 5.1 Values Used for the Calculation of Transformation Strains

Transformation temperatures:

	^{o}F	^{o}C
A_1	1210	654
A_3	1415	768
B_s	840	449
M_s	715	379
M_f	415	213

Thermal expansion coefficients:

	in/in.^{o}F	mm/mm.^{o}C
α_A	8.9×10^{-6}	4.9×10^{-6}
α_M	7.5×10^{-6}	4.2×10^{-6}
α_B	6.7×10^{-6}	3.7×10^{-6}

Transformation strains:

$\epsilon^{TR}_{M \to A}$	-0.10×10^{-2}
$e^{TR}_{A \to B}$	0.25×10^{-2}
$e^{TR}_{A \to M}$	0.38×10^{-2}

course, depend on the correct evaluation of the required input.

5.5 Weld Model Using the FEM

In this section all the necessary considerations for the modelling of a multipass weldment between two relatively thick plates will be discussed. They include the geometry and boundary conditions, the mechanical properties of the material, and some thoughts on the solution strategy.

5.5.1 Geometry - Boundary Conditions

A cross-section of the weldment in its midlength was used to calculate the transient strains, transient stresses, and residual stresses due to welding. This is rationalized by the fact that for relatively long plates the maximum stresses are developed in this region.

Furthermore, the plane strain assumption was used. This implies that all sections normal to the weld line remain plane during the entire welding process. Though this assumption is probably adequate in regions somewhat removed from the weld puddle, it may not be valid in the neighborhood of the molten metal. The approach employed therefore prevents calculation of distortions ahead of the welding arc, and may inhibit accurate computations of deformations in the immediate vicinity of the weld puddle. Because of the various other assumptions involved in the material modelling of the weld metal (as outlined in Section 5.5.2), however, the plane strain conditions should be adequate. Furthermore, the method enables one to determine

complete transient strain, transient stress, and residual stress distributions, transverse distortions, and estimates of the damage (permanent plastic strains) accumulated during the welding process.

To be able to characterize the longitudinal bending distortion as well one can utilize three-dimensional analysis. It can be noted, however, that by introducing three additional degrees of freedom per node, in other words by resorting to the generalized plastic strain approach, one could conceivably obtain similar results. Such an approach would let the longitudinal strain, e_{xx}, be a linear function of the longitudinal extension and the two rotations about the y and z axes of Figure 4.1. It is recommended that an effort towards this direction be undertaken by future investigators.

The boundary conditions used in the analysis should be such so as to allow free expansion of the weldment in the transverse direction as well as bending. At the same time the structure should be properly restrained to eliminate all possible modes of rigid body motion; otherwise the stiffness matrix will not be positive definite. The exact boundary conditions used will be discussed when the finite element mesh used is introduced.

5.5.2 Material Properties

The temperature dependence of the Young's modulus, E, Poisson's ratio, ν, virgin yield stress, σ_{vy}, and strain hardening modulus, E_T, are all required input for the thermo-

elastic-plastic and creep material model incorporated in ADINA. This dependence has been explained and evaluated in Section 3.3.1 for the case of HY-130 and the values obtained there were used in this analysis. The temperature dependence of the average thermal expansion coefficient, α, is also a required input, but it has been overriden in this study by the phase transformation model discussed in the previous Section.

A word of caution is appropriate at this point as far as the material properties above the liquidus temperature is concerned. The material does not have any strength when molten since all its mechanical properties are zero. But due to numerical considerations, zero properties cannot be entered as input to the program. Hence to avoid any instabilities (or even divisions by zero) very small values for E, σ_{vy}, and E_T should be used above the liquidus temperature.

Another point is the accumulation of plastic strains in the regions that become molten during the welding cycle. When the temperature reaches the liquidus these plastic strains are physically relieved, starting to accumulate again when the metal solidifies. The presence of nonzero material properties above the liquidus, however, would cause the plastic strains not only to continue accumulating but also to reach artificially high values owing to the very low magnitude of the mechanical properties. It was therefore necessary to modify ADINA by imposing a total relief of plastic strains when the material melts.

5.5.3 Solution Strategy

One of the most important decisions an analyst has to make when performing a nonlinear incremental stress analysis is the solution strategy to be followed, because the accuracy and the convergence characteristics of the solution depend very much on it. This is especially true for complex situations involving highly nonlinear material behavior like the one encountered in the welding problem. Bathe and Cimento [102] provide some guidelines to be followed in such cases. Based on this article and on experience gained in making simpler nonlinear analyses, a discussion will be made on the solution strategy used in analyzing the welding problem.

As mentioned in Section 5.3 the solution of the incremental equations can be made using either the modified Newton-Raphson iterative technique (with or without the Aitken acceleration) or the BFGS matrix updating method. Both were tried for the initial steps of the analysis (the first 100 steps). The Newton-Raphson technique did not exhibit, however, good behavior signaling on several occasions increase in the out-of-balance loads owing to the sudden stiffening of the structure during elastic unloading from the plastic stage at several integration points. On the contrary, using BFGS updates no such behavior was observed. This last method was thus used for the entire analysis.

As far as the displacement and force convergence tolerances are concerned, the default value of $\varepsilon_F = 0.1$ was used

for the latter, whereas one hundredth of the default value, namely $\varepsilon_D = 1x10^{-5}$, was used for the former because of the softening involved in the problem (plasticity). Iterations and stiffness reformation were required at each time step because of the complex material behavior.

Table 5.2 provides a summary of the solution strategy. Also shown are the parameters used in integrating the stresses at each time step.

TABLE 5.2 Solution Parameters Used with ADINA

Equilibrium Iteration Parameters	Stess Integration Parameters
METHØD = 2	ALPHA = 0.0
IATKEN = 0	XISUBM = 150.
DTØL = 0.00001	XNITE = 15.
RTØL = 0.1	XNALG = 2.
STØL = 0.5	TØLIL = 0.005
	TØLPC = 0.1

Note: The above symbols refer to the ones used for the variables in ADINA [100].

5.6 Results

The same finite element mesh as the one used for the heat transfer analysis and shown in Figures 4.8a and 4.8b was initially utilized to analyze the strains and stresses developed during the welding experiments described in Section 4.4. Figure 5.6 shows the constraints imposed; nodes 6, 68, and 70 are

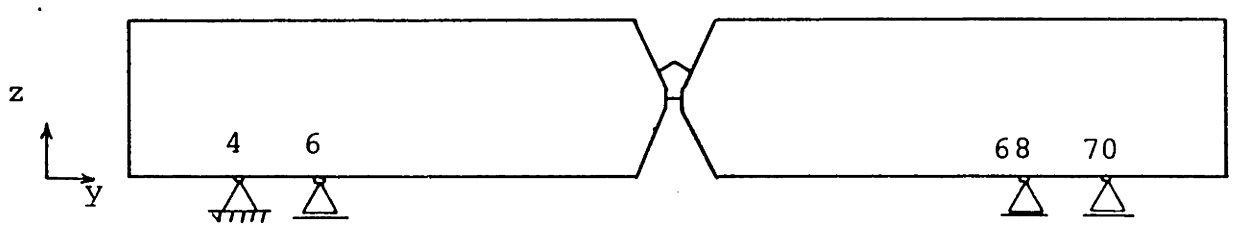

FIGURE 5.6 Constraints Applied to the Finite Element Model.

not allowed to move in the z-direction, whereas node 4 is not allowed to move at all. It is thus possible for the weld to freely expand in the y-direction and also to bend transversly.

This case was analyzed for three seconds before and three seconds after the arc center passed over the middle of the cross-section. The obtained results were not satisfactory, however, owing to the crudeness of the mesh around the weld metal. Based on these facts and considering the long computer time and large cost required for the analysis, it was decided to analyze only the first welding pass (of the twelve involved) using a finer mesh to more accurately capture the rapid variation of the problem's variables close to the weld centerline, while at the same time taking advantage of the geometric symmetry of the first welding pass. Figures 5.7a and 5.7b show the finer mesh used in the right half part of the cross-section. In the first figure the rightmost 11.5 in are shown, whereas in the second one the 0.5 in to the right of the weld centerline are depicted in different scale.

Four- to six-node isoparametric elements were used; special care was given not to include any triangular elements in the mesh. A total of 77 nodes and 47 elements were utilized. Nodes 2 and 4 were restrained in the z-direction, and nodes 74 through 77 in the y-direction.

Figure 5.8 shows the accumulation of the effective plastic strain, $\bar{e}^P$, at three points on the midthickness of the plate up to four seconds after the center of the arc has passed

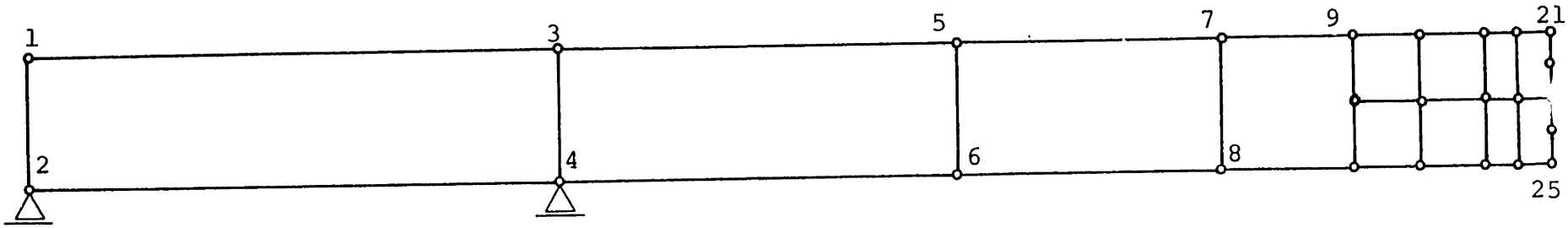

FIGURE 5.7a Finer Finite Element Mesh Used in Stress Analysis of Welding Problem.

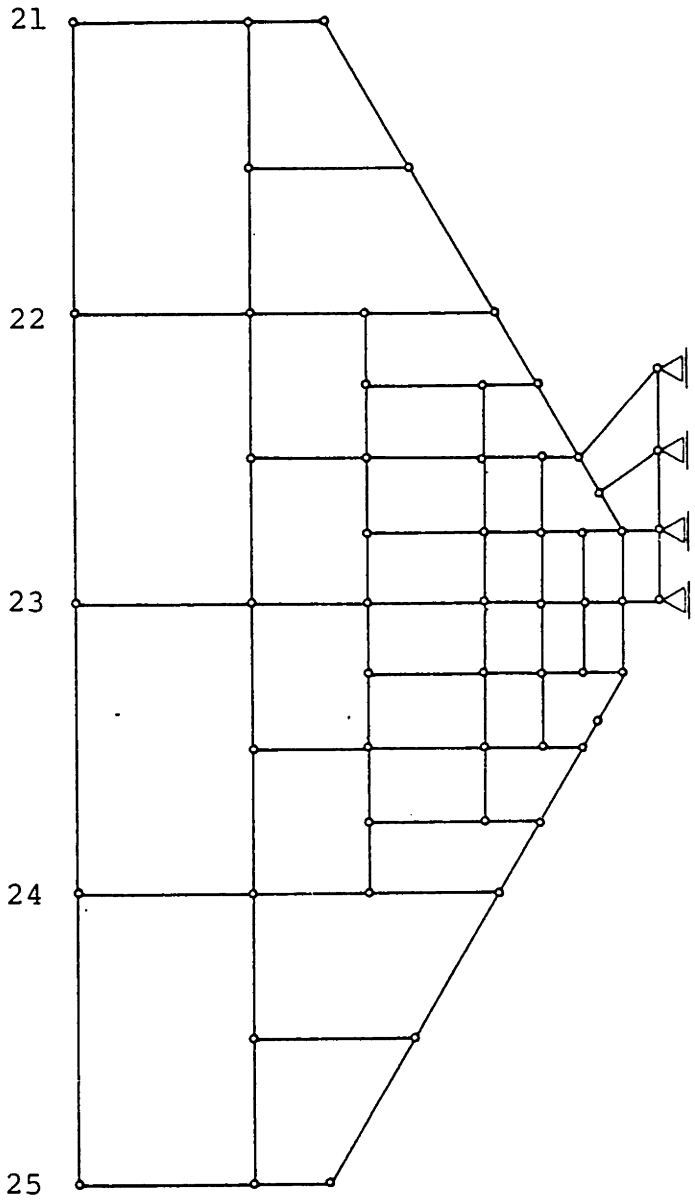

FIGURE 5.7b Finer Finite Element Mesh, cont. (0.5 in to the right of weld centerline).

FIGURE 5.8

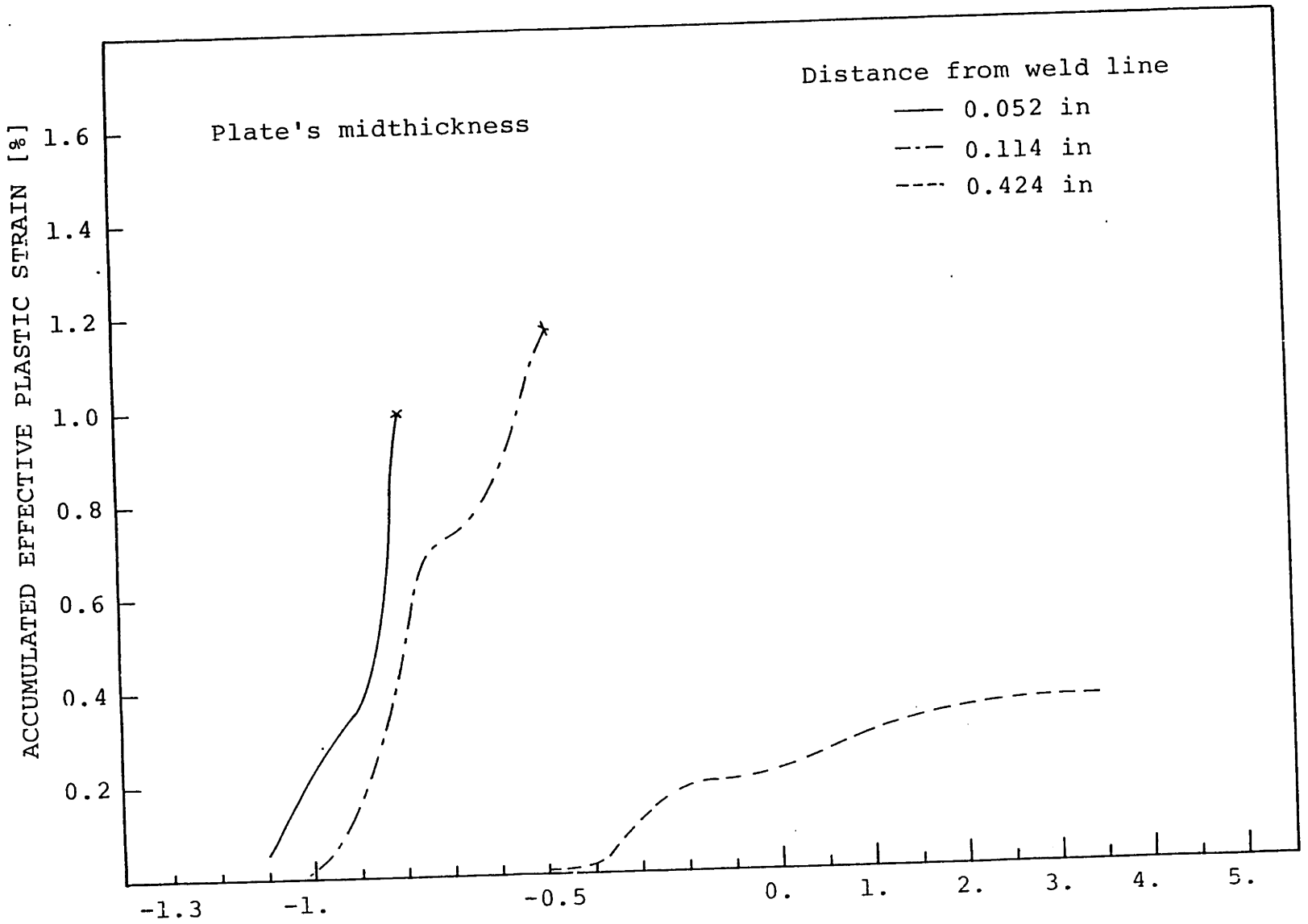
Plate's midthickness
Distance from weld line
0.052 in
0.114 in
0.424 in
ACCUMULATED EFFECTIVE PLASTIC STRAIN [%]
1.6
1.4
1.2
1.0
0.8
0.6
0.4
0.2
-1.3
-1.
-0.5
0.
1.
2.
3.
4.
5.

the middle of the cross section. The rapid accumulation of $\bar{e}^P$ at the two points closest to the weld centerline is evident. Also shown is the relaxation of these strains as soon as melting occurs. On the other hand, for the point located 0.424 in (10.8 mm) away from the welding centerline, the accumulation is much slower. This is the pattern observed for the whole HAZ region.

Figure 5.9 depicts the longitudinal transient stress, σ_x, history at the same points and for the same time interval. These stresses are compressive as would have been expected since at the instances shown the material expansion is hindered by the relatively colder bulk of the metal located outside the HAZ. For the two points closest to the weld centerline these stresses become negligibly small as soon as melting occurs.

The transverse transient strain, e_{yy}, history for two points on the top surface of the plate are compared with experimental measurements in Figure 5.10. Good correlation is observed.

A more complete history of the accumulated plastic strain, the longitudinal stress and the transverse strain is shown in the next three figures. Plots of accumulated effective plastic strain versus time at various locations on the plate's mid-thickness are shown in Figure 5.11. In the weld metal zone, plastic strain is built up rapidly as the material yields in compression. At the melting region this plastic strain is completely relieved, to rapidly reach again a level in close pro-

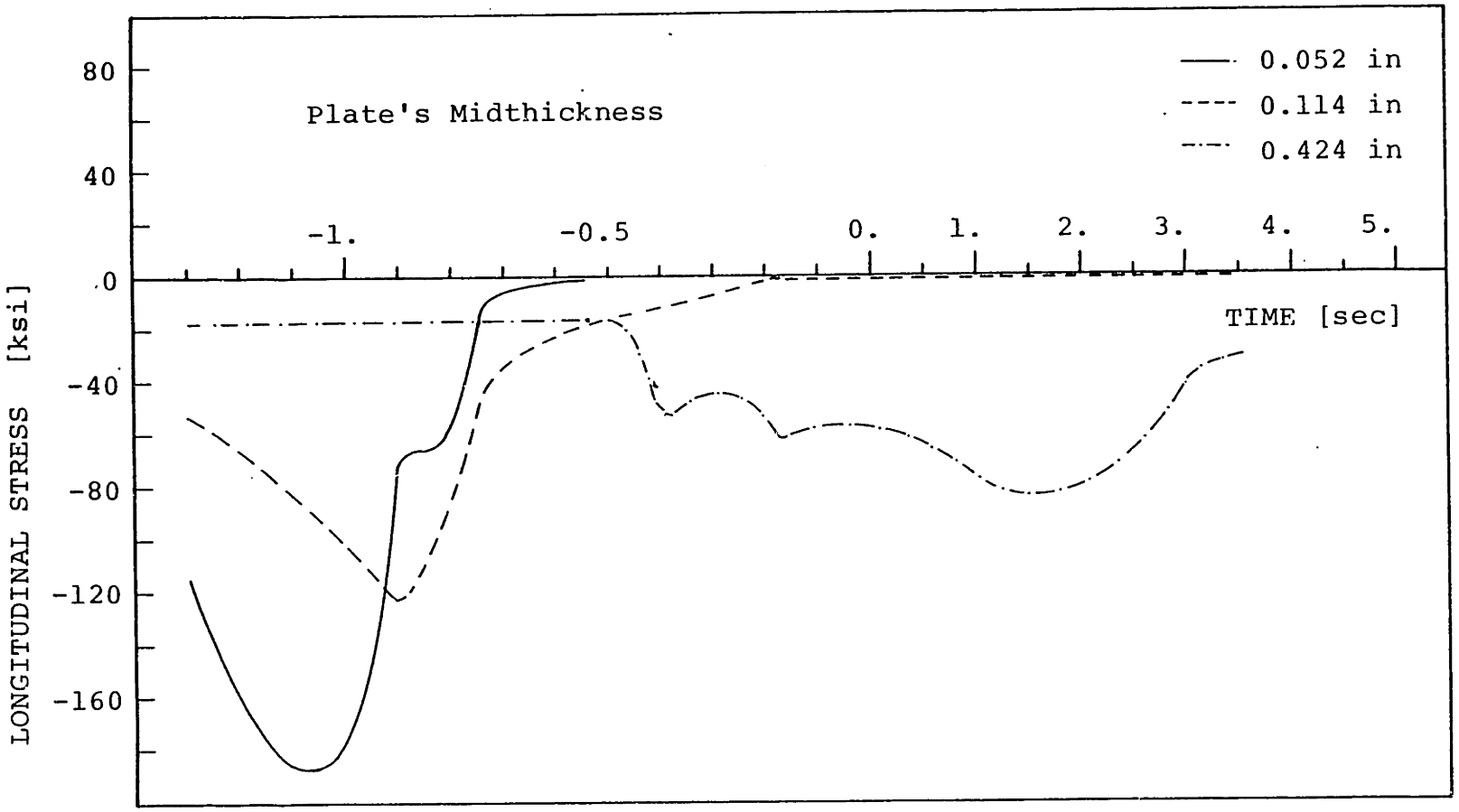

FIGURE 5.9 Transient Stress History at Various Distances from Weld Centerline (initial 5 sec).

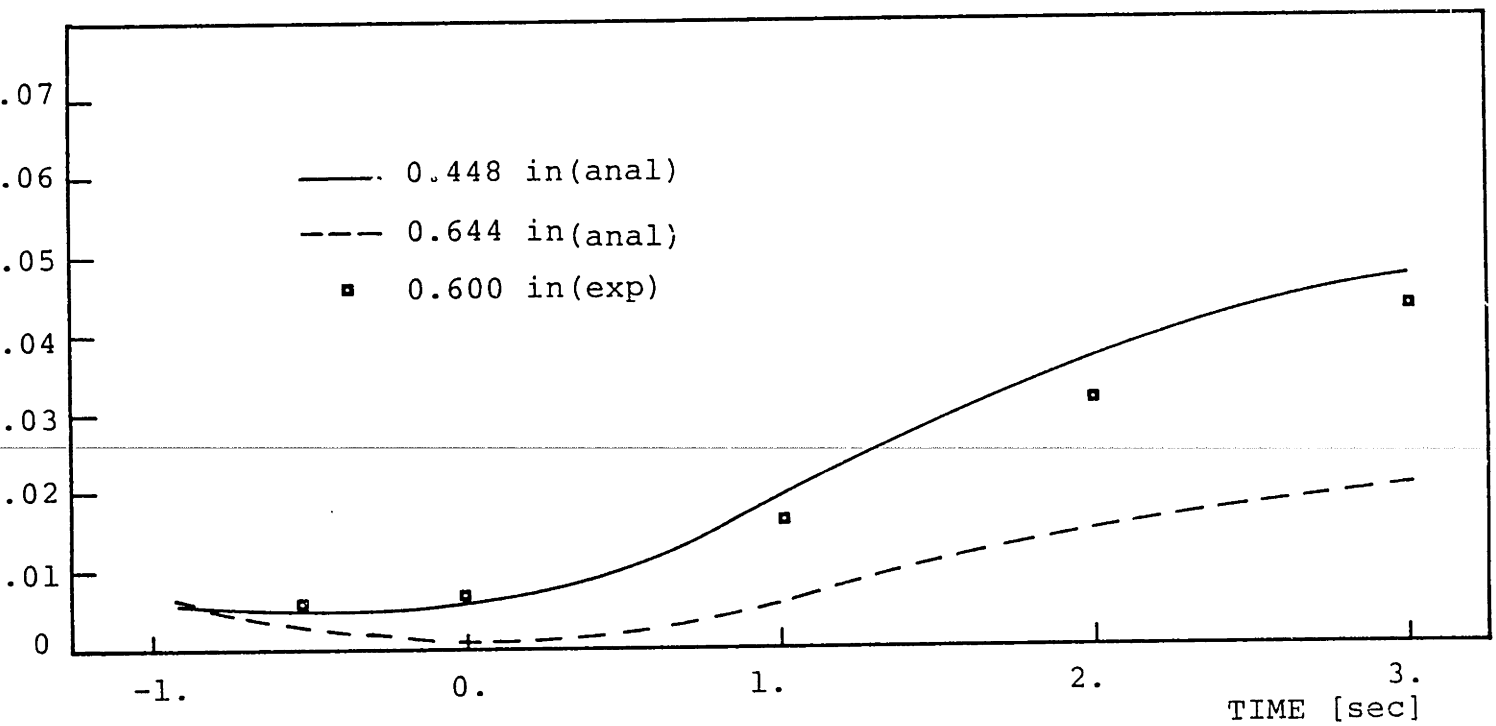

FIGURE 5.10 Comparison of Transverse Transient Strain Histories - Experimental Data vs. Analytical Predictions (initial 4 sec).

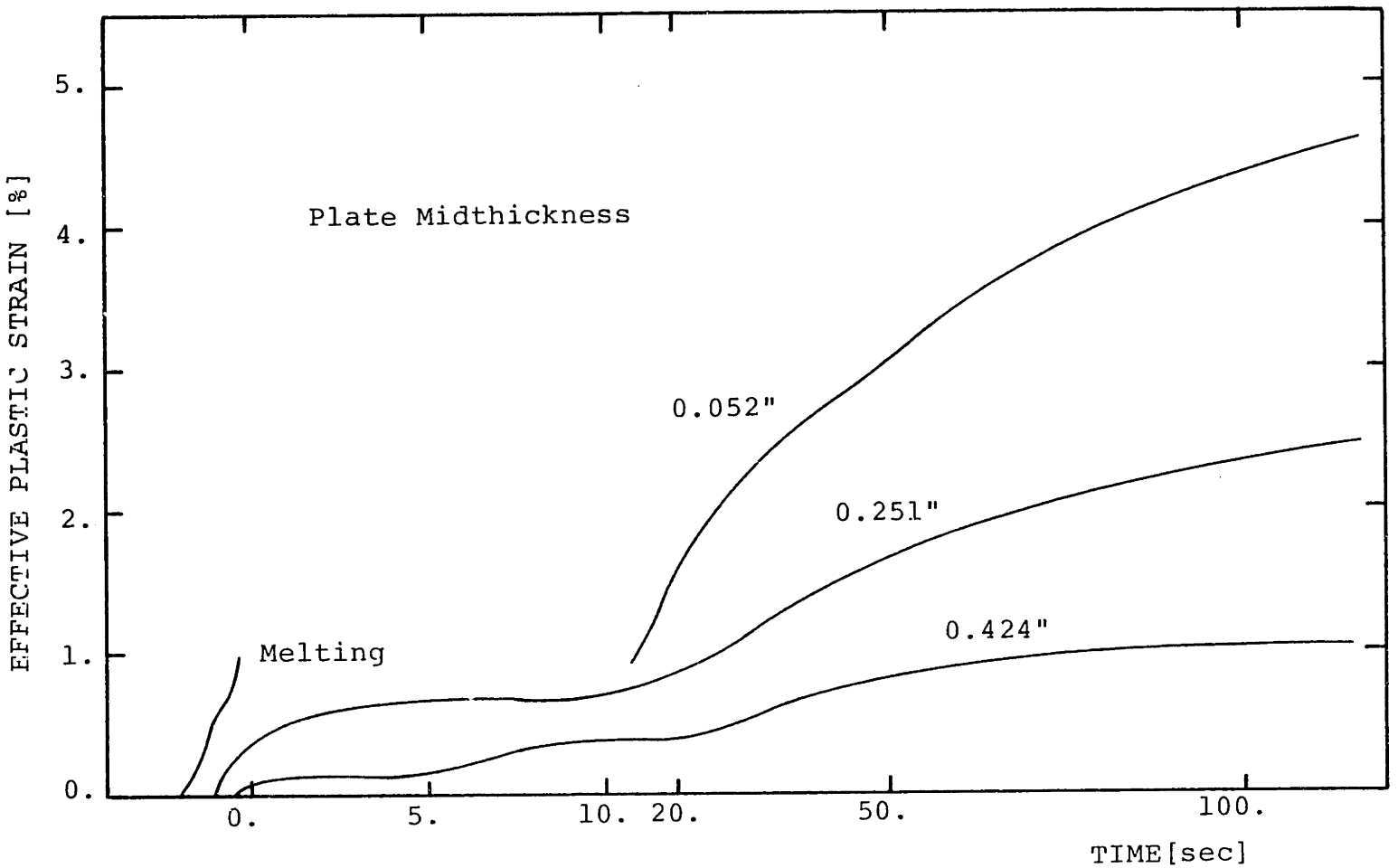

FIGURE 5.11 Accumulated Effective Plastic Strain History at Various Distances from the Weld Center-line.

ximity to that existing prior to melting upon solidification. As cooling continues and yielding in tension progresses, the plastic strain steadily increases but at a smaller rate than before. In the heat-affected zone, plastic strain is accumulated during heat-up in much the same way as in the weld metal zone but not quite as rapidly. As the material cools, it yields in tension and further plastic strain is accumulated.

Figure 5.12 shows calculated transient longitudinal stress distributions. Compressive stresses exist in the weld metal prior to melting. When the metal is in its molten stage, negligible compressive or tensile stresses were calculated.* As cooling commences, tensile stresses start appearing in the weld metal. These stresses then build up to the residual stress pattern when ambient temperature is reached. For self-equilibrating purposes, compressive stresses exist in areas removed from the weld centerline. Note in Figure 5.12 the effect of phase transformation, causing a sudden decrease in the tensile stresses.

Comparison of the experimentally measured transverse transient strain history at a point located on the top surface of the plate is made with the numerically obtained results in Figure 5.13. The correlation is relatively good if one takes

---

*Note that in reality the molten metal has no strength. For numerical reasons, however, a very small amount of strength had to be assumed as explained in previous Sections.

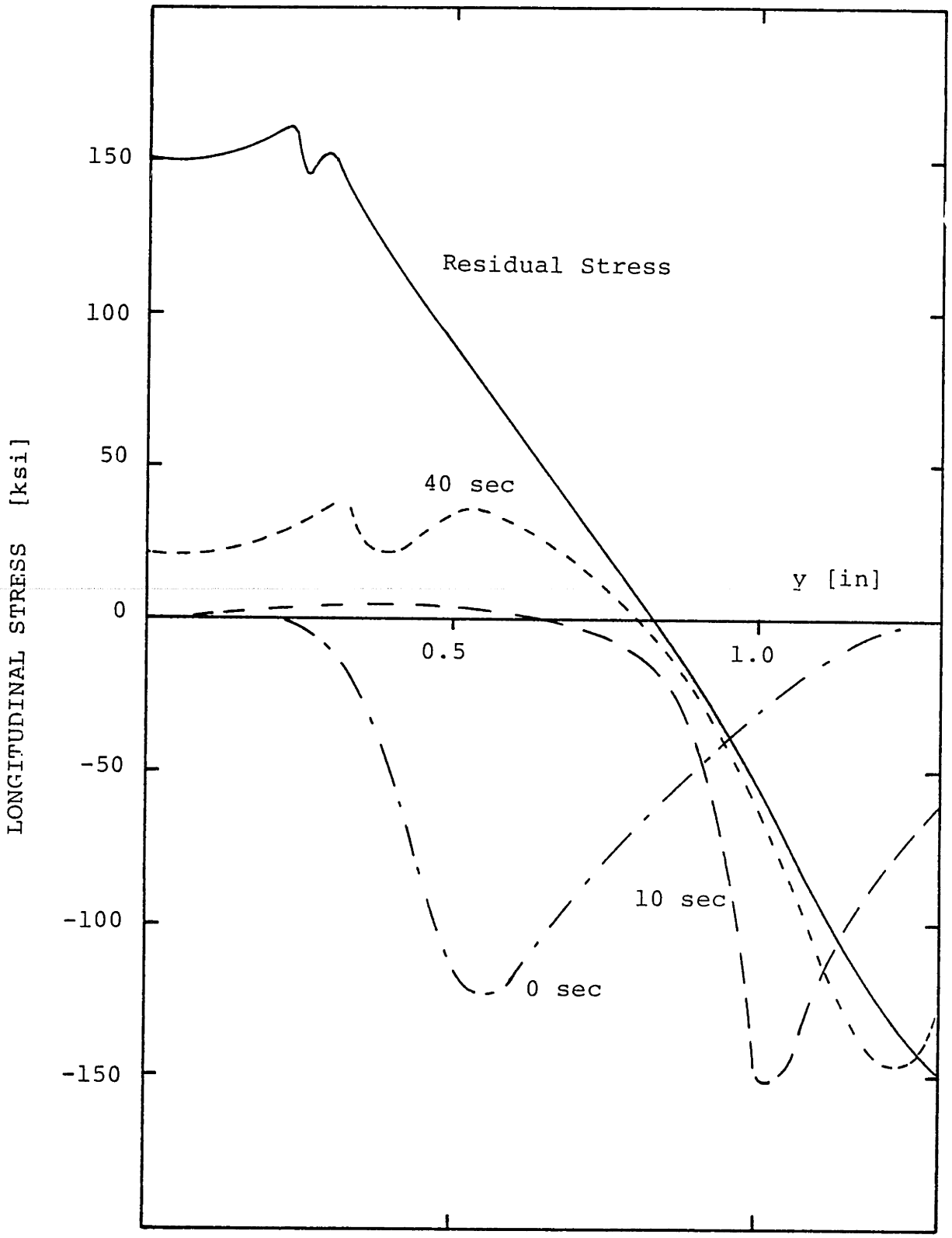

FIGURE 5.12 Longitudinal Stress Distribution at Several Time Instances.

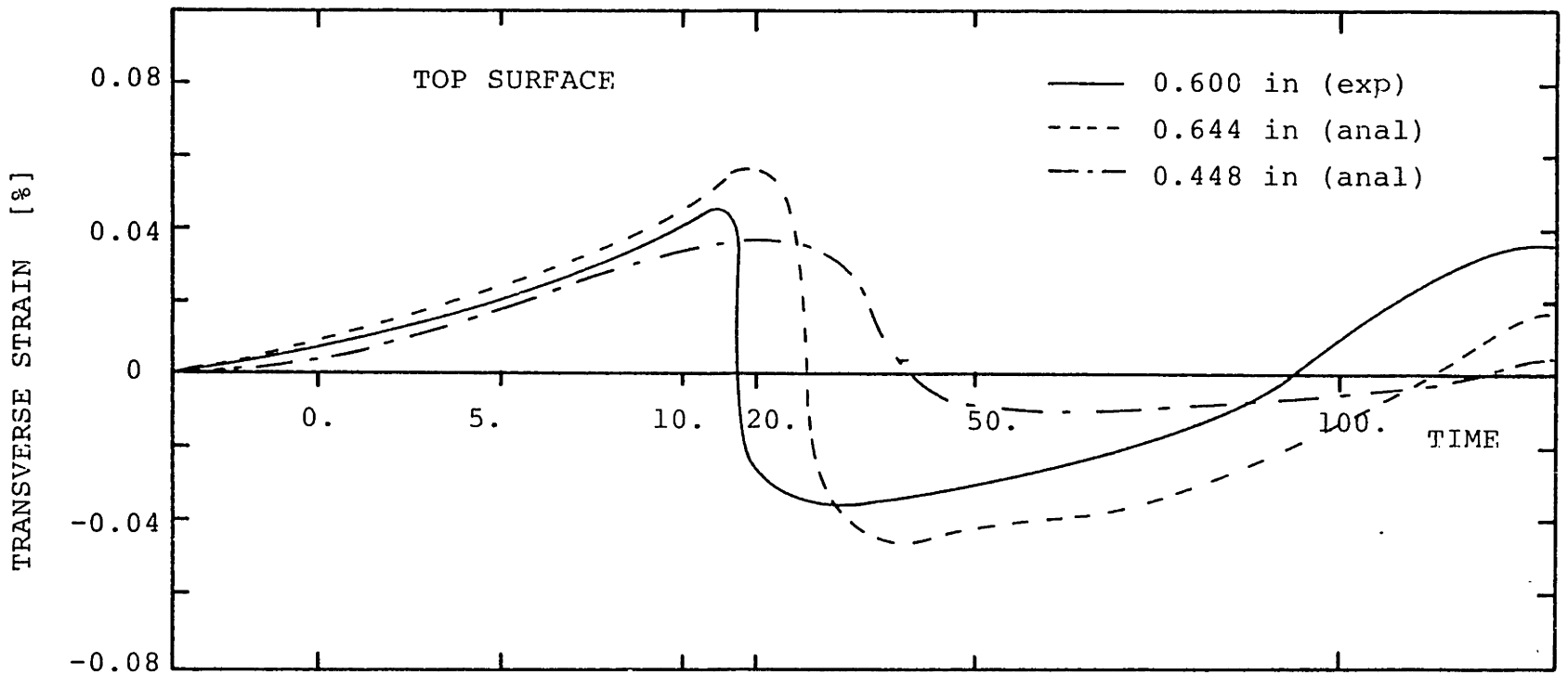

FIGURE 5.13 Comparison of Experimentally Measured Transverse Transient Strains on the Plate's Top Surface with Numerical Predictions.

into account the various assumptions involved in modeling the complex welding problem. A delay in the transition from tensile to compressive and again from compressive to tensile strains is observed in the analysis. The same delay as far as the occurence of the maximum strain is also exhibited. It is believed that this phenomenon is primarily due to the relative coarseness of the finite element mesh, and the complex loading history present in the welding problem.

Summarizing it can be said that the finite element model developed based on ADINA modified for phase transformation effects captures most of the important aspects of the welding stress analysis. Although some discrepancies have been observed between the obtained results and experimental data, considerations of cost and the assumptions made do not allow much more sophisticated analyses at present. It is expected, however, that the dramatically decreasing computer costs, together with developments in the areas of coupled thermoplasticity, will enable investigators to perform more accurate analyses in the future.

CHAPTER VI

CONCLUSIONS AND RECOMMENDATIONS

6.1 Conclusions

A closed-form analytical solution capable of predicting temperature distributions in a finite thickness plate caused by a moving three-dimensional finite heat source on its top surface has been developed in this study. The linear temperature dependence of the material's thermal conductivity and heat losses from the top and bottom surfaces of the plate have been taken into account in the analysis. A parametric investigation of the effects the magnitude of the heat input, the concentration of the heat source and the heat losses have on the results obtained by using this model was undertaken. Comparison of the model's predictions with experimental results show good correlation in the cases of thin-plate welding and bead-on-plate welding.

The classical point heat source solution was also modified to enable it to predict temperatures during multipass welding. The obtained results showed good agreement with experimental data.

Since the high strength quenched and tempered HY-130 steel was the material used in this investigation, a thorough examination of its transformation kinetics and of the temperature dependence of its mechanical and physical properties was made. In the absence of available data on the continuous cooling transformation kinetics, existing methods for estimating

them on the basis of isothermal data were modified and applied in the case of the HY-130 steel. The modifications involved the use of log-linear cooling curves instead of the linear ones presently used.

Plate specimens made of HY-130 steel and measuring 24 in x 12 in x 1 in were welded using the multipass GMA process. Temperatures and transient strains were measured during each welding pass. The collected data were compared with numerical predictions as discussed in the following paragraphs.

Using the multipurpose nonlinear finite element program ADINAT, the heat transfer of the above mentioned experiments was modelled. The temperature variation of the material properties, nonlinear convection and radiation heat losses, and the appearance of each welding pass through the birth-and-death option, all features of ADINAT, were taken into consideration. Four different analyses were performed to better establish the magnitude of the heat input and the temperature dependence of the convection coefficient. Very good agreement of the results obtained was observed upon comparison with experimental data.

Finally, a stress analysis of the welding problem was made using the thermo-elastic-plastic and creep material model of the nonlinear finite element program ADINA. This model was further developed by including the effects of phase transformation, being of particular importance when welding quenched and tempered steels such as the HY-130 one. These effects were calculated by first evaluating the microstructure history ba-

sed on an idealization of the CCT diagram previously derived; then the dilatational curve for the cooling curve of each integration point in the finite element mesh was found using data for each of the phases present at any time during the welding cycle. These dilatational curves were then used to replace the conventional thermal strains of the program's model.

Comparison of the obtained results with experimental data were good confirming the importance of phase transformation effects.

6.2 Recommendations for Future Research

Based on the findings and observations made in this study the following topics for future research can be recommended:

1. One of the basic assumptions underlying all efforts towards analyzing the temperature and stress fields during welding is the uncoupling of the thermal and mechanical problems. This assumption may be good in most cases but there is always the question regarding its validity in and around the molten pool. The development of a coupled thermo-plasticity theory, currently in its initial stages, should therefore be further pursued so that a better understanding of the phenomena involved and consequently a test of the uncoupling postulate can be accomplished.

2. In the heat transfer analysis using numerical techniques, such as the finite element method, the assumption is made that the heat transfer mechanism is pure conduction even when the weld metal is in a molten stage. The combined conduction

and convection mechanisms that are actually present in the liquid metal are treated by an apparent increase in the value of the material thermal conductivity. Although this method has in general yielded satisfactory results, it is recommended that a more fundemental modelling of the phenomena be undertaken by including the convection heat transfer mechanism in the analysis as well. It is of course understood that such an objective will be a long range one because of the complexities and uncertainties present inside the weld fusion zone.

3. An initial effort towards including the effects of phase transformation in the stress analysis of a welded structure has been undertaken in this study. The model developed made use of the CCT diagrams to predict the microstructrure history in the weld metal and the HAZ. A more fundamental approach would have made use of the rate equations of transformation kinetics. Such equations, however, are not available in general; the ones already developed pertain to very simple alloys, usually steels of the eutectoid composition. It is therefore recommended that research in the direction of developing rate equations for more complicated alloys, high strength quenched and tempered steels for example, be undertaken.

4. One of the inputs required in both the heat transfer and stress analyses of welded structures is the temperature dependence of the physical and mechanical properties of the material under consideration. The available data on this dependence are, however, scarce and whenever present do not cover the

whole temperature range encountered during welding, i.e. from room to above liquidus temperature. At the same time slight variations in alloy composition can have a drastic impact on the material properties. As a consequence, a significant amount of rational judgement is involved in estimating them, with usually uncertain results regarding the accuracy of the obtained values. It is therefore recommended that an experimental program be undertaken to measure the temperature variation of these properties, at least for some materials. The obtained results could then be compared with the statistical thermodynamic theories that have been developed over the years for estimating these values. This effort could conceivably improve these theories and hence provide the analyst with a more reliable tool for calculating the material properties.

5. The plane strain material nonlinear finite element analysis performed in this study to calculate the strains and stresses during welding was adequate for our purposes. To study the longitudinal bending distortion of a welded structure, though, either a three-dimensional or a generalized plane strain analysis should be performed. The latter analysis is preferable due to cost considerations. It is thus recommended that efforts should be undertaken to modify the multipurpose finite element program ADINA by including the generalized plane strain case, not currently present.

REFERENCES

1. Masubuchi, K., Analysis of Welded Structures, Pergamon Press, New York, 1980.

2. Macherauch, E., and Wohlfahrt, H., "Different Sources of Residual Stress as a Result of Welding", Int'l Conf. on Residual Stresses in Welded Construction and their Effects, The Welding Institute, London, 1977, Paper 11, pp. 267-282.

3. Mróz, Z., and Raniecki, B., "Variational Principles in Uncoupled Thermoplasticity", Int. J. Engng. Sci., 11, 1973, pp. 1133-1141.

4. Mróz, Z., and Raniecki, B. "On the Uniqueness Problem in Coupled Thermoplasticity", Int. J. Engng., 14, 1976, pp. 211-221.

5. Mróz, Z., and Raniecki, B. "A Derivation of the Uniqueness Conditions in Coupled Thermoplasticity", Int. J. Engng. Sci., 14, 1976, pp. 395-401.

6. Hibbitt, H. D.,"A Numerical Thermo-Mechanical Model for the Welding and Subsequent Loading of a Fabricated Structure", Ph.D. Thesis, Brown University, June 1972.

7. Rosenthal, D., "Étude théorique du régime thermique pendant la soudure de l'arc", 2-me Congres National des Sciences, Brussels, 1935, pp. 1277-1292.

8. Rosenthal, D., "Mathematical Theory of Heat Distribution During Welding and Cutting", Welding Journal, 20 (5), 1941, pp. 220s-234s.

9. Rosenthal, D., "The Theory of Moving Sources of Heat and its Application to Metal Treatment", Transactions ASME, Nov. 1946, pp. 849-866.

10. Boulton, N. S., and Lance Martin, H. E., "Residual Stresses in Arc-Welding Plates", Proc.Inst. Mech. Engrs. (London), 133, 1936, pp. 295-347.

11. Myers, P. S., Uyehara, O. A., and Borman, G. L., "Fundanentals of Heat Flow in Welding", WRC Bulletin, 123, July 1967.

12. Rosenthal, D, and Schmerber, R., "Thermal Study of Arc Welding—Experimental Verification of Theoretical Formulas", Welding Journal, 17 (4), 1938, pp. 2-8.

13. Mahla, E., Rowland, M., Shook, C. and Doan, G.,"Heat Flow in Arc Welding", Welding Journal, 20 (10), 1941, pp. 559s-568s.

14. Wells, A. A.,"Heat Flow in Welding", Welding Journal, 31 (5), 1952, pp. 263s-267s.

15. Jackson, C. E., and Shrubsall, A. E.,"Energy Distribution in Electric Welding", Welding Journal, 29 (5), 1950, pp. 231s-241s.

16. Apps, R. L., and Milner, D. R., "Heat Flow in Argon-Arc Welding", British Welding Journal, Oct. 1955, pp. 475-485.

17. Roberts, D. K., and Wells, A. A., "Fusion Welding of Aluminum Alloys, Part V. A Mathematical Examination of the Effect of Bounding Planes on the Temperature Distribution Due to Welding", Brit. Weld. Jnl., Dec 1954, pp. 553-560.

18. Adams, C. M., Jr., "Cooling Rate and Peak Temperatures in Fusion Welding", Welding Journal, 37 (5), 1958, pp. 210s-215s.

19. Jhaveri, Pravin, Moffat, W. G., and Adams, C. M., Jr., "The Effect of Plate Thickness and Radiation on Heat Flow in Welding and Cutting", Welding Journal, 41 (1), 1962, pp. 12s-16s.

20. Christensen, N., and Davies, V.,"Distribution of Heat Around Finite Moving Sources", Report on Army Contract CA-91-508-EVC-378, Sept. 10, 1959.

21. Christensen, N., Davies, V. and Gjermundsen, K., "The Distribution of Temperatures in Arc Welding", Brit. Weld. Jnl., Feb. 1965, pp. 54-75.

22. Grosh, R. J., Trabant, E. A., and Hawkins, G. A., "Temperature Distribution in Solids of Variable Thermal Properties Heated by Moving Heat Sources", Quart. Appl. Mech., 13 (2), 1955, pp. 161-167.

23. Grosh, R. J., and Trabant, E. A., "Arc-Welding Temperatures", Welding Journal, 35 (8), 1956, pp. 396s-400s.

24. Masubuchi, K., et al., "Analysis of Thermal Stresses and Metal Movements of Weldments: A Basic Study towards Computer-Aided Analysis and Control of Welded Structures", Transactions SNAME, 83, 1975.

25. Nishida, M., "Analytical Prediction of Distortion in Welded Structures", S.M. Thesis, M.I.T., May 1976.

26. Papazoglou, V. J. ,"Computer Programs for the One-Dimensional Analysis of Thermal Stresses and Thermal Movement During Welding", Manual #2 of Report under Contract N00014-75-C-0469 to).N.R., M.I.T., 1977.

27. Rykalin, N. N., "Calculation of Heat Processes in Welding", Lecture presented before the A.W.S., April 1961.

28. Rykalin, N. N., and Nikolaev, A. V., "Welding Arc Heat Flow", Welding in the World, 9 (3/4), 1971, pp. 112-132.

29. Tsai, C. L., "Parametric Study on Cooling Phenomena in Underwater Welding", Ph.D. Thesis, M.I.T.,Sept. 1977.

30. Rykalin, N. N., "Energy Sources Used for Welding", Welding in the World, 12 (9/10), 1974, pp.227-247.

31. Carslaw, H. S., and Jaeger, J. C., Conduction of Heat in Solids, 2nd ed.,Oxford Univ. Press,London, 1969.

32. Hildebrand, F. B., Advanced Calculus for Applications, Prentice-Hall Inc., Englewood Cliffs, N.J., 1962.

33. Arpaci, V. S., Conduction Heat Transfer, Addison-Wesley Publ. Co., Reading, Mass., 1966.

34. Wessel, E. T., and Hays, L. E., "Development of a High-Strength, Tough, Weldable, Structural Steel", Welding Journal, 43 (5), 1964, pp. 215s-231s.

35. Heuschkel, J., "Ultra-High Steel Weld Metals", Welding Journal, 46 (2), 1967, pp. 74s-93s.

36. Gross, J. H., "The New Development of Steel Weldments", Welding Journal, 47 (6), 1968, pp. 241s-270s.

37. Shackleton, D. N., "Welding HY-100 and HY-130 Steels: A Literature Review", The Welding Institute, Abington, England, Report Series C287/3/72, Sept. 1973.

38. Flax, R. W., Keith, R. E., and Randall, M. D., "Welding the HY Steels", ASTM Special Technical Publication 494, 1971.

39. Schrodt, C. J., "Fracture of High Restraint Welds in High Strength Quenched and Tempered Steel", Ocean Engineer Thesis, M.I.T., May 1974.

40. Porter, L. F. et al., "Ultraservice Steels with Yield Strengths of 130 to 200 ksi", ASM Tech. Rept. No. D5-22.4, Presented at the 1965 Metals and Materials Congress, Detroit Mich., Oct. 18-22, 1965.

41. Manganello, S. J. et al., "Development of a High-Toughness Alloy Plate Steel with a Minimum Yield of 140 ksi", Welding Journal, 43 (11), 1964, pp. 514s-520s.

42. Heuschkel, J., "Composition Controlled, High-Strength, Ductile, Tough, Steel Weld Metals", Welding Journal, 43 (8), 1964, pp. 361s-384s.

43. Dorschu, K. E., and Lesnewich, A., "Development of a Filler Metal for a High-Toughness Alloy Plate Steel with a Minimum Yield Strength of 140 ksi", Welding Journal, 43 (12), 1964, pp. 564s-576s.

44. Manganello, S. J. et al., "Isothermal Transformation Diagram for 5Ni-Cr-Mo-V Steel", U.S. Steel Applied Research Lab. Rept. 39.018-001(63), July 1967.

45. Andrews, K. W., "Empirical Formulae for the Calculation of Some Transformation Temperatures", Journal of the Iron and Steel Institute, 203 (7), 1965, pp. 721-727.

46. Holsberg, P. W., "High-Strength Steel Weldment Subcritical Cracking Program - Relationship of Transformations, Microstructure, and Properties in the HY-130 System", DTNSRDC Report SME-79-29, July 1979.

47. Savage, W. F., "Apparatus for Studying the Effects of Rapid Thermal Cycles and High Strain Rates on the Elevated Temperature Behavior of Materials", Jn. of Applied Polymer Science, VI (21), pp. 303-315.

48. Nippes, E.F., and Nelson, E. C., "Prediction of Weld Heat-Affected Zone Microstructures from Continuous Cooling Transformation Data", Welding Journal, 37 (7), 1958, pp. 289s-294s.

49. Brick, R.M., Pense, A.W., and Gordon, R.B., Structure and Properties of Engineering Materials, 4th ed., McGraw-Hill Book Co., New York, 1977.

50. Schreitz, W. G., and Thompson, R. E., "Relationship of Welding Parameters to Structure and Properties of HY-130 Steel and Weld Metal", DTNSRDC Report 2599, March 1968.

51. Wyckoff, R. D., Brenna, R. T., and Pollack, A., "Continuous Cooling Transformations in HY-130 Steel Weld Metal", DTNSRDC Report 4446, Febr. 1975.

52. Stoop, J., and Metzbower, E. A., "A Metallurgical Characterization of HY-130 Steel Welds", Welding Journal, 57 (11), 1978, pp. 345s-353s.

53. Tall, L., "Residual Stresses in Welded Plates - A Theoretical Study", Welding Journal, 43 (1), 1964, pp. 10s-23s.

54. Willner, A. R., and Salive, M. L., "Materials Survey for the Rescue and Search Vehicles of the Deep-Submergence Systems Project", DTMB Report 1987, March 1965.

55. Phillips, A., "The Foundations of Thermoplasticity - Experiments and Theory", Symposium on Topics in Applied Continuum Mechanics, Vienna, March 1-2, 1974.

56. Pugh, C. E., Liu, K. C., Corum, J. M., and Greenstreet, W. L., "Currently Recommended Constitutive Equations for Inelastic Design of FFTF Components", Oak Ridge National Laboratory Report ORNL-TM-3602, Sept. 1972.

57. Corum, J. M., et al., "Interim Guidelines for Detailed Inelastic Analysis of High Temperature Reactor System Components", Oak Ridge National Laboratory Report ORNL-5014, Dec. 1974.

58. Aerospace Structural Metals Handbook, AFML-TR-68-115, Air Force Materials Laboratory, Air Force Systems Command, Wright-Patterson Air Force Base, Ohio, 1970.

59. Wessel, E. T., and Hovan, R. R., "Effect of Long Time Exposures at 400 to 1000 F On the Strength and Toughness of a Ni-Cr-Mo-V High Strength, Weldable Steel", Symposium on Heat-Treated Steels for Elevated Temperature Service, ASME, New Orleans, Louis., Sept. 19-20, 1966, pp. 86-112.

60. Hibbitt, H. D., and Marcal, P. V., "A Numerical, Thermo-Mechanical Model for the Welding and Subsequent Loading of a Fabricated Structure", Computers and Structures, 3, 1973, pp. 1145-1174.

61. Cacciatore, P. J., and Morante, R., "Analytical Modelling of Structural Distortion in Ship Structures Produced by Welding", Technical Report to O.N.R. from Electric Boat Division, General Dynamics, Contract No. N00014-76-C-0808, Dec. 1979.

62. Friedman, E., "Thermodynamical Analysis of the Welding Process Using the Finite Element Method", ASME Transactions, Jn. of Pressure Vessel Technology, Aug. 1975, pp. 206-213.

63. Elridge, E. A., and Deem, H. W., "Report on Physical Properties of Metals and Alloys from Cryogenic to Elevated Temperatures", ASTM Special Technical Publication (296), 1961.

64. Friedman, E., and Glickstein, S. S., "An Investigation of the Thermal Response of Stationary Gas Tungsten Arc Welds", Welding Journal, 55 (12), 1976, pp. 408s-420s.

65. Cavanagh, A. K., "Discussion of Schematic Transformation Diagrams for Steel", Metallurgical Transactions, 10A, Jan. 1979, pp. 129-131.

66. Bain, E. C., "Factors Affecting Inherrent Hardenability of Steel", Trans. Amer. Soc. Steel Treating, 20, 1932, pp. 385-428.

67. Grange, R. A., and Kiefer, J. M., "Transformation of Austenite on Continuous Cooling and its Relation to Transformation at Constant Temperature", ASM Transactions, 29 (3), 1941, pp. 85-115.

68. Manning, G. K., and Lorig, C. H., "The Relationship Between Transformation at Constant Temperature and Transformation During Cooling", AIME Transactions, 167, 1946, pp. 442-463.

69. Scheil, E., "Initiation Period of the Austenite Transformation", Archiv für Eisenhuttenwesen, 8, 1935, pp. 565-567.

70. Cahn, J. W., "Transformation Kinetics During Continuous Cooling", Acta Metallurgica, 4 (11), 1956, pp. 572-575.

71. Markowitz, L. M., and Richman, M. H., "The Computation of Continuous Transformation Diagrams from Isothermal Data", AIME Transactions, 239 (1), 1967, pp. 131-132.

72. Kennon, N. F., "Schematic Transformation Diagrams for Steel", Metallurgical Transactions, 9A, 1978, pp. 57-66.

73. McCullough, T. W., "Using Rate Equations and Numerical Techniques to Predict Metallurgical Structures formed During Arc Welding", Ph.D. Thesis, Univ. of Wisconsin, 1969.

74. Burke, J., The Kinetics of Phase Transformations in Metals, Pergamon Press, London, 1965.

75. Wilson, E. L., Bathe, K. J., and Peterson, F. E., "Finite Element Analysis of Linear and Nonlinear Heat Transfer", J. Nuclear Eng. and Design, 29, 1974, pp. 110-124.

76. Bathe. K. J., "ADINAT - A Finite Element Program for Automatic Dynamic Incremental Nonlinear Analysis of Temperature", AVL Report 82448-5, Mech. Eng. Dept., M.I.T., May 1977 (revised Dec. 1978).

77. Bathe, K. J., and Khoshgoftaar, M. R., "Finite Element Formulation and Solution of Nonlinear Heat Transfer", J. Nuclear Eng. and Design, 51, 1979, pp. 389-401.

78. Hsu, M. B., "Analysis of Welds by the Finite Element Method", Proc. of Numerical Modelling of Manuf. Processes, ASME Winter Annual Meeting, Atlanta, Georgia, 1977, pp. 97-115.

79. Nickell, R. E., and Hibbitt, H. D., "Thermal and Mechanical Analysis of Welded Structures", J. Nuclear Eng. and Design, 32, 1975, pp. 110-120.

80. Masubuchi, K., "Numerical Modeling of Thermal Stresses and Metal Movement During Welding", Proc. of Numerical Modeling of Manuf. Processes, ASME Winter Annual Meeting, Atlanta, Georgia, 1977, pp. 1-17.

81. Masubuchi, K., "Thermal Stresses and Metal Movement During Welding Structural Materials, especially High Strength Steels", Int'l. Conf. on Residual Stresses in WElded Construction and their Effects, The Welding Institute, London, 1977, Paper 1, pp. 1-13.

82. Masubuchi, K., "Applications of Numerical Analysis in Welding - Present State-of-the-Art and Future Possibilities", Colloquim on Application of Numerical Analysis in Welding, I.I.W. Annual Assembly, Dublin, Ireland, 1978.

83. Muraki, T., Bryan, J. J., and Masubuchi, K., "Analysis of Thermal Stresses and Metal Movement During Welding, Part II: Comparison of Experimental Data and Analytical Results", ASME Trans., J. of Eng. Materials and Technology, Jan. 1975, pp. 85-91.

84. Friedman, E., "A Direct Iteration Method for the Incorporation of Phase Change in Finite Element Heat Conduction Programs", Bettis Atomic Power Laboratory report # WAPD-TM-1133, March 1974.

85. Friedman, E., "Numerical Simulation of the Gas Tungsten Arc Welding Process", Proc. of Numerical Modeling of Manuf. Processes, ASME Winter Annual Meeting, Atlanta, Georgia, 1977, pp. 35-47.

86. Hughes, T., "Unconditionally Stable Algorithms for Nonlinear Heat Conduction", Comp. Meth. in Appl. Mechanics and Engineering, 10, 1977, pp. 135-139.

87. Andersson, B. A. B., "Thermal Stresses in a Submerged-Arc Welded Joint Considering Phase Transformations", Transactions of the ASME, Jn. of Eng. Mat. and Technology, 100, Oct. 1978, pp. 356-362.

88. Pavelic, V., et al., "Experimental and Computed Temperature Histories in Gas Tungsten-Arc Welding of Thin Plates", Welding Journal, 48 (7), 1969, pp. 295s-305s.

89. Bathe, K. J., and Wilson, E. L., Numerical Methods in Finite Element Analysis", Prentice-Hall, Englewood Cliffs, New Jersey.

90. Coneybear, G. W., "Analysis of Thermal Stresses and Metal Movement During Welding", S.M. Thesis, M.I.T., May 1978.

91. Rogalsky, W. J., "An Economic and Technical Study on the Feasibility of Using Advanced Joining Techniques in Constructing Critical Naval Marine Structures", O.E. Thesis, M.I.T., May 1979.

92. Coumis, G. A., "An Experimental Investigation of the Transient Thermal Strain Variation and the Triaxial Residual Stress Field Generated due to Electron Beam Welding of Thick HY-130 Plates", S.M. Thesis, M.I.T., June 1980.

93. Lipsey, M. D., "Investigation of Welding Thermal Strains in High Strength Quenched and Tempered Steel", O.E Thesis, M.I.T., June 1978.

94. Perry, C. C., and Lissner, H. R., The Strain Gage Primer, 2nd ed., McGraw-Hill Book Co., New York, 1962.

95. Tall, L., "The Calculation of Residual Stresses-in-Perspective", Int'l. Conf. on Residual Stresses in Welded Construction and their Effects, The Welding Institute, London, 1977, Paper 7, pp. 49-62.

96. Masubuchi, K., Simons, F. B., and Monroe, R. E., "Analysis of Thermal Stresses and Metal Movement During Welding", Battelle Memorial Institute, RSIC-820, Redstone Scientific Information Center, NAGA-TM-X-613000, N68-37857, July 1968.

97. Andrews, J. B., Arita, M., and Masubuchi, K., "Analysis of Thermal Stresses and Metal Movement During Welding", Contract Report NASA CR-61351, prepared for the G. C. Marshall Space Flight Center, NASA, Dec. 1970.

98. DeYoung, R. M., and Chiu, S. S., "Some Applications of Numerical Methods to Practical Welding Problems", Proc. of Numerical Modeling of Manuf. Processes, ASME Annual Winter Meeting, Atlanta, Georgia, 1977, pp. 143-156.

99. Zienckiewicz, O. C., The Finite Element Method in Engineering Science, McGraw-Hill, London, 1971.

100. Bathe, K. J., "ADINA-A Finite Element Program for Automatic Dynamic Incremental Nonlinear Analysis", AVL Report 82448-1, Mechanical Engineering Dept., M.I.T., Sept. 1975 (revised Dec. 1978)

101. Bathe, K. J., "An Assessment of Current Finite Element Analysis of Nonlinear Problems in Solid Mechanics" in Numerical Solution of Partial Differential Equations III, Academic Press, 1976.

102. Bathe, K. J., and Cimento, A. P., "Some Practical Procedures for the Solution of Nonlinear Finite Element Equations", Comp. Meth. in Appl. Mech. and Eng., 22, 1980, pp. 59-85.

103. Snyder, M. D., and Bathe, K. J., "A Solution Procedure for Thermo-Elastic-Plastic and Creep Problems", J. Nuclear Eng. and Design (to be published)

104. Inoue, T., and Tanaka, K., "Temperature Dependent Analysis of Elastoplastic Thermal Stresses by Finite Element Method", Memoirs of the Faculty of Engineering, Kyoto Univ., 35, Part I, Jan. 1973, pp. 1-14.

105. Lobitz, D. W., McClure, J. D., and Nickell, R. E., "Residual Stresses and Distortions in Multi-Pass Welding", Proc. of Numerical Modeling of Manuf. Processes, ASME Winter Annual Meeting, Atlanta, Georgia, 1977, pp. 81-96.

106. Rybicki, E. F., et al., "Residual Stresses at Girth-Butt Welds in Pipes and Pressure Vessels", Batelle Columbus Laboratory Report to U.S. Nuclear Regulatory Commission, NUREG-0376, 1977.

107. Rybicki, et al., "A Finite Element Model for Residual Stresses in Girth-Butt Welded Pipes", Proc. of Numerical Modeling of Manuf. Processes, ASME Winter Annual Meeting, Atlanta, Georgia, 1977, pp. 131-142.

108. Rybicki, E. F., Ghadiali, N. D., and Schmueser, D. W., "An Analytical Technique for Evaluating Residual Deformations in Butt Welded Plates", Proc. of Numerical Modeling of Manuf. Processes, ASME Annual Winter Meeting, Georgia, 1977, pp. 157-166.

109. Ueda, Y., and Yamakawa, T., "Analysis of Thermal Elastic-Plastic Stress and Strain Analysis During Welding by Finite Element Method", Trans. of J. W. S., 2 (2), Sept. 1971, pp. 90-100. Also IIW Doc. X-616-71.

110. Ueda, Y., and Yamakawa, T., "Thermal Stress Analysis of Metals with Temperature Dependent Mechanical Properties", Proc. of the Int'l. Conf. on Mech. Behavior of Materials, Kyoto, Japan, 1971, III, pp. 10-20.

111. Ueda, Y., and Fukuda, K., "Analysis of Welding Stress Relieving by Annealing Based on Finite Element Method", IIW Doc. X-773-75. Also Trans. of JWRI, 4 (1), 1975. Also Trans. of JWS, 8 (1), April 1977.

112. Ueda, Y., et al., "Multipass Welding Stresses in Very Thick Plates and Their Reduction from Stress Relief Annealing", IIW Doc. X-850-77. Also Trans. of JWRI, 5 (2), 1976.

113. Ueda, Y., Fukuda, K., and Nakacho, K., "Basic Procedures in Analysis and Measurement of Welding Residual Stresses by the Finite Element Method", Int'l Conf. on Residual Stresses in Welded Construction and their Effects, The Welding Institute, London, 1977, Paper 3, pp. 27-37.

114. Satoh, K., Seo, K, Iwai, K, and Takahashi, D., "Thermal Elasto-Plastic Analysis on Stress and Strain in Weld Metal During Multi-pass Welding", IIW Document, X-706-73, May 1973.

115. Fujita, Y., Nomoto, T., and Ohtsuta, M., "On Transient Stress-Strain Problems During Welding", IIW Doc. X-804-76, May 1976.

116. Fujita, Y., Nomoto, T., and Sato, K., "Thermal Stress Analysis Based on Inherrent Strain", IIW Doc. X-855-77, April 1977.

117. Fujita, Y., Nomoto, T., and Hagesawa, H., "Thermal Stress Analysis Based on Initial Strain Method", IIW Doc. X-926-79, April 1979.

118. Inoue, T., and Tanaka, K., "An Elastic-Plastic Stress Analysis of Quenching When Considering a Transformation", Int't. J. Mech. Sci., 17, 1975, pp. 361-367.

119. Toshioka, Y., "Deformation of a Quenched Bar", M.I.T. internal report, 1974 (unpublished)

120. Toshioka, Y., "Effects of Material Properties on Residual Stresses and Deformation of Welded Parts", M.I.T. interim report, 1974 (unpublished)

121. Jones, W. K. C., and Alberry, P. J., "A Model for Stress Accumulation in Steels During Welding", Int'l Conf. on Residual Stresses in Welded Construction and their Effects, The Welding Institute, London, 1977, Paper 2, pp. 15-26.

122. Mendelson, A., Plasticity: Theory and Application, Macmillan, New York, 1968.

123. Martin, J. B., Plasticity: Fundamentals and General Results, M.I.T. Press, Cambridge, Mass., 1975.

124. Prager, W., "Non-Isothermal Plastic Deformation", Proc. Koninklijke Nederlandse Akademie van Wetenschappen, Ser. B, 61, 1958, pp. 176-182.

125. Shield, R. T., and Ziegler, H., "On Prager's Hardening Rule", Z. angew. Math. Phys., IXa, 1958, pp. 260-276.

126. Ziegler, H., "A Modification of Prager's Hardening Rule", Quart. Appl. Math, 17, 1959, pp. 55-65.

127. Naghdi, P. M., "Stress-Strain Relations in Plasticity and Thermoplasticity", Proc. of the 2nd Symposium on Naval Structural Mechanics, Brown University, 1960, pp. 121-169.

128. Cyr, N. A., and Teter, R. D., "Finite Element Elastic-Plastic-Creep-Analysis of Two-Dimensional Continuum With Temperature Dependent Material Properties", Computers and Structures, 3, 1973, pp. 849-863.

129. Sharifi, P., and Yates, D. N., "Nonlinear Thermo-Elastic-Plastic and Creep Analysis by the Finite Element Method", AIAA/ASME/SAE 14th Structures, Structural Dynamics, and Material Conference, March 1973.

130. Chang, T. Y., "Nonisothermal Kinematic Hardening Law in Plasticiy", J. Engng. Mech. Div., ASCE, 99, 1973, pp. 423-428.

131. Linnert, G. E., Welding Metallurgy, 2 vols., AWS, New York, 3rd ed., 1967.

132. Dorn, W. S., and McCracken, D. D., Numerical Methods with Fortran IV Case Studies, John Wiley, New York, 1972.

133. Abramowitz, M., and Stegun, I. A., Handbook of Mathematical Functions , National Bureau of Standards, 1967.

134. Grandshteyn, I. S., and Ryzhik, I. M., Table of Integrals, Series, and Products, 4th ed., Academic Press, New York, 1695.

A P P E N D I C E S

APPENDIX A

COMPUTER IMPLEMENTATION OF THE THREE-DIMENSIONAL FINITE HEAT SOURCE SOLUTION

Some notes on the computer implementation of the three-dimensional finite heat source solution derived in Section 2.3.3 will be presented in this Appendix. The computer program has been written in the FORTRAN IV language using double precision arithmetic. Runs of the program have been made in both the Digital Equipment Co.'s VAX and IBM's 370 systems at the Joint Computer Facilities and the Information Processing Services respectively at M.I.T.

A.1 Solution of the Transcedental Equation (2.43)

The characteristic values of the outer solution, ω_n, were found in part A of Section 2.3.3 to be the roots of the following equation:

$$(k_o \cdot \omega_n^2 - h_1 \cdot h_2) \cdot \tan(\omega_n H) = k_o \cdot \omega_n \cdot (h_1 + h_2), \quad n=1,2,3... \qquad (2.43)$$

which can be written as

$$(A \cdot \lambda_n^2 - B) \cdot \tan(\lambda_n) = C \cdot \lambda_n, \quad n = 1,2,3,... \qquad (A.1)$$

where

$$\lambda_n = \omega_n \cdot H$$
$$A = (k_o/H)^2$$
$$B = h_1 \cdot h_2$$
$$C = k_o \cdot (h_1 + h_2)/H$$

with all constants A, B, and C being non-negative; A is always positive, whereas B and C are zero only under the adiabatic

boundaries assumption ($h_1 = h_2 = 0$).

Letting

$$f(\lambda_n) = (A \cdot \lambda_n^2 - B) \cdot \tan(\lambda_n), \quad n = 1,2,3,... \tag{A.2}$$

it can be seen that the roots of this function are $(B/A)^{1/2}$ and $\ell\pi$, $\ell = 0,1,2,...$, where the first root is such that

$$(i-1) \cdot \frac{\pi}{2} < \left(\frac{B}{A}\right)^{1/2} < i \cdot \frac{\pi}{2}, \quad i = 1,2,3,... \tag{A.3}$$

Based on the above and a thorough investigation of the analytical properties of eqn. (A.2), it was concluded that the roots of equation

$$g(\lambda_n) = f(\lambda_n) - C \cdot \lambda_n \tag{A.4}$$

could be pinpointed as follows, depending on the value of i:

1. For i odd, $g(\lambda_n)$ has

   (a) $(i-1)/2$ number of roots $\lambda_n < (i-1)\pi/2$, one in each of the intervals

$$\left(\frac{(j-2)\pi}{2}, \frac{(j-1)\pi}{2}\right), \quad j = 3,5,7,...,i$$

   (b) one root in the interval

$$\left(\frac{(i-1)\pi}{2}, \frac{i\pi}{2}\right)$$

   (c) the remaining roots $\lambda_n > i\pi/2$, one in each of the intervals

$$\left(\frac{i\pi}{2} + (2j-1)\frac{\pi}{2}, \frac{i\pi}{2} + j\pi\right), \quad j = 1,2,3,...$$

2. For i even, $g(\lambda_n)$ has

(a) $i/2-1$ number of roots $\lambda_n < (i-1)\pi/2$, one in each of the intervals

$$\left(\frac{(j-3)\pi}{2}\ ,\ \frac{(j-2)\pi}{2}\right),\ j = 4,6,8,\ldots,i$$

(b) one root in the interval

$$\left(\frac{(i-1)\pi}{2}\ ,\ \frac{i\pi}{2}\right)$$

(c) the remaining roots $\lambda_n > i\pi/2$, one in each of the intervals

$$\left(\frac{i\pi}{2} + (j-1)\pi\ ,\ \frac{i\pi}{2} + (2j-1)\frac{\pi}{2}\right),\quad j = 1,2,3,\ldots$$

These roots were calculated using the so-called half-interval method [132]. As it will be later explained, only twenty roots need to be found.

In the computer program the necessary calculations for the determination of the characteristic values ω_n are performed in subroutines OMEGA and ROOT and the function FUNC.

A.2 Numerical Calculation of Integral (2.63)

In the expressions giving the inner solution, $\phi^i(r,z)$, and the constants, C_n, the integral

$$K_n = \int_o^1 x.e^{-Cr_h^2x^2}\ .\ J_o(\delta_n r_h x).dx,\quad n = 1,2,3,\ldots \qquad (2.63)$$

is involved and since no closed-form solution exists, it must be calculated numerically. Letting

$z_n = \delta_n \cdot r_h$ and $y = z_n \cdot x$

the above equation can be written as

$$K_n = \frac{1}{z_n^2} \int_o^{z_n} f_n(y) \cdot dy \tag{A.5}$$

where

$$f_n(y) = y.\exp(-\frac{C}{\delta_n^2}.y^2) \cdot J_o(y) \tag{A.6}$$

or, equivalently

$$K_n = \frac{1}{z_n^2} \cdot \sum_{i=1}^{n} \left\{ \int_{z_{i-1}}^{z_i} f_n(y) \cdot dy \right\} \tag{A.7}$$

where $z_o = 0$.

Applying the trapezoidal numerical integration scheme [132], each of the integrals in the series can be approximated as

$$\int_{z_{i-1}}^{z_i} f_n(y) \cdot dy \simeq \frac{h_i}{2} \cdot \left\{ f_n[y_{(i-1).N+1}] + \right.$$

$$\left. 2 \cdot \sum_{j=1}^{N-1} f_n [y_{(i-1).N+j+1}] + f_n [y_{i.N+1}] \right\} \tag{A.8}$$

where

$$h_i = \frac{z_i - z_{i-1}}{N} \quad , \quad i = 1,2,3,\ldots,n$$

are the lengths of the N equal subintervals into which each interval $[z_{i-1}, z_i]$, $i = 1,2,\ldots, n$ is divided and y_ℓ, $\ell = 1,2,\ldots, nN+1$ are the resulting nN+1 values of the parameter y. Note that due to the special construction of

the scheme (see Fig. A.1)

$$y_{(i-1).N+1} = z_{i-1} \quad , \; i = 1,2,3,\ldots, \; n+1$$

and

$$y_{(i-1).N+k+1} = z_{i-1} + k.h_i \quad , \; i = 1,2,3,\ldots,n$$

Furthermore, recalling that $z_n = \delta_n \cdot r_h$ are the zeros of $J_o(x)$, it can be seen that the function $f_n(y)$ vanishes at the limits of each interval. Equation (A.8) can thus be written as

$$\int_{z_{i-i}}^{z_i} f_n(y).dy \simeq h_i \cdot \sum_{j=1}^{N-1} f_n[y_{(i-1).N+j+1}]$$

and going back to eqn. (A.7)

$$K_n \simeq \frac{1}{z_n^2} \cdot \sum_{i=1}^{n} \left\{ h_i \cdot \sum_{j=1}^{N-1} f_n[y_{(i-1).N+j+1}] \right\} \qquad (A.9)$$

This last equation is evaluated numerically in subroutine KAPPA and function WAX, with each interval $[z_{i-1}, z_i]$ divided into ten subintervals (N=10).

A.3 Calculation of Maximum Heat Flux

The maximum heat flux, q_o, can be found as outlined in section 2.2 from

$$Q = 2.q_o \cdot \int_o^{r_h} \int_o^{\pi} \exp(-C.r^2 - \lambda v.r.\cos\psi).r.d\psi.dr \qquad (2.14)$$

where

$$Q = \eta_a \cdot V \cdot I \qquad (2.7)$$

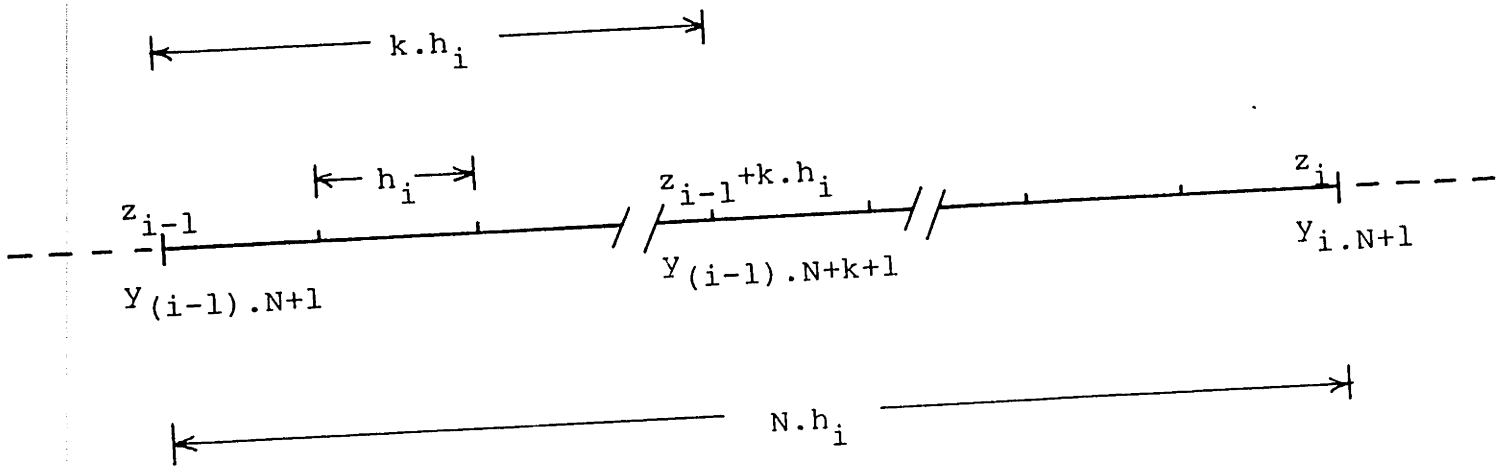

FIGURE A.1 Representative Interval Used in Numerical Integration.

Using again the trapezoidal scheme for the numerical integration, it can be found that

$$Q = q_o \cdot \frac{r_h}{N} \cdot \left[2 \cdot \sum_{n=2}^{N-1} r_n \cdot \exp(-C \cdot r_n^2) \cdot g(r_n) + r_h \cdot \exp(-C \cdot r_h^2) \cdot g(r_h) \right] \qquad (A.10)$$

where

$$g(r) = \frac{\pi}{2M} \cdot \left[e^{-\lambda vr} + e^{\lambda vr} + 2 \cdot \sum_{m=2}^{M-1} e^{-\lambda vr \cdot \cos\psi_m} \right]$$

$$\psi_m = (m-1) \cdot \frac{\pi}{M} \quad , \quad m = 1,2,3,\ldots,M$$

$$r_n = (n-1) \cdot \frac{r_h}{N} \quad , \quad n = 1,2,3,\ldots,N$$

and M, N are the number of subintervals into which the intervals $[0,\pi]$ and $[0, r_h]$ are divided respectively.

The calculations are performed in subroutine QMAX.

A.4 Calculation of Bessel Functions

The Bessel and modified Bessel functions appearing in the various equations of the solution have been calculated using the well known approximate product formulae [133]. Several subroutines have been written for this purpose as follows (the Bessel function calculated is shown in parenthesis): J1BES ($J_1(x)$), J0BES ($J_o(x)$), I1BES ($I_1(x)$), I0BES, ($I_o(x)$), K1BES ($K_1(x)$), and K0BES ($K_o(x)$).

Finally, to calculate the characteristic values, δ_n, of the first part of the inner solution the zeros of $J_o(x)$ have to be found according to eqn. (2.57). The first twenty zeros can be found tabulated in many mathematical handbooks and are given in the program in BLOCK DATA. In case, however, more than twenty zeros are required, i.e. if more than twenty terms of the series solutions must be added for convergence, the following expansion can be used for the mth zero, $m \geq 20$

$$x_m \sim \frac{\pi}{4}(4m-1) + \frac{1}{2\pi(4m-1)} - \frac{1}{6\pi^3(4m-1)^3} + \frac{3779}{15\pi^5(4m-1)^5} - \ldots \qquad \text{(A.11)}$$

with an accuracy of at least five digits [134].

A.5 Program Listing

A listing of the developed program is given in the following pages. Enough comment statements have been inserted into the program to facilitate easier understanding.

```
                C     PROGRAM MAIN                                                THR00010
                C                                                                 THR00020
                C     THIS PROGRAM CALCULATES THE TEMPERATURE DISTRIBUTION IN A   THR00030
                C     PLATE OF INFINITE LENGTH, FINITE WIDTH, AND FINITE          THR00040
                C     THICKNESS DUE TO A THREE-DIMENSIONAL GAUSSIAN DISTRIBUTED   THR00050
                C     HEAT SOURCE MOVING ALONG ITS SURFACE                        THR00060
                C                                                                 THR00070
                C     PROGRAM DEVELOPED BY V.J.PAPAZOGLOU        JULY 1979        THR00080
                C                                                                 THR00090
0001                  IMPLICIT REAL*8(A-H,O-Z)                                    THR00100
0002                  COMMON/S1/ZERO(100)                                         THR00110
0003                  COMMON/S2/QC                                                THR00120
0004                  COMMON/S3/A,B,S                                             THR00130
0005                  DIMENSION XN(100),YN(100),ZN(100),TEMP(100)                 THR00140
0006                  DIMENSION O(100),D(100),CHI(100),ZET(100)                   THR00150
0007                  DIMENSION P(100),C(100)                                     THR00160
0008                  DIMENSION CK(6)                                             THR00170
0009                  DIMENSION ANAME(20)                                         THR00180
0010                  DATA CK/-.002515,.005879,-.010624,.021896,-.07832,1.253314/ THR00190
                C                                                                 THR00200
                C     * * *   I N P U T   D A T A   * * *                         THR00210
                C                                                                 THR00220
0011                  READ(5,490) (ANAME(I),I=1,20)                               THR00230
0012                  READ(5,500) AV,AI,V,QC,EFF                                  THR00240
0013                  READ(5,500) CKO,G,ALPHA,H1,H2                               THR00250
0014                  READ(5,510) H,TO,TE,TLIQ,NN,NOUT,NIN,MCON                   THR00260
0015                  READ(5,530) (XN(I),YN(I),ZN(I),I=1,NN)                      THR00270
0016              500 FORMAT(6F10.5)                                              THR00280
0017              510 FORMAT(4F10.5,8I3)                                          THR00290
0018              530 FORMAT(2(3F10.4))                                           THR00300
0019              490 FORMAT(20A4)                                                THR00310
0020                  WRITE(6,1000) (ANAME(I),I=1,20)                             THR00320
0021                  WRITE(6,1050)                                               THR00330
0022                  WRITE(6,1100) AV,AI,EFF,V,QC                                THR00340
0023                  WRITE(6,1150) CKO,G,ALPHA,H1,H2                             THR00350
0024                  WRITE(6,1200) H,TO,TE,TLIQ                                  THR00360
0025                  WRITE(6,1250) (I,XN(I),YN(I),ZN(I),I=1,NN)                  THR00370
0026                  WRITE(6,2000)                                               THR00380
0027             1000 FORMAT('1',21('****')/1H ,'* ',80X,' *'/                    THR00390
                     11H ,'* ',20A4,' *'/1H ,'* ',80X,' *'/                       THR00400
                     21H ,21('****'))                                             THR00410
0028             1050 FORMAT('0','****** ANALYTICAL SOLUTION OF THE HEAT CONDUCTION PROBTHR00420
                     1LEM - 3D HEAT SOURCE - STEADY STATE ******'///)             THR00430
0029             1100 FORMAT('0',' WELDING CONDITIONS'/                           THR00440
                     1/6X,'ARC VOLTAGE (VOLTS) --------------------',F12.5/      THR00450
                     2/6X,'ARC CURRENT (AMPERES) ------------------',F12.5/      THR00460
                     3/6X,'ARC EFFICIENCY -------------------------',F12.5/      THR00470
                     4/6X,'ARC TRAVEL SPEED (IN/SEC) --------------',F12.5/      THR00480
                     5/6X,'CONCENTRATION COEFFICIENT (1/IN.IN) ----',F12.5///)   THR00490
0030             1150 FORMAT('0',' THERMAL PROPERTIES'/                           THR00500
                     1/6X,'THERMAL CONDUCTIVITY (BTU/SEC.IN.F) --------------',F12.5/ THR00510
                     2/6X,'CONDUCTIVITY COEFFICIENT -------------------------',F12.5/ THR00520
                     3/6X,'THERMAL DIFFUSIVITY (IN.IN/SEC) ------------------',F12.5/ THR00530
```

```
                 4/6X,'CONVECTICN COEFFICIENT-TOP (BTU/SEC.IN.IN.F) -----',F12.5/   THR00540
                 5/6X,'CONVECTICN COEFFICIENT-BOTTOM (BTU/SEC.IN.IN.F) --',F12.5///)THR00550
0031          1200 FORMAT('0',' PLATE THICKNESS (IN) -------------------',F10.5///   THR00560
                 12X,'INITIAL TEMPERATURE (F) ----------------',F10.5///            THR00570
                 22X,'ENVIRONMENTAL TEMPERATURE (F) ----------',F10.5///            THR00580
                 32X,'MAXIMUM TEMPERATURE (F) ----------------',F10.5)              THR00590
0032          1250 FORMAT('1',' COORDINATES  (X,Y,Z)'///                            THR00600
                 1(6X,3(I5,'*',3F10.4)))                                            THR00610
0033          2000 FORMAT('1','******* R E S U L T S *******')                      THR00620
              C                                                                     THR00630
0034                PI=3.141592                                                     THR00640
0035                CL=1./(2.*ALPHA)                                                THR00650
0036                RO=1.73/DSQRT(QC)                                               THR00660
0037                KMAX=MAX0(NOUT,NIN)                                             THR00670
0038                LMAX=MAX0(NIN,MCON)                                             THR00680
              C                                                                     THR00690
              C     CALCULATE CHARACTERISTIC VALUES                                 THR00700
              C                                                                     THR00710
0039                A5=CKO/H                                                        THR00720
0040                A=A5**2                                                         THR00730
0041                B=H1*H2                                                         THR00740
0042                S=A5*(H1+H2)                                                    THR00750
0043                PAR=(CL*V)**2                                                   THR00760
0044                IF(H1.EQ.0.0.AND.H2.EQ.0.0) GO TO 30                            THR00770
0045                CALL OMEGA(A,B,H,O,KMAX)                                        THR00780
0046                GO TO 50                                                        THR00790
0047             30 CONTINUE                                                        THR00800
0048                DO 20 L=1,KMAX                                                  THR00810
0049             20 O(L)=DFLOAT(L)*PI/H                                             THR00820
0050             50 CONTINUE                                                        THR00830
0051                DO 10 I=1,KMAX                                                  THR00840
0052             10 ZET(I)=DSQRT(O(I)**2+PAR)                                       THR00850
0053                IF(LMAX.LE.20) GO TO 15                                         THR00860
0054                DO 25 M=21,LMAX                                                 THR00870
0055                CNT=(4.*DFLOAT(M)-1.)*PI                                        THR00880
0056             25 ZERO(M)=CNT/4.+1./(2.*CNT)-31./(6.*CNT**3)+3779./(15.*CNT**5)   THR00890
0057             15 CONTINUE                                                        THR00900
0058                DO 35 J=1,LMAX                                                  THR00910
0059                D(J)=ZERO(J)/RO                                                 THR00920
0060             35 CHI(J)=DSQRT(D(J)**2+PAR)                                       THR00930
              C                                                                     THR00940
              C     CALCULATE INTEGRAL KN                                           THR00950
              C                                                                     THR00960
0061                CALL KAPPA(D,P,LMAX)                                            THR00970
              C                                                                     THR00980
              C     CALCULATE MAXIMUM HEAT FLUX                                     THR00990
              C                                                                     THR01000
0062                Q=EFF*AV*AI/1055.                                               THR01010
0063                CALL QMAX(Q,QC,CL,V,RO,PINT,QO)                                 THR01020
              C                                                                     THR01030
              C     CALCULATE COEFFICIENTS CN OF SERIES SOLUTION                    THR01040
              C                                                                     THR01050
0064                IF(H1*H2.NE.0.0) GO TO 700                                      THR01060
```

```
0065          CLVA=CL*V*BO                                          THR01070
0066          CALL K1BES(CLVA,BEK1)                                 THR01080
0067          CO=Q/(2.*CKO*CLVA*H*BEK1*PINT)                        THR01090
0068      700 CONTINUE                                              THR01100
0069          DO 200 N=1,KMAX                                       THR01110
0070          ZRO=ZET(N)*BO                                         THR01120
0071          CALL K0BES(ZRO,BK0)                                   THR01130
0072          CALL K1BES(ZRO,BK1)                                   THR01140
0073          CALL I0BES(ZRO,BI0)                                   THR01150
0074          CALL I1BES(ZRO,BI1)                                   THR01160
0075          DEN1=ZET(N)*(BK1+BK0*BI1/BI0)                         THR01170
0076          IF(H1.EQ.0.0.AND.H2.EQ.0.0) GO TO 710                 THR01180
0077          V1=H2/CKO/O(N)**2                                     THR01190
0078          V2=H2*V1/CKO                                          THR01200
0079          V3=O(N)*H                                             THR01210
0080          DEN2=.5*H*(1.+V2)+(1.-V2)*DSIN(2.*V3)/(4.*O(N))+V1*DSIN(V3)**2  THR01220
0081          GO TO 715                                             THR01230
0082      710 V3=O(N)*H                                             THR01240
0083          DEN2=0.5*H                                            THR01250
0084      715 DEN=DEN1*DEN2                                         THR01260
0085          U=CKO*O(N)                                            THR01270
0086          SINO=DSIN(V3)                                         THR01280
0087          COSO=DCOS(V3)                                         THR01290
0088          SUM=0.0                                               THR01300
0089          DO 100 M=1,MCON                                       THR01310
0090          CH2=CHI(M)**2                                         THR01320
0091          W1=CKO*CHI(M)                                         THR01330
0092          H1=H2*(O(N)+CH2/O(N))*SINO                            THR01340
0093          H2=(CKO*CH2-H2**2/CKO)*COSO                           THR01350
0094          D1=H1+H2                                              THR01360
0095          D2=CHI(M)*(U+H2**2/U)*SINO                            THR01370
0096          D3=W1*(H1+H2)                                         THR01380
0097          D4=W1*W1+H1*H2                                        THR01390
0098          W2=CHI(M)*H                                           THR01400
0099          W3=D(M)*RO                                            THR01410
0100          IF(W2.GT.80.) GO TO 70                                THR01420
0101          EX1=DEXP(W2)                                          THR01430
0102          GO TO 80                                              THR01440
0103       70 EX1=1.0E+35                                           THR01450
0104       80 EX2=1./EX1                                            THR01460
0105          HYPT=(EX1-EX2)/(EX1+EX2)                              THR01470
0106          CALL J1BES(W3,BJ1)                                    THR01480
0107          U1=2.*QO*P(M)*D(M)*(D1*HYPT+D2)                       THR01490
0108          VCH=CH2+O(N)**2                                       THR01500
0109          U2=VCH*BJ1*(D3+D4*HYPT)                               THR01510
0110      100 SUM=SUM+U1/U2                                         THR01520
0111          C(N)=SUM/DEN                                          THR01530
0112      200 CONTINUE                                              THR01540
        C                                                           THR01550
        C     INPUT                                                 THR01560
        C     TM=TIME AT WHICH TEMPERATURES ARE TO BE CALCULATED    THR01570
        C     ISTOP=INDEX TO TERMINATE CALCULATIONS                 THR01580
        C                 EQ.0  CONTINUE                            THR01590
```

```
                C                EQ.1  STOP                                    THR01600
                C                                                              THR01610
0113              800 READ(5,520) TM,ISTOP                                     THR01620
0114              520 FORMAT(F10.4,I5)                                         THR01630
0115                  IF(ISTOP.NE.0) GO TO 999                                 THR01640
0116                  DO 400 I=1,NN                                            THR01650
0117                  XI=XN(I)-V*TM                                            THR01660
0118                  RADI2=XI**2+YN(I)**2                                     THR01670
0119                  RADI=DSQRT(RADI2)                                        THR01680
0120                  CLV=CL*V*XI                                              THR01690
0121                  CLVR=CL*V*RADI                                           THR01700
0122                  IF(RADI.LT.RO) GO TO 350                                 THR01710
                C                                                              THR01720
                C     SOLUTION FOR OUTER REGION                                THR01730
                C                                                              THR01740
0123                  SUM=0.0                                                  THR01750
0124                  IF(H1*H2.NE.0.0) GO TO 40                                THR01760
                C     FOR H1=H2=0. CALCULATE THE ZEROTH TERM OF SERIES SOLUTION THR01770
0125                  IF(CLVR.LE.170.0) GO TO 42                               THR01780
0126                  XS=2./CLVR                                               THR01790
0127                  SK=0.00053208                                            THR01800
0128                  DO 45 L=1,6                                              THR01810
0129               45 SK=SK*XS+CK(L)                                           THR01820
0130                  EKR=SK/DSQRT(CLVR)/DEXP(CLV+CLVR)                        THR01830
0131                  GO TO 43                                                 THR01840
0132               42 CALL KOBES(CLVR,BKK)                                     THR01850
0133                  EKR=0.0                                                  THR01860
0134                  IF(CLV.GE.15.0) GO TO 43                                 THR01870
0135                  EKR=BKK/DEXP(CLV)                                        THR01880
0136               43 SUM=SUM+EKR*CC                                           THR01890
0137               40 CONTINUE                                                 THR01900
                C     CALCULATE THE SERIES TERMS FROM 1 TO NOUT                THR01910
0138                  DO 220 N=1,NOUT                                          THR01920
0139                  U5=O(N)*ZN(I)                                            THR01930
0140                  FACTOR=H2*DSIN(U5)/O(N)/CKO+DCOS(U5)                     THR01940
0141                  U6=ZET(N)*RADI                                           THR01950
0142                  IF(U6-2.) 240,240,260                                    THR01960
0143              240 CALL KOBES(U6,BK)                                        THR01970
0144                  FN=BK/DEXP(CLV)                                          THR01980
0145                  GO TO 230                                                THR01990
0146              260 C1=CLV+U6                                                THR02000
0147                  IF(C1.LE.-170.0)    GO TO 270                            THR02010
0148                  IF(C1.GE.170.0)     GO TO 310                            THR02020
0149                  CEX=DEXP(C1)                                             THR02030
0150                  GO TO 320                                                THR02040
0151              310 CEX=1.0E+60                                              THR02050
0152              320 XS=2./U6                                                 THR02060
0153                  SK=.00053208                                             THR02070
0154                  DO 280 L=1,6                                             THR02080
0155              280 SK=SK*XS+CK(L)                                           THR02090
0156                  FN=SK/CEX/DSQRT(U6)                                      THR02100
0157                  GO TO 230                                                THR02110
0158              270 FN=1.0E+60                                               THR02120
```

```
0159          230  SUM=SUM+C(N)*FACTOR*FN                                THR02130
0160          220  CONTINUE                                              THR02140
0161               UT=SUM+(TO-TE)                                        THR02150
0162               GO TO 600                                             THR02160
                 C                                                       THR02170
                 C     SOLUTION FOR INNER REGION                         THR02180
                 C                                                       THR02190
0163          350  SUM=0.0                                              THR02200
0164               IF(H1*H2.NE.0.0) GO TO 90                             THR02210
                 C     FOR H1=H2=0. CALCULATE ZEROTH TERM OF SERIES SOLUTION THR02220
0165               CALL KOBES(CLVA,BK3)                                  THR02230
0166               CALL IOBES(CLVA,BI3)                                  THR02240
0167               CALL IOBES(CLVR,BI4)                                  THR02250
0168               SUM=SUM+CO*BK3*BI4/BI3                                THR02260
0169            90 CONTINUE                                              THR02270
                 C     CALCULATE THE SERIES TERMS FROM 1 TO NOUT         THR02280
0170               DO 360 N=1,NIN                                        THR02290
0171               U7=D(N)*RADI                                          THR02300
0172               U8=CHI(N)*ZN(I)                                       THR02310
0173               U9=O(N)*ZN(I)                                         THR02320
0174               U10=D(N)*RO                                           THR02330
0175               CALL JOBES(U7,BJ0)                                    THR02340
0176               CALL J1BES(U10,BJ)                                    THR02350
0177               IF(U8.GT.170.)GO TO 120                               THR02360
0178               E10=DEXP(U8)                                          THR02370
0179               GO TO 130                                             THR02380
0180          120  E10=1.0E+60                                           THR02390
0181          130  E11=1./E10                                            THR02400
0182               COSHU8=.5*(E10+E11)                                   THR02410
0183               SINHU8=.5*(E10-E11)                                   THR02420
0184               FACT1=P(N)*BJ0*(H2*SINHU8+CKO*CHI(N)*COSHU8)          THR02430
0185               U11=CHI(N)*H                                          THR02440
0186               U12=CKO*CHI(N)                                        THR02450
0187               IF(U11.GT.170.)GO TO 160                              THR02460
0188               E15=DEXP(U11)                                         THR02470
0189               GO TO 170                                             THR02480
0190          160  E15=1.0E+60                                           THR02490
0191          170  E16=1./E15                                            THR02500
0192               COSH11 =.5*(E15+E16)                                  THR02510
0193               SINH11 =.5*(E15-E16)                                  THR02520
0194               FACT2=BJ**2*(U12*(H1+H2)*COSH11 +(U12**2+H1*H2)*SINH11) THR02530
0195               U13=ZET(N)*RO                                         THR02540
0196               U14=ZET(N)*RADI                                       THR02550
0197               CALL KOBES(U13,BK2)                                   THR02560
0198               CALL IOBES(U14,BI2)                                   THR02570
0199               CALL IOBES(U13,BI)                                    THR02580
0200               FACT3=C(N)*BK2*BI2/BI*(H2*DSIN(U9)/CKO/O(N)+DCOS(U9)) THR02590
0201          360  SUM=SUM+2.*QO*FACT1/FACT2+FACT3                      THR02600
0202               PHI=SUM                                               THR02610
0203               UT=PHI/DEXP(CLV)+(TO-TE)                              THR02620
                 C                                                       THR02630
                 C     CALCULATE THE TEMPERATURES                        THR02640
                 C                                                       THR02650
```

```
0204          600 IF(UT.GT.1.0E+20) GO TO 420                                THR02660
0205              IF(G.EQ.0.) GO TO 450                                      THR02670
0206              G1=DSQRT(1.+2.*G*(UT-TO+TE))                               THR02680
0207              IF(G.LT.0.0) GO TO 430                                     THR02690
0208              TEMP(I)=TO+(G1-1.)/G                                       THR02700
0209              GO TO 480                                                  THR02710
0210          430 TEMP(I)=TO-(G1+1.)/G                                       THR02720
0211              GO TO 480                                                  THR02730
0212          420 TEMP(I)=1.0E+30                                            THR02740
0213              GO TO 480                                                  THR02750
0214          450 TEMP(I)=TE+UT                                              THR02760
0215          480 IF(TEMP(I).GT.TLIQ) TEMP(I)=TLIQ                           THR02770
0216          400 CONTINUE                                                   THR02780
            C                                                                THR02790
            C     P R I N T   R E S U L T S                                  THR02800
            C                                                                THR02810
                                                                             THR02820
0217              WRITE(6,2100) TM                                           THR02830
0218              WRITE(6,2200) (I,TEMP(I),I=1,NN)                           THR02840
0219         2100 FORMAT(//////' TIME=',F10.4)                               THR02850
0220         2200 FORMAT('0',' TEMPERATURE DISTRIBUTION ( AT THE POINTS IN CONSIDERATHR02860
            1TION)'//(1H ,7(I4,3X,F9.2)))                                    THR02870
0221              GO TO 800                                                  THR02880
0222          999 CONTINUE                                                   THR02890
0223              STOP                                                       THR02900
0224              END
```

```
0001          SUBROUTINE OMEGA(A,B,H,O,KMAX)                                THR02910
        C                                                                   THR02920
        C     THIS SUBROUTINE CALCULATES THE CHARACTERISTIC VALUES OMEGA    THR02930
0002          IMPLICIT REAL*8(A-H,O-Z)                                      THR02940
0003          REAL R                                                        THR02950
0004          DIMENSION O(100)                                              THR02960
0005          PI=3.141593                                                   THR02970
0006          H=.5*DSQRT(B/A)/PI                                            THR02980
0007          I=IFIX(H)+1                                                   THR02990
0008          IF(I.EQ.1) GO TO 40                                           THR03000
0009          K=2                                                           THR03010
0010          L=3                                                           THR03020
0011     10   IF(I.EQ.K) GO TO 100                                          THR03030
0012          IF(I.EQ.L) GO TO 200                                          THR03040
0013          K=K+2                                                         THR03050
0014          L=L+2                                                         THR03060
0015          GO TO 10                                                      THR03070
0016     40   CONTINUE                                                      THR03080
0017          DO 20 J=1,KMAX                                                THR03090
0018          ZL=(DFLOAT(J)-1.)*PI                                          THR03100
0019          CALL ROOT(ZL,U)                                               THR03110
0020     20   O(J)=U/H                                                      THR03120
0021          RETURN                                                        THR03130
0022     100  K=0                                                           THR03140
0023          DO 120 J=4,I,2                                                THR03150
0024          ZL=(DFLOAT(J)-3.)*PI/2.                                       THR03160
0025          CALL ROOT(ZL,U)                                               THR03170
0026          M=(J-2)/2                                                     THR03180
0027     120  O(M)=U/H                                                      THR03190
0028          ZL=(DFLOAT(I)-1.)*PI/2.                                       THR03200
0029          CALL ROOT(ZL,U)                                               THR03210
0030          M=I/2                                                         THR03220
0031          O(M)=U/H                                                      THR03230
0032          K=KMAX-I/2                                                    THR03240
0033          DO 150 N=1,K                                                  THR03250
0034          ZL=(DFLOAT(I)/2.+DFLOAT(N)-1.)*PI                             THR03260
0035          CALL ROOT(ZL,U)                                               THR03270
0036          M=I/2+N                                                       THR03280
0037     150  O(M)=U/H                                                      THR03290
0038          RETURN                                                        THR03300
0039     200  L=0                                                           THR03310
0040          DO 220 J=3,I,2                                                THR03320
0041          ZL=(DFLOAT(J)-2.)*PI/2.                                       THR03330
0042          CALL ROOT(ZL,U)                                               THR03340
0043          M=(J-1)/2                                                     THR03350
0044     220  O(M)=U/H                                                      THR03360
0045          ZL=(DFLOAT(I)-1.)*PI/2.                                       THR03370
0046          CALL ROOT(ZL,U)                                               THR03380
0047          M=(I+1)/2                                                     THR03390
0048          O(M)=U/H                                                      THR03400
0049          L=KMAX-(I+1)/2                                                THR03410
0050          DO 250 N=1,L                                                  THR03420
0051          ZL=.5*(DFLOAT(I)+2.*DFLOAT(N)-1.)/PI                          THR03430
```

```
0052                CALL BOOT(ZL,U)                                THR03440
0053                M=(I+1)/2+N                                    THR03450
0054          250   O(M)=U/H                                      THR03460
0055                RETURN                                         THR03470
0056                END                                            THR03480
```

```
0001                SUBROUTINE ROOT(W,Z)                                    THR03490
                C                                                           THR03500
                C   THIS  SUBROUTINE FINDS THE ROOT OF A FUNCTION           THR03510
                C   BY THE HALF-INTERVAL METHOD                             THR03520
                C                                                           THR03530
0002                IMPLICIT REAL*8(A-H,O-Z)                                THR03540
0003                ITER=ALOG(.1/1.0E-6)/ALOG(2.)+1.                        THR03550
0004                ZLE=W+.001                                              THR03560
0005            1   IF (FUNC(ZLE)*FUNC(ZLE+.1).LT.0.) GO TO 3              THR03570
0006                ZLE=ZLE+.1                                              THR03580
0007                GO TO 1                                                 THR03590
0008            3   ZR=ZLE+.1                                              THR03600
0009                FZL=FUNC(ZLE)                                           THR03610
0010                DO 6 J=1,ITER                                           THR03620
0011                ZHALF=(ZLE+ZR)/2.                                       THR03630
0012                FZHALF=FUNC(ZHALF)                                      THR03640
0013                IF (FZHALF*FZL.LE.0.) GO TO 5                           THR03650
0014                ZLE=ZHALF                                               THR03660
0015                FZL=FZHALF                                              THR03670
0016                GO TO 6                                                 THR03680
0017            5   ZR=ZHALF                                               THR03690
0018            6   CONTINUE                                                THR03700
0019                Z=(ZLE+ZR)/2.                                           THR03710
0020                RETURN                                                  THR03720
0021                END                                                     THR03730
```

```
0001          FUNCTION FUNC(R)                                  THR03740
0002          IMPLICIT REAL*8(A-H,O-Z)                          THR03750
0003          COMMON/S3/A,B,S                                   THR03760
0004          FUNC=(A*R**2-B)*DTAN(R)-S*R                       THR03770
0005          RETURN                                            THR03780
0006          END                                               THR03790
```

```
0001                SUBROUTINE KAPPA(D,P,LMAX)                                THR03800
                C                                                             THR03810
                C   THIS SUBROUTINE CALCULATES THE INTEGRAL KN                THR03820
                C   USING THE TRAPEZOIDAL RULE                                THR03830
                C                                                             THR03840
0002                IMPLICIT REAL*8(A-H,O-Z)                                  THR03850
0003                COMMON/S1/ZERO(100)                                       THR03860
0004                DIMENSION P(100),H(100),Y(1000),BJ(1000),D(100)           THR03870
0005                NINTG=10                                                  THR03880
0006                H(1)=ZERO(1)/DFLOAT(NINTG)                                THR03890
0007                DO 5 L=2,LMAX                                             THR03900
0008            5   H(L)=(ZERO(L)-ZERO(L-1))/DFLOAT(NINTG)                    THR03910
0009                N=1                                                       THR03920
0010                I=1                                                       THR03930
0011                Y(I)=0.                                                   THR03940
0012           10   CALL JOBES(Y(I),B)                                        THR03950
0013                BJ(I)=B                                                   THR03960
0014                I=I+1                                                     THR03970
0015                IF(I.EQ.N*NINTG+1) GO TO 20                               THR03980
0016                Y(I)=Y(I-1)+H(N)                                          THR03990
0017                GO TO 10                                                  THR04000
0018           20   Y(I)=ZERO(N)                                              THR04010
0019                BJ(I)=0.                                                  THR04020
0020                N=N+1                                                     THR04030
0021                IF(N.GT.LMAX) GO TO 30                                    THR04040
0022                I=I+1                                                     THR04050
0023                Y(I)=Y(I-1)+H(N)                                          THR04060
0024                GO TO 10                                                  THR04070
0025           30   CONTINUE                                                  THR04080
0026                NN=NINTG-1                                                THR04090
0027                DO 100 N=1,LMAX                                           THR04100
0028                ATHR=0.0                                                  THR04110
0029                DO 60 K=1,N                                               THR04120
0030                M=(K-1)*NINTG+1                                           THR04130
0031                SUM=0.0                                                   THR04140
0032                DO 50 L=1,NN                                              THR04150
0033                J=M+L                                                     THR04160
0034           50   SUM=SUM+WAX(Y(J),D(N),BJ(J))                              THR04170
0035           60   ATHR=ATHR+H(K)*SUM                                        THR04180
0036          100   P(N)=ATHR/ZERO(N)**2                                      THR04190
0037                RETURN                                                    THR04200
0038                END                                                       THR04210
```

```
0001              FUNCTION WAX(A,B,C)                                THR04220
0002              IMPLICIT REAL*8(A-H,O-Z)                           THR04230
0003              COMMON/S2/QC                                       THR04240
0004              R=-QC*A**2/B**2                                    THR04250
0005              IF (R.GT.170.)GO TO 5                              THR04260
0006              WAX=A*C*DEXP(R)                                    THR04270
0007              GO TO 10                                           THR04280
0008         5    WAX=1.0E+70                                        THR04290
0009        10    RETURN                                             THR04300
0010              END                                                THR04310
```

```
0001                SUBROUTINE QMAX(Q,QC,CL,V,RO,PINT,QO)                THR04320
                    C                                                    THR04330
                    C   THIS SUBROUTINE CALCULATES THE HEAT FLUX AT THE  THR04340
                    C   CENTER OF THE GAUSSIAN DISTRIBUTION              THR04350
                    C                                                    THR04360
0002                IMPLICIT REAL*8(A-H,O-Z)                             THR04370
0003                PI=3.141592                                          THR04380
0004                CV=CL*V                                              THR04390
0005                IM=30                                                THR04400
0006                IN=30                                                THR04410
0007                DM=PI/DFLOAT(IM)                                     THR04420
0008                DN=RO/DFLOAT(IN)                                     THR04430
0009                SUM1=0.0                                             THR04440
0010                RN=0.0                                               THR04450
0011                DO 200 N=2,IN                                        THR04460
0012                RN=RN+DN                                             THR04470
0013                F=CV*RN                                              THR04480
0014                THM=0.0                                              THR04490
0015                SUM2=0.0                                             THR04500
0016                DO 100 M=2,IM                                        THR04510
0017                THM=THM+DM                                           THR04520
0018                CTM=DCOS(THM)                                        THR04530
0019                E1=DEXP(F*CTM)                                       THR04540
0020            100 SUM2=SUM2+1./E1                                      THR04550
0021                E2=DEXP(F)                                           THR04560
0022                PF=0.5*DM*(E2+1./E2+2.*SUM2)                         THR04570
0023                E3=DEXP(QC*RN**2)                                    THR04580
0024            200 SUM1=SUM1+RN*PF/E3                                   THR04590
0025                CLVA=CV*RO                                           THR04600
0026                ATHR=0.0                                             THR04610
0027                TH=0.0                                               THR04620
0028                DO 300 L=2,IM                                        THR04630
0029                TH=TH+DM                                             THR04640
0030                COSTH=DCOS(TH)                                       THR04650
0031                EX3=DEXP(CLVA*COSTH)                                 THR04660
0032            300 ATHR=ATHR+1./EX3                                     THR04670
0033                EX4=DEXP(CLVA)                                       THR04680
0034                PINT=0.5*DM*(EX4+2.*ATHR+1./EX4)                     THR04690
0035                E4=DEXP(QC*RO**2)                                    THR04700
0036                QO=Q/(DN*(2.*SUM1+RO*PINT/E4))                       THR04710
0037                RETURN                                               THR04720
0038                END                                                  THR04730
```

```
0001              SUBROUTINE J1BES(X,B)                                          THR04740
0002              IMPLICIT REAL*8(A-H,O-Z)                                       THR04750
0003              DIMENSION C(6),CF(6),CTH(6)                                    THR04760
0004              DATA C/-.0003176,.0044332,-.0395429,.2109357,-.5624998,.5/     THR04770
0005              DATA CF/.0011365,-.0024951,.0001711,.0165967,.0000016,.7978846/ THR04780
0006              DATA CTH/.0007982,.0007435,-.0063788,.0000565,.1249961,-2.3561945/THR04790
0007              IF(X) 10,20,20                                                 THR04800
0008        10    X=-X                                                           THR04810
0009        20    IF(X-3.) 30,50,50                                              THR04820
0010        30    XS=X**2/9.                                                     THR04830
0011              SI=.00001109                                                   THR04840
0012              DO 35 L=1,6                                                    THR04850
0013        35    SI=SI*XS+C(L)                                                  THR04860
0014              B=X*SI                                                         THR04870
0015              RETURN                                                         THR04880
0016        50    XS=3./X                                                        THR04890
0017              SF=-.00020033                                                  THR04900
0018              STH=-.00029166                                                 THR04910
0019              DO 55 L=1,6                                                    THR04920
0020              SF=SF*XS+CF(L)                                                 THR04930
0021        55    STH=STH*XS+CTH(L)                                              THR04940
0022              B=SF*DCOS(X+STH)/DSQRT(X)                                      THR04950
0023              RETURN                                                         THR04960
0024              END                                                            THR04970
```

```
0001          SUBROUTINE JOBES(X,B)                                    THR04980
0002          IMPLICIT REAL*8(A-H,O-Z)                                 THR04990
0003          DIMENSION C(6),CF(6),CTH(6)                              THR05000
0004          DATA C/-.0039444,.0444479,-.3163866,1.2656208,-2.2499997,1./  THR05010
0005          DATACF/-.00072805,.0013724,-.0000951,-.0055274,-.00000077,  THR05020
             1.7978846/                                                THR05030
0006          DATA CTH/-.0002933,-.00054125,.002625730,-.0000395,       THR05040
             0-.04166397,-.78539816/                                   THR05050
0007          IF(X) 10,20,20                                           THR05060
0008     10   X=-X                                                     THR05070
0009     20   IF(X-3.) 30,50,50                                        THR05080
0010     30   XS=X**2/9.                                               THR05090
0011          SI=.00021                                                THR05100
0012          DO 35 L=1,6                                              THR05110
0013     35   SI=SI*XS+C(L)                                            THR05120
0014          B=SI                                                     THR05130
0015          RETURN                                                   THR05140
0016     50   XS=3./X                                                  THR05150
0017          SF=.00014476                                             THR05160
0018          STH=.00013558                                            THR05170
0019          DO 55 L=1,6                                              THR05180
0020          SF=SF*XS+CF(L)                                           THR05190
0021     55   STH=STH*XS+CTH(L)                                        THR05200
0022          B=SF*DCOS(X+STH)/DSQRT(X)                                THR05210
0023          RETURN                                                   THR05220
0024          END                                                      THR05230
```

```
0001          SUBROUTINE I1BES(X,B)                                          THR05240
0002          IMPLICIT REAL*8(A-H,O-Z)                                       THR05250
0003          DIMENSION C(6),D(8)                                            THR05260
0004          DATA C/.00301532,.02658733,.15084934,.51498869,.8789059,.50/   THR05270
0005          DATA D/.0178765,-.0289531,.0228297,-.0103155,.0016380,         THR05280
             1-.0036202,-.0398802,.3989423/                                  THR05290
0006          IF(X) 10,20,20                                                 THR05300
0007     10   X=-X                                                           THR05310
0008     20   IF(X-3.75) 30,50,50                                            THR05320
0009     30   XS=X**2/14.0625                                                THR05330
0010          SI=.00032411                                                   THR05340
0011          DO 35 L=1,6                                                    THR05350
0012     35   SI=SI*XS+C(L)                                                  THR05360
0013          B=X*SI                                                         THR05370
0014          RETURN                                                         THR05380
0015     50   IF(X.GT.170.)GO TO 60                                          THR05390
0016          XRE=DEXP(X)/DSQRT(X)                                           THR05400
0017          XS=3.75/X                                                      THR05410
0018          SI=-.00420059                                                  THR05420
0019          DO 55 L=1,8                                                    THR05430
0020     55   SI=SI*XS+D(L)                                                  THR05440
0021          B=XRE*SI                                                       THR05450
0022          RETURN                                                         THR05460
0023     60   B=1.0E+70                                                      THR05470
0024          RETURN                                                         THR05480
0025          END                                                            THR05490
```

```
0001                SUBROUTINE IOBES(X,B)                                   THR05500
0002                IMPLICIT REAL*8(A-H,O-Z)                                THR05510
0003                DIMENSION C(6),D(8)                                     THR05520
0004                DATA C/.036076,.2659732,1.2067492,3.0899424,3.5156229,1./ THR05530
0005                DATA D/-.01647633,.0263554,-.0205771,.0091628,-.0015756, THR05540
                   1.0022532,.0132859,.3989423/                             THR05550
0006                IF(X) 10,20,20                                          THR05560
0007           10   X=-X                                                    THR05570
0008           20   IF(X-3.75) 30,50,50                                     THR05580
0009           30   XS=X**2/14.0625                                         THR05590
0010                SI=.0045813                                             THR05600
0011                DO 35 L=1,6                                             THR05610
0012           35   SI=SI*XS+C(L)                                           THR05620
0013                B=SI                                                    THR05630
0014                RETURN                                                  THR05640
0015           50   IF(X.GT.170.)GO TO 60                                   THR05650
0016                XRE=DEXP(X)/DSQRT(X)                                    THR05660
0017                XS=3.75/X                                               THR05670
0018                SI=.00392377                                            THR05680
0019                DO 55 L=1,8                                             THR05690
0020           55   SI=SI*XS+D(L)                                           THR05700
0021                B=XRE*SI                                                THR05710
0022                RETURN                                                  THR05720
0023           60   B=1.0E+70                                               THR05730
0024                RETURN                                                  THR05740
0025                END                                                     THR05750
```

```
0001          SUBROUTINE K1BES(X,B)                                          THR05760
0002          IMPLICIT REAL*8(A-H,O-Z)                                       THR05770
0003          DIMENSION C(6),CI(6),CK(6)                                     THR05780
0004          DATA C/.0032561,-.0078035,.0150426,-.0365562,.02349862,1.2533141/ THR05790
0005          DATA CI/.0030153,.0265873,.1508493,.5149887,.8789059,.5/        THR05800
0006          DATA CK/-.0011040,-.0191940,-.1815689,-.6727858,.1544314,1./    THR05810
0007          IF(X) 11,10,20                                                 THR05820
0008       10 B=1.0E+70                                                      THR05830
0009          RETURN                                                         THR05840
0010       11 X=-X                                                           THR05850
0011       20 IF(X-2.) 30,50,50                                              THR05860
0012       30 XL=X*DLOG(.5*X)                                                THR05870
0013          XSK=X**2/4.                                                    THR05880
0014          XSI=X**2/14.0625                                               THR05890
0015          SI=.00032411                                                   THR05900
0016          SK=-.00004686                                                  THR05910
0017          DO 35 L=1,6                                                    THR05920
0018          SI=SI*XSI+CI(L)                                                THR05930
0019       35 SK=SK*XSK+CK(L)                                                THR05940
0020          B=(SK+XL*X*SI)/X                                               THR05950
0021          RETURN                                                         THR05960
0022       50 IF(X-170.)60,60,70                                             THR05970
0023       60 XRE=DSQRT(X)*DEXP(X)                                           THR05980
0024          XS=2./X                                                        THR05990
0025          SK=-.00068245                                                  THR06000
0026          DO 65 L=1,6                                                    THR06010
0027       65 SK=SK*XS+C(L)                                                  THR06020
0028          B=SK/XRE                                                       THR06030
0029          RETURN                                                         THR06040
0030       70 B=1.0E-70                                                      THR06050
0031          RETURN                                                         THR06060
0032          END                                                            THR06070
```

```
0001          SUBROUTINE KOBES(X,B)                                          THR06080
0002          IMPLICIT REAL*8(A-H,O-Z)                                       THR06090
0003          DIMENSION C(6),CI(6),CK(6)                                     THR06100
0004          DATA C/-.0025154,.00587887,-.0106244,.0218956,-.0783235,       THR06110
             11.2533141/                                                     THR06120
0005          DATA CI/.0360768,.2659732,1.2067492,3.0899424,3.5156229,1./    THR06130
0006          DATA CK/.0001075,.0026269,.0348859,.2306975,.4227842,-.577215/ THR06140
0007          IF(X) 11,10,20                                                 THR06150
0008       10 B=1.0E+70                                                      THR06160
0009          RETURN                                                         THR06170
0010       11 X=-X                                                           THR06180
0011       20 IF (X-2.) 30,50,50                                             THR06190
0012       30 XL=DLOG(.5*X)                                                  THR06200
0013          XSK=X**2/4.                                                    THR06210
0014          XSI=X**2/14.0625                                               THR06220
0015          SI=.0045813                                                    THR06230
0016          SK=.0000074                                                    THR06240
0017          DO 35 L=1,6                                                    THR06250
0018          SI=SI*XSI+CI(L)                                                THR06260
0019       35 SK=SK*XSK+CK(L)                                                THR06270
0020          B=SK-SI*XL                                                     THR06280
0021          RETURN                                                         THR06290
0022       50 IF(X-170.)60,60,70                                             THR06300
0023       60 XRE=DSQRT(X)*DEXP(X)                                           THR06310
0024          XS=2./X                                                        THR06320
0025          SK=.00053208                                                   THR06330
0026          DO 55 L=1,6                                                    THR06340
0027       55 SK=SK*XS+C(L)                                                  THR06350
0028          B=SK/XRE                                                       THR06360
0029          RETURN                                                         THR06370
0030       70 B=1.0E-70                                                      THR06380
0031          RETURN                                                         THR06390
0032          END                                                            THR06400
```

```
0001          BLOCK DATA                                                THR06410
0002          IMPLICIT REAL*8(A-H,O-Z)                                  THR06420
0003          COMMON/S1/ZERO(100)                                       THR06430
0004          DATA ZERO/2.40482,5.52007,8.65372,11.79153,14.93091,18.07106,  THR06440
             121.21163,24.35247,27.49347,30.63460,33.77582,36.91709,40.05842,  THR06450
             243.19979,46.34118,49.48260,52.62405,55.76551,58.90698,  THR06460
             362.04846/                                                THR06470
0005          END                                                       THR06480
```

APPENDIX B

MODIFICATION OF THE CONVENTIONAL POINT HEAT SOURCE SOLUTION

The solution to the problem of a point heat source moving on the top surface of a finite thickness plate was given in Section 2.1.1 as eqn. 2.4. It was there pointed out that the method of images had to be applied to satisfy the adiabatic boundary conditions on the top and bottom surfaces of the plate. This solution has been found to be satisfactory by previous investigators in the case of bead-on-plate welds, especially if the temperature dependence of material properties was taken into account through an iterative approach.

For the multipass welding case, however, the solution failed to give good correlation with experimental results owing to the location of the point source on the top surface of the plates. To accomodate this possibility, a modification of the solution was accomplished in this study enabling one to locate the point source at any point through the plate's thickness. It thus becomes possible to simulate each welding pass by positioning a point source at the center of the pass.

Figure B.1 shows the superposition of heat sources necessary to obtain the desired solution. At point O the welding heat source WS is situated. To satisfy the adiabatic boundary conditions on the top and bottom surfaces of the plate, two imaginary heat sources T_1 and B_1 are required, being the mirror images of WS with respect to the two surfaces. These new sour-

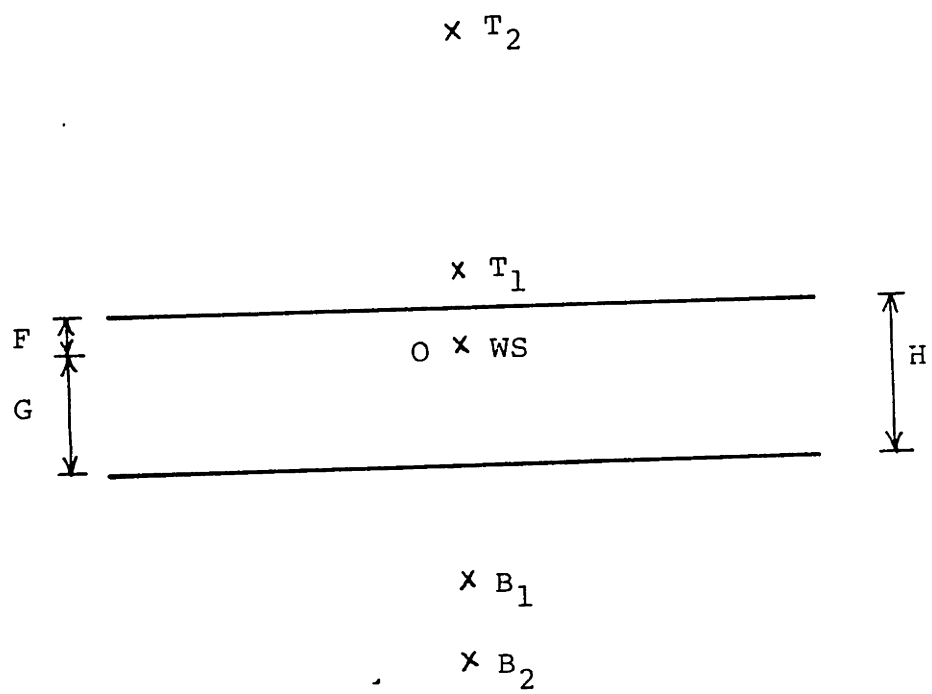

FIGURE B.1 Superposition of Heat Sources.

ces, however, produce heat transfer through the two surfaces. Consequently new image sources of them should be taken, etc. ad infinitum. For practical purposes around 30 total imaginary sources are required to obtain the solution.

This solution can now be expressed by the following equation:

$$\theta = \theta_o + \frac{Q}{4\pi k} \cdot e^{-\lambda \bar{v} \xi} \cdot \left\{ \frac{e^{-\lambda v R}}{R} + \sum_{n=1}^{\infty} \left[\frac{e^{-\lambda v R_n}}{R_n} + \frac{e^{-\lambda v R_{n'}}}{R_{n'}} \right] \right\} \qquad (B.1)$$

where

$$R_n = \sqrt{\xi^2 + y^2 + (OT_n + z)^2}$$

$$R_{n'} = \sqrt{\xi^2 + y^2 + (OB_n - z)^2}$$

$$OT_n = OB_{n-1} + 2.F$$

$$OB_n = OT_{n-1} + 2.G$$

and all other quantities have been previously defined or can be found in Figure B.1.

A computer program has been written in FORTRAN to implement this solution. In addition, the program can take into account the temperature variation of the material properties as well as the effect of each pass on the weld joint shape.

B.1 Program Listing

A listing of the computer program developed to implement the point heat source solution is given in the following pages.

```
                C     QUASI-STATIONARY STATE                                          POI00010
                C     TEMPERATURE DISTRIBUTION DUE TO A MOVING POINT HEAT SOURCE      POI00020
                C     ON A PLATE OF FINITE THICKNESS .                                POI00030
                C     USE OF ITERATION METHOD FOR TEMPERATURE DEPENDENCE OF           POI00040
                C     MATERIAL PROPERTIES                                             POI00050
                C                                                                     POI00060
                C     COMPILED BY V. J. PAPAZOGLOU          DECEMBER 1980             POI00070
                C                                                                     POI00080
                      IMPLICIT REAL*8 (A-H,O-Z)                                       POI00090
0001                  DIMENSION T(200),XY(100),XZ(100),Z(100),TY(100),RAT(20),TNEW(200) POI00100
0002                  DIMENSION TEMP(10),COND(10),CAP(10),RHO(10)                     POI00110
0003                  DIMENSION F(20),G(20),YTHN(20,100),THEFN(20,100)                POI00120
0004                  DIMENSION STATE(2)                                              POI00130
0005                  DATA STATE /8HCONSTANT,8HVARIABLE/                              POI00140
0006                                                                                  POI00150
                C                                                                     POI00160
                C        * * *   I N P U T   P H A S E   * * *                        POI00170
                C                                                                     POI00180
0007              870 READ(5,100) VOLT,AMP,EFF,THICK,V                                POI00190
0008                  IF(VOLT.EQ.0.) GO TO 999                                        POI00200
0009                  READ(5,110) (RAT(K),K=1,20)                                     POI00210
0010                  READ(5,120) (TEMP(I),I=1,10)                                    POI00220
0011                  READ(5,120) (COND(I),I=1,10)                                    POI00230
0012                  READ(5,120) (CAP(I),I=1,10)                                     POI00240
0013                  READ(5,120) (RHO(I),I=1,10)                                     POI00250
0014                  READ(5,130) NPASS,NPNC,NSMAX,NPROP                              POI00260
0015                  DO 3 I=1,NPASS                                                  POI00270
0016                3 READ(5,120)  (YTHN(I,J),J=1,NPNC)                               POI00280
0017                  READ(5,150) (F(I),G(I),I=1,NPASS)                               POI00290
0018                  READ(5,160) TMAX,THEF,TIX                                       POI00300
0019                  READ(5,160) T1,T2,T3,T4,T5,TLAST                                POI00310
0020                  READ(5,160) TI1,TI2,TI3,TI4,TI5                                 POI00320
0021                  READ(5,150) (XY(N),XZ(N),N=1,NPNC)                              POI00330
                C                                                                     POI00340
0022              100 FORMAT(5F10.4)                                                  POI00350
0023              110 FORMAT(20A4)                                                    POI00360
0024              120 FORMAT(10F8.3)                                                  POI00370
0025              130 FORMAT(4I5)                                                     POI00380
0026              150 FORMAT(8F10.4)                                                  POI00390
0027              160 FORMAT(8F10.4)                                                  POI00400
                C                                                                     POI00410
                C     WRITE IDENTIFICATION INFORMATION                                POI00420
                C                                                                     POI00430
0028                  WRITE(6,200)                                                    POI00440
0029              200 FORMAT(1H1,48X,'POINT HEAT SOURCE'//30X,'CALCULATION OF TEMPERATURE POI00450
                     1E DISTRIBUTION DURING WELDING'///49X,'WELDING CONDITIONS'/)     POI00460
0030                  WRITE(6,205) VOLT,AMP,EFF,V,THICK                               POI00470
0031              205 FORMAT(/28X,5HVOLT=,F5.1,5H AMP=,F5.1,5H EFF=,F4.2,7H SPEED=,F7.5, POI00480
                     111H THICKNESS=,F6.3/)                                           POI00490
0032                  NPROP1=NPROP+1                                                  POI00500
0033                  WRITE(6,210) (RAT(K),K=1,20),STATE(NPROP1)                      POI00510
0034              210 FORMAT(/10X,20A4,'(',A8,2X,'PROPERTIES)')                       POI00520
0035                  WRITE(6,215)                                                    POI00530
0036              215 FORMAT(/40X,'MATERIAL PROPERTIES VS. TEMPERATURE'/)
```

```
0037          WRITE(6,220) (TEMP(I),I=1,10)                                  POI00540
0038      220 FORMAT(/3X,'TEMPERATURE',4X,10(2X,F8.1))                       POI00550
0039          WRITE(6,221) (COND(I),I=1,10)                                  POI00560
0040      221 FORMAT(/3X,'CONDUCTIVITY',3X,10(2X,F8.6))                      POI00570
0041          WRITE(6,222) (CAP(I),I=1,10)                                   POI00580
0042      222 FORMAT(/3X,'SPECIFIC HEAT',2X,10(2X,F8.6))                     POI00590
0043          WRITE(6,223) (RHO(I),I=1,10)                                   POI00600
0044      223 FORMAT(/3X,'DENSITY',8X,10(2X,F8.6))                           POI00610
0045          WRITE(6,224) TMAX,TIX,TREF                                     POI00620
0046      224 FORMAT(///12X,'TMAX=',F8.1,4X,'TIX=',F8.2,4X,'TREF=',F8.1)     POI00630
0047          WRITE(6,225) 1ST,T1,T2,T3,T4,T5                                POI00640
0048      225 FORMAT(//5X,'TST =',F8.3,5X,'T1 =',F8.3,5X,'T2 =',F8.3,5X,'T3 =',FPOI00650
             18.3,5X,'T4 =',F8.3,5X,'T5 =',F8.3)                             POI00660
0049          WRITE(6,226) TI1,TI2,TI3,TI4,TI5                               POI00670
0050      226 FORMAT(//23X,'TI1=',F8.3,5X,'TI2=',F8.3,5X,'TI3=',F8.3,5X,'TI4=',FPOI00680
             18.3,5X,'TI5=',F8.3)                                            POI00690
0051          WRITE(6,230) NPASS,TLAST,NPNC,NSMAX                            POI00700
0052      230 FORMAT(1H1,'NUMBER OF WELDING PASSES=',I2,5X,'TIME INTERVAL FOR EAPOI00710
             1CH PASS=',F10.1//1X,'NUMBER OF OUTPUT POINTS =',I3/1X,'NUMBER OF IPOI00720
             2MAGE SOURCES =',I3)                                            POI00730
0053          WRITE(6,231) (I,F(I),I=1,NPASS)                                POI00740
0054      231 FORMAT(1H0,10X,'DISTANCE OF SOURCE FROM TOP OF PLATE   ---INCHES',POI00750
             1//3X,'(PASS NO. * DIST.)',6(I2,1X,'*',1X,F8.4))                POI00760
0055          WRITE(6,232)                                                   POI00770
0056      232 FORMAT(1H0,10X,'CHANGE OF JOINT SHAPE BY EFFECT OF MULTIPASS') POI00780
0057          DO 5 K=1,NPASS                                                 POI00790
0058          WRITE(6,233) K,(I,YTHN(K,I),I=1,NPNC)                          POI00800
0059      233 FORMAT(//4X,'PASS=',I2/(4X,10(I2,'*',F6.3,2X)))                POI00810
0060        5 CONTINUE                                                       POI00820
0061          WRITE(6,240) (N,XY(N),XZ(N),N=1,NPNC)                          POI00830
0062      240 FORMAT(1H1,'COORDINATES  (Y,Z)'///(6X,4(I5,'*',2F10.4)))       POI00840
        C                                                                    POI00850
        C        * * *   S O L U T I O N   P H A S E   * * *                 POI00860
        C                                                                    POI00870
0063          NSMAX2=NSMAX/2                                                 POI00880
0064          P=EFF*VOLT*AMP/1055.                                           POI00890
        C                                                                    POI00900
        C     DEFINITION OF TIME INSTANCES                                   POI00910
        C                                                                    POI00920
0065          TI=TI1                                                         POI00930
0066          N=1                                                            POI00940
0067          T(1)=1ST+TI                                                    POI00950
0068       40 IF(T(N).GE.T1) TI=TI2                                          POI00960
0069          IF(T(N).GE.T2) TI=TI3                                          POI00970
0070          IF(T(N).GE.T3) TI=TI4                                          POI00980
0071          IF(T(N).GE.T4) TI=TI5                                          POI00990
0072          IF(T(N).GE.T5) GO TO 41                                        POI01000
0073          T(N+1)=T(N)+TI                                                 POI01010
0074          N=N+1                                                          POI01020
0075          GO TO 40                                                       POI01030
0076       41 CONTINUE                                                       POI01040
0077          N=N+1                                                          POI01050
0078          T(N)=TLAST                                                     POI01060
```

```
0079                DO 300 I=1,N                                          POI01070
0080            300 TNEW(I)=T(I)                                          POI01080
              C                                                           POI01090
0081                IF(TIX.NE.0.) GO TO 55                                POI01100
0082                IX=0.45/V**2+1.                                       POI01110
0083                TIX=FLOAT(IX)                                         POI01120
0084             55 WRITE(6,270) TIX                                      POI01130
0085            270 FORMAT(//18H HEAT SOURCE AT T=,F8.2)                  POI01140
0086                DO 700 J=1,NPNC                                       POI01150
0087            700 TY(J)=TEMP(1)                                         POI01160
0088                WRITE(50) TST,TY                                      POI01170
              C     INITIALIZE TEMPERATURES FOR FIRST PASS                POI01180
0089                DO 668 J=1,NPNC                                       POI01190
0090                TY(J)=TREF                                            POI01200
0091            668 TREFN(1,J)=TREF                                       POI01210
              C                                                           POI01220
              C     FIND TEMPERATURE AT ALL TIME INSTANCES I FOR ALL WELDING PASSES K POI01230
              C                                                           POI01240
0092                DO 666 K=1,NPASS                                      POI01250
0093                DO 777 I=1,N                                          POI01260
0094                XT=(TIX-T(I))*V                                       POI01270
0095                WRITE(6,280) TNEW(I)                                  POI01280
0096            280 FORMAT( //1X,5HTIME=,F10.3)                           POI01290
0097                WRITE(6,285) K                                        POI01300
0098            285 FORMAT(1H+,20X,'INVOLVES MULTIPASS EFFECT - PASS NO.',I2) POI01310
              C                                                           POI01320
              C     FOR ALL CONSIDERED POINTS                             POI01330
              C                                                           POI01340
0099                DO 70 J=1,NPNC                                        POI01350
0100                Z(J)=XZ(J)-F(K)                                       POI01360
0101                RO2=XT*XT+XY(J)*XY(J)                                 POI01370
0102                R=DSQRT(RO2+Z(J)*Z(J))                                POI01380
0103                IF(R.LT..001) GO TO 11                                POI01390
              C                                                           POI01400
              C     CHOICE OF PROPERTIES TO INITIALIZE ITERATION          POI01410
              C                                                           POI01420
0104                CON=COND(3)                                           POI01430
0105                CA=CAP(3)                                             POI01440
0106                RH=RHO(3)                                             POI01450
0107                IF(NPROP.EQ.0) GO TO 500                              POI01460
              C                                                           POI01470
0108                TO=TY(J)                                              POI01480
0109                CON=FILLIN(TO,TEMP,COND,10)                           POI01490
0110                CA=FILLIN(TO,TEMP,CAP,10)                             POI01500
0111                RH=FILLIN(TO,TEMP,RHO,10)                             POI01510
0112                IT=0                                                  POI01520
0113             10 CONTINUE                                              POI01530
0114                IT=IT+1                                               POI01540
              C                                                           POI01550
              C     MODIFICATION OF PROPERTIES TO TAKE INTO ACCOUNT WELD PASS POI01560
              C                                                           POI01570
0115            500 CON=CON*YTHN(K,J)/THICK                               POI01580
0116                RH=RH*YTHN(K,J)/THICK                                 POI01590
```

```
                C     TEMPERATURE DUE TO ACTUAL POINT SOURCE                    POI01600
0117                  C1=V*CA*RH/2./CON                                         POI01610
0118                  C2=P/12.56637/CON                                         POI01620
0119                  CR=C1*(XT+R)                                              POI01630
0120                  IF(CR.LT.0.) CEX=0.                                       POI01640
0121                  IF(CR.GT.0.) CEX=1.0E+30                                  POI01650
0122                  IF(DABS(CR).LT.170.) CEX=DEXP(CR)                         POI01660
0123                  IF(CEX.EQ.0.) GO TO 11                                    POI01670
0124                  TP0=1./CEX/R                                              POI01680
                C                                                               POI01690
                C     TEMPERATURE DUE TO IMAGE SOURCES                          POI01700
                C                                                               POI01710
0125                  TP1=0.                                                    POI01720
0126                  TP2=0.                                                    POI01730
0127                  L=1                                                       POI01740
0128                  ON1=2.*G(K)                                               POI01750
0129                  ON2=2.*F(K)                                               POI01760
0130               30 Z1=ON1-Z(J)                                               POI01770
0131                  Z2=ON2+Z(J)                                               POI01780
0132                  R1=DSQRT(RO2+Z1*Z1)                                       POI01790
0133                  R2=DSQRT(RO2+Z2*Z2)                                       POI01800
0134                  CR1=C1*(XT+R1)                                            POI01810
0135                  CR2=C1*(XT+R2)                                            POI01820
0136                  IF(CR1.LT.0.) CEX1=0.                                     POI01830
0137                  IF(CR2.LT.0.) CEX2=0.                                     POI01840
0138                  IF(CR1.GT.0.) CEX1=1.0E+30                                POI01850
0139                  IF(CR2.GT.0.) CEX2=1.0E+30                                POI01860
0140                  IF(DABS(CR1).LT.170.) CEX1=DEXP(CR1)                      POI01870
0141                  IF(DABS(CR2).LT.170.) CEX2=DEXP(CR2)                      POI01880
0142                  IF(CEX1.EQ.0.0.OR.CEX2.EQ.0.0) GO TO 11                   POI01890
0143                  TP1=TP1+1./CEX1/R1                                        POI01900
0144                  TP2=TP2+1./CEX2/R2                                        POI01910
0145                  L=L+1                                                     POI01920
0146                  IF(L.GT.NSMAX2) GO TO 80                                  POI01930
0147                  ONIN=ON2+2.*G(K)                                          POI01940
0148                  ON2=ON1+2.*F(K)                                           POI01950
0149                  ON1=ONIN                                                  POI01960
0150                  GO TO 30                                                  POI01970
                C                                                               POI01980
                C     FINAL TEMPERATURE                                         POI01990
                C                                                               POI02000
0151               80 TP=C2*(TP0+TP1+TP2)                                       POI02010
0152                  TN=TP+TREFN(K,J)                                          POI02020
0153                  IF(TN.GT.TMAX) TN=TMAX                                    POI02030
0154                  IF(NPROP.EQ.0) GO TO 15                                   POI02040
                C                                                               POI02050
                C     CHECK FOR CONVERGENCE                                     POI02060
                C                                                               POI02070
0155                  AB=DABS(TN-TO)                                            POI02080
0156                  IF(AB.LE.2.0) GO TO 15                                    POI02090
0157                  TM=0.5*(TO+TN)                                            POI02100
0158                  IF(IT.GT.90) GO TO 998                                    POI02110
0159                  TO=TN                                                     POI02120
```

```
                C     NEW PROPERTIES                                          POI02130
                      CON=FILLIN(TM,TEMP,COND,10)                             POI02140
0160                  CA=FILLIN(TM,TEMP,CAP,10)                               POI02150
0161                  RH=FILLIN(TM,TEMP,RHO,10)                               POI02160
0162                  GO TO 10                                                POI02170
0163                 11 TN=TMAX                                               POI02180
0164                 15 TY(J)=TN                                              POI02190
0165                    GO TO 888                                             POI02200
0166                998 WRITE(6,290) J,TM,TO,TN                               POI02210
0167                290 FORMAT( 1X,22HTEMP DOES NOT CONVERGE,' J=',I2,' TM,TO,TN=',3F10.2,POI02220
0168                   1'*** TM IS USED ***')                                 POI02230
                                                                              POI02240
0169                    TY(J)=TM                                              POI02250
0170                888 CONTINUE                                              POI02260
0171                 70 CONTINUE                                              POI02270
0172                    WRITE(6,295) (J,TY(J),J=1,NPNC)                       POI02280
0173                295 FORMAT(1H0,'TEMPERATURES AT CONSIDERED POINTS'//(1H ,7(I4,'*',F9.2POI02290
                       1,3X)))                                                POI02300
0174                    WRITE(56) TNEW(I),TY                                  POI02310
0175                777 CONTINUE                                              POI02320
0176                    DO 667 J=1,NPNC                                       POI02330
0177                667 TREPN(K+1,J)=TY(J)                                    POI02340
0178                    DO 350 I=1,N                                          POI02350
0179                350 TNEW(I)=TNEW(I)+TLAST                                 POI02360
0180                666 CONTINUE                                              POI02370
0181                    GO TO 870                                             POI02380
0182                999 CONTINUE                                              POI02390
0183                    STOP                                                  POI02400
0184                    END
```

```
0001          FUNCTION FILLIN(X,AB,OR,NO)                                    POI02410
        C     *** FILLIN ***  LINEAR    INTERPOLATION                        POI02420
        C     FINDS Y(X) FROM TABLE OF                                       POI02430
        C     AB(N) AND OR(N) CONTAINING NO POINTS.                          POI02440
0002          IMPLICIT REAL*8(A-H,O-Z)                                       POI02450
0003          DIMENSION AB(NO),OR(NO)                                        POI02460
        C                                                                    POI02470
0004          IF(X.GE.AB(1)) GO TO 10                                        POI02480
0005          WRITE(6,3001)                                                  POI02490
0006     3001 FORMAT(//,'    ERROR   TEMPERATURE OUTSIDE RANGE OF MATERIAL PROPEPOI02500
            1RTY TEMPERATURES  (FUNCTION FILLIN)')                           POI02510
0007          STOP                                                           POI02520
        C                                                                    POI02530
        C     DETERMINE INTERPOLATION FACTOR                                 POI02540
        C                                                                    POI02550
0008       10 L=0                                                            POI02560
0009          DO 20 K=2,NO                                                   POI02570
0010          L=L+1                                                          POI02580
0011          DUM=AB(K)                                                      POI02590
0012          IF(K.EQ.NO) DUM=AB(NO)                                         POI02600
0013          IF(X.GT.DUM) GO TO 20                                          POI02610
0014          GO TO 25                                                       POI02620
0015       20 CONTINUE                                                       POI02630
0016          WRITE(6,3001)                                                  POI02640
0017          STOP                                                           POI02650
        C                                                                    POI02660
0018       25 XRATIO=(X-AB(L))/(AB(L+1)-AB(L))                               POI02670
        C                                                                    POI02680
0019          IF(XRATIO.GT.1.0) XRATIO=1.0                                   POI02690
0020          IF(XRATIO.LT.0.0) XRATIO=0.0                                   POI02700
        C                                                                    POI02710
        C     INTERPOLATE THE MATERIAL PROPERTY                              POI02720
        C                                                                    POI02730
0021          FILLIN=OR(L)+XRATIO*(OR(L+1)-OR(L))                            POI02740
0022          RETURN                                                         POI02750
0023          END                                                            POI02760
```

APPENDIX C

DERIVATION OF SCHEMATIC CONTINUOUS COOLING TRANSFORMATION DIAGRAMS

A brief description of the methods proposed by Grange and Kiefer [67] and Manning and Lorig [68] for the derivation of schematic CCT diagrams based on isothermal data are presented in this Appendix. The necessary modifications to enable one to use log-linear as well as the traditional linear cooling curves are also outlined. Finally, the computer implementation (made on an IBM 370 machine) is discussed.

C.1 The Grange-Kiefer Approach

A part of the isothermal transformation diagram showing the starting curve for an allotropic transformation (say austenite to bainite) is shown in Figure C.1. A cooling curve is superimposed on the diagram starting from the A_1 (eutectoid) temperature assuming that the transformation product is bainite*. The cooling curve intersects the isothermal starting curve at the point x corresponding to a temperature θ_x and a time t_x (time zero is defined as the time at which the cooling curve intersects the A_1 temperature). An arbi-

*Note that the starting temperature should be A_3 if the primary product is ferrite and A_{cm} if proeutectoid cementite.

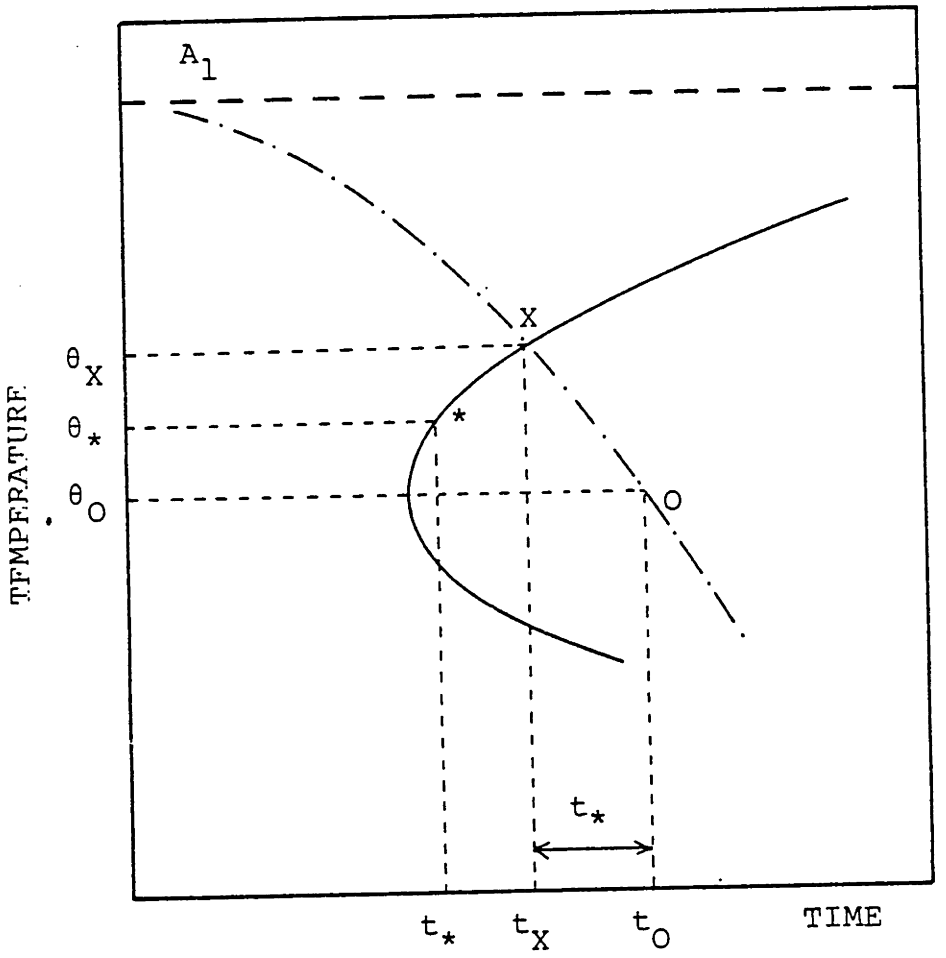

FIGURE C.1 Schematic Representation of the Grange-Kiefer Method.

trary lower point 0 is taken on the cooling curve corresponding to temperature θ_0 and time t_0. To describe what happens between points x and 0, two assumptions are made:

(1) The extent of transformation of the austenite at the instant it cools to the intersection point x is not substantially different than it would have been if quenched instantly to θ_x.

(2) On cooling through the limited temperature range θ_x to θ_0, the amount of transformation is approximately equal to the amount indicated by the isothermal diagram at the mean temperature $\theta_* = (\theta_x + \theta_0)/2$ after a time interval $t_* = t_0 - t_x$.

Based on the second assumption, point 0 will be on the starting curve of the CCT diagram if point * is on the starting curve of the TTT diagram. It is therefore evident that a number of iterations are required for the determination of a point on the starting curve of the CCT diagram, a fact that makes the process ideally suited for computer implementation. Furthermore, the whole starting CCT curve can be obtained by joining several points obtained using different cooling curves.

C.2 The Manning-Lorig Approach

This approach is based on the rule of additivity. The cooling curve is approximated by a step curve so that for a time interval Δt_i the temperature is assumed to be constant and equal to θ_i. This time interval Δt_i is then divided by

the time τ_i required for the transformation to begin isothermally at temperature θ_i (see Figure C.2), and the resulting quantity is considered to represent a fraction of the total nucleation time required. When the sum of a number of such fractions equals one, that is, when

$$\sum_{\substack{t=0 \\ (\theta=A_1)}}^{t_n} \frac{\Delta t_i(\theta)}{\tau_i(\theta)} = 1$$

then transformation commences. The point on the cooling curve at which this occurs is thus considered to be a point on the starting curve of the CCT diagram. By employing several cooling curves, the starting CCT curve can be adequately described.

It is again evident that the nature of the method makes it appropriate for computer implementation. Furthermore, the note regarding the A_1 temperature (which can be A_3 or A_{cm} depending on the nature of the transformation) mentioned in the Grange-Kiefer approach holds true here as well.

Finally, it should be mentioned that when the sum of the fractions does not reach 1 before the M_s temperature is encountered, then only the martensitic transformation takes place. This will happen when the cooling rates are relatively high, exceeding the so-called critical cooling rate.

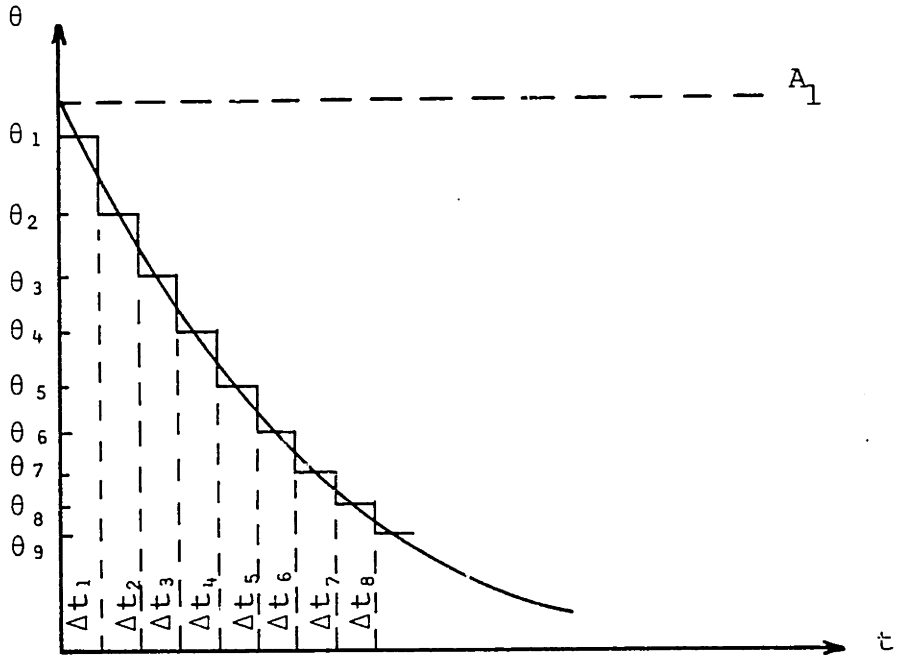

TIME FOR COOLING

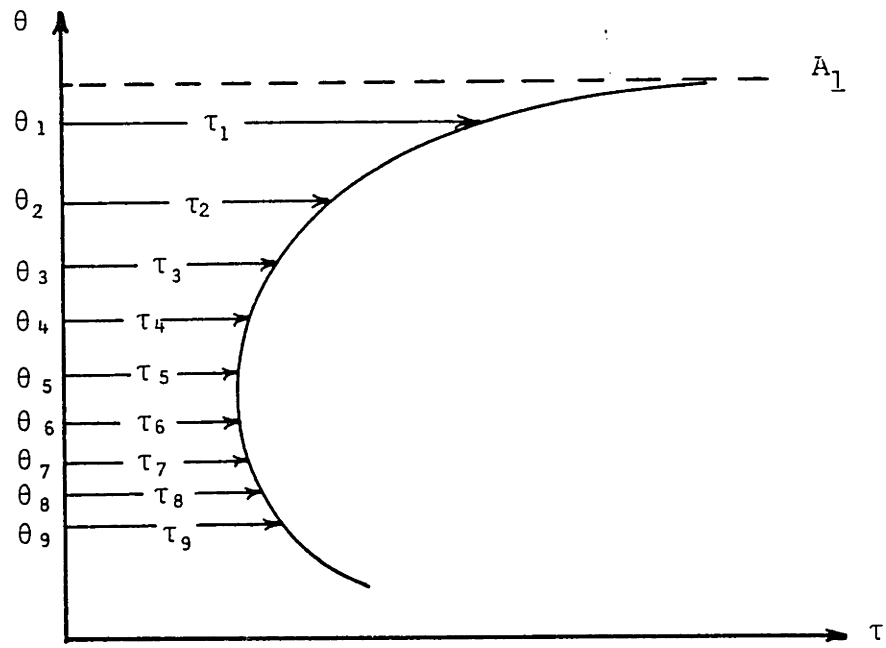

TIME FOR ISOTHERMAL NUCLEATION

FIGURE c.2 Schematic Representation of the Manning-Lorig Method.

C.3 Log-linear Cooling Rates

As noted in Section 3.4.1, the cooling stage of the welding temperature history can be approximated by a linear curve in a θ -$\log_{10}t$ graph, and thus represented by an equation of the form

$$\theta = A.\log_{10}t + B$$

where A and B are parameters chosen to curve-fit representative welding temperature curves using the least-squares method (see Table C.1).

TABLE C.1 Values of Parameters A and B

A	B
-1000.0	2000.0
- 780.0	1960.0
- 700.0	1980.0
- 650.0	2050.0
- 535.0	1985.0
- 500.0	2000.0
- 463.3	2000.0
- 425.1	2000.0
- 384.3	2000.0

Note: The parameters A and B pertain to the log-linear equation $\theta = A.\log_{10}t + B$.

From the discussion of the two previous sections it is moreover evident that cooling curves of this type are appropriate and compatible with both methods, the only difficulty being lengthier calculations, a fact that does not pose any problems when a computer is used.

C.4 Computer Implementation

A double precision computer program was written using the FORTRAN IV language to implement the two methods of calculating schematic CCT diagrams. Some notes on the program follow:

1. The TTT ciagram is expressed in terms of N data points. Since the program consequently approximates the transformation curve with linear segments, care should be taken in spacing the input data points closer in the regions where abrupt slope changes occur, as for example, near the nose of the diagram.

2. The log-linear cooling curve is approximated by a piecewise linear curve when the Grange-Kiefer approach is used so that its intersection with the TTT curve can be calculated.

3. About 10 cooling curves are adequate for determining the CCT diagram.

4. The time step size, Δt, in the case of linear cooling curves, and the temperature step size, $\Delta\theta$, in the case of log-linear ones, should be selected according to the trans-

formation times depicted in the TTT diagram. For example, short times require relatively small step sizes. In the case of HY-130 Δt was chosen to be from 0.2 to 2.0 sec., increasing with decreasing cooling rates; whereas $\Delta\theta$ was chosen to be from 5.0 to 2.0°F respectively.

5. The maximum number of iterations allowed for the selection of point 0 in the Grange-Kiefer approach was set to 100.

6. The convergence criterion in the Grange-Kiefer approach for the selection of point 0, i.e., the distance between t_* and the time of the point on the TTT curve at temperature θ_*, was set equal to 1 sec. Use of a smaller convergence criterion will usually require a larger maximum number of iterations allowed.

APPENDIX D

EVALUATION OF COMBINED THERMAL AND TRANSFORMATION STRAIN

The equations developed for the evaluation of the combined thermal and transformation strain will be discussed in this Appendix. As mentioned in Section 5.4.2 this strain was used to replace the conventional thermal strain, e_{rs}^{TH}, in the thermo-elastic-plastic and creep constitutive model incorporated into the finite element stress analysis program ADINA.

The heating and cooling stages of the welding cycle will be treated separately. Furthermore, and given the incremental nature of the solution process, a time step will be considered that brings the solution from time t to time t+Δt. Finally, for each of the three terms in equation (5.13), namely e_1 for the thermal strain in a mixture of phases, e_2 for the transformation strain, and e_3 for the thermal strain in a single phase, a separate equation will be established.

D.1 Heating Stage

Depending on the relative position of the temperatures t_θ and $^{t+\Delta t}\theta$ with respect to A_{c1} and A_{c3}, the following cases are possible.

D.1.1 $t_\theta < {}^{t+\Delta t}\theta \leqslant A_{c1}$

No transformation has started taking place, so the

structure is still martensitic. Therefore:

$$^{t+\Delta t}e_1 = 0 \tag{D.1a}$$

$$^{t+\Delta t}e_2 = 0 \tag{D.1b}$$

$$^{t+\Delta t}e_3 = \alpha_M.(^{t+\Delta t}\theta - \theta_R) \tag{D1.c}$$

where α_M is the thermal expansion coefficient of martensite and θ_R the ambient temperature.

D.1.2 $\underline{A_{c1} < {}^{t+\Delta t}\theta \leqslant A_{c3}}$

Austenitization has started at the A_{c1} temparature, and has already produced a fraction f^A of austenite with the remaining $1-f^A$ still being martensite. Using eqn. (5.11) for the calculation of f^A, we have

$$^{t+\Delta t}e_1 = \alpha_A \cdot \int_{A_{c1}}^{t+\Delta t_\theta} f^A.d\theta + \alpha_M \cdot \int_{A_{c1}}^{t+\Delta t_\theta} (1-f^A).d\theta$$

or

$$^{t+\Delta t}e_1 = \left[\alpha_A - \left(\frac{A_{c3}}{A_{c3}-A_{c1}}\right)^2 (\alpha_A-\alpha_M)\right] \cdot \left(^{t+\Delta t}\theta - A_{c1}\right) - (\alpha_A-\alpha_M) \cdot \frac{\left(^{t+\Delta t}\theta^3 - A_{c1}^3\right)/3 - \left(^{t+\Delta t}\theta^2 - A_{c1}^2\right).A_{c3}}{\left(A_{c3}-A_{c1}\right)^2} \tag{D2.a}$$

$$^{t+\Delta t}e_2 = \left\{1 - \left[\frac{A_{c3} - {}^{t+\Delta t}\theta}{A_{c3} - A_{c1}}\right]^2\right\} e^{TR}_{M\to A} \tag{D.2b}$$

$$^{t+\Delta t}e_3 = \alpha_M \cdot (A_{c1} - \theta_R) \qquad \text{(D.2c)}$$

where all variables have been defined in Section 5.4.

D.1.3 $\underline{A_{c3} < {}^{t+\Delta t}\theta}$

Full austenitization has taken place when the temperature is above A_{c3}. One therefore obtains

$$^{t+\Delta t}e_1 = \alpha_A \cdot \int_{A_{c1}}^{A_{c3}} f^A . d\theta + \alpha_M \cdot \int_{A_{c1}}^{A_{c3}} (1-f^A) . d\theta$$

or

$$^{t+\Delta t}e_1 = \left[\alpha_A - \left(\frac{A_{c3}}{A_{c3}-A_{c1}}\right)^2 . (\alpha_A - \alpha_M)\right] . (A_{c3}-A_{c1})$$

$$-(\alpha_A - \alpha_M) . \frac{\left(A_{c3}^3 - A_{c1}^3\right)/3 - A_{c3} . \left(A_{c3}^2 - A_{c1}^2\right)}{\left[A_{c3}-A_{c1}\right]^2} \qquad \text{(D.3a)}$$

$$^{t+\Delta t}e_2 = e_{M\to A}^{TR} \qquad \text{(D3.b)}$$

$$^{t+\Delta t}e_3 = \alpha_M \cdot (A_{c1} - \theta_R) + \alpha_A \cdot ({}^{t+\Delta t}\theta - A_{c3}) \qquad \text{(D3.c)}$$

D.2 Cooling Stage

The equations for the cooling stage of the temperature cycle depend on the maximum temperature reached, θ_{max}, during the heating phase. They have been derived in such a way that the total thermal and transformation strain can be written

$$^{t+\Delta t}e_{rs} = (e_{max} + e_1 + e_2 + e_3).\delta_{rs} \tag{D.4}$$

where e_{max} is the total strain at the maximum temperature reached and all other variables have been previously defined.

D.2.1 $\underline{\theta_{max} \leqslant A_{c1}}$

Cooling started before the temperature of the point under consideration has exceeded the A_{c1} temperature. As a consequence, no austenitization took place, so

$$^{t+\Delta t}e_1 = 0 \tag{D.5a}$$

$$^{t+\Delta t}e_2 = 0 \tag{D.5b}$$

$$^{t+\Delta t}e_3 = \alpha_M.(^{t+\Delta t}\theta - \theta_{max}) \tag{D.5c}$$

D.2.2 $\underline{A_{c1} < \theta_{max}}$

Since the maximum temperature has exceeded the A_{c1} one, at least partial austenitization has taken place. The austenite can therefore (under the conditions described in Section 5.4.1) be transformed upon cooling into bainite and/or martensite. To study the various possibilities, each of the three terms e_1, e_2, and e_3 will be considered separately.

D.2.2.1 Thermal Expansion of the Untransformed Martensite.

Depending on the relative magnitude of θ_{max} with respect to the A_{c3} temperature, two subcases are possible.

(1) $\underline{A_{c3}<\theta_{max}}$: Full austenitization has taken place upon heating, so

$$^{t+\Delta t}e_3 = 0 \tag{D.6a}$$

(2) $\underline{A_{c1}<\theta_{max}\leqslant A_{c3}}$: Since only partial austenitization took place upon heating, there is a fraction of untransformed martensite equal to $1-f^A$ giving

$$^{t+\Delta t}e_3 = (1-f^A).\alpha_M.(^{t+\Delta t}\theta-\theta_{max}) \tag{D.6b}$$

D.2.2.2 Transformation Expansion

Four subcases are considered for the calculation of the transformation expansion.

(1) $\underline{B_s\leqslant {}^{t+\Delta t}\theta}$: The temperature has not yet reached the bainite start transformation one upon cooling, therefore

$$^{t+\Delta t}e_2 = 0 \tag{D.7a}$$

(2) $\underline{M_s\leqslant {}^{t+\Delta t}\theta<B_s}$: The existing fraction of austenite, f^A, can be transformed into bainite within this temperature region if the precipitation starting time is exceeded (refer to Section 5.4.1), so

$$^{t+\Delta t}e_2 = f^A.f_F^B.\left[1-\left(\frac{^{t+\Delta t}\theta-M_s}{B_s-M_s}\right)^2\right].e_{A\to B}^{TR} \tag{D.7b}$$

where f_F^B is the final fraction of bainite to be transformed at the M_s temperature for the cooling curve under consideration.

(3) $\underline{M_f \leqslant {}^{t+\Delta t}\theta < M_s}$: Any remaining austenite (not previously transformed into bainite) will be transformed to martensite in this temperature region, the transformation extent being a function of the undercooling below the M_s temperature. It can thus be written

$$
{}^{t+\Delta t}e_2 = f^A \cdot \left\{ f_F^B \cdot e_{A\to B}^{TR} + (1-f_F^B) \cdot \left[1 - \left(\frac{{}^{t+\Delta t}\theta - M_f}{M_s - M_f} \right)^2 \right] \cdot e_{A\to M}^{TR} \right\} \tag{D.7c}
$$

(4) $\underline{{}^{t+\Delta t}\theta < M_f}$: All transformations have already being made and there may still be some remaining austenite. Eqn. (D.7c) also holds for this subcase.

D.2.2.3 Thermal Expansion of Mixed Region

The same four subcases considered in Section D.2.2.2 are distinguished here as well.

(1) $\underline{B_s \leqslant {}^{t+\Delta t}\theta}$: Only the transformed fraction of austenite is present, so

$$
{}^{t+\Delta t}e_1 = f^A \cdot \alpha_A \cdot ({}^{t+\Delta t}\theta - \theta_{max}) \tag{D.8a}
$$

Note that the possibly present untransformed martensite has already been taken into account in eqn. (D.6).

(2) $\underline{M_s \leqslant {}^{t+\Delta t}\theta < B_s}$: To arrive at this temperature from θ_{max} the point under consideration went through a temperature region (from θ_{max} to B_s) where only the transformed austenite

was present and a region (from B_s to $^{t+\Delta t}\theta$) in which the fraction of bainite was continuously increasing accompanied by a conqurrent decrease in austenite. Therefore

$$^{t+\Delta t}e_1 = f^A \left\{ \alpha_A \cdot (B_s - \theta_{max}) + \int_{B_s}^{t+\Delta t_\theta} \left[\alpha_B \cdot f^B + \alpha_A \cdot (1-f^B) \right] \cdot d\theta \right\}$$

or, using eqn. (5.11)

$$^{t+\Delta t}e_1 = f^A \cdot \left\{ \alpha_A \cdot (B_s - \theta_{max}) + \left[f_F^B \cdot (\alpha_B - \alpha_A) + \alpha_A - \frac{f_F^B \cdot (\alpha_B - \alpha_A)}{(B_s - M_s)^2} \cdot \left(\frac{1}{3} \cdot ({}^{t+\Delta t}\theta^2 + {}^{t+\Delta t}\theta \cdot B_s + B_s^2) + M_s \cdot (M_s - {}^{t+\Delta t}\theta - B_s) \right) \right] \cdot ({}^{t+\Delta t}\theta - B_s) \right\} \qquad \text{(D.8b)}$$

(3) $\underline{M_f \leqslant {}^{t+\Delta t}\theta < M_s}$: Similar thoughts to the ones described in the previous subcase lead to the following equation

$$^{t+\Delta t}e_1 = f^A \cdot \left\{ \alpha_A \cdot (B_s - \theta_{max}) + \int_{B_s}^{M_s} \left[\alpha_B \cdot f^B + \alpha_A \cdot (1-f^B) \right] \cdot d\theta \right.$$

$$+ f_F^B \cdot \alpha_B \cdot ({}^{t+\Delta t}\theta - M_s)$$

$$+ \int_{M_s}^{t+\Delta t_\theta} \left[\alpha_M \cdot f^M + \alpha_A \cdot (1 - f_F^B - f^M)\right] \cdot d\theta$$

where f^M is the fraction of transformed martensite and is given by

$$f^M = (1 - f_F^B) \cdot \left[1 - \left(\frac{\theta - M_f}{M_s - M_f}\right)^2\right]$$

After some algebra one finds

$$\begin{aligned}
{}^{t+\Delta t}e_1 = f^A \cdot \Big\{ & \alpha_A \cdot (B_s - \theta_{max}) \\
& + \left[\frac{2}{3} \cdot f_F^B \cdot (\alpha_B - \alpha_A) + \alpha_A\right] \cdot (M_s - B_s) \\
& + \alpha_B \cdot f_F^B \cdot ({}^{t+\Delta t}\theta - M_s) \\
& + (1 - f_F^B) \cdot \left[\alpha_M + \frac{\alpha_A - \alpha_M}{(M_s - M_f)^2} \cdot \left[({}^{t+\Delta t}\theta^2 + \right.\right. \\
& \left.\left. {}^{t+\Delta t}\theta \cdot M_s + M_s^2)/3 + M_f \cdot (M_f - {}^{t+\Delta t}\theta - M_s)\right]\right] \cdot \\
& ({}^{t+\Delta t}\theta - M_s) \Big\}
\end{aligned} \tag{D.8c}$$

(4) $\underline{{}^{t+\Delta t}\theta < M_f}$: In this subcase eqn. (D.8c) also holds if the variable ${}^{t+\Delta t}\theta$ is replaced by M_f and the additional

term

$$f^{A}.\alpha_{M}.(1-f_{F}^{B}).({}^{t+\Delta t}\theta-M_{f})$$

is taken into account.